Diagonal Cracking in Reinforced Concrete Deep Beams - An Experimental Investigation

Marco Rigotti

A Thesis

in

The Department

of

Building, Civil and Environmental Engineering

Presented in Partial Fulfillment of the Requirements

for the Degree of Doctor of Philosophy at

Concordia University

Montreal, Quebec, Canada

November 2002

ABSTRACT

Diagonal Cracking in Reinforced Concrete Deep Beams - An Experimental Investigation

Marco Rigotti, Ph.D.
Concordia University, 2002

Concrete deep beams with a shear span to depth ratio of less than 2.32 [73] will work as tied arches after flexural cracking, provided there is sufficient reinforcement. The compression strut formed between the support and the loading points is under biaxial compressive and tensile stresses.

The current Canadian Code[5] stipulates that deep beams and corbels should be designed using the Strut-and-Tie Method. This method incorporates the work done by Collins and Mitchell[8][9] where the cracked concrete behaves as a new material and that the compressive strength of concrete is reduced due to strain-softening. Here-in lies an area of discrepancy. The work done by Collins and Mitchell utilizes beam theory which requires that plane sections remain plane. However, deep beams and corbels are classified as "regions of discontinuity" consequently beam theory does not apply to these structures. An area of the Canadian code which needs to be examined is the dimensioning of the compression strut. To date there is no clear explanation as to how the design guidelines of the compression strut were developed. A weakness of the design code is that numerous assumptions must be made. The designer first assumes that the compression strut reaches a maximum concrete strain of 0.002[5], and then must assume the strains in the tension ties.

The focus of this research has been to investigate diagonal splitting strength of reinforced concrete deep beams. In conducting this study, twelve deep beams, categorized in four groups were tested. The test variables included the shear span, the amount of web reinforcement and the concrete compressive strength. Surprisingly, no researcher has published measured strain incurred by the

compression strut in deep beams. In our research, a single beam from each of the four test groups was fitted with strain gauges to measure the tensile strain in the main tensile reinforcement. As well, the concrete strains along the main diagonal formed between the support and the loading points as well as perpendicular to the strut were measured.

The experimental work demonstrated the development of diagonal cracking. These cracks appeared above the supports and propagated towards the loading points. The strain gauges on the concrete surface confirmed that the stresses along the compression strut were under biaxial compression tension stresses. A finite element analysis determined that the compression stress acting parallel to the diagonal were uniform in distribution and symmetrical. Perpendicular to the diagonal, high compressive stresses were seen at the supports and the loading points. However, the stresses in between these areas were uniformly distributed in tension. The measured compressive strains were much less than the recommended value of 0.002, and the compression strut was found to be much wider than that defined by the Canadian Code. As a consequence of these the findings, a truss model was defined using a biaxial concrete strength envelope. This truss model was applied to the test beams of this study as well as too ninety-nine test beams available in literature. In all cases, the truss model was able to accurately predict the strength of these test beams.

Acknowledgments

I would like to express my sincerest gratitude to Professor Zenon A. Zielinski for his unwavering support, encouragement, and generous willingness to share his insight in my pursuit of this research.

I would like to extend my gratitude to the support staff in the department of Building, Civil and Environmental Engineering at Concordia University. A special thank you to Rocco Lombardo for the long hours spent in the lab, and more importantly, for the time spent talking while having coffee at lunch.

Table of Contents

CHAPTER 1 Introduction 1

1.1 Introduction 1
1.1.1 Concrete failure modes 2
1.1.2 Current Research 5

CHAPTER 2 Literature Review 7

2.1 Introduction 7
2.2 Corbels - Shear Friction 7
2.2.1 Kriz & Raths 7
2.2.2 Mast 11
2.2.3 Mattock 13
2.2.4 Hermansen & Cowan 17
2.3 Corbels - Truss Analogy 19
2.3.1 Franz & Niedenhoff 19
2.3.2 Somerville 21
2.3.3 Hagberg 24
2.3.4 Solanki & Sabnis 28
2.3.5 Hwang, Lu and Lee 31
2.4 Deep Beams 34
2.4.1 Leonhardt & Walther 34
2.4.2 Kong et al. 35
2.4.3 Smith & Vantsiotis 37
2.4.4 Besser and Cusens 39
2.4.5 Mau & Hsu 41
2.4.6 Kotsovos 44
2.4.7 Siao 46
2.4.8 Rogowsky and MacGregor 48
2.4.9 Collins and Mitchell 50
2.4.10 Schlaich and Schafer 55
2.4.11 Tan and Lu 57
2.4.12 Hwang, Lu and Lee 59
2.5 Current Canadian Code 64
2.6 Summary 67

CHAPTER 3 Experimental Program 68

3.1 Test Program 68
3.1.1 Introduction 68
3.1.2 Beam Details 69
3.2 Materials 77
3.2.1 Concrete 77
3.2.2 Steel 78

3.3 Instrumentation 79
3.3.1 Strain Gauges 80
3.3.2 Displacements 80
3.4 Testing 80
3.4.1 Testing Procedure 80
3.4.2 Test Setup 82
3.5 Objective 82

CHAPTER 4 Test Results 83

4.1 Presentation of Results 83
4.2 Failure Loads 84
4.3 Deflections 85
4.4 Individual Beam Results 94
4.4.1 Beam B150S6 94
4.4.2 Beam B250S6 95
4.4.3 Beam B350S6 96
4.4.4 Beam B150S19 103
4.4.5 Beam B250S19 104
4.4.6 Beam B350S19 105
4.4.7 Beam B160S6 112
4.4.8 Beam B260S6 113
4.4.9 Beam B360S6 114
4.4.10 Beam B160S25 121
4.4.11 Beam B260S25 122
4.4.12 Beam B360S25 123
4.5 Modes of failure 129

CHAPTER 5 Non-Linear Finite Element Analysis 130

5.1 Introduction 130
5.1.1 Material Properties 130
5.1.1.1 Concrete 130
5.1.1.2 Steel 131
5.1.1.3 Concrete Post Tensile Failure 132
5.1.1.4 Post Compression Failure 133
5.1.2 Modeling of Reinforcement 133
5.1.3 Elements 134
5.1.3.1 Plane Stress Element 134
5.1.3.2 Truss Element 135
5.2 Finite Element Models 135
5.3 Finite Element Results 137
5.3.1 Beams B150S6, B150S19, and B250S19 137
5.3.2 Beams B260S6, B360S6 and B260S25 142

CHAPTER 6 Analysis of F.E.M. Results 148

6.1 Introduction 148

6.2 Finite Element Model 148
6.2.1 Stress and strain distribution 158
6.2.2 Strain along the compression strut 166
6.2.3 Stress along the compression strut 185
6.2.4 Summary 193

CHAPTER 7 Truss Model 194

7.1 Truss Model 194
7.1.1 Compression strut 195
7.1.2 Tension tie 201
7.2 Comparison to Other Research 205

CHAPTER 8 Conclusion 211

8.1 Conclusion 211
8.2 Recommendations for future study 214

Bibliography 215

List of Figures

CHAPTER 1 Introduction 1

Figure 1-1. Basic failure modes of concrete 3
Figure 1-2. Typical crack pattern of a deep beam with two point loading 4

CHAPTER 2 Literature Review 7

Figure 2-1. Corbel test specimen variables used by Kriz and Raths 8
Figure 2-2. Reinforcement details for corbels test specimen Kriz and Raths 9
Figure 2-3. Shear friction model with reinforcement as proposed by Mattock 13
Figure 2-4. Flexural model proposed by Mattock 14
Figure 2-5. Truss model proposed by Franz and Niedenhoff 20
Figure 2-6. Truss model as proposed by Somerville 22
Figure 2-7. Assumed internal force distribution for Hagberg's model 25
Figure 2-8. Truss model as proposed by Solanki and Sabnis 29
Figure 2-9. Strut and tie model for internal forces 32
Figure 2-10. Reinforcement details for deep beams tested by Kong et al. 35
Figure 2-11. Web reinforcement for beams tested by Smith and Vantsiotis 38
Figure 2-12. Proposed truss model by Kotsovos 45
Figure 2-13. Truss model as proposed by Siao 46
Figure 2-14. Diagonal compression field 51
Figure 2-15. Compression Field Theory linked to plane sections 52
Figure 2-16. Test panel after failure 52
Figure 2-17. Stress strain relationship for cracked concrete 53
Figure 2-18. D-regions with non-linear strain distributions 56
Figure 2-19. Web reinforcement for beams tested byTan and Lu 58
Figure 2-20. Strut and tie development in deep beams 60
Figure 2-21. Strut and tie model for a deep beam 61
Figure 2-22. Flow chart showing solution algorithm 63
Figure 2-23. Orientation of tension tie with respect to the compression strut 65
Figure 2-24. Guidelines for determining the dimensions of the strut and tie 66

CHAPTER 3 Experimental Program 68

Figure 3-1. Reinforcement details for test beams B150S6, B250S6 and B350S6. 70
Figure 3-2. Reinforcement details for test beams B150S19, B250S19 and B350S19. 71
Figure 3-3. Reinforcement details for test beams B160S6, B260S6 and B360S6. 72
Figure 3-4. Reinforcement details for test beams B160S25, B260S25 and B360S25. 73
Figure 3-5. Locations of strain gauges placed on steel reinforcement. 74
Figure 3-6. Location of concrete strain gauges on the left side of test beam. 75
Figure 3-7. Location of concrete strain gauges on the right side of test beam. 75
Figure 3-8. Placement of concrete strain gauges. 76
Figure 3-9. Concrete compressive stress-strain relationship 78
Figure 3-10. Steel tensile stress-strain relationship 79
Figure 3-11. Schematic of test loading setup. 81

CHAPTER 4 Test Results 83

Figure 4-1. Deflection of beam B150S19. 86

Figure 4-2. Deflection of beam B250S19. 87
Figure 4-3. Deflection of beam B150S6. 88
Figure 4-4. Deflection of beam B250S6. 89
Figure 4-5. Deflection of beam B160S25. 90
Figure 4-6. Deflection of beam B260S25. 91
Figure 4-7. Deflection of beam B160S6. 92
Figure 4-8. Deflection of beam B260S6. 93
Figure 4-9. Crack pattern detail of left side of test beam B150S6. 94
Figure 4-10. Left side crack pattern for beam B250S6. 95
Figure 4-11. Left side crack pattern for beam B350S6. 96
Figure 4-12. Main tension steel strain versus load for beam B350S6. 97
Figure 4-13. Diagonal steel strain versus load for beam B350S6. 98
Figure 4-14. Concrete compression strain along diagonal versus load for beam B350S6. 99
Figure 4-15. Concrete compression strain across the diagonal versus load for beam B350S6. 100
Figure 4-16. Concrete tension strain for beam B350S6. 101
Figure 4-17. Right side crack pattern for beam B150S19. 103
Figure 4-18. Right side crack pattern for beam B250S19. 104
Figure 4-19. Right side crack pattern for beam B350S19. 105
Figure 4-20. Main tension steel strain versus load for beam B350S19. 106
Figure 4-21. Diagonal steel strain versus load for beam B350S19. 107
Figure 4-22. Concrete compression strain along diagonal versus load for beam B350S19. 108
Figure 4-23. Concrete compression strain across the diagonal versus load for beam B350S19. 109
Figure 4-24. Concrete tension strain for beam B350S19. 110
Figure 4-25. Left side crack pattern for beam B160S6. 112
Figure 4-26. Right side crack pattern for beam B260S6. 113
Figure 4-27. Right side crack pattern for beam B360S6. 114
Figure 4-28. Main tension steel strain versus load for beam B360S6. 115
Figure 4-29. Diagonal steel strain versus load for beam B360S6. 116
Figure 4-30. Concrete compression strain along diagonal versus load for beam B360S6. 117
Figure 4-31. Concrete compression strain across the diagonal versus load for beam B360S6. 118
Figure 4-32. Concrete tension strain for beam B360S6. 119
Figure 4-33. Right side crack pattern for beam B160S25 121
Figure 4-34. Right side crack pattern for beam B260S25. 122
Figure 4-35. Right side crack pattern for beam B360S25. 123
Figure 4-36. Main tensile steel strain versus load for beam B360S25. 124
Figure 4-37. Diagonal steel strain versus load for beam B360S25. 125
Figure 4-38. Concrete compression strain along diagonal versus load for beam B360S25. 126
Figure 4-39. Concrete compression strain across the diagonal versus load for beam B360S25. 127
Figure 4-40. Concrete tension strain versus load for beam B360S25. 128

CHAPTER 5 Non-Linear Finite Element Analysis.... 130

Figure 5-1. Concrete stress-strain curve used in the finite element analysis 131
Figure 5-2. Stress-strain relationship for steel used in the finite element analysis 132
Figure 5-3. Alternate representation for steel reinforcement 133
Figure 5-4. Eight node plane stress element 134
Figure 5-5. Three node truss element used to model the steel reinforcement 135
Figure 5-6. Finite element models used to simulate experimental tests 136
Figure 5-7. Deflection of series B50 as determined by the finite element analysis 138
Figure 5-8. Steel strain at midpoint and leftside determined by finite element analysis 139

Figure 5-9. Compressive stresses at a loading of 50 kN, 150 kN and 250 kN 140
Figure 5-10. Compressive stresses at a loading of 321 kN, 362 kN and 375 kN 141
Figure 5-11. Deflection of deep beam series B60 as determined by finite element analysis.143
Figure 5-12. Steel strain at midpoint and leftside determined by finite element analysis 144
Figure 5-13. Compressive stresses at a loading of 80 kN, 160 kN and 227 kN 145
Figure 5-14. Compressive stresses at a loading of 280 kN, 334 kN and 343 kN 146
Figure 5-15. Cracking patterns as predicted by the finite element analysis.....147

CHAPTER 6 Analysis of F.E.M. Results 148

Figure 6-1. Midpoint deflection from experimental test results and finite element analysis ...150
Figure 6-2. Left side deflection from experimental test results and finite element analysis ...151
Figure 6-3. Midpoint deflection from experimental test results and finite element analysis ...152
Figure 6-4. Left side deflection from experimental test results and finite element analysis ...153
Figure 6-5. Comparison of main tension steel strain at midpoint for series B350.....154
Figure 6-6. Comparison of main tension steel strain at left side for series B350 155
Figure 6-7. Comparison of main tension steel strain at midpoint for series B360.....156
Figure 6-8. Comparison of main tension steel strain at left side for series B360 157
Figure 6-9. Load transmission for test beams at a loading of 333.6 kN.....159
Figure 6-10. Effective stress of left side for beams B150S6, B150S19, and B250S19.....160
Figure 6-11. Effective stress of left side for beams B260S6, B360S6, and B260S25.....161
Figure 6-12. Left side stress distribution for beams B150S6, B150S19, and B250S19 162
Figure 6-13. Left side stress distribution for beams B260S6, B360S6, and B260S25 163
Figure 6-14. Left side strain distribution for beams B150S6, B150S19, and B250S19 164
Figure 6-15. Left side strain distribution for beams B260S6, B360S6, and B260S25 165
Figure 6-16. Location of left side strain gauges on lines A-A and B-B.....166
Figure 6-17. Location of right side strain gauges on lines A-A and B-B 167
Figure 6-18. Strain perpendicular to B-B for sample B350S19 at 200 kN 168
Figure 6-19. Strain perpendicular to B-B for sample B350S19 at 289 kN 169
Figure 6-20. Strain perpendicular to B-B for sample B350S6 at 200 kN 170
Figure 6-21. Strain perpendicular to B-B for sample B350S6 at 289 kN 171
Figure 6-22. Strain perpendicular to B-B for sample B360S25 at 67 kN 172
Figure 6-23. Strain perpendicular to B-B for sample B360S25 at 89 kN 173
Figure 6-24. Strain perpendicular to B-B for sample B360S6 at 200 kN 174
Figure 6-25. Strain perpendicular to B-B for sample B360S6 at 289 kN 175
Figure 6-26. Strain perpendicular to A-A for sample B350S19 at 44 kN 177
Figure 6-27. Strain perpendicular to A-A for sample B350S19 at 67 kN 178
Figure 6-28. Strain perpendicular to A-A for sample B350S6 at 44 kN 179
Figure 6-29. Strain perpendicular to A-A for sample B350S6 at 67 kN 180
Figure 6-30. Strain perpendicular to A-A for sample B360S25 at 44 kN 181
Figure 6-31. Strain perpendicular to A-A for sample B360S25 at 67 kN 182
Figure 6-32. Strain perpendicular to A-A for sample B360S6 at 44 kN 183
Figure 6-33. Strain perpendicular to A-A for sample B360S6 at 67 kN 184
Figure 6-34. Internal force diagram strut and tie schematic.....185
Figure 6-35. Finite element stress perpendicular to B-B for sample B350S19 187
Figure 6-36. Finite element stress perpendicular to B-B for sample B360S25 188
Figure 6-37. Finite element stress perpendicular to A-A for sample B350S19 189
Figure 6-38. Finite element stress perpendicular to A-A for sample B360S25 190
Figure 6-39. ASTM (C496) split cylinder test 191
Figure 6-40. Tension stresses perpendicular to compression strut.....192

CHAPTER 7 Truss Model 194

Figure 7-1. Schematic detailing main diagonal and perpendicular diagonal 194
Figure 7-2. Simplified compressive stress distribution 196
Figure 7-3. Assumed compression stress distribution 197
Figure 7-4. Internal force distribution of the compression strut 198
Figure 7-5. Biaxial strength envelope for concrete as proposed by Zielinski 199
Figure 7-6. Projection of reinforcement along compression strut 201
Figure 7-7. Comparison of Equation7-18 to force in reinforcement as determined by ADINA 203
Figure 7-8. Calculated versus measured failures for various shear span to depth ratios 210

CHAPTER 8 Conclusion 211

List of Tables

CHAPTER 1 Introduction 1

CHAPTER 2 Literature Review 7

Table 2-1. Shear design methods as recommended by CSA A23.3-94 64

CHAPTER 3 Experimental Program 68

Table 3-1. Concrete strength determined from test cylinders. 77

CHAPTER 4 Test Results 83

Table 4-1. Measured failure loads of the test beams. 84

CHAPTER 5 Non-Linear Finite Element Analysis 130

CHAPTER 6 Analysis of F.E.M. Results 148

Table 6-1. Measured failure loads of the test samples 149
Table 6-2. Force along the compression strut 186

CHAPTER 7 Truss Model 194

Table 7-1. Truss model equations applied to experimental results 204
Table 7-2. Comparison to work done by Smith and Vantsiotis 205
Table 7-3. Comparison to work done by Kong, Robbins and Cole 207
Table 7-4. Comparison to work done by Mattock et al. 208

CHAPTER 8 Conclusion 211

NOTATION

a	Shear span
A_s	Area of steel reinforcement
b	Width of the beam
C	Compression force of the concrete strut
C'	Compressive force in free body diagram
d	Effective depth (distance from top fiber to reinforcement)
E_c	Modulus of elasticity of concrete
E_s	Modulus of elasticity of steel
f'_c	Concrete compression capacity
f_{ct}	Concrete compression stress/capacity under biaxial compression-tension
f_{tc}	Concrete tensile stress/capacity under biaxial tension-compression
f_t, f_{to}	Concrete tensile capacity under uniaxial tension
f_{tt}	Concrete tensile capacity under biaxial tension
f_y	Yield strength of steel reinforcement
h	Total depth of the beam
P	Load applied to the beam
T	Capacity of the tension tie
T'	Tensile force in free body diagram
V	Shear load corresponding to applied load
V_u	Ultimate shear load at failure
V_{calc}	Calculated shear load at failure
w	Width of the support

1 Introduction

1.1 Introduction

The design of flexural reinforced concrete structures was revolutionized in 1912 when Morsch[45] first introduced a truss design model comprised of steel tension ties with concrete compression struts. Many variations of truss models have been used over the years, first using allowable stress then later using ultimate strength design methods.

Zielinski[69][70] introduced "economy girders" in 1950. These girders were designed using the "tied arch" model. The tied arch model differs from truss models in that the latter have stringent demand on the bond between the steel tension ties and the concrete. Tied arch models diminish the demand for bond in all locations except for where the steel tension tie is anchored. Structures designed using this model usually allow for a reduction of both concrete and steel material and generally result in a more efficient design.

The current Canadian Code[5] stipulates that deep beams and corbels should be designed using the Strut-and-Tie Method. This method hinges on the work done by Collins and Mitchell[8][9] where the cracked concrete behaves as a new material and that the compressive strength of concrete is reduced due to strain-softening. Here-in lies an area of discrepancy. The work done by Collins and Mitchell utilizes beam theory, which requires that plane sections remain plane. However, deep beams and corbels are classified as "regions of discontinuity" and that beam theory does not apply to these structures. Another area of the Canadian code which needs to be examined is the dimensioning of the compression strut. There is no clear explanation as to how the design recommendations of the compression strut were developed. One significant weakness of the design code is that numerous

assumptions must be made. The designer must assume that the compression strut reaches a maximum concrete strain of 0.002[5], as well, the strains in the tension ties must also be assumed.

The purpose of this research is to present our findings with new test results, to propose new comprehensive methods of analysis which reflect the true structural behaviour, and finally to redefine diagonal cracking strength limits for reinforced concrete deep beams.

1.1.1 Concrete failure modes

Reinforced concrete, being a heterogeneous material, depends on the strength of both concrete and steel. Failure will occur when either of these materials fail separately or if they fail simultaneously. Complications in design arise due to the tensile strength of concrete being approximately one tenth that in compression.

Tests carried out by Zielinski[71][72][73] identified four basic causes of concrete failure. Figure 1-1 illustrates the four cases.

Cause I. Under uniaxial tension, concrete fails by rupture and cracking perpendicular to tension direction.

Cause II. Under biaxial tension - compression, concrete fails by rupture and cracking perpendicular to tension direction. Strength of concrete under biaxial tension - compression is less than that under uniaxial compression.

Cause III. Under biaxial tension, failure occurs by inclined cracking. The angle of cracking ranges from 45^0 to 90^0 from the larger tension load. In the case of equal tension stresses, failure occurs at an angle of 45^0. Strength of concrete under biaxial tension is approximately 3/4 of the strength under uniaxial tension.

Cause IV. Under uniaxial compression, concrete fails by cohesion loss and cracking parallel to loading. Under biaxial compression,

concrete strength is greater (up to $1.25f'_c$) than under uniaxial stresses.

Tension failures occur when the strain in the tension direction reaches ε_{ct} = 0.0015 to 0.0025. Compression failures occur when the ultimate strain reaches ε_{cu} = 0.0035.

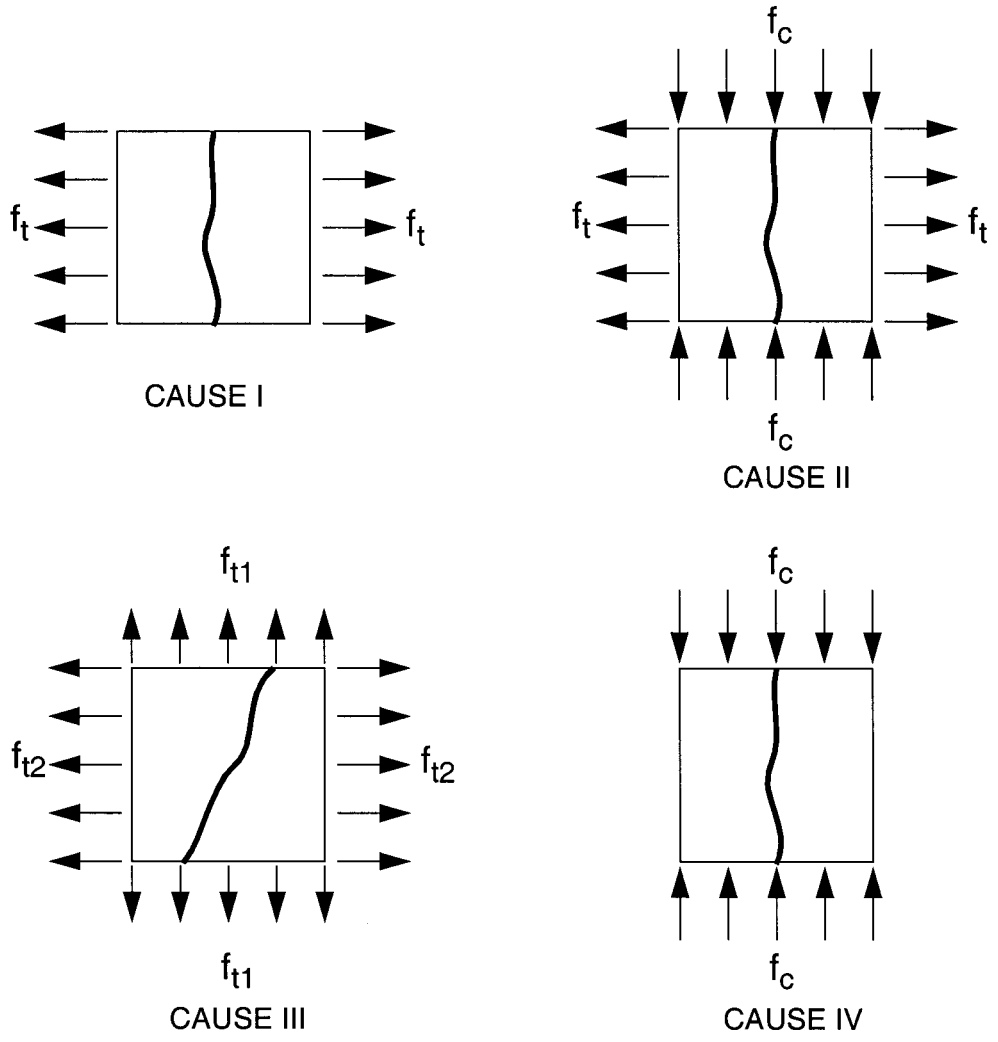

Figure 1-1. Basic failure modes of concrete[73]

Research[73] has shown that after cracking, all beams begin to act as tied arches. This leads to four strength limits of reinforced concrete beams shown in Figure 1-2.

Limit I. Appearance of first crack due to flexure. This will result in the failure of the beam if there is no reinforcement or the reinforcement is insufficient.

Limit II. The appearance of inclined cracks due to beam action as the limit strength of combined stresses is reached.

Limit III. Diagonal splitting crack appearance caused by combined beam and tied arch action or only under tied arch action.

Limit IV. Ultimate flexural capacity.

Extensive research has been done for Limits I, II, and IV. This research examines diagonal splitting, or Limit III. It is important to remember that tied arch action is only possible when the reinforcement is extended beyond the support and is well anchored. Research conducted by Zielinski[73] demonstrated that diagonal splitting is the prominent mode of failure when the shear span to depth ratio is less than 2.32 (i.e. $\frac{a}{h} < 2.32$).

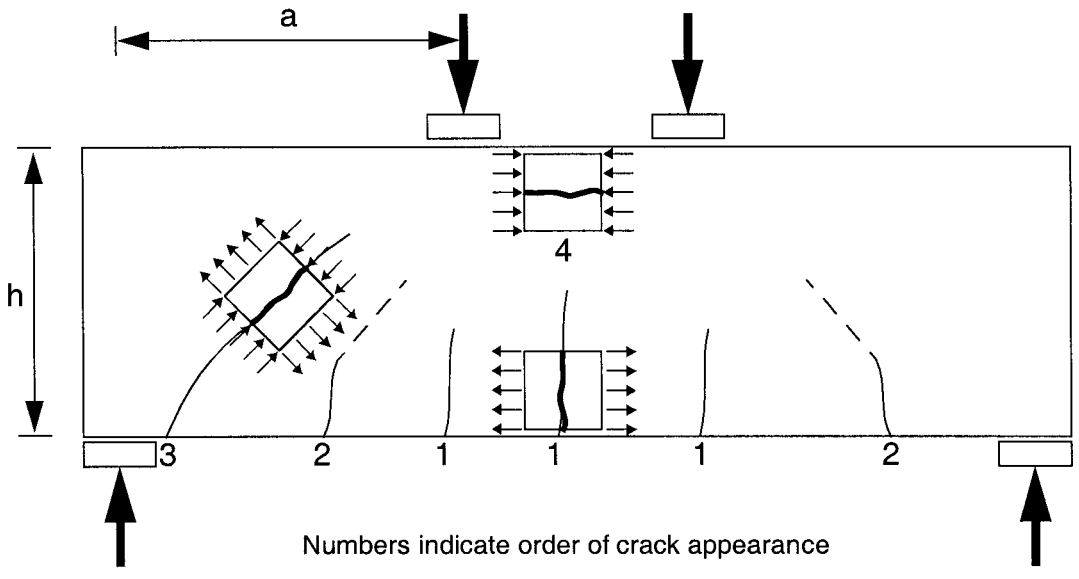

Figure 1-2. Typical crack pattern of a deep beam with two point loading

Flexural cracks are usually the first cracking to appear. They are the result of the concrete reaching its tensile strength, Cause I. Appearing in the centre of the beam, these develop vertically and straight (labeled as "1" in Figure 1-2).

The next type of cracking to appear is generally caused by beam action (i.e. due to moment and shear). These cracks are labeled as "2" in Figure 1-2. They propagate vertically, until reaching the main reinforcement, they then incline at an angle of approximately 45^0. Generally referred to as shear cracks, they appear as a result of biaxial compression and tension stresses (cracking Cause III).

The final cracking to appear is splitting or diagonal cracks, labeled as "3" in Figure 1-2. Diagonal cracking is directed from the support to the point of loading. This appears to be due to arch action of the beam and occurs when the stresses reach f_{ct}, which is the ultimate compressive strength of concrete under biaxial compression - tension (Figure 1-1 Cause II).

1.1.2 Current Research

The focus of this research is to investigate diagonal splitting strength of reinforced concrete deep beams. In conducting this study, twelve deep beams, categorized in four groups were tested. The test variables included the shear span, the amount of web reinforcement and the concrete compressive strength. Surprisingly, no researcher has published measured strain data incurred by the compression strut in deep beams. In our research, a single beam from each of the four test groups was fitted with strain gauges to measure the tensile strain in the main tensile reinforcement. As well, the concrete strains along the main diagonal formed between the support and the loading points as well as perpendicular to the strut were measured.

The experimental work demonstrated the development of diagonal cracking. These cracks appeared above the supports and propagated towards the loading points. The strain gauges on the concrete surface confirmed that the stresses along the compression strut were under biaxial compression tension stresses. A finite element analysis determined that the compression stress acting parallel to

the diagonal were uniform in distribution and symmetrical. Perpendicular to the diagonal, high compressive stresses were seen at the supports and the loading points. However, the stresses in between these areas were uniformly distributed in tension. The measured compressive strains were much less than the recommended value of 0.002, and the compression strut was found to be much wider than that defined by the Canadian Code. As a consequence of these findings, a truss model was defined using a biaxial concrete strength envelope. This truss model was applied to the test beams of this study as well as 114 deep beams and corbels available in literature. In all cases, the truss model was able to accurately predict the strength of these test beams.

2 Literature Review

2.1 Introduction

This chapter will outline some of the more significant studies conducted on reinforced concrete corbels and deep beams. The first two sections will outline a brief research history of both corbels and deep beams. Following these two sections, the work done by Rogowsky et al. and Schlaich et al. whose works have led to a "consistent design of structural concrete"[54] will be presented. The final section will examine the current Canadian design practice.

2.2 Corbels - Shear Friction

2.2.1 Kriz & Raths

In 1965, Kriz and Raths[28] undertook an extensive experimental study into the behaviour of reinforced concrete corbels. The purpose of the study was directed towards the development of design criteria for corbels. The existing method of design given by the ACI code made no distinction between corbels and other members such as beams or slabs, which are very different from corbels.

For their experimental work, 195 corbels were tested, of which 124 were loaded vertically while the remaining 71 corbels were loaded both vertically and horizontally. Details of the corbel test specimen are shown in Figure 2-1 and Figure 2-2. Variables in their study included:

- shear span to the effective depth ratio,
- concrete strength,
- ratio of horizontal load to vertical load,

- the amount of main tension reinforcement and stirrups, and
- the detailing of the corbel.

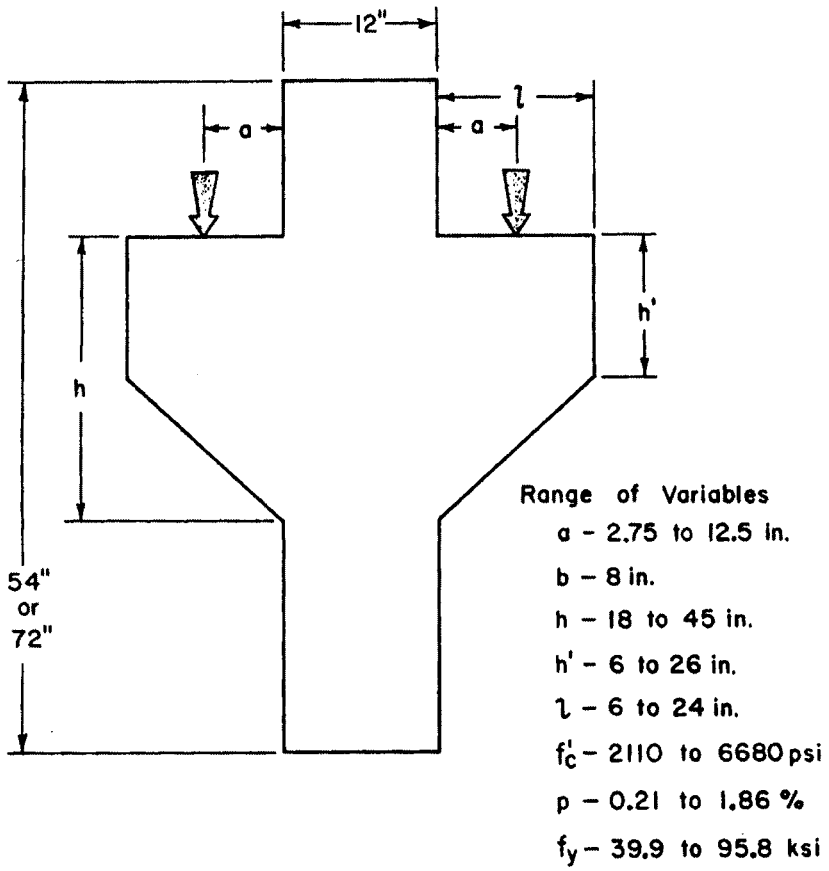

Figure 2-1. Corbel test specimen variables used by Kriz and Raths[28]

In relation to the ultimate load achieved by a corbel, it was noted that:

- the corbel strength was significantly reduced by horizontal forces acting outward from the column, and
- the strength of a corbel (subject to vertical loads only) can be increased by adding extra tension reinforcement and/or horizontal stirrups until a maximum amount of reinforcement is reached

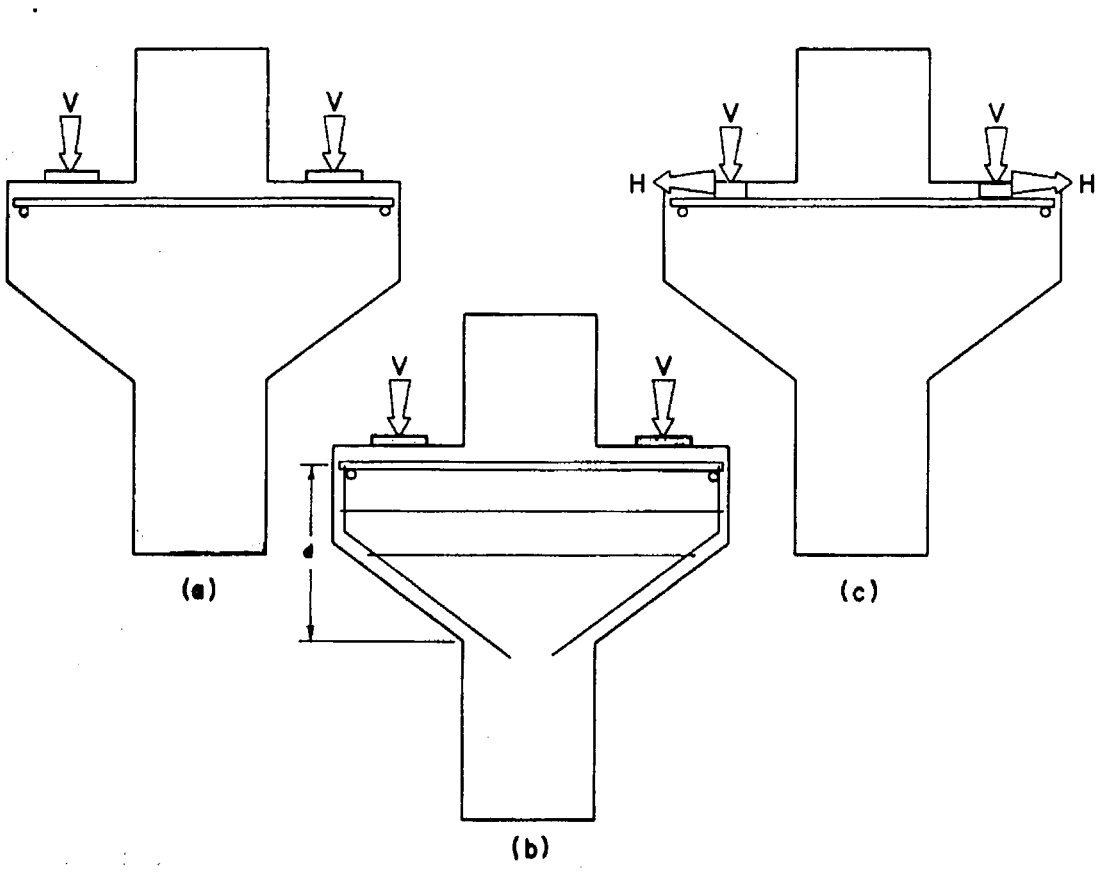

Figure 2-2. Reinforcement details for corbels test specimen Kriz and Raths[28]

Design Method

Empirical design equations were developed by fitting curves to the experimental data. The design method is expressed by two equations:

for corbels subject to vertical loads only

$$V_u = 6.5bd\sqrt{f'_c}(1-0.5^{d/a})(1000\rho)^{1/3} \qquad \textbf{Equation 2-1.}$$

corbels subject to both vertical and horizontal load

$$V_u = 6.5bd\sqrt{f'_c}(1-0.5^{d/a})\left(\frac{1000\rho^{(1/3+0.4(H/V))}}{10^{0.8(H/V)}}\right) \qquad \textbf{Equation 2-2.}$$

where V_u = ultimate load capacity (lb),

b = width of corbel (in),

d = effective depth of the centroid of the main steel (in),

f'_c = concrete cylinder compressive strength (psi),

a = shear span measured from the column face to the resultant of the applied load (in),

H = horizontal applied load (lb),

V = vertical applied load (lb), and

ρ = reinforcement ratio.

The reinforcement ratio, ρ, is defined differently in each of the above equations:

for Eq 2.1 $\left(\frac{H}{V} = 0\right)$: $\rho = \left(\frac{A_s + A_v}{bd}\right)$ **Equation 2-3.**

for Eq 2.2 $\left(\frac{H}{V} \neq 0\right)$: $\rho = \left(\frac{A_s}{bd}\right)$ **Equation 2-4.**

where A_s is the area of main tension steel, and

A_v is the area of horizontal stirrups.

The design method is applicable when:

- the shear span to depth ratio is less than one,
- the area of tension reinforcement (A_s) is greater than 0.004bd,
- closed horizontal stirrups are provided having a total cross sectional area greater than $0.5A_s$,
- detailing measures are undertaken to prevent a premature secondary failure.

The empirical design approach presented by Kriz and Raths was adopted by ACI318-71[1] for corbels where the shear span to depth ratio was greater than 0.55, but less than 1 ($0.55 < a/d < 1.0$).

Hagberg[11] commented that the design formulas presented by Kriz and Raths do not include the strength of steel which contrary to common reinforced concrete design. Somerville[60] expressed concern that the different modes of failure were largely ignored by Kriz and Raths. He also felt that when horizontal forces were introduced, the design requirements were over conservative. Hermansen and Cowan[14] claimed that the diagonal splitting failures described by Kriz and Raths were in fact compression failures, which would not occur if secondary reinforcement was provided.

2.2.2 Mast

Mast[36] applied the shear friction theory to the design of concrete connections. To support his theory, he included the experimental data provided by Kriz and Raths[28]. Mast showed that the shear friction theory can predict a safe lower bound for the strength of a corbel.

In his work, Mast stated that:

- shear friction theory applies directly to corbels with a/d ratios less than 0.7,
- for a/d ratios greater than 0.7, the main reinforcement is controlled by flexure,
- some tension reinforcement must be placed throughout the upper half of the corbel to prevent the external corner of the corbel from splitting, and
- a mechanical anchor should be provided to ensure that yield stress can be developed between the potential crack and the face of the corbel.
- though the test data showed that the shear friction model can provide good results, the research did not prove that the model represents the true behaviour of the concrete.

Mast supported the following shear friction equation:

$$V_u = (A_{sv}f_y - H)(\tan\alpha_f)$$ **Equation 2-5.**

where V_u = total ultimate shear force,

H = total horizontal force (from creep or temperature changes, etc.),

A_{sv} = total cross-sectional area of reinforcement across the corbel-column interface,

f_y = yield strength of reinforcing steel, and

α_f = the angle of internal friction determined from tests; concrete to concrete (rough interface) α_f =1.4, concrete to steel (composite beams) α_f =1.0, concrete to steel (field-welded inserts) α_f =0.7, concrete to concrete (smooth interface) α_f =0.7

To use the above shear friction equation, the following conditions must be ensured:

- reinforcement crossing cracks must be fully anchored,
- additional reinforcement must be provided for any applied external tension,
- the cohesive strength of the concrete is ignored, and
- the angle of internal friction (α_f) is independent of both the concrete strength and the level of stress applied to the concrete.

2.2.3 Mattock

Mattock[37][38][39][40][41] conducted experimental research relating to shear transfer in concrete. He showed that the shear friction theory can be extended to include the case of concrete with reinforcement at an angle to the shear plane.

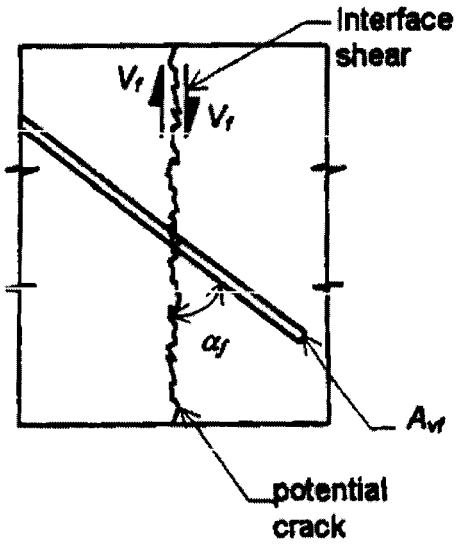

Figure 2-3. Shear friction model with reinforcement as proposed by Mattock[38]

Where the shear friction reinforcement lies at an angle to the shear plane, Mattock proposed that the maximum shear capacity be taken as:

$$V_u = A_{vf} f_y (\mu \sin\alpha_f + \cos\alpha_f) \qquad \textbf{Equation 2-6.}$$

where V_u = total ultimate shear force,

A_{vf} = total cross-sectional area of reinforcement of the vertical reinforcement,

f_y = yield strength of reinforcing steel,

μ = coefficient of friction used in shear friction calculations, and

α_f = the angle between the shear friction reinforcement and the shear plane.

In 1974, Mattock also showed that a moment applied over a cracked section does not reduce the shear that can be transferred across the crack. Mattock proposed that the a/d limit of 0.5 as set by ACI 318-71[1] was unwarranted in relation to corbel design.

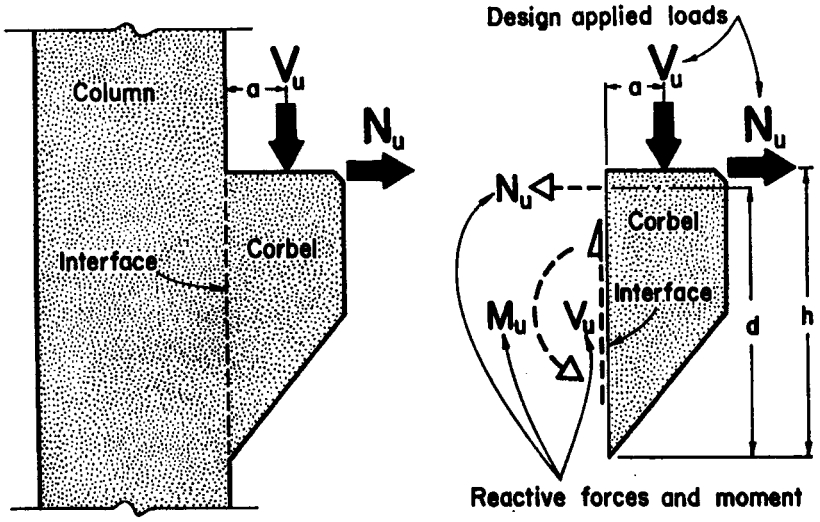

Figure 2-4. Flexural model proposed by Mattock[37][39][40][41]

Mattock proposed a flexural model which considers the corbel as a free body cut from the corbel-column interface. The corbel is designed to resist a combination of vertical and horizontal loads using the laws of statics. For static equilibrium, the reactive forces V_u and N_u must be equal to the design vertical and horizontal loads V_u and N_u, respectively. Hence, the reactive moment M_u must equal:

$$M_u = V_u a + N_u(h - d) \qquad \textbf{Equation 2-7.}$$

where N_u = total ultimate horizontal force,

h = total depth of corbel,

d = distance from extreme compression fiber to centroid of tension reinforcement, and

a = shear span, distance between vertical load and face of column.

The suggested design method was tested using an experimental study of 28 corbels. The study was also directed towards extending the existing shear friction provisions for corbel design beyond the a/d limit of 0.5 recommended by ACI 318-71[1].

Following his study, Mattock proposed that the design of corbels be based on "useful ultimate strength" to maintain a safety margin against wide cracking (cracks widths should not exceed 0.33mm (0.013in) for exterior exposures and 0.41mm (0.016in) for interior exposures. Useful ultimate strength was defined as the vertical load at yield of the tension reinforcement, or the vertical load at failure if yielding does not occur.

The useful ultimate strength of corbels subject to both vertical and horizontal loads can be calculated by using the lesser of:

- the shear friction provisions as per ACI 318-71[1], and
- the vertical load derived from the flexural ultimate strength of the corbel-column interface.

Additionally, a minimum amount of horizontal reinforcement must be provided to eliminate the possibility of premature diagonal tension failure.

Design Method

1. Given V_u, b, ϕ (capacity reduction factor) and assuming that the nominal shear stress (v_u) is not greater than $0.2f'_c$ or 5.52MPa, the depth of the corbel is calculated from:

$$d = \frac{V_u}{\phi v_u b}$$ **Equation 2-8.**

2. The area of shear friction steel can be determined by:

$$A_{vf} = \frac{V_u}{\phi f_y \mu}$$ **Equation 2-9.**

3. Given a, h, and the corbel depth (d) the moment capacity is determined from Equation 2-7 on page 14. Thus the required area of flexural reinforcement can be calculated from:

$$A_f = \frac{M_u}{\phi f_y\left(d - \frac{x}{2}\right)}$$ **Equation 2-10.**

where x (depth of the compression stress block) is initially estimated and then checked using:

$$x = \frac{A_f f_y}{0.85 f'_c b}$$ **Equation 2-11.**

4. The area of reinforcement necessary to resist the applied horizontal force is determined from:

$$A_t = \frac{H}{\phi f_y}$$ **Equation 2-12.**

5. The total area of main tension reinforcement is calculated from the greater of:

(a) $A_s = A_f + A_t \quad$ when $\quad A_f \geq \frac{2A_{vf}}{3}$ **Equation 2-13.**

(b) $A_s = \frac{2A_{vf}}{3} + A_t \quad$ when $\quad A_f \leq \frac{2A_{vf}}{3}$ **Equation 2-14.**

6. The reinforcement ratio is checked such that:

$$\rho = \frac{A_s}{bd} \geq 0.04\left(\frac{f'_c}{f_y}\right)$$ **Equation 2-15.**

7. The area of stirrup reinforcement (A_h) is calculated using Equation 2-16, and distributed over the top two-thirds of the effective depth of the corbel.

$$A_h = 0.5(A_s - A_t)$$ **Equation 2-16.**

8. Recheck the dimensions of the corbel and ensure that the depth of the corbel at the outside edge of bearing is not less than one-half the effective depth adjacent to the face of the support.

Mattock believed that his design method offered the following advantages:

- the concept is simple and avoids complicated empirical equations,
- compared to the existing shear friction method, the model predicts less conservative results thereby providing reinforcement economy.

2.2.4 Hermansen & Cowan

Hermansen and Cowan[14][15] presented a modified shear friction design method, adding a cohesion term into the shear friction equation. The authors based their design proposal on an experimental study of 40 corbels performed by Hermansen combined with data from Kriz and Raths[28]. Hermansen and Cowan showed that the modified shear friction theory provided greater accuracy than the shear friction theory, particularly at low reinforcement ratios.

Hermansen and Cowan's design method called for the design of three main modes of failure. These modes of failure included shear failure, flexural failure, and secondary failure (anchorage, bearing).

Shear Failure

The shear failure mode was most likely to occur in an efficiently designed connection. Push-off tests performed by Mattock[39] and Hermansen[13] have shown that the ultimate shear stress, v_{uf}, for a pure shear failure of an uncracked concrete specimen is:

$$v_{uf} = 4.0 + 0.8\rho f_y \qquad N/mm^2$$ **Equation 2-17.**

The above equation can be written in the form:

$$v_{uf} = c + \rho f_y \tan\alpha_f \qquad N/mm^2$$ **Equation 2-18.**

where c is an apparent cohesive stress and tan α_f is the coefficient of friction.

This equation implies that the amount of tensile reinforcement to prevent a shear failure in a corbel carrying a shear load, V_u, will be:

$$A_{sf} = \frac{V_u - 4.0bd}{0.8f_y}$$ **Equation 2-19.**

Flexural Failure

Flexural failure occurs due to yielding of the main reinforcement or due to crushing or buckling of the concrete in compression. The load to cause yielding of the main steel can be calculated with reasonable accuracy for a/d < 2.0. Using truss analogy, the area of main reinforcement (A_{sm}) to resist flexural failure is:

$$A_{sm} = \frac{V_u a}{df_y}$$ **Equation 2-20.**

Secondary Failure

Hermansen and Cowan believed that secondary failures (inadequate anchorage of the reinforcement or crushing of the concrete under the bearing area) could be eliminated provided that appropriate detailing measures relating to anchorage, shape and bearing were undertaken.

Mattock[40] expressed concern that there was no limit on ρf_y. Therefore, it could not be guaranteed that the main reinforcement would reach its potential strength. As well, the shear friction model, where a crack exists in the shear plane before the concrete is subjected to shear, has been replaced with an empirical equation based on initially uncracked concrete.

2.3 Corbels - Truss Analogy

2.3.1 Franz & Niedenhoff

A photo-elastic study of resin model corbels was performed by Franz and Niedenhoff[10]. Their goal was to analyze the behaviour of corbels under shear loads. Their findings showed that the structural action of a corbel resembles that of a simple determinant truss. The truss model consisted of compression struts and tension ties.

Their results revealed that:

- the tensile stress at the upper edge of the corbel is relatively constant from the load to the root of the bracket,
- an approximately straight strut develops at the compressive face where the stresses are relatively constant,
- stress concentrations were found to develop at the root of the corbel, both at the top (tensile root) and at the bottom (compressive root), and
- the shape of the corbel has little influence on the state of the stress within the corbel.

Design Method

The proposed truss analogy is one where the corbel is viewed as containing a strut and tie system acted on by an external vertical force V. Although, the tensile force F_t, is regarded as being slightly inclined, for design purposes it can be taken as horizontal.

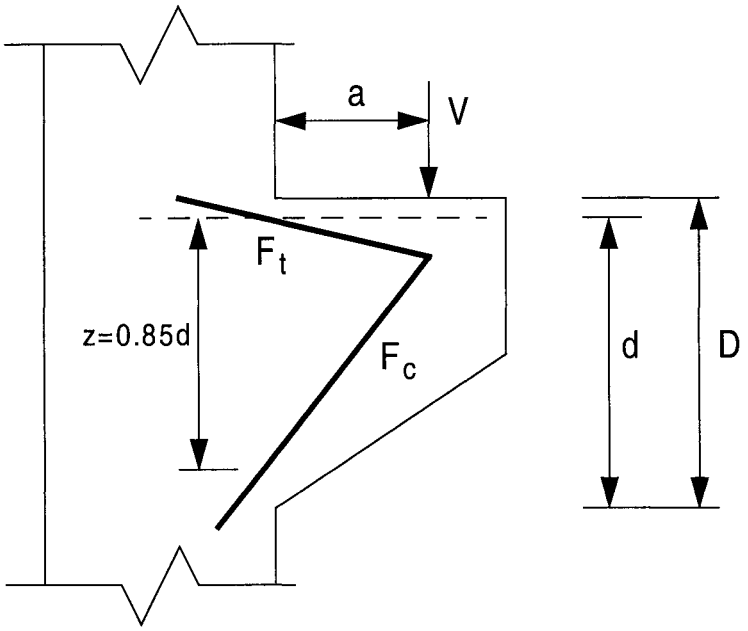

Figure 2-5. Truss model proposed by Franz and Niedenhoff[10]

The tensile force is given by:

$$F_t = \frac{Va}{z} \qquad \textbf{Equation 2-21.}$$

where z = 0.85d

a = shear span, and

V = total shear load.

The required area of main reinforcement (A_{st}) is given by:

$$A_{st} = \frac{F_t}{f_{adm}} \qquad \textbf{Equation 2-22.}$$

where f_{adm} is the allowable tensile stress of the reinforcement.

The depth of the corbel and the concrete strength are determined from flexural considerations at the corbel-column interface.

Franz and Niedenhoff recommended that:

- reinforcement be placed in the compression zone of the corbel,
- the area of horizontal or inclined web reinforcement should be greater than 25% of the main tension reinforcement,
- the column reinforcement should be supplemented in the tensile zone area of the corbel, and
- a distinction should be made as to whether the loading is imposed at the top or the bottom of the corbel.

While this method has the advantage of simplicity and ease of use, Somerville[60] stated that this method does not take into account the cracking which occurs, as the forces are represented only in the elastic range. He also pointed out that the above method does not consider horizontal loads.

2.3.2 Somerville

Somerville[60] considered several points that had emerged from previous studies which are summarized as follows:

- evidence exists which suggests that a simple strut and tie approach provides the best physical model of a corbel's behaviour under load,
- the main factors influencing the behaviour of a corbel under load are:
  - the shear span to depth ratio (a/d)
  - percentage of reinforcement
  - concrete strength
- many common types of failure are due to secondary failures which can be avoided through consideration of the:
  - corbel proportions
  - methods for anchoring the main reinforcement
  - provision for secondary reinforcement

- horizontal forces can influence both the strength and behaviour of a corbel.

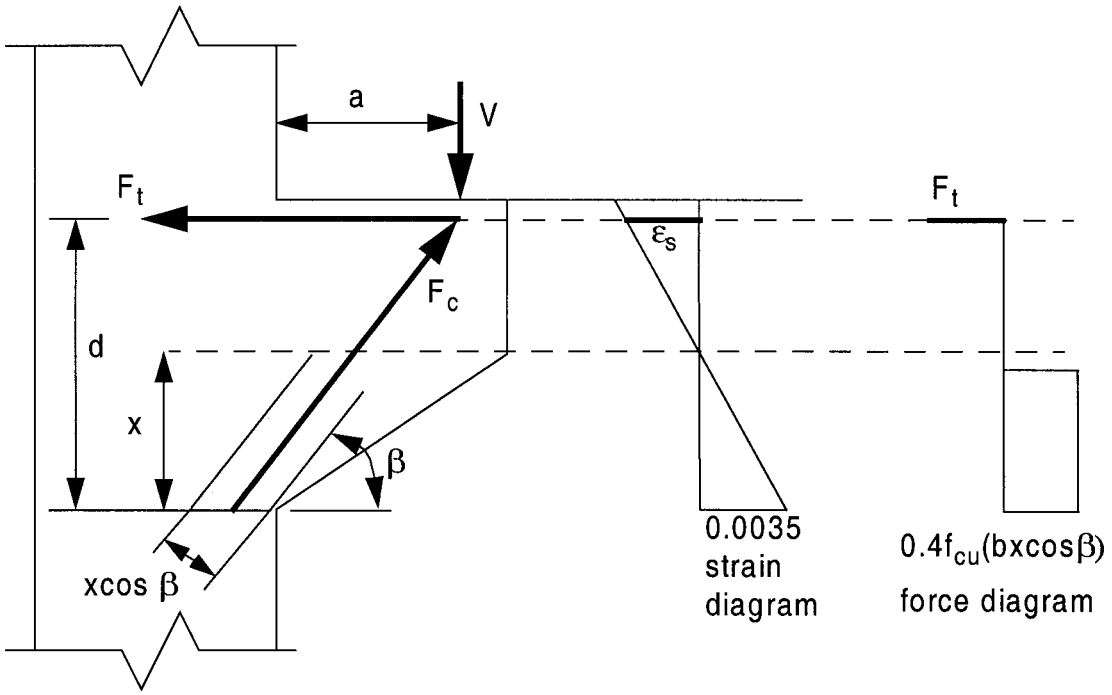

Figure 2-6. Truss model as proposed by Somerville[60]

Design Method

The Somerville design method can be summarized in five steps:

1. With V_u, the shear span (a), and the width of the corbel (b), the depth of the corbel is estimated using the empirical shear provisions in CP110-1972[7]. The code allows the maximum nominal shear stress (v_{max}) to be as high as:

$$v_{max} = \frac{2v_c d}{a}$$ **Equation 2-23.**

where $a/d \leq 2$ and v_c is the maximum compression stress of the concrete.

2. Calculate the bearing area, with the maximum allowable bearing stress equal to $0.8f_{cu}$ (compressive strength of the concrete),

3. The area of main reinforcement is calculated using the truss analogy:

   - the internal compression force, F_c, and tensile force, F_t, are calculated from truss analogy
   - the location of the neutral axis (x) is calculated from:

$$bx\cos\beta(0.4f_{cu}) = \frac{V_u}{\sin\beta} \qquad \textbf{Equation 2-24.}$$

Initially, β is assumed to be $\tan^{-1}\left(\frac{0.8d}{a}\right)$ and then the tensile force F_t is calculated from:

$$F_t = \frac{V_u a}{\left(d - \frac{x}{2}\right)} \qquad \textbf{Equation 2-25.}$$

4. Tension reinforcement (A_{st}) is calculated using stress compatibility (CP110-1972[7]),

5. Anchorage and other detailing matters are handled.

Hagberg[11][12] mentioned that Somerville's proposed formulas were not based on shear failures, but are instead based on various forms of failures.

2.3.3 Hagberg

Hagberg[11][12] devised a truss model using a geometrical method of force distribution. He felt that the advantages of this model were:

- it can effectively predict the capacity of a corbel,
- it provides a rational basis for corbel detailing, and
- it is suited to computer aided design.

Hagberg's model makes the following assumptions:

- failure is caused by yielding of the reinforcement or by crushing of the concrete (shear failure is not considered as a failure criterion),
- uniaxial tests are used to determine the strength of materials,
- the concrete strength is equal to the cylinder test strength,
- the strength of concrete in tension is neglected, and
- the geometry of the corbel shall conform with the mathematical model.

The structural model used is based on the model developed by Franz and Niedenhoff[10]. The concrete is assumed to act as inclined struts between the cracks, thereby transmitting only compression forces as shown in Figure 2-7. The reinforcement is assumed to act as a linear tension member. The effect of dowel action by the reinforcement is ignored.

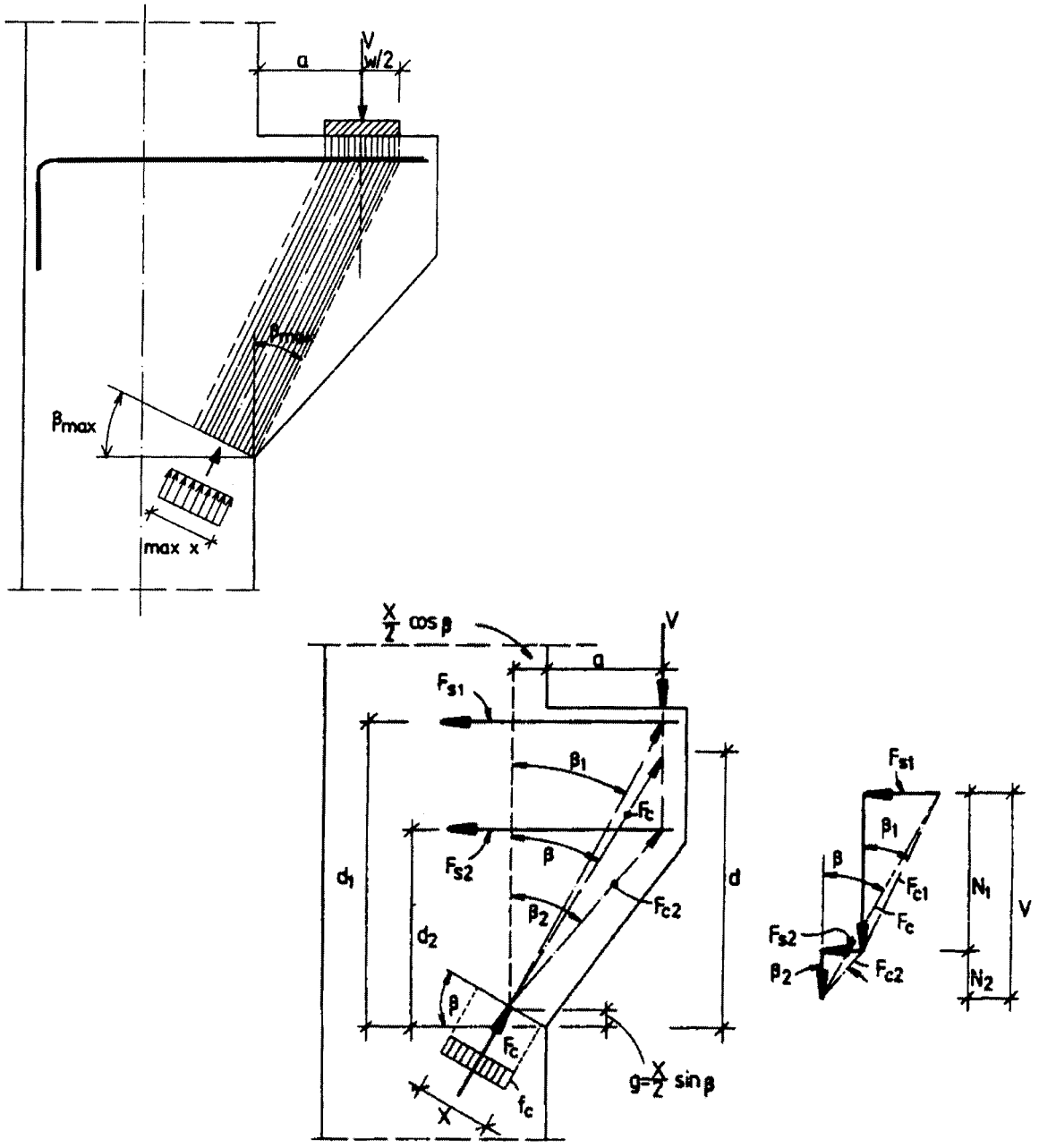

Figure 2-7. Assumed internal force distribution for Hagberg's[11][12] model

For a corbel with horizontal stirrups the following equations are considered:

Equilibrium Conditions

$$F_c = \frac{V}{\cos\beta}$$ **Equation 2-26.**

$$F_t = V\tan\beta$$ **Equation 2-27.**

where β = angle of inclination of compression member

$$F_s = F_{s1} + F_{s2}$$ **Equation 2-28.**

$$V = N_1 + N_2 = \frac{F_{s1}}{\tan\beta_1} + \frac{F_{s2}}{\tan\beta_2}$$ **Equation 2-29.**

Geometry

$$\tan\beta_1 = \frac{a + 0.5x\cos\beta}{d_1 - 0.5\sin\beta}$$ **Equation 2-30.**

$$\tan\beta_2 = \frac{a + 0.5x\cos\beta}{d_2 - 0.5\sin\beta}$$ **Equation 2-31.**

Strength of Materials

$$F_c = f'_c bx$$ **Equation 2-32.**

$$F_{s1} = A_{s1}f_{s1}$$ **Equation 2-33.**

$$F_{s2} = A_{s2}f_{s2}$$ **Equation 2-34.**

where A_{s1} = the area of the main tension reinforcement, and

A_{s2} = the area of the stirrups.

By equating the basic equations it can be shown that:

$$\left(1 - \frac{2f'_c bd}{F_s}\right)\tan^2\beta + \frac{2f'_c ba}{F_s}\tan\beta + 1 = 0$$ **Equation 2-35.**

where $d = \frac{d_1 F_{s1}}{F_s} + \frac{d_2 F_{s2}}{F_s}$ **Equation 2-36.**

$$\text{and } x = \frac{F_s}{f'_c b \sin\beta} \qquad \textbf{Equation 2-37.}$$

The strength of the corbel in compression is a function of the concrete strength, corbel dimensions, and the amount of tension resistance available. The maximum load that can be carried by the corbel in compression is given as:

$$V_{max} = f'_c bw \cos^2(\beta_{max}) \qquad \textbf{Equation 2-38.}$$

$$\tan(\beta_{max}) = \frac{a + \frac{w}{2}}{d} \qquad \textbf{Equation 2-39.}$$

Design Method

Hagberg also considered failure at the balanced condition, i.e. the corbel fails by simultaneous yielding of the reinforcement and crushing of the concrete. Formulas were derived to calculate the required area of reinforcement to achieve a balanced failure. The following design steps were recommended.

1. With the corbel width (b), calculate the minimum width of the bearing plate:

$$w = \frac{V}{\lambda f_{cd} b} \qquad \textbf{Equation 2-40.}$$

where f_{cd} = the concrete strength,

λ = strength reduction factor such that $\lambda < 1$.

2. The effective height (d) is calculated from:

- corbels subjected to vertical load only

$$d \geq \left(a + \frac{w}{2}\right)\sqrt{\frac{V}{f_{cd} bw - V}} \qquad \textbf{Equation 2-41.}$$

- corbels subjected to both vertical and horizontal loads

$$d \geq \left(a + \frac{w}{2} + (h-d)\right)\tan\alpha \sqrt{\frac{V}{2f_{cd}b\left(\frac{w}{2} - t\tan\alpha\right) - V}}$$ **Equation 2-42.**

where t = the thickness of the bearing plate.

The reinforcement area required for the balanced condition using horizontal stirrups is calculated from:

- corbels subject to vertical load only

$$A_s = \left(\frac{f_{cd}}{f_{sd}}\right) bw \sin(\beta_{max}) \cos(\beta_{max})$$ **Equation 2-43.**

- corbels subject to both vertical and horizontal loads

$$A_s = \left(\frac{f_{cd}}{f_{sd}}\right) 2b\left(\frac{w}{2} - t\tan\alpha\right) \times .....$$

$$.... \left(\tan\alpha + \frac{a + \frac{w}{2} + (h-d)\tan\alpha}{d}\right) \cos^2\beta_{max}$$ **Equation 2-44.**

where f_{sd} is the yield strength of the reinforcement.

3. The tension force (from the reinforcement) is located a distance "d", from the compressive edge. If the capacity of the stirrups is to be taken into account, a proportion of the main reinforcement (say 25%) should be assumed to consist of stirrups.

Hagberg believed his design approach to be valid for corbels having a/d ratios between 0.15 - 1.0, subjected to combinations of vertical and horizontal loads.

2.3.4 Solanki & Sabnis

Solanki and Sabnis[59] describe their design method as a "simplified approach" using truss analogy. Based on the results of 398 tests from 16 different investigations, they showed that their design approach was effective.

The structural model used by Solanki and Sabnis was based on that proposed earlier by Leonhardt and Monning[32]. The following assumptions were made:

- concrete acts as inclined struts between cracks carrying compressive forces only,
- shear transmitted across a crack through either aggregate interlock or dowel action is neglected,
- local effects caused by reactions or loads are neglected,
- equilibrium conditions are satisfied,
- failure occurs through yielding of the reinforcement or concrete crushing,
- the strength of concrete in tension is neglected,
- the maximum concrete strain is equal to 0.003,
- the concrete strength is equal to t he cylinder strength.

The strut and tie action at failure is shown in and is represented by the following equation:

$$Dx = V_u a + N_u \Delta h$$ **Equation 2-45.**

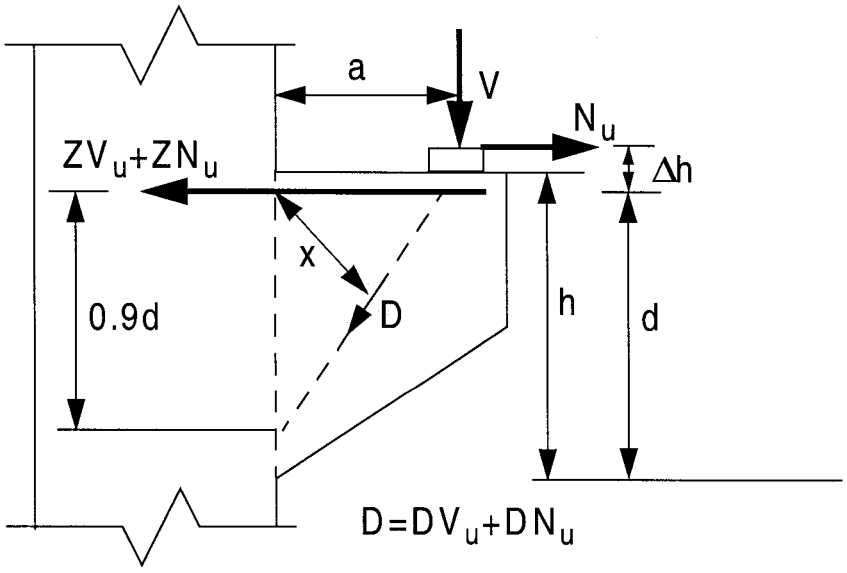

Figure 2-8. Truss model as proposed by Solanki and Sabnis[59]

where x = perpendicular distance of the force to the inclined strut such that:

$$x = \frac{0.9ad}{\sqrt{(0.9d)^2 + a^2}}$$ **Equation 2-46.**

a = the shear span and Δh is the distance from the horizontal load to the main reinforcement.

D = assumed to be the compressive force in the strut based on the work of Leonhardt[30] and others, and is equal to:

$$D = 0.25bd(\beta_1 f'_c)$$ **Equation 2-47.**

$$\beta_1 = 0.85 - 0.08\left(\frac{f'_c - 30}{10}\right) \geq 0.65$$

Substituting the above two equations into Equation 2-45 yields:

$$\frac{bdf'_c}{V_u} = \frac{4.45}{\beta_1}\left(1 + \frac{N_u \Delta h}{V_u a}\right)\sqrt{(0.9d)^2 + a^2}$$ **Equation 2-48.**

By assuming that $\Delta h/a = 0.3$, Equation 2-48 simplifies to:

$$\frac{bdf'_c}{V_u} = \frac{4.45}{\beta_1}\left(1 + \frac{0.3N_u}{V_u a}\right)\sqrt{(0.9d)^2 + a^2}$$ **Equation 2-49.**

The effect of the bracketed component in the above equation is small and can be ignored for $\frac{N_u}{V_u} \leq 0.2$, and thus:

$$\frac{bdf'_c}{V_u} = \frac{4.45}{\beta_1}\sqrt{(0.9d)^2 + a^2}$$ **Equation 2-50.**

Design Method

Solanki and Sabnis recommended the following design steps:

1. Given V_u, N_u, f'_c, a and b; d is estimated using Equation 2-49 or Equation 2-50.

2. The area of shear reinforcement (A_v) is calculated from a free body analysis of the corbel (as proposed by Mattock[37][38][39][40][41]).

$$A_v = \frac{V_u a + N_u(h-d)}{jdf_y}$$ **Equation 2-51.**

where "j" is the lever arm between the resultant tensile force and the compression force acting on the corbel/column interface.

3. The area of tension reinforcement (A_n) is calculated from:

$$A_n = \frac{N_u}{f_y}$$ **Equation 2-52.**

4. The total area of reinforcement (A_s) is

$$A_s = A_v + A_n$$ **Equation 2-53.**

5. The corbel is appropriately detailed.

The design method is valid for:

- a/d ratios between 0.1 and 1.0,
- any combination of vertical and/or horizontal loads, and
- combinations of horizontal and inclined reinforcement.

2.3.5 Hwang, Lu and Lee

In 2000, Hwang, Lu and Lee[17] presented a theoretical softened strut-and-tie model for shear strength predictions of reinforced concrete corbels. The model was applied to corbels of different concrete strengths, shear span to depth ratios, and horizontal and vertical web reinforcement. The proposed model originates from the strut-and-tie concept and satisfies equilibrium, compatibility and constitutive laws of cracked reinforced concrete. The shear strength predictions of the proposed

model were applied to 178 corbels available in literature and compared to the ACI 318-95 Code[2].

The strut-and-tie model for corbels is shown in Figure 2-9. As can be seen, the angle of inclination of the strut can be defined as:

$$\theta = \tan^{-1}\left(\frac{jd}{a}\right)$$ **Equation 2-54.**

where: jd = the lever arm

a = the shear span

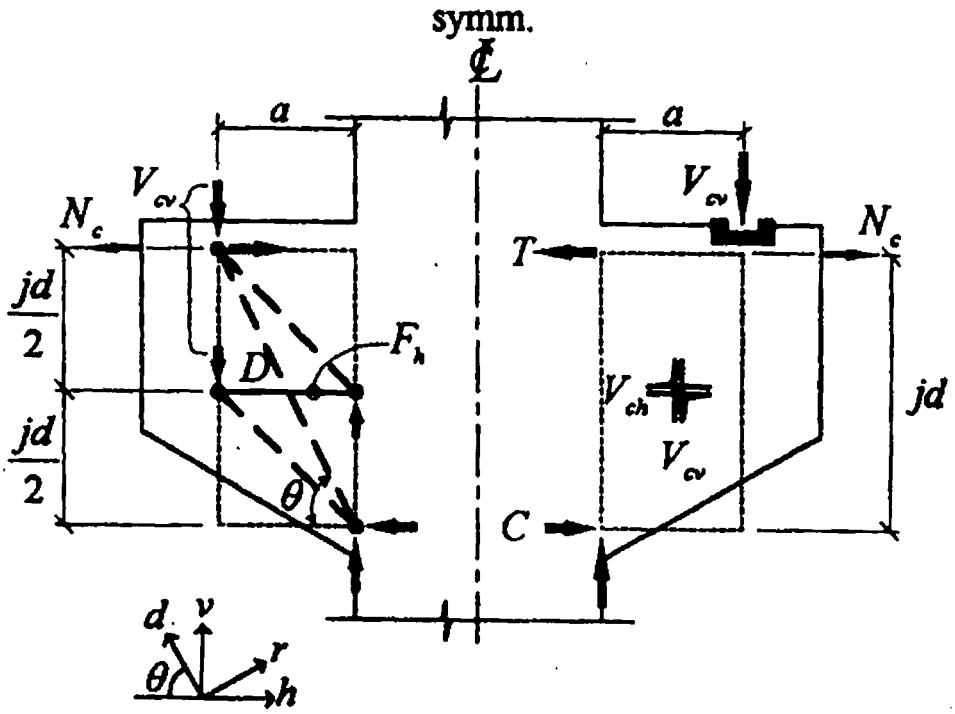

Figure 2-9. Strut and tie model for internal forces

The direction of the principal compressive stress of the concrete is assumed to coincide with the direction of the diagonal concrete strut.

The maximum compressive stress σ_d max resulting from the summation of the compressive forces shown in Figure 2-9 can be estimated as:

$$\sigma_{d,\max} = \frac{1}{A_{str}}\left(D - \frac{\cos\left(\theta - \tan^{-1}\left(\frac{jd}{2a}\right)\right)}{\cos\left(\tan^{-1}\left(\frac{jd}{2a}\right)\right)}F_h\right) \qquad \textbf{Equation 2-55.}$$

where A_{str} = effective area of diagonal strut

D = compression force in diagonal strut (negative for compression)

F_h = Tension force in horizontal ties (positive for tension)

Cracked reinforced concrete in compression exhibits lower strength than uniaxially compressed concreted as shown in Figure 2-17 on page 53. The stress-strain softening curve of cracked concrete is represented as follows.

$$\sigma_d = -\zeta f'_c\left[2\left(\frac{-\varepsilon_d}{\zeta\varepsilon_o}\right) - \left(\frac{-\varepsilon_d}{\zeta\varepsilon_o}\right)^2\right] \text{ for } \frac{-\varepsilon_d}{\zeta\varepsilon_o} \le 1 \qquad \textbf{Equation 2-56.}$$

$$\sigma_d = -\zeta f'_c\left[1 - \left(\frac{-\varepsilon_d/\zeta\varepsilon_o - 1}{2/\zeta - 1}\right)^2\right] \text{ for } \frac{-\varepsilon_d}{\zeta\varepsilon_o} > 1 \qquad \textbf{Equation 2-57.}$$

$$\zeta = \frac{5.8}{\sqrt{f'_c}}\frac{1}{\sqrt{1+400\varepsilon_r}} \le \frac{0.9}{\sqrt{1+400\varepsilon_r}} \qquad \textbf{Equation 2-58.}$$

where σ_d = the average principal stress in the d-direction

ζ = the softening coefficient

f'_c = the compressive strength of concrete

ε_d = average principal strain in the d-direction

ε_r = average principal strain in the r-direction

ε_o = concrete cylinder strain corresponding to the cylinder strength

The softened truss model was applied to 178 corbels available in literature from such researchers as Kriz and Raths, Mattock et al., Fattuhi and Hughes, Her, Yong and Balaguru, Fattuhi and Foster et al. The following conclusions were drawn from this study.

- The softened strut-and tie model presented was able to accurately predict the shear strength of 178 corbels available in literature
- The crushing and splitting failures of the diagonal struts of corbels were found to be identical and could be reliably predicted using the same analytical model
- The ACI empirical equations are conservative for the selected test data
- For crack control, it is recommended that the vertical stirrups within the corbels be detailed at a/d>0.5.

2.4 Deep Beams

2.4.1 Leonhardt & Walther

An experimental investigation in 1966 by Leonhardt and Walther[31] clearly demonstrated the formation of the tied arch in deep beams. Large scale tests were carried out on nine single span and two double span deep beams. They noticed that the main flexural reinforcement retained a large proportion of its force close to the support and therefore required a full strength anchorage. In continuous deep beams, they noticed that the interior negative moments tended to decrease and the positive moments increased as compared with the values obtained by an elastic analysis.

Leonhardt and Walther concluded that for beams with clear span to depth ratios less than two, vertical or inclined web reinforcement was of no benefit, because the concrete always failed by crushing under the bearing area.

Their work formed the basis for the European Code[6] (CEB-FIP Model Code, 1978) design recommendations for deep beams.

2.4.2 Kong et al.

Kong et al.[18][19][20][21][22][23][24][25] performed numerous tests during the 1970's on reinforced concrete deep beams.

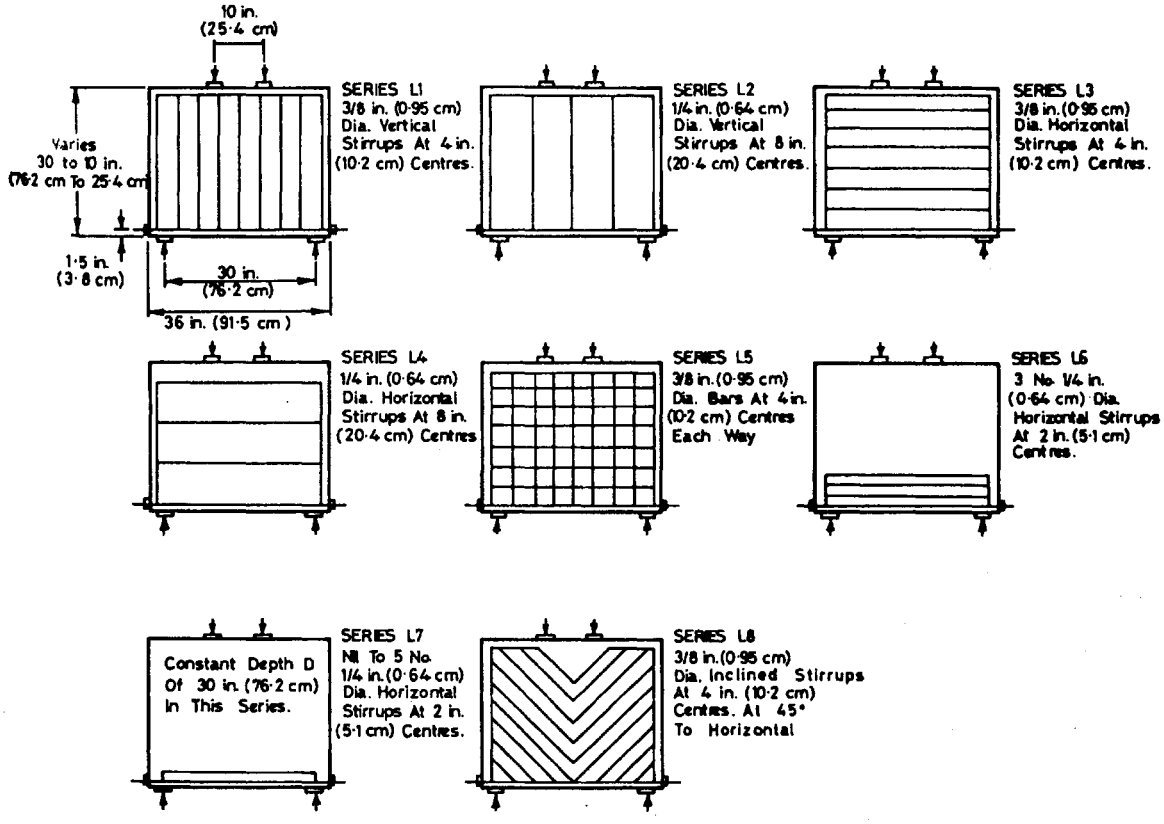

Figure 2-10. Reinforcement details for deep beams tested by Kong et al.[18][19][20][21][22][23][24][25]

Parameters investigated included:

- span to depth (l/d) ratios,
- shear span to depth (a/d) ratios,
- vertical and horizontal web reinforcement ratios,
- effect of inclined web reinforcement,
- weight of concrete and size, and
- position of web openings, if any.

Among the various tests conducted, a test to determine the influence of web reinforcement on the shear strength of deep beams was performed. Thirty-five specimens were tested, with l/d ratios varying from 1 to 3 and a/d ratios varying from 0.23 to 0.70. Web reinforcement ratios varied from; light to heavy vertical stirrups, light to heavy horizontal reinforcement and orthogonal mats.

Findings of the investigation included:

1. The effectiveness of web reinforcement depends to a large extent on the length to depth ratio (l/d) and shear span to depth (a/d) ratios. For low l/d, and a/d ratios (less than 1.5 and 0.35, respectively), only horizontal web reinforcement placed close to the bottom had an effect. For larger l/d and a/d ratios, vertical web reinforcement (stirrups) was more effective than the horizontal web reinforcement in increasing the shear strength.
2. Failure occurred most often by diagonal splitting followed by crushing of the concrete at the bearing blocks or crushing of the compression strut between the diagonal cracks (occurred in a few beams). Diagonal cracking generally occurred when the load reached 70-90% of ultimate load.
3. The failure load was compared with the theoretical values obtained from various methods available at the time from a number of sources, including those in the then current editions of the British and American codes. Good agreement was found with a modified de Paiva and Siess[48] formula, as follows:

$$P_u = 0.0016bD\left(1 - 0.6\frac{a}{D}\right)(1.38 + 0.188f'_c + 147\rho_t) \qquad \textbf{Equation 2-59.}$$

and with the Ramakrishnan and Ananthanarayana's[49] formula;

$$P_u = 2Kf'_{sp}bD \qquad \textbf{Equation 2-60.}$$

where P_u = ultimate load capacity (kN),

a = shear span (mm),

b = width of beam (mm),

D = depth of beam (mm),

f'_c = cylinder strength of the concrete (MPa),

f'_{sp} = concrete cylinder splitting strength (MPa),

$\rho_t = \frac{A_s}{bD}$, where A_s is the area of the longitudinal reinforcement only,

$K = \frac{\pi}{2}$, a splitting coefficient.

2.4.3 Smith & Vantsiotis

Smith and Vantsiotis[58] furthered this experimental work by conducting a series of tests on 52 deep beams. They studied the effects of web reinforcement, a/d ratios and concrete strength on the strength and behaviour of deep beams.

Smith and Vantsiotis were interested in the shear behaviour of deep beams and therefore designed their specimens to fail by shear. The shear span-to-depth (a/d) ratios varied from 0.77 to 2.01 and web reinforcement ratios varied from 0 to 0.91% for horizontal reinforcement and from 0 to 1.25% for vertical reinforcement. Concrete strengths ranged from 16 to 23 MPa.

All beams tested failed by crushing or splitting of the compression strut and all beams failed in the same way regardless of a/d ratio or amount of web reinforcement.

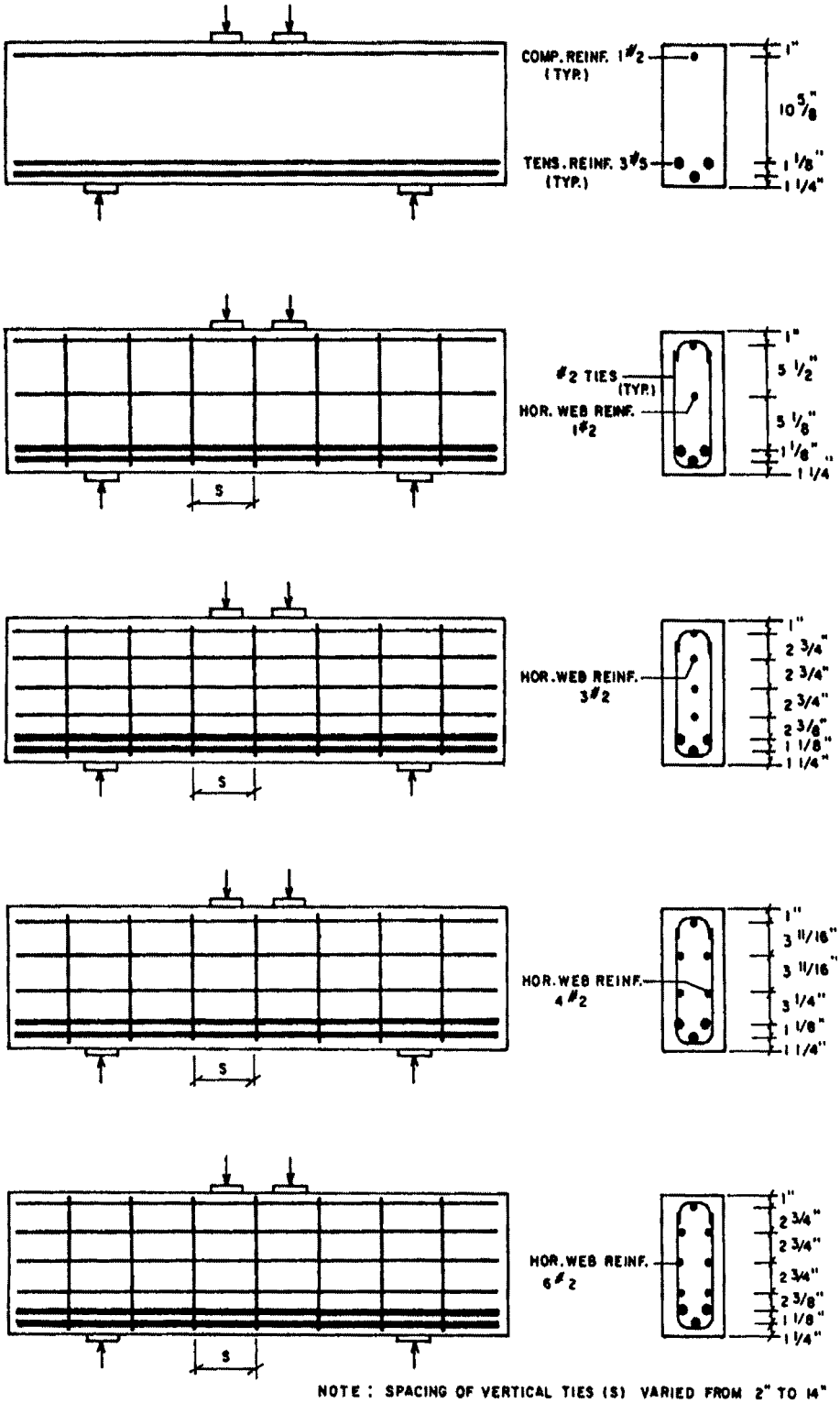

Figure 2-11. Web reinforcement for beams tested by Smith and Vantsiotis[58]

The main findings included:

1. a minimum amount of web reinforcement ($\rho_v = 0.18$, $\rho_h = 0.23$) was found to reduce crack widths and deflections considerably after inclined cracking,
2. inclined cracking occurred at about 40-50% of the ultimate load whether or not web reinforcement was present, however, less damage at failure was observed in beams with web reinforcement,
3. the amount of web reinforcement had no influence on the cracking load,
4. web reinforcement increased the ultimate shear strength, but never more than 30% (compared to beams without web reinforcement).
5. vertical web reinforcement had the most beneficial effect; however, the value of vertical stirrups tended to reduce for a/d ratios < 1,
6. horizontal reinforcement appeared to have had negligible influence on the ultimate shear strength, and
7. the ultimate shear strength was strongly influenced by concrete strength, particularly for low a/d ratios.

Smith and Vantsiotis' results indicated strut and tie behaviour and confirmed that a different set of design rules was needed from those that existed at that time in the codes.

2.4.4 Besser and Cusens

Besser and Cusens[4] carried out an investigation on deep beams with depth to span (d/l) ratios of greater than or equal to 1. They performed seven tests on simply supported beams with d/l ratios of 1.0 to 4.0. At the higher end of the range, specimens became very slender and out of plane buckling became a problem.

All specimens had a constant span of 720 mm, constant thickness of 72 mm with only the height varied. The concrete strength was typically about 50 MPa and all beams were subjected to 2-point loading at one third span.

It was found that the beams with depth-to-span ratios of 1.5 to 3.5 all failed in bearing at the supports. Specimens with a depth-to-span ratio of 1.0, failed by diagonal splitting, while specimens with a depth-to-span ratio of 4.0 failed by buckling. Besser and Cusens also reported that a linear relationship existed between depth-to-span ratios up to 3.0 and the loads which caused the first diagonal crack. For depth-to-span ratios greater than 3.0, the cracking load became independent of the d/l ratio.

Besser and Cusens found that for specimens with a depth-to-span ratio of 1.0, good agreement existed between the experimentally determined cracking load and that predicted by Kong et al. for deep beam design as follows;

$$\frac{V_u}{bd} < \lambda_1\left(1 - 0.35\frac{a}{d}\right)\sqrt{f_{cu}} + \lambda_2 \sum \frac{100 A_i y_i \sin^2\theta_i}{bd^2} \qquad \textbf{Equation 2-61.}$$

where the first term is the contribution from the concrete and the second term is contribution from the reinforcement.

In the above equation:

V_u = ultimate shear capacity (kN),

b = panel thickness (mm),

d = effective depth to centroid of the main tensile reinforcement (mm),

a = the shear span (mm),

f_{cu} = cube crushing strength of the concrete (MPa),

A_i = area of web reinforcement (mm^2) at spacing "y" (mm),

λ_1 = factor dependent on aggregate type (0.44 for normal weight concrete),

λ_2 = factor dependent on reinforcement type (1.95 for deformed bars), and

θ_i = angle between shear crack and web reinforcement.

For specimens with higher depth-to-span ratios, Besser and Cusens defined the cracking load as:

$$V_{cr} = 0.375V_1\left(\frac{5}{3}+\frac{D}{L}\right)$$ **Equation 2-62.**

where V_1 is the cracking load given by Equation 2-61 for a beam with d/l = 1.0.

Besser and Cusens concluded from this work that a significant enhancement of the shear strength is available for beams whose depth exceeds their span. Their study also indicated that the shear strength is dependent on both the web reinforcement and the bearing area. They also recommended that when sufficient web reinforcement is provided to resist both the bending moments and shear forces, the bearing stress at the supports should be limited to $0.4f_{cu}$.

2.4.5 Mau & Hsu

Mau and Hsu[42][43] proposed a theoretical model for the shear resistance of deep beams in 1987. They considered that the shear force in a deep beam is resisted by a shear element bounded by the line of action between the load and support reactions, and of depth d_v (where d_v is the distance between the centroid of the main longitudinal compressive and tensile forces).

Deep beams tend to have a loading point close to the support point, and so the shear element is subject to substantial compressive forces parallel to the line connecting the load and support points, that is the "compression strut". The magnitude of these compressive forces tends to reduce as the shear span increases.

Mau and Hsu proposed the use of a "softened truss model" to represent the shear resistance of deep beams, in which the material characteristics of the concrete are represented by the stress-strain curve. The coefficient λ is the softening coefficient, and is given by:

$$\lambda = \sqrt{\left(0.7-\frac{\varepsilon_r}{\varepsilon_d}\right)}$$ **Equation 2-63.**

where ε_r = the normal strain in the principle tensile direction (i.e. normal to the strut), and

ε_d = the normal strain in the principle compression direction (i.e. parallel to the strut).

The softening coefficient was introduced to account for the experimentally confirmed reduction in compressive strength of struts subject to shear stresses. They also observed that the magnitude of the compressive stresses in the strut tends to decrease as the shear span-to-depth ratio increases. This observation was modeled using the relationship:

$$p = 2\frac{V}{bh} \quad \text{for } \frac{a}{h} < 0.5$$

$$p = \frac{V}{bh}\left[\frac{h}{a}\left(\frac{4}{3} - \frac{2a}{3h}\right)\right] \quad \text{for } 0.5 \le \frac{a}{h} < 2 \qquad \textbf{Equation 2-64.}$$

$$p = 0 \quad \text{for } \frac{a}{h} < 2$$

where p = effective transverse compression acting on the shear element,

V = the shear force in the shear span,

a = the shear span,

h = height of the beam, and

b = thickness of beam.

The above equation implies that a parabolic relationship exists for a/h ratios between 0.5 and 2.0.

Combining the above with equations of equilibrium and compatibility, Mau and Hsu obtained five simultaneous equations which they were able to solve numerically to obtain the predicted shear response of an element. Their criteria for establishing the strength of an element was the attainment of the maximum shear stress on the stress-strain curve.

Mau and Hsu compared their results with 64 test results which were available in literature (Smith and Vantsiotis[58], Kong[18], and de Paiva and Siess[48]). These results were selected on the basis that the predominant mode of failure was web shear cracking.

Good agreement was found with the test results. Eighty percent of the test results fell within 10% of the computer analyzed results. It was further found from a parametric study, that while varying the shear span to depth ratio had a significant effect on the maximum shear strength of the element, varying the longitudinal reinforcement had a more noticeable effect for low a/d ratios only, and varying the vertical web reinforcement had a noticeable effect only for shear span to depth ratios above 0.5.

Mau and Hsu performed algebraic manipulations of their preceding theory and calibrated the resulting equations with the test data. They ultimately derived the following non-dimensioned formula for the shear strength of deep beams:

$$\frac{\tau}{f'_c} = \frac{1}{2}K_1(\omega_h + 0.03) + \frac{1}{2}\left[\sqrt{K_1^{\,2}(\omega_h + 0.03)^2 + 4(\omega_h + 0.03)(\omega_v + 0.03)}\right] \le 0.3$$

Equation 2-65.

where $\omega_h = \frac{\rho_h f_{yv}}{f'_c}$ and $\omega_v = \frac{\rho_v f_{yv}}{f'_c}$ are the horizontal and vertical web reinforcement indices respectively, within the limits $0 \le \omega_h \le 0.26$ and $0 \le \omega_v \le 0.12$.

K_1 represents the effect of the shear span on the shear strength.

$$K_1 = \frac{2d_v}{D} \qquad 0 \le \frac{a}{D} \le 0.5$$

$$K_1 = \frac{d_v}{D}\left[\frac{D}{a}\left(\frac{4}{3} - \frac{2a}{3D}\right)\right] \quad 0.5 \le \frac{a}{D} \le 2 \qquad \textbf{Equation 2-66.}$$

$$K_1 = 0 \qquad \frac{a}{D} > 2$$

f_{yv} = the yield stress of the web reinforcement,

f'_c = the cylinder strength of the concrete,

ρ_v = the vertical web reinforcement ratios,

ρ_h = the horizontal web reinforcement ratios, and

τ = the shear stress = $\frac{V}{bd_v}$.

The resulting formula provided accurate predictions of shear strength for the experimental test results. However, since it was calibrated with a particular set of test data, it is only applicable to single span beams subject to point loads at midspan.

2.4.6 Kotsovos

Kotsovos[26][27], proposed a simple design procedure for deep beams, based on his concept of the "compressive force path". Kotsovos theorizes that the shear resistance of a member is provided by a direct compressive force transmitted to the supports along a load path. In deep beams, the existence of this direct compression strut has long been accepted.

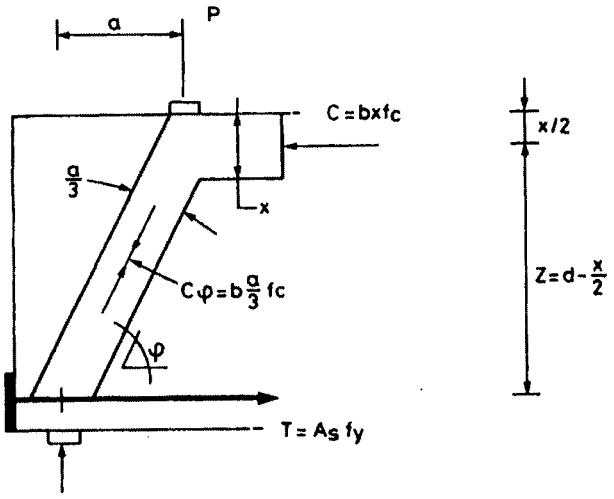

Figure 2-12. Proposed truss model by Kotsovos[26][27]

Shear failures are associated with the presence of tensile stresses developing perpendicular to the direction of the compressive force path. These tensile stresses may be caused by:

- changes in the path direction, which in deep beams usually occurs at the loaded cross section,
- varying intensities of the compressive stress field caused by the changing trajectories of the compressive forces,
- high stresses existing at the tip of inclined flexural cracks, and
- bond failure in the tensile reinforcement causing changes in the stress conditions in the compressive zones of the beam.

The actual shape of the stress field and the magnitude of the tensile stresses are difficult to determine without sophisticated nonlinear finite element analysis programs. To circumvent these difficulties, Kotsovos proposed an idealized model for the compressive force path which is essentially bi-linear. The model has parallel sides with a width of one third of the shear span (a/3). However, if a/3 is smaller than the effective width of bearing, then the bearing width should be used for the width of the compression strut. The design method then follows from the principles of statics.

The results were verified against the experimental results of de Paiva and Siess[48], Ramakrishnan and Ananthanarayana[49], Kong[18], Smith and Vantsiotis[58] and also the continuous deep beam test results of Rogowsky et al[50][51][52]. The method showed a reasonable correlation with experimental values, with the predicted values generally on the conservative side. Greater reliability existed for beams without web reinforcement.

The procedure from Kotsovos does not take into account the contribution of web reinforcement to the shear strength. The justification for this is the conclusion made by de Paiva and Siess, Smith and Vantsiotis and Kong et al. among others, that the presence of web reinforcement has little, if any, effect on the load carrying capacity of deep beams. The method also assumes that the strut can develop the full cylinder strength of the concrete in compression.

2.4.7 Siao

Siao[55][56][57] proposed another model based on a refined strut and tie model for deep beams. He assumed that the compression strut can be divided into two components dispersing at angles of 2:1 from the line connecting the load and support points. At the mid-depth of the member, two tensile ties are required for equilibrium.

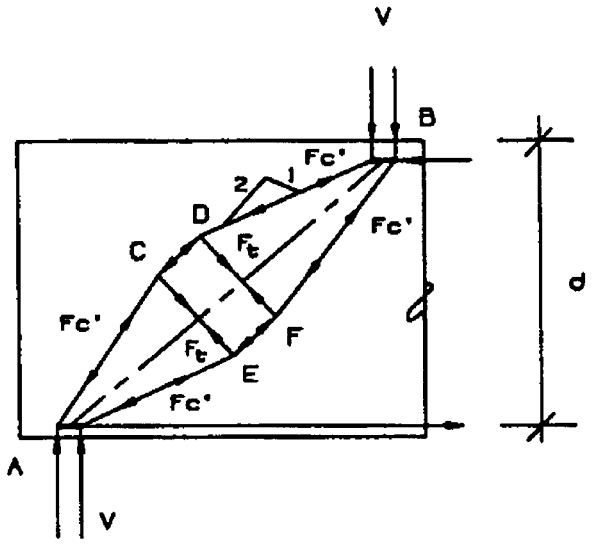

Figure 2-13. Truss model as proposed by Siao[55][56][57]

On the basis of this model, assuming that the lever arm between the centroid of the top compression force and the main tension reinforcement is 0.9d, he derived that the ultimate shear strength of the beam could be represented by the equation;

$$V_u = 1.8 f_t b d \qquad \textbf{Equation 2-67.}$$

where b = the thickness of the beam (mm)

d = the effective depth (mm),

f_t = the tensile strength of the concrete = $0.52\sqrt{f'_{cu}}$ N/mm^2, and

f_{cu} = cube strength in N/mm^2

When web reinforcement is present, he proposed the following modified expression for f_t:

$$f_t = 6.96\sqrt{f'_c}[1 + n(\rho_h \sin^2\theta + \rho_v \cos^2\theta)] \qquad \textbf{Equation 2-68.}$$

where the second and third terms in the brackets are the contribution from the reinforcement.

In the above equation:

n = the modular ratio E_s/E_c,

ρ_h = the horizontal reinforcement ratio,

ρ_v = the vertical reinforcement ratio, and

θ = the angle of the compressive strut to the horizontal.

Comparing these equations to the experimental data indicated good agreement for specimens with shear span to depth (a/d) ratios less than 1.0. However, for a/d ratios greater than this, the gap between the experimental and theoretical results widened progressively. For a/d ratios greater than 1.3, the accuracy dropped off rapidly. Therefore, he suggested the use of a modification factor k_1 to account for this reduced shear strength for higher a/d ratios, where $k_1 = 1$ for $a/d \leq 1.0$, and

$k_1 < 1.0$ for higher values of a/d. No guidance was given for the value of k_1 beyond a/d=1.0.

Siao also observed that after cracking, all of the tensile forces would have to be resisted by the web reinforcement, therefore, he proposed that where web reinforcement was present, the minimum shear strength of the beam would be:

$$V_u = 1.8 f_{yv}(\rho_h \sin^2\theta + \rho_v \sin^2\theta) \qquad \textbf{Equation 2-69.}$$

where f_{yv} is the yield strength of the web reinforcement. This equation assumes that the web reinforcement has adequate anchorage to develop its full yield strength.

2.4.8 Rogowsky and MacGregor

Rogowsky and MacGregor[50][51][52] conducted an extensive experimental investigation into the behaviour of both simple span and continuous deep beams. Their work demonstrated that a plastic truss model can provide accurate predictions of stresses and the ultimate strength of deep beams.

A deep beam is defined as "any beam in which a substantial portion of the load is transferred to the support by a direct compression strut". Corbels are included under this definition of a deep beam and it was proposed that they also be designed using the plastic truss model.

Rogowsky and MacGregor based their model on work conducted by Marti[33][34], Mueller[46], Thurlimann[62][63][64], and Nielson et al.[47]. The basis of the model is that an applied load is resisted internally by a pin jointed truss (or strut and tie model), composed of compression (concrete) and tension (steel) members.

The basic assumptions for the model are:

- equilibrium must be satisfied,
- elastic strains are negligible compared to the yield strains,

- the concrete only resists compression and has an effective compressive strength $f^*_c = vf'_c$, where $v < 1.0$,
- the steel resists all tensile forces, and
- failure of the truss occurs when either the steel yields or the concrete crushes.

From the above assumptions, the following can be derived:

- The lines of action of all applied loads must coincide with the centroid of each truss member,
- At ultimate load, concrete struts are in uniaxial compression with a uniform stress, and
- Bearing plates, support conditions and details must be designed so that bearing and anchorage failures do not occur.

The basic equations relating to materials, geometry and equilibrium for the plastic truss model for corbels are:

Materials

$$F_s = A_{st} f_s \qquad \textbf{Equation 2-70.}$$

$$F_c = f^*_c b d_c \qquad \textbf{Equation 2-71.}$$

$$f^*_c = v f'_c \qquad \textbf{Equation 2-72.}$$

Geometry

$$\Omega = d - \sqrt{d^2 - 2aw - w^2} \qquad \textbf{Equation 2-73.}$$

$$V_u = \frac{F_s w}{\Omega} \qquad \textbf{Equation 2-74.}$$

From materials and geometry:

$$V_u = \frac{A_{st} f_{st} w}{\Omega}$$ **Equation 2-75.**

From materials and equilibrium and noting that $d_c = w/\sin\theta$:

$$V_u = f^*_c b w$$ **Equation 2-76.**

Design Method

1. Given f^*_c, estimate the corbel dimensions with:

$$\frac{V_u}{bd} = 0.8\sqrt{f^*_c}$$ **Equation 2-77.**

2. The minimum bearing width of the loading plate, w_{min}, can be calculated from:

$$w_{min} = \frac{V^*}{bvf'_c}$$ **Equation 2-78.**

3. The depth of the node Ω is given by:

$$\Omega = d - \sqrt{d^2 - 2aw - w^2} \leq 2(D - d)$$ **Equation 2-79.**

4. The area of reinforcement is calculated from:

$$A_{st} = \frac{V^* \Omega}{f_{sy} w}$$ **Equation 2-80.**

5. Proper detailing including secondary reinforcement is considered.

2.4.9 Collins and Mitchell

Collins and Mitchell[8][9][44] adapted work done by Wagner[68] in 1929 on steel beams. Wagner assumed that after web buckling, the thin webs could no longer support compression. Collins and Mitchell proposed that after cracking, a concrete beam can no longer carry tension, and that the shear is carried by a diagonal field

of compression as shown in Figure 2-14. The angle of inclination of the compression stresses can be found from the following equation.

$$\tan^2\theta = \frac{\varepsilon_x - \varepsilon_2}{\varepsilon_t - \varepsilon_2}$$ **Equation 2-81.**

where ε_s = longitudinal strain at mid-depth of the web,

ε_t = transverse strain, and

ε_2 = principal compressive strain.

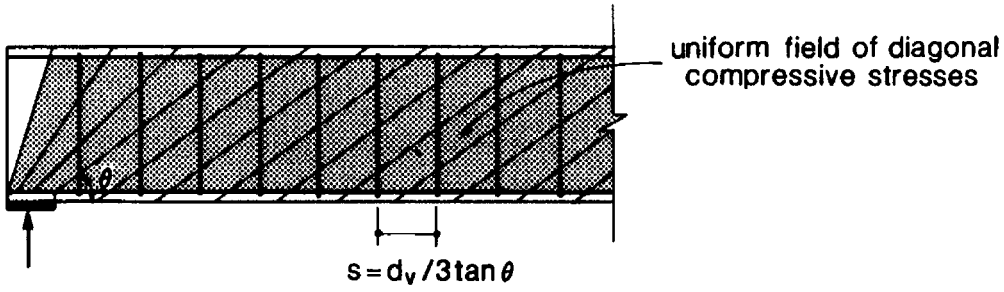

Figure 2-14. Diagonal compression field[9]

Considering a symmetrically reinforced prestressed concrete beam subjected to shear, five unknowns need to be solved. The stress in the reinforcement, the stress in the prestressing tendon, the stress in the stirrups, compressive stress in the concrete, and the angle of inclination. To solve for these unknowns, three equilibrium equations, two compatibility equations and the constitutive relationship of the materials. This approach was named the Compression Field Theory.

The design approach used by the Compression Field Theory uses plane sections theory to consider the resistance and behaviour of beams under shear load. The cross section of the beam is divided into a series of horizontal layers. Longitudinal strains, shear stress, and angle of principal compressive stress is assumed to be constant. At each layer, biaxial stresses are calculated.

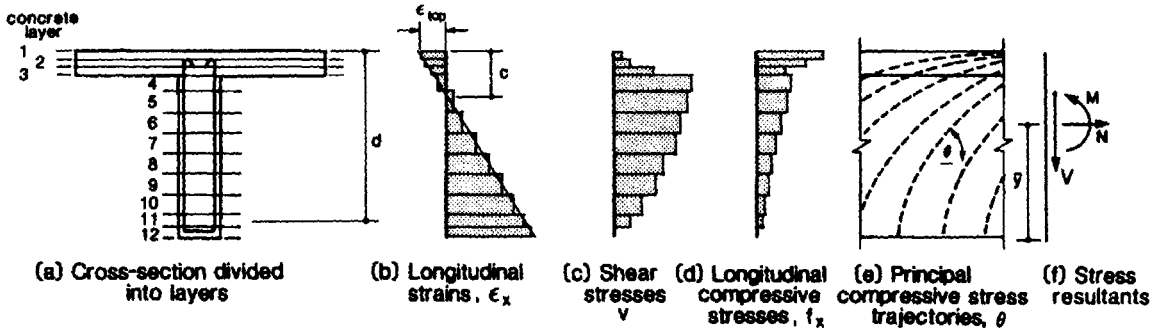

Figure 2-15. Compression Field Theory linked to plane sections[9]

Vecchio and Collins[65][66][67] in 1986 tested thirty square reinforced concrete panels measuring 890mm x 890mm by 70mm. The panels were reinforced with two layers of welded wire mesh placed parallel to the edges of the panels. The smooth wire meshes had typically 50 mm grid spacing with a clear cover of 6 mm. The maximum size aggregate used in the concrete mix was 6 mm. Five steel shear keys were cast into each of the four edges of the test panel and anchored by concrete shear studs. Thirty-seven hydraulic jacks applied the loading to the test panel.

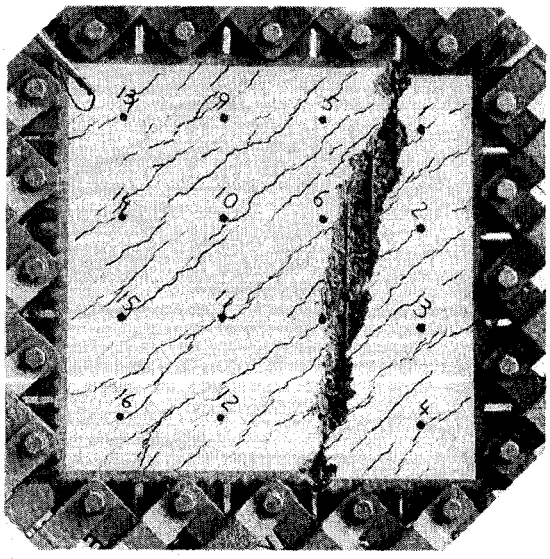

Figure 2-16. Test panel after failure[9]

Their results lead to the formation of the "modified compression-field theory". In this model, cracked concrete is treated a new material with its own stress-strain properties. To establish these properties, equilibrium, compatibility and stress-strain relationships were formulated in terms of average strains and stresses. It was assumed that the direction of principle strain axes coincides with the direction of the principle stresses.

The principal compressive stress in the concrete was found to be a function of the co-existing principal tensile strain. Concrete subjected to high tensile strains normal to the compressive strain is "softer" and weaker than concrete subjected to a standard cylinder stress (where the tensile strain is due to the Poisson's ratio).

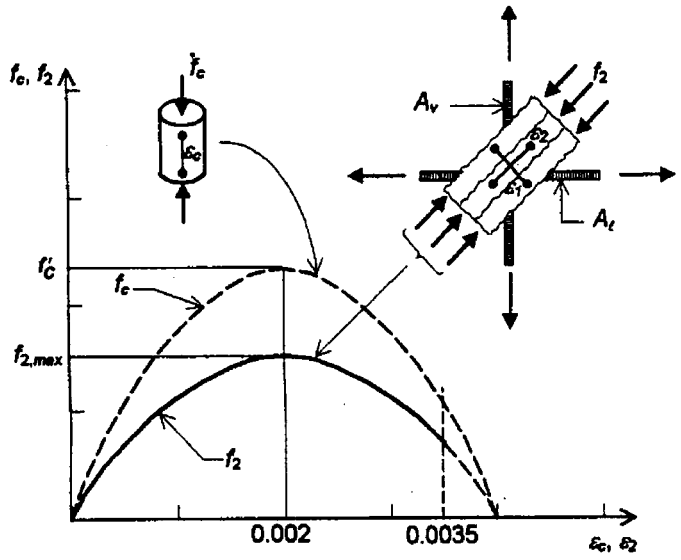

Figure 2-17. Stress strain relationship for cracked concrete[9]

The following equations were derived to describe this effect.

$$f_{c2} = f_{c2max}\left[2\left(\frac{\varepsilon_2}{\varepsilon'_c}\right) - \left(\frac{\varepsilon_2}{\varepsilon'_c}\right)^2\right] \qquad \textbf{Equation 2-82.}$$

$$\frac{f_{c2max}}{f'_c} = \frac{1}{0.8 - 0.34\frac{\varepsilon_1}{\varepsilon'_c}} \leq 1.0 \qquad \textbf{Equation 2-83.}$$

$$\varepsilon_1 = \varepsilon_s + \frac{(\varepsilon_s + 0.002)}{\tan^2 \alpha_s}$$ **Equation 2-84.**

where ε'_c = negative quantity assumed to be -0.002 which corresponds to the highest point in the stress-strain curve

ε_s = tensile strain in tension tie due to factored loads

α_s = angle between tension tie and compression strut

Assuming $\varepsilon'_c = -0.002$, Equation 2-83 can be re-written as:

$$f_{c2max} = \frac{f'_c}{0.8 + 170\varepsilon_1} \leq f'_c$$ **Equation 2-85.**

Though the Compression Field Theory has been shown to accurately describe the strength of reinforced concrete beams, its application to deep beams and corbels is questionable. Firstly, the theory is based on the use plane sections theory, which does not apply to deep beams and corbels (and other areas of discontinuities). Of the panels that were tested, twenty-two were tested in monotonic pure shear, four in combined shear and biaxial stresses (of which one failed prematurely due to poor casting), two in uniaxial compression, one in reverse cyclic shear and one with a changing load ratio. When tested under biaxial stresses, each side was equally loaded. A shortcoming of the test procedure is that no panels were tested under unequal biaxial compression-tension stress conditions. These loading conditions would have reflected the stress state that exists along the compression strut that develops from the loading point to the support of deep beams and corbels.

As well, all test panels were reinforced with two layers of welded wire mesh, other reinforcement configurations, or no reinforcement at all, would have provided meaningful results, and would have representative of deep beams and corbels with such reinforcement. The cracking pattern shown in Figure 2-16 on page 52 is not representative of deep beams or corbels. From this figure you can see that failure occurred at an angle to the cracks, while with deep beams and corbels, diagonal

cracking failures occur in the same direction of cracking. The equations are complex and many assumptions are made; the designer must assume the strain in the concrete and the strain in the reinforcement. Equation 2-85 shows that the strain, ε_1, must be greater than 0.00117 before a reduction of compression strength is considered. Such a high strain is probably due to the amount of reinforcement used in the test panels.

2.4.10 Schlaich and Schafer

In 1987, Schlaich and Schafer[53][54] introduced a design method based on plasticity theory using a strut and tie model. The model could be used for both ultimate load and serviceability check. Concrete only allows a limited plastic deformation. Therefore, the model must be designed in such a way that the rotation deformation capacity is not exceeded at any point until the state of stress is reached by the rest of the structure. In areas of high stress, the size of the struts as well as their direction are designed according to elastic theory.

Design Method

The structure is divided into "B" and "D" regions. "B" regions occur where the Bernoulli hypothesis of linear strain distribution applies. In these areas, internal stresses are calculated from statics. "D" (discontinuity, disturbance, or detail) regions occur where strain distribution is non-linear. Internal forces can be calculated using strut and tie models. The model proposed by Schlaich and Schafer has three components, the strut, tie, and the nodes.

Schlaich and Schafer described three strut configurations that should adequately cover all cases of compression stress fields:

- fan shaped stress field which does not develop transverse stresses,
- the bottle shaped stress field which develops considerable transverse stresses, and
- prismatic stress fields

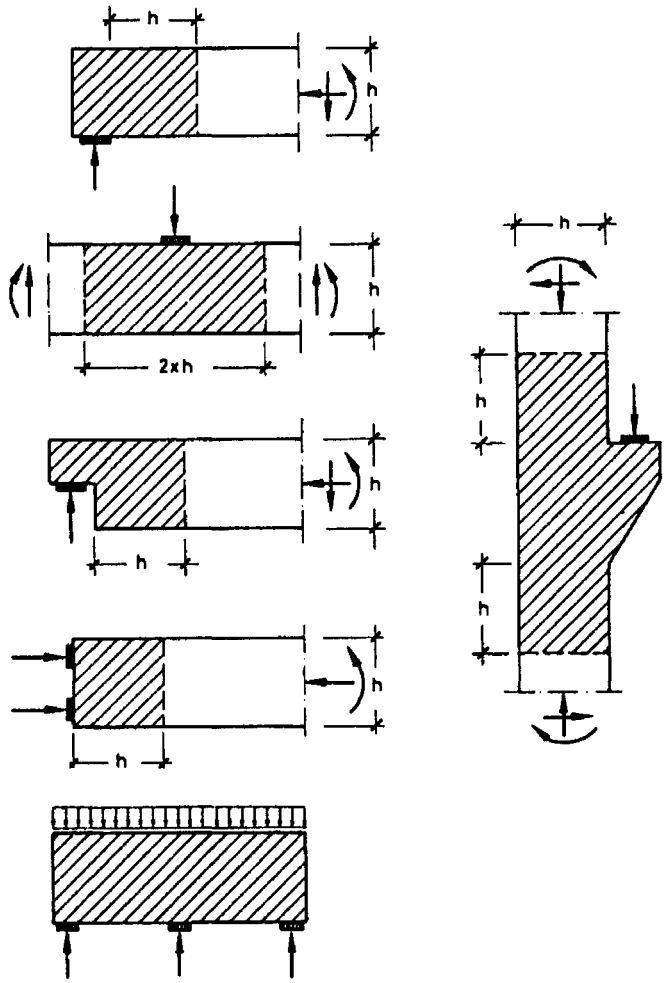

Figure 2-18. D-regions with non-linear strain distributions[53][54]

The fan and bottle shaped stress fields are normally found in "D" regions, while the prismatic stress field is found in "B" regions. The compressive strength of the concrete in the stress field depends largely on the state of stress. Schlaich and Schafer proposed a simplified design strength as follows:

$f^{*}_{cd} = 1.0f_{cd}$ for an undisturbed, uniaxial state of stress

$= 0.8f_{cd}$ where compression cracks are present and parallel to the compressive stresses

$= 0.6f_{cd}$ for compressive stress fields with skew cracks

where f_{cd} is the compressive strength of concrete.

Tension forces are carried by the reinforcement. The required area of the tension tie is calculated from the ultimate tie force and the yield strength of the reinforcement. Reinforcement is placed uniformly over the tensile zone.

Regions where forces change direction are called nodes. Nodes can be divided into two main types:

- smeared or continuous nodes in which wide concrete stress fields join each other, and
- singular or concentrated nodes in which the deviation of the loads is locally concentrated.

Nodes are designed empirically using the following guidelines:

- the geometry of the node must agree with the applied forces,
- the average compressive stresses in the node must be less than:

$f^*_{cd} = 1.0 f_{cd}$ where only compression struts meet, or

$f^*_{cd} = 0.8 f_{cd}$ in nodes where tensile reinforcement is anchored.

2.4.11 Tan and Lu

In 1999, Tan and Lu[61] presented their investigation on the size effect in large reinforced concrete deep beams. Twelve concrete deep beams varying in height from 500 to 1750mm were tested and compared to strength predictions from the ACI Code[2], the UK CIRIA Guide, and the CSA Code[5].

The test beams are shown in Figure 2-19. The width of the beams was held constant, while the shear span to depth ratio varied from 0.5 to 1.0. All beams with a height greater than 500mm were provided with a 6mm square wire mesh of 350mm grid to prevent sudden spalling of the concrete. A high percentage of main steel reinforcement (ρ=2.60) was used to prevent a flexural failure.

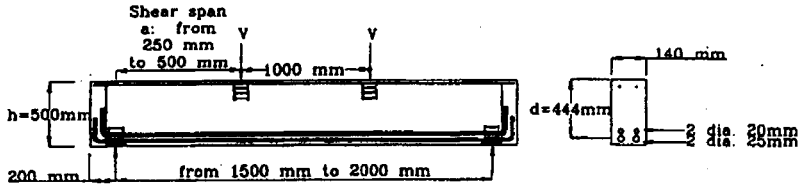

(a) Group 1 – h=500mm

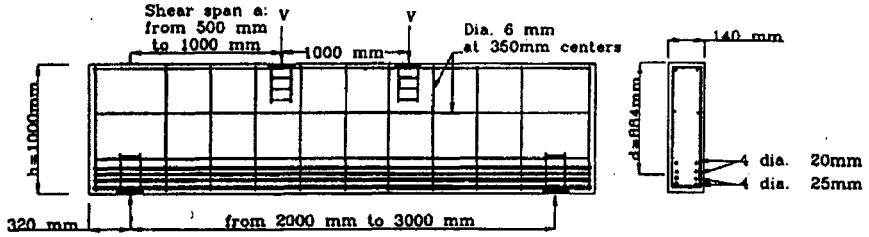

(b) Group 2 – h=1000mm

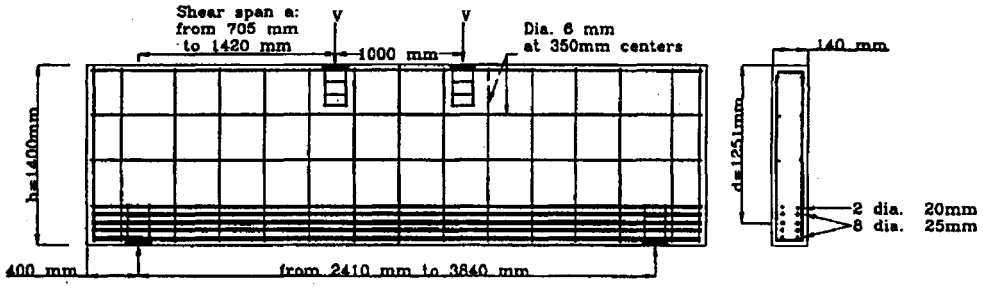

(c) Group 3 – h=1400mm

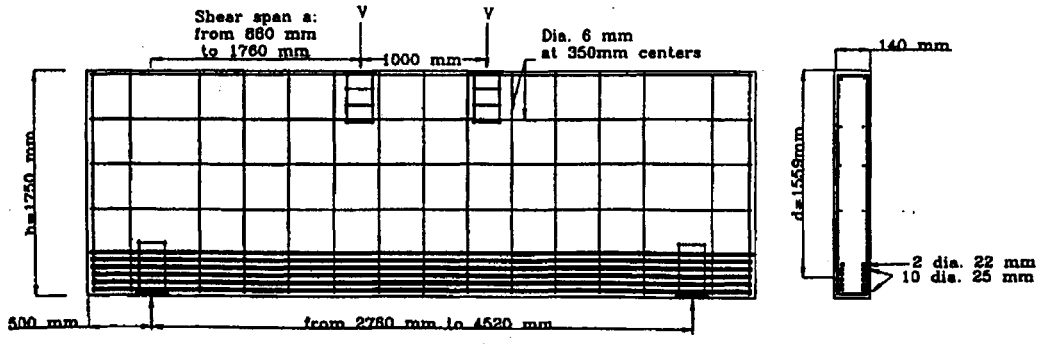

(d) Group 4 – h=1750mm

Figure 2-19. Web reinforcement for beams tested by Tan and Lu[61]

Among their findings:

1. An increase in height for geometrically similar beams leads to a more extensive crack patterns at the same shear stress
2. Size effect in diagonal cracking stress is small or negligible
3. There is a pronounced size effect on the ultimate shear stress, however the size effect seems relatively independent of the shear span to depth ratio (a/h)
4. The ACI Code predictions were generally conservative for all size beams, however the diagonal cracking strengths for beams with h=1750mm were overestimated.
5. The CIRIA predictions were unsafe for beams with heights greater than 1000mm
6. The Canadian Code predictions provided uniform safety margin for all beams tested. The strut-and-tie model predictions did not deteriorate with increasing height of the beam.

2.4.12 Hwang, Lu and Lee

In 2000, Hwang, Lu and Lee[16] presented a theoretical softened strut-and-tie model for shear strength predictions of deep beams. The model was applied to deep beams of different concrete strengths, shear span to depth ratios, and horizontal and vertical web reinforcement. The proposed model originates from the strut-and-tie concept and satisfies equilibrium, compatibility and constitutive laws of cracked reinforced concrete. The shear strength predictions of the proposed model was applied to 123 deep beams available in literature and compared to the ACI 318-95 Code[2]. The strut-and-tie development for a deep beam is shown in Figure 2-20.

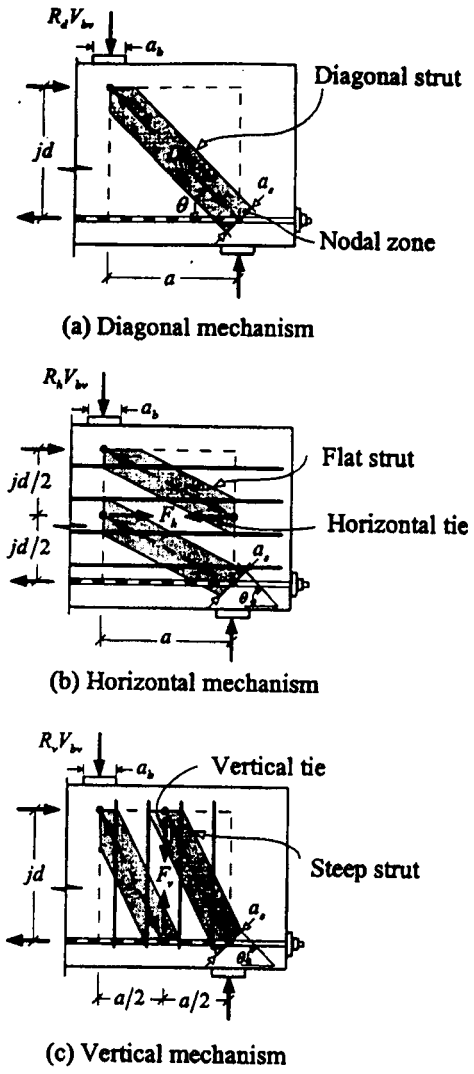

Figure 2-20. Strut and tie development in deep beams

After first cracking of a deep beam, the steel reinforcement bars are subjected to tension and the concrete acts as the compressive struts. The angle of inclination of the strut can be defined as:

$$\theta = \tan^{-1}\left(\frac{jd}{a}\right)$$ **Equation 2-86.**

where: jd = the lever arm

a = the shear span

The direction of the principal compressive stress of the concrete is assumed to coincide with the direction of the diagonal concrete strut.

The maximum compressive stress σ_d max resulting from the summation of the compressive forces shown in Figure 2-21 can be estimated as:

$$\sigma_{d,max} = \frac{1}{A_{str}}\left(D - \frac{\cos\left(\theta - \tan^{-1}\left(\frac{jd}{2a}\right)\right)}{\cos\left(\tan^{-1}\left(\frac{jd}{2a}\right)\right)}F_h - \frac{\cos\left(\tan^{-1}\left(\frac{2jd}{a}\right) - \theta\right)}{\sin\left(\tan^{-1}\left(\frac{2jd}{a}\right)\right)}F_v \right) \quad \textbf{Equation 2-87.}$$

where A_{str} = effective area of diagonal strut

D = compression force in diagonal strut (negative for compression)

F_h = Tension force in horizontal ties (positive for tension)

F_v = Tension force in vertical ties (positive for tension)

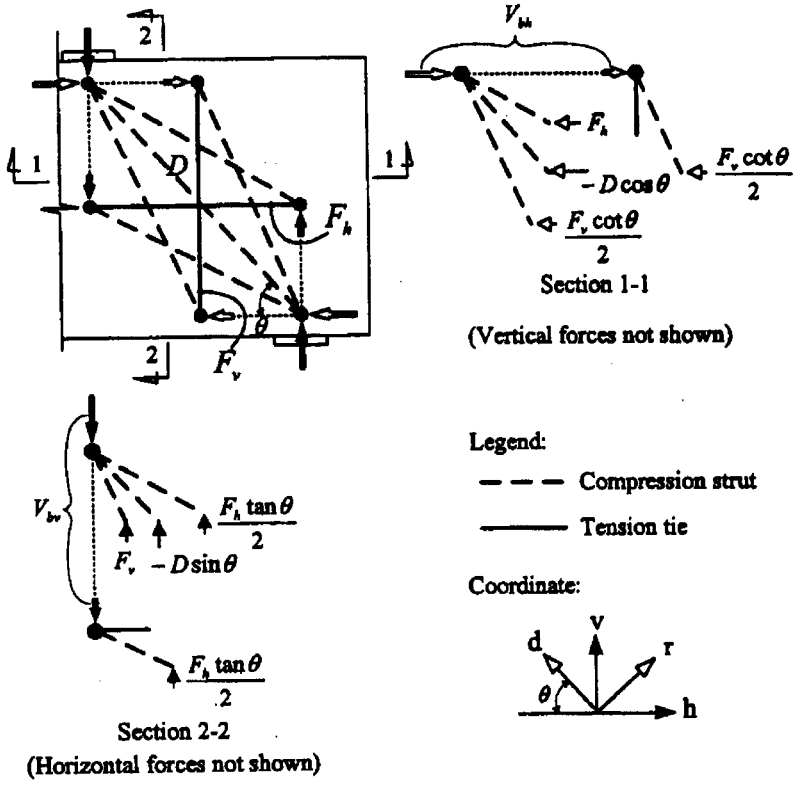

Figure 2-21. Strut and tie model for a deep beam

Cracked reinforced concrete in compression exhibits lower strength than uniaxially compressed concreted as shown in Figure 2-17 on page 53. The stress-strain softening curve of cracked concrete is represented as follows.

$$\sigma_d = -\zeta f'_c\left[2\left(\frac{-\varepsilon_d}{\zeta\varepsilon_o}\right)-\left(\frac{-\varepsilon_d}{\zeta\varepsilon_o}\right)^2\right] \text{ for } \frac{-\varepsilon_d}{\zeta\varepsilon_o} \le 1 \qquad \textbf{Equation 2-88.}$$

$$\sigma_d = -\zeta f'_c\left[1-\left(\frac{-\varepsilon_d/\zeta\varepsilon_o - 1}{2/\zeta - 1}\right)^2\right] \text{ for } \frac{-\varepsilon_d}{\zeta\varepsilon_o} > 1 \qquad \textbf{Equation 2-89.}$$

$$\zeta = \frac{5.8}{\sqrt{f'_c}}\frac{1}{\sqrt{1+400\varepsilon_r}} \le \frac{0.9}{\sqrt{1+400\varepsilon_r}} \qquad \textbf{Equation 2-90.}$$

where σ_d = the average principal stress in the d-direction

ζ = the softening coefficient

f'_c = the compressive strength of concrete

ε_d = average principal strain in the d-direction

ε_r = average principal strain in the r-direction

ε_o = concrete cylinder strain corresponding to the cylinder strength

The proposed design solution is shown in Figure 2-22. The softened truss model was applied to 123 test beams available in literature from such researchers as de Paiva and Siess, Kong et al., Smith and Vantsiotis, Fang et al., and Chen. The following conclusions were drawn from this study.

- The softened strut-and tie model consistently predicted 123 deep beams measured shear strengths with a reasonable accuracy. These beams had a wide range of horizontal and vertical web reinforcement ratios, concrete strengths and shear to depth spans.
- The ACI 318-95 Code was found to underestimate the contribution of concrete and overestimated the contribution of web reinforcement on the shear strength of deep beams.

- The ACI 318-95 Code predictions are conservative
- The proposed model provides valuable insight into the shear strength and behaviour of reinforced concrete deep beams.

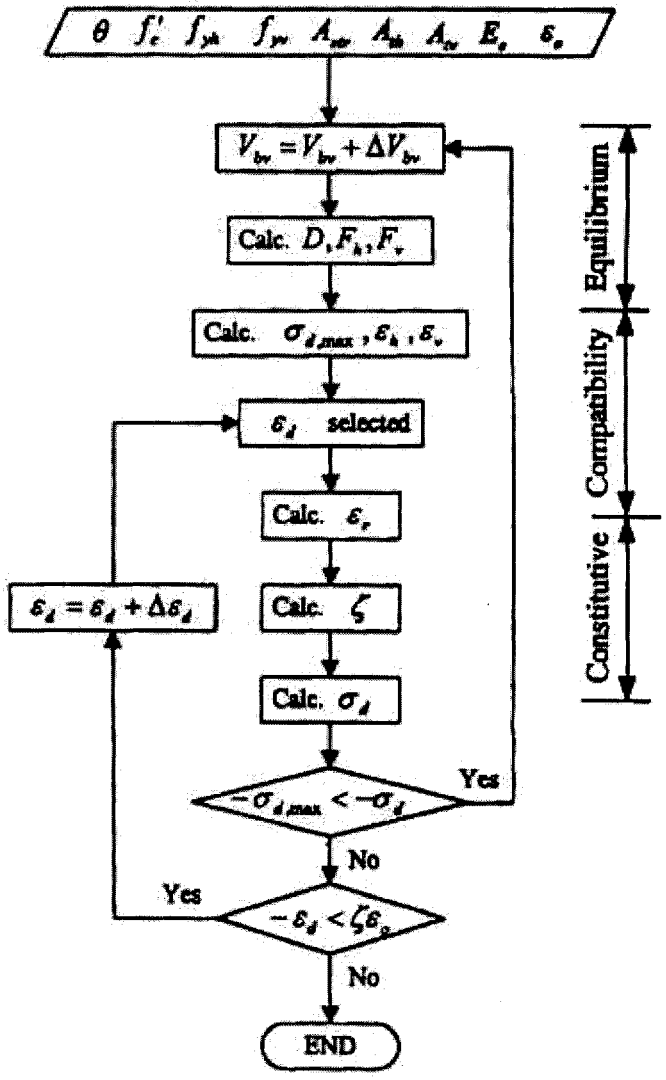

Figure 2-22. Flow chart showing solution algorithm[17]

2.5 Current Canadian Code

The current Canadian Standard (CSA A23.3-94)[5] recommends five different design procedures for shear. These recommendations are outlined in the following table.

Table 2-1. Shear design methods as recommended by CSA A23.3-94

Method	Applicability
Simplified Method, (Cl. 11.3)	Flexural regions not subjected to significant axial tension
General Method, or the Strut-and-tie Model (Cl. 11.4 or 11.5)	Flexural regions where traditional beam theory (plane sections remain plane) is reasonably applicable.
Strut-and-tie Model (Cl. 11.5)	Regions near discontinuity where plane section remaining plane is not applicable, including affects of axial forces. (deep beams and corbels)
Shear Friction (Cl. 11.6)	Interface shear transfer, situations where failure occurs by sliding along a plane of weakness
Two-way shear or punching shear (Cl. 13.4 & Cl. 13.5)	Thin slabs and footings with two-way action, subjected to concentrated loads

As can be seen from Table 2-1, the strut-and-tie method as outlined by Clause 11.5 of CSA A23.3-94[5] is applicable to the design of reinforced concrete deep beams and corbels.

Clause 11.5 states:

> *"The strength of reinforced concrete structures, members, or regions may be investigated by idealizing the reinforced concrete as series of reinforcing steel tensile ties and concrete compressive struts interconnected at nodes to form a truss capable of carrying all factored loads to the supports. In determining the geometry of the truss, account shall be taken of the required dimensions of the compressive struts and tension ties."*

Strength of the compression strut

The dimensions of the strut shall be large enough that the calculated compressive force does not exceed:

$$C \le \phi_c A_{cs} f_{cu}$$ **Equation 2-91.**

where A_{cs} = the area of the compression strut defined by clause 11.5.2.2,

$$f_{cu} = \frac{f'_c}{0.8 + 170\varepsilon_1} \le 0.85f'_c$$ **Equation 2-92.**

$$\varepsilon_1 = \varepsilon_s + (\varepsilon_s + 0.002)\cot^2\theta_s$$ **Equation 2-93.**

ϕ_s = the smallest angle between the compression strut and the adjoining tension ties as shown in, and

ε_s = the tensile strain in the tension tie inclined at ϕ_s to the compression strut.

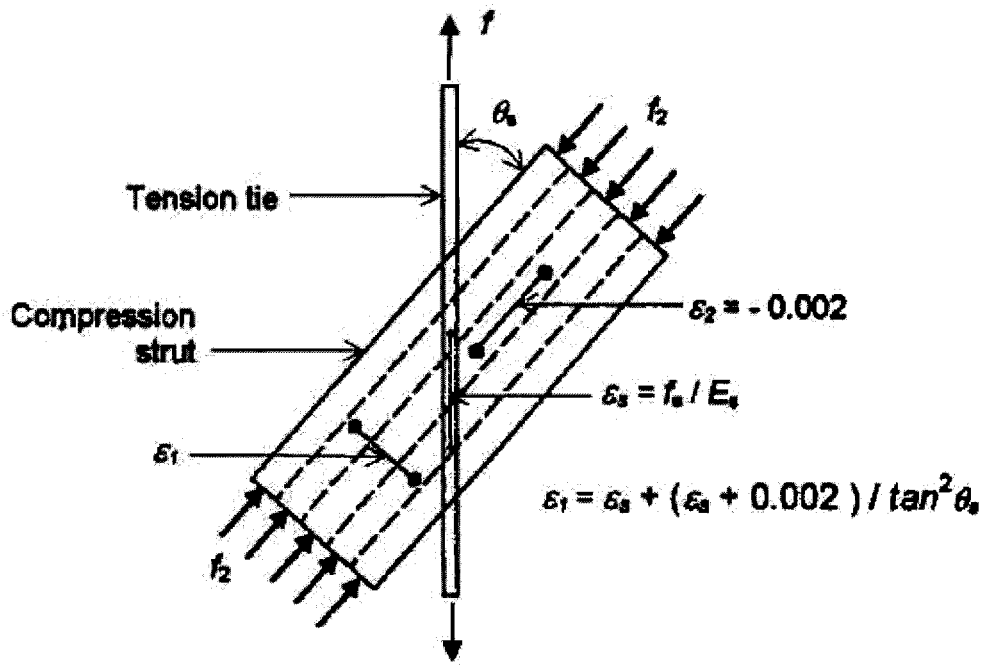

Figure 2-23. Orientation of tension tie with respect to the compression strut[8]

For regions of the compression strut not crossed by a tension tie, the limit for compression resistance by the strut is $0.85f'_c$. The expression for ε_s is based on

the assumption that the principal compression strain in the direction of the strut is equal to 0.002 (which corresponds to the highest point in the stress-strain curve).

Guidelines for the dimension of the compression strut are shown in the following figure.

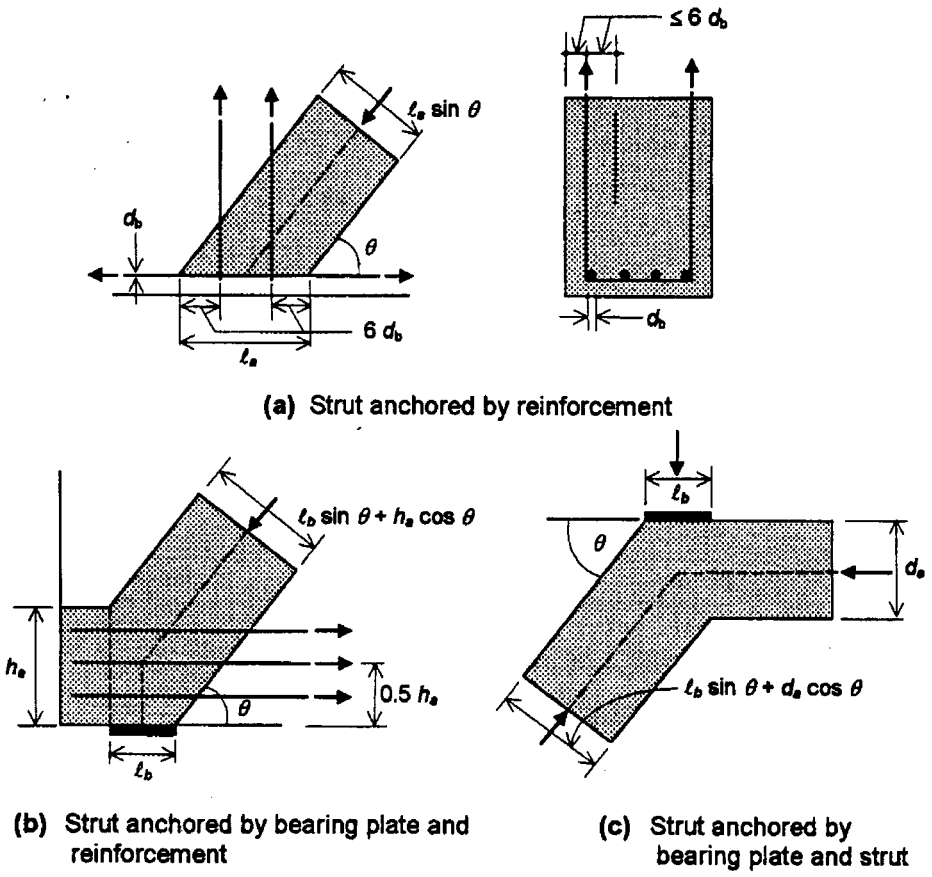

Figure 2-24. Guidelines for determining the dimensions of the strut and tie[5]

Strength of the tension tie

The area of reinforcement required for the tension tie, much ensure that the calculated tensile force in the tie does not exceed:

$$T_{calc} \leq \phi_s A_{st} f_y \qquad \textbf{Equation 2-94.}$$

where A_{st} = area of the tension tie, and

f_y = yield strength if the reinforcement.

Stress limits in node regions

The Canadian code also places a limit on nodal stresses. Concrete compressive stresses cannot exceed the following limits:

$0.85\phi_c f'_c$ in node regions bounded by compression struts and bearing areas,

$0.75\phi_c f'_c$ in node regions anchoring a tension tie in only one direction, and

$0.65\phi_c f'_c$ in node regions anchoring tension ties in more than one direction.

The Canadian code seems to contradict itself, on one hand it clearly indicates that the Compression Field Theory should only be used on flexural regions where traditional beam theory (plane sections remain plane) is reasonably applicable, yet the code then uses the equations derived by this theory to define the strength of the compression strut. The main problems with this are that Equation 2-92 is applicable only if a tension tie crosses a compression strut. If no stirrups are used, then there is no reduction of compressive strength at the midpoint of the strut for example. Other problems are, that the maximum compressive strain is assumed to reach 0.002 along the strut, that the strain in the tension tie must be assumed, and that no reasoning is given for the strut dimensions given in Figure 2-24.

2.6 Summary

The literature review presented here has clearly shown that a lot of research has been done in this area. While each researcher presented a different approach, one thing is certain, deep beams and corbels should be designed using some sort of compression strut and tension tie system. There has been no research done on measuring the actual compressive strains along the strut and the corresponding tensile strains perpendicular to the strut on a deep beam subjected to a point load. The research done here will try to address this problem using experimental and finite element analysis.

3 Experimental Program

3.1 Test Program

3.1.1 Introduction

The current study consists of twelve deep beams fabricated and tested in four groups of three beams. After an extensive literature review, it was evident that deep beams can be defined as having up to five strength limits.

1. First flexural cracking which may result in ultimate failure in the case of deep beams without or with very little tension reinforcement,
2. Inclined cracking under moment and shear due to beam action,
3. Inclined splitting due to arch action,
4. Ultimate flexural failure due to yield of tensile steel or crushing of concrete in compression, and
5. Excessive deformation of the beam.

The twelve beams tested were designed to study the ultimate strength behaviour of deep beams and to develop a simplified design model. Sufficient reinforcement was used to ensure a diagonal cracking failure. Stirrups were provided in only half of the test beams. In this way it was possible to study the stress-strain distribution along the compression strut for deep beams with and without stirrups.

It was decided to keep the beam depth constant while varying the shear span. In addition, sufficient tension reinforcement was used to ensure failure in the compression strut.

3.1.2 Beam Details

The overall dimensions and reinforcement arrangement for the twelve beams tested are shown in Figure 3-1, Figure 3-2, Figure 3-3 and Figure 3-4. In all cases the main reinforcement consisted of horizontal M20 bars. Anchorage of the main tension reinforcement was enhanced by providing 180-degree hooks at the bar ends. The vertical reinforcement consisted of 6mm-closed stirrups.

Strain gauges were attached to one specimen from each of the four groups. Steel strain gauges were applied to the main tensile reinforcement as well as to a 6mm non-deformed steel bar situated along the diagonal compression strut as shown in Figure 3-5. Strain gauges were also attached to the surface of the concrete test beams as shown in Figure 3-6, Figure 3-7 and Figure 3-8.

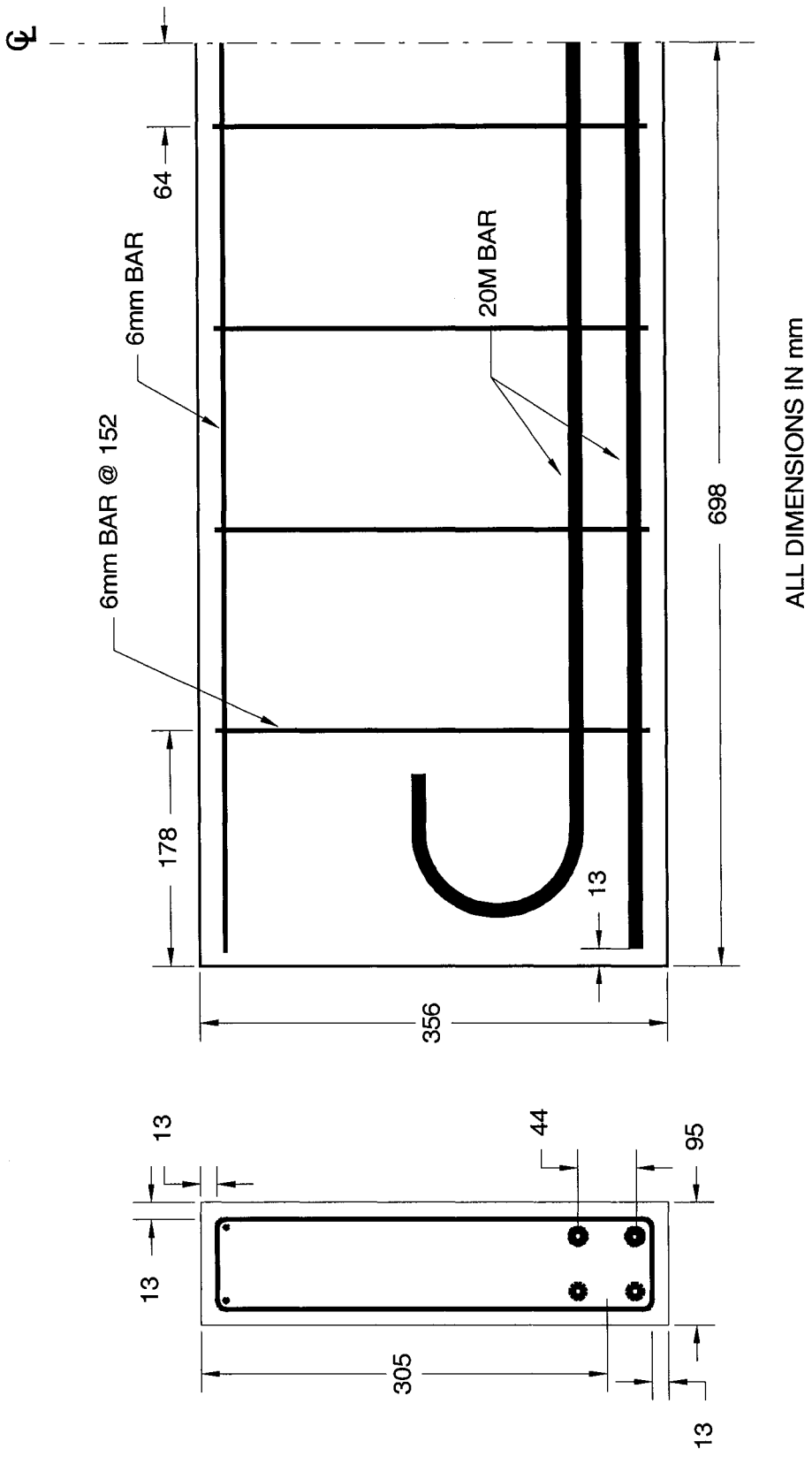

Figure 3-1. Reinforcement details for test beams B150S6, B250S6 and B350S6.

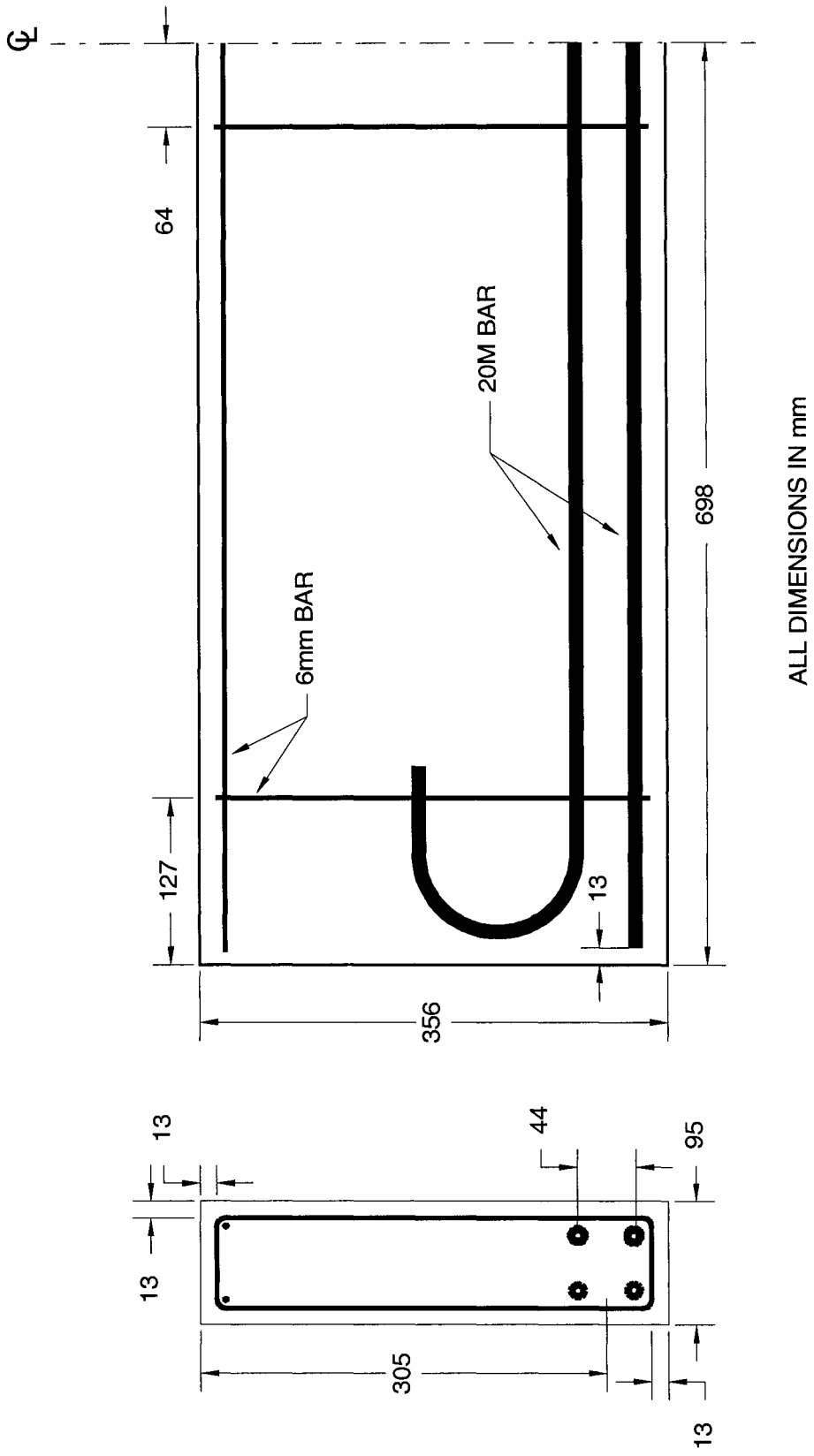

Figure 3-2. Reinforcement details for test beams B150S19, B250S19 and B350S19.

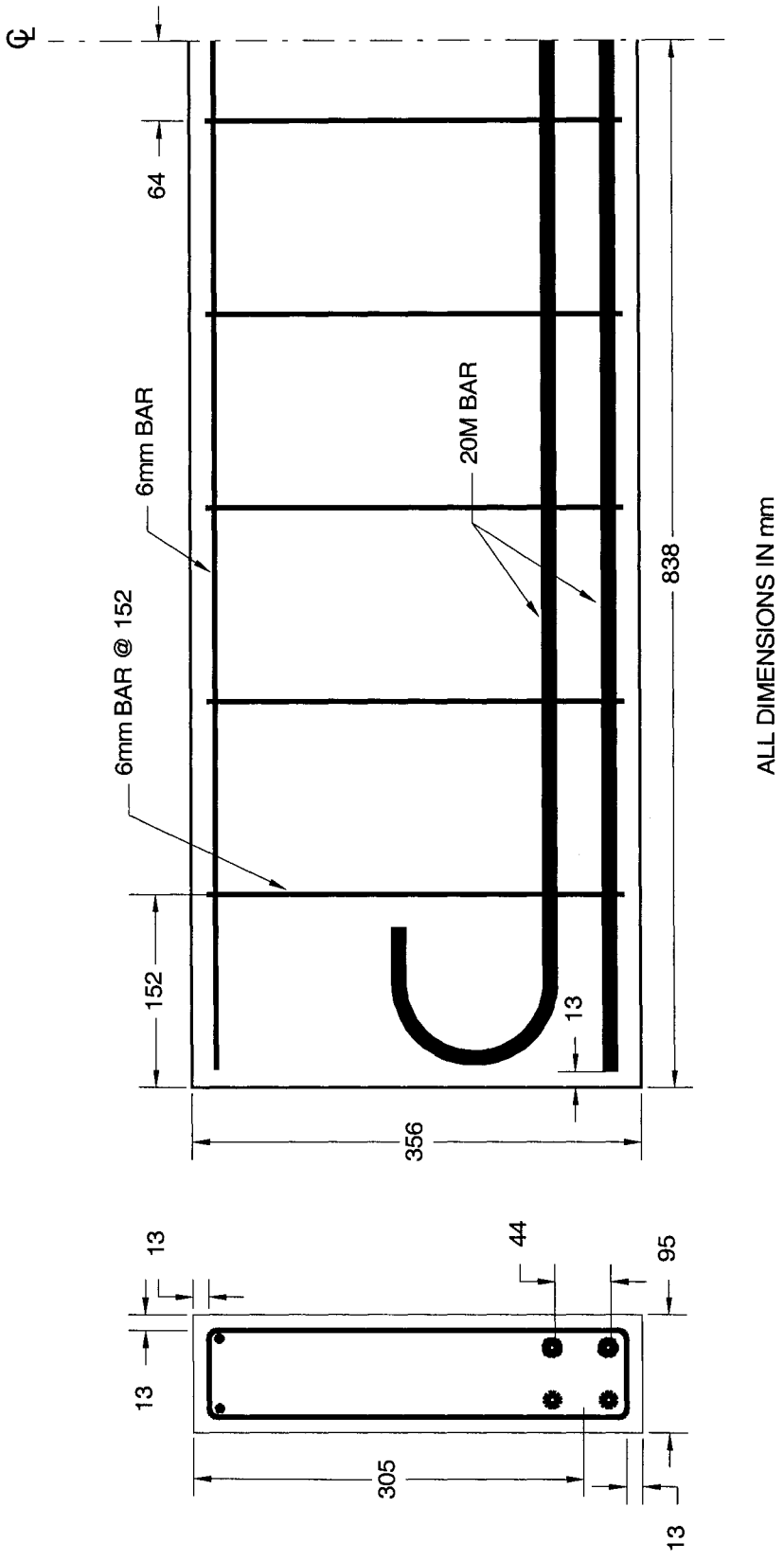

Figure 3-3. Reinforcement details for test beams B160S6, B260S6 and B360S6.

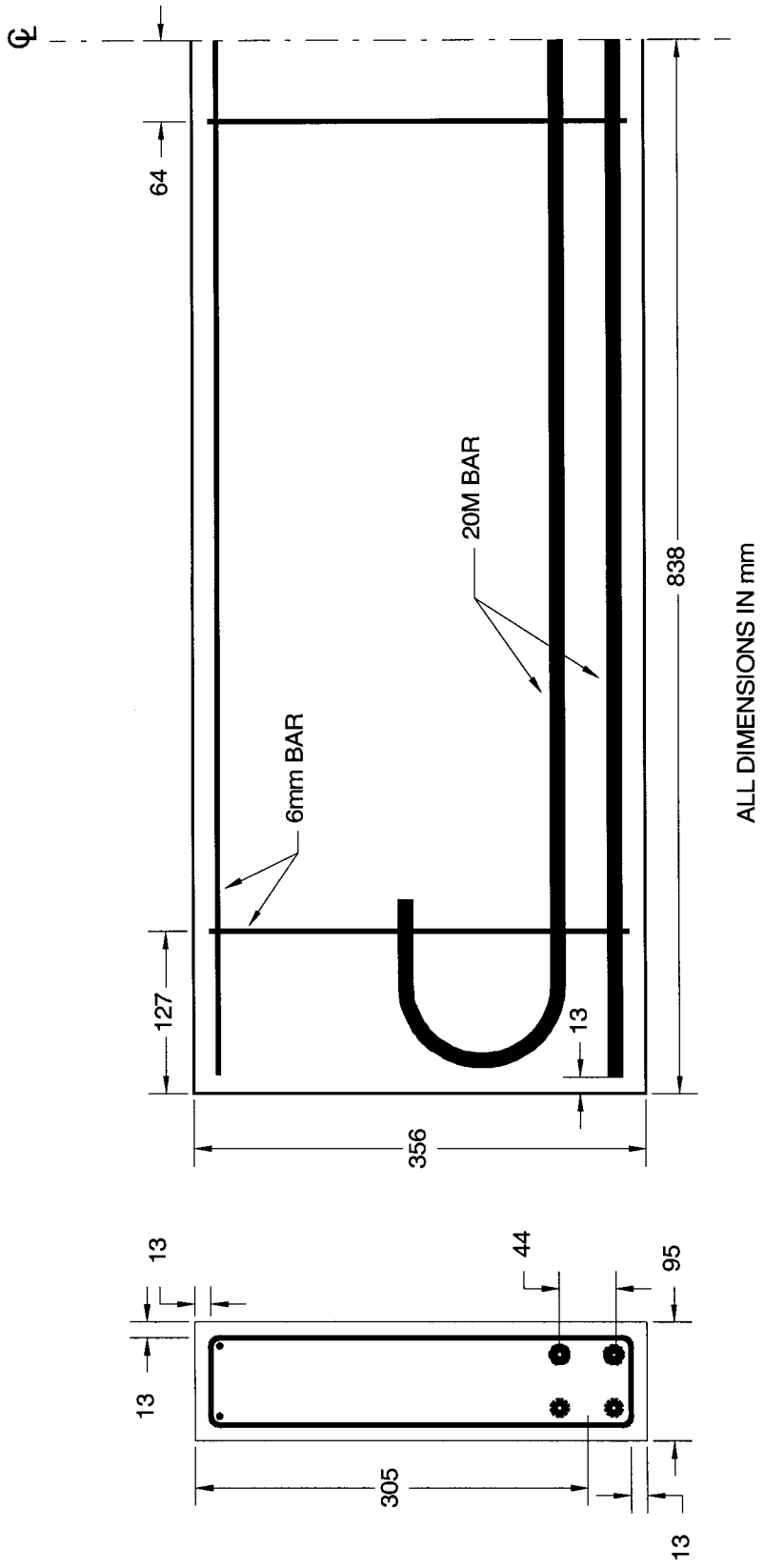

Figure 3-4. Reinforcement details for test beams B160S25, B260S25 and B360S25.

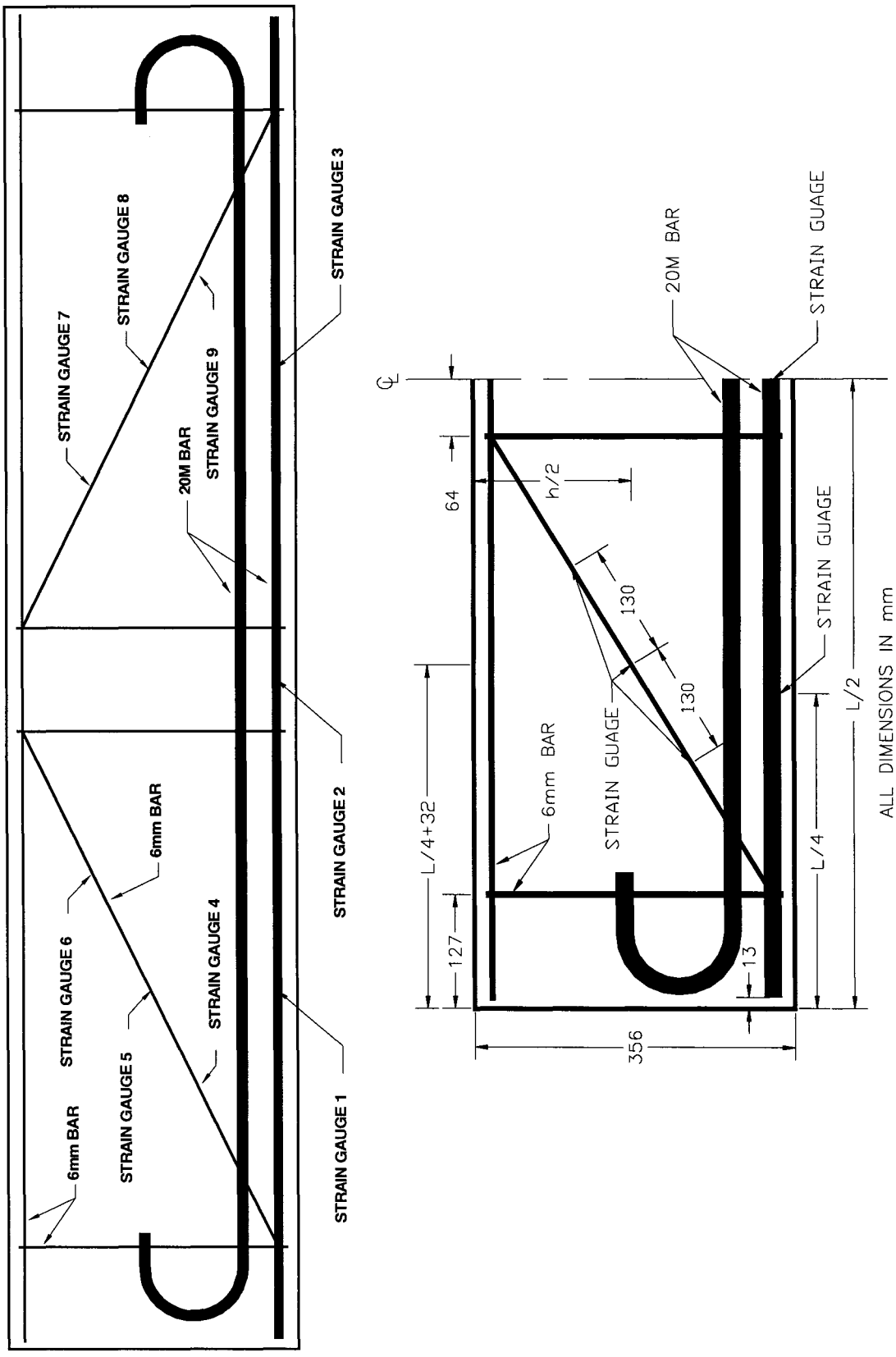

Figure 3-5. Locations of strain gauges placed on steel reinforcement.

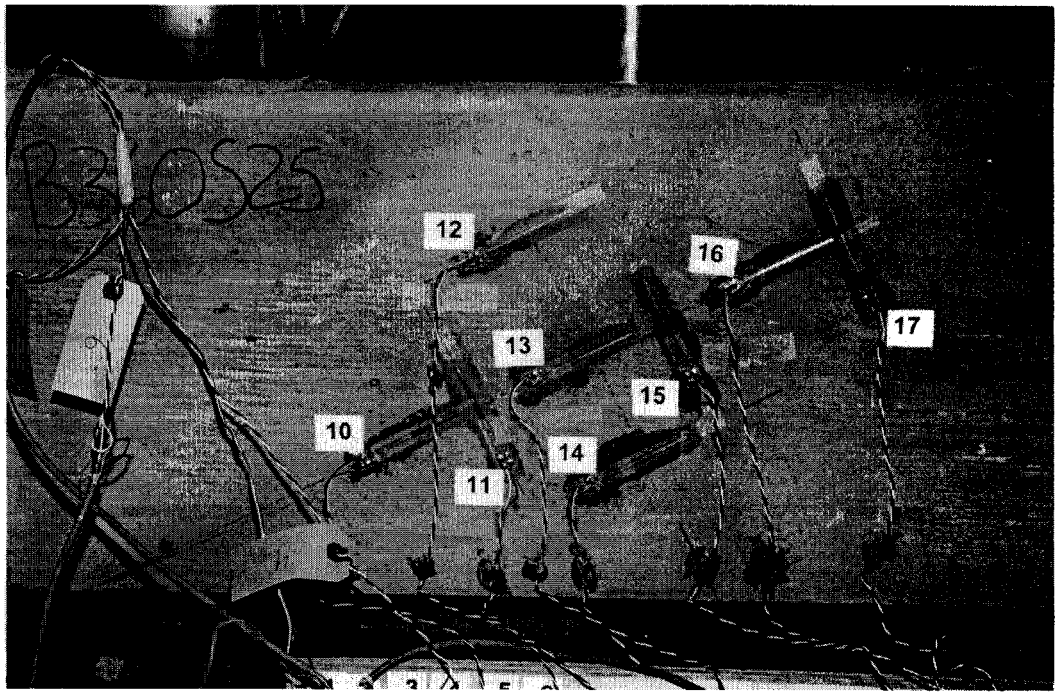

Figure 3-6. Location of concrete strain gauges on the left side of test beam.

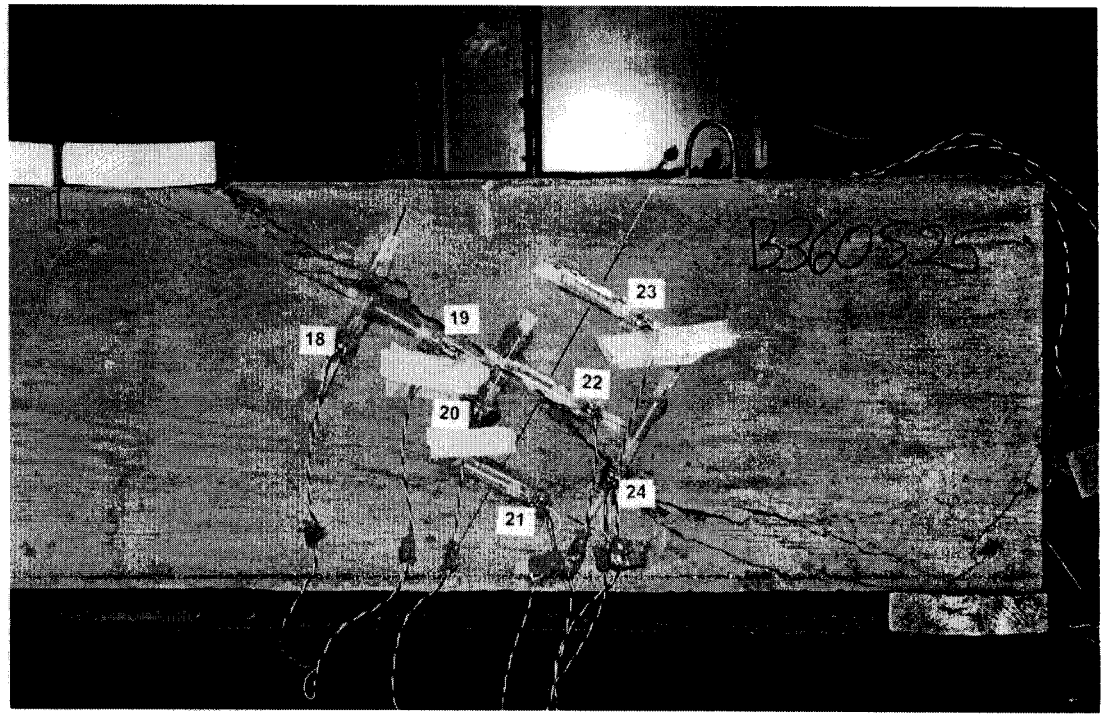

Figure 3-7. Location of concrete strain gauges on the right side of test beam.

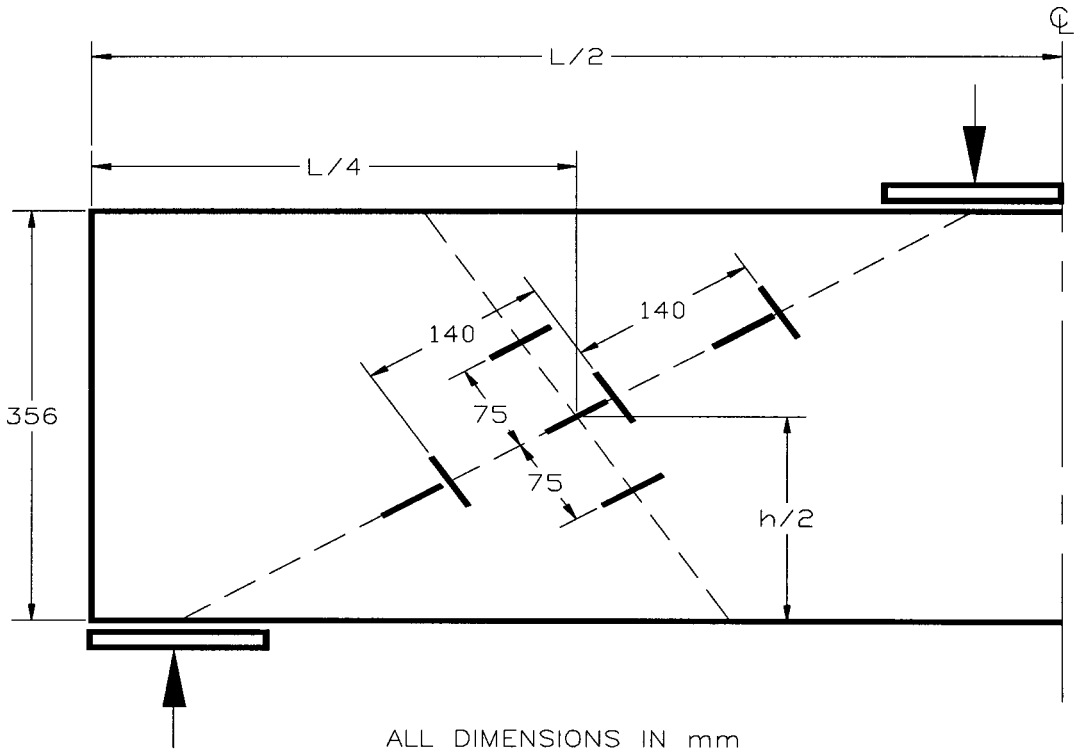

Figure 3-8. Placement of concrete strain gauges.

3.2 Materials

3.2.1 Concrete

The concrete used in the study was supplied by a local ready-mix concrete supplier and had the following specifications:

- 6mm (1/4") crushed stone aggregate,
- 0.5 water to cement ratio, and
- 80mm slump.

Although 25 MPa concrete was requested, the 28-day concrete strength varied from 16.5 MPa (2400 psi) to 34.5 MPa (5000 psi). Three 76mm (3") diameter and 152mm (6") high concrete cylinders were cast for each of the test beams. A summary of the concrete strength for each of the test beams is given in Table 3-1.

Table 3-1. Concrete strength determined from test cylinders.

Test Sample	f'_c (MPa)	f'_c (psi)
B150S6	28.9	4191
B250S6	34.5	5003
B350S6	28.9	4191
B150S19	28.9	4191
B250S19	28.9	4191
B350S19	25.5	3698
B160S6	28.9	4191
B260S6	28.9	4191
B360S6	34.5	5003
B160S25	16.5	2393
B260S25	34.5	5003
B360S25	16.5	2393

At the time of casting, the concrete beams and test cylinders were vibrated using a pencil vibrator. Within a few hours of casting, the test samples and cylin-

ders were covered with canvas and plastic. The canvas was watered twice daily for 14 days after which the formwork was removed.

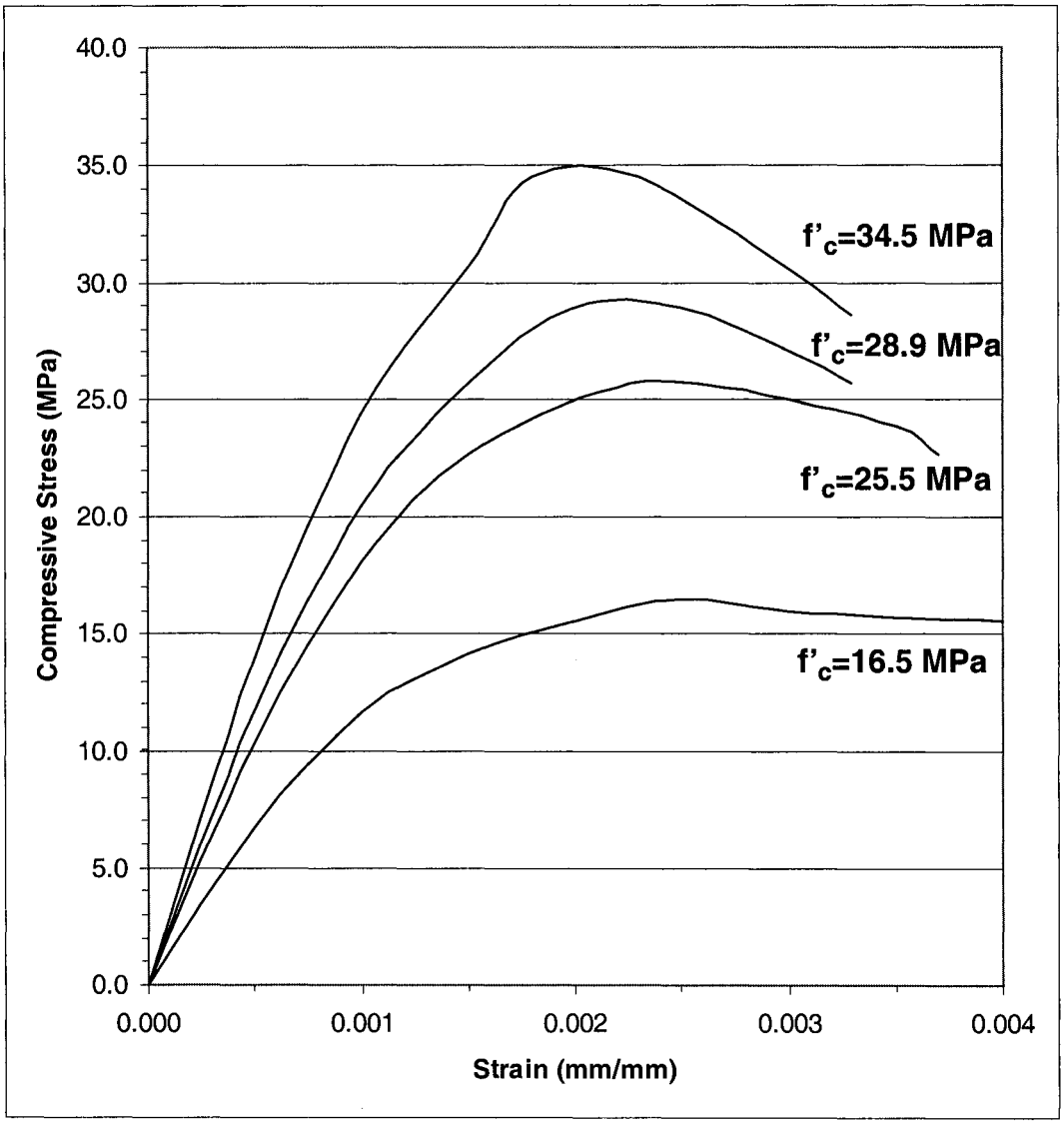

Figure 3-9. Concrete compressive stress-strain relationship

3.2.2 Steel

The main tensile reinforcement consisted of deformed M20 bars (bar diameter = 19.5mm), with a yield strength of 440 MPa (63.8 ksi). Non-deformed 6mm steel bars were used as vertical reinforcement. In addition, one sample from each of the four test groups had a 6mm non-deformed steel bar placed along a diagonal line

from the loading point to the support. Three steel strain gauges were placed on these bars to measure strains along the compression strut.

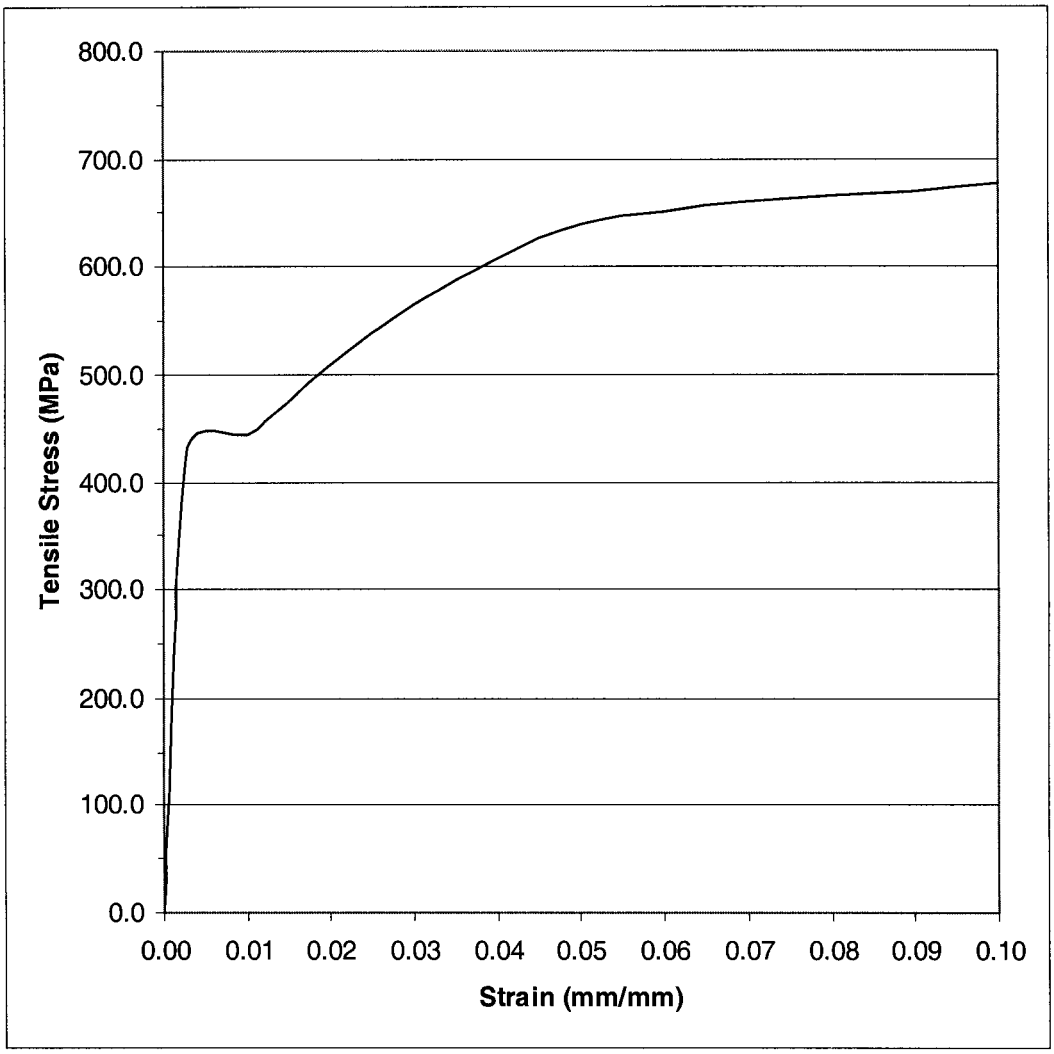

Figure 3-10. Steel tensile stress-strain relationship

3.3 Instrumentation

Monitoring equipment was set up to measure loads, displacements, and concrete and steel strains. The following sections describe the system of instrumentation.

3.3.1 Strain Gauges

Strain gauges were applied to one sample from each of the four test groups. Showa strain gauges (N11-FA-60-120-11) were used to measure the strain on the main steel reinforcement as well as a steel rod placed along the compression strut. Precision strain gauges (CEA-06-125UN-120) were used to measure strains in the concrete. Strain gauges placed on the reinforcement were covered with epoxy to protect them during casting. In all, four samples had three strain gauges placed on the main tensile reinforcement, six gauges on the steel rods placed along the compression struts, and 15 gauges placed on the concrete surface.

3.3.2 Displacements

Displacements were measured at the midspans of the beams as well as at 305mm (12" for the shorter test samples) or 406mm (16" for the longer test samples) from each end. Location of deflection gauges are shown in Figure 3-11. Digital gauges with a least count of ± 0.01 mm were used to measure the displacements.

3.4 Testing

3.4.1 Testing Procedure

Testing was done using a Tinius Olsen compression machine. The test setup is shown in Figure 3-11. The supports, as well as the loading points measured 127mm (5") in length. The load was applied at midpoint as two point loads. Loading was applied at 11 kN (2.5 kips) intervals until the total load was 133 kN (30 kips). Loading was then applied at 22 kN (5 kips) intervals until specimen failure. The initial load increment was small in order to collect many readings from the strain gauges. After the load reached 133 kN it was found that many of the strain gauges on the concrete had failed due to cracks passing through them, therefore the load increment was increased.

At each increment, the load was held constant so that deflection and electronic strain gauge readings could be taken. After the readings were taken, the test beam was inspected for any new or extended cracks. These observations were recorded on the beam using felt tipped markers. Once the readings and observations were taken, the loading was then increased by the next increment and the procedure was repeated.

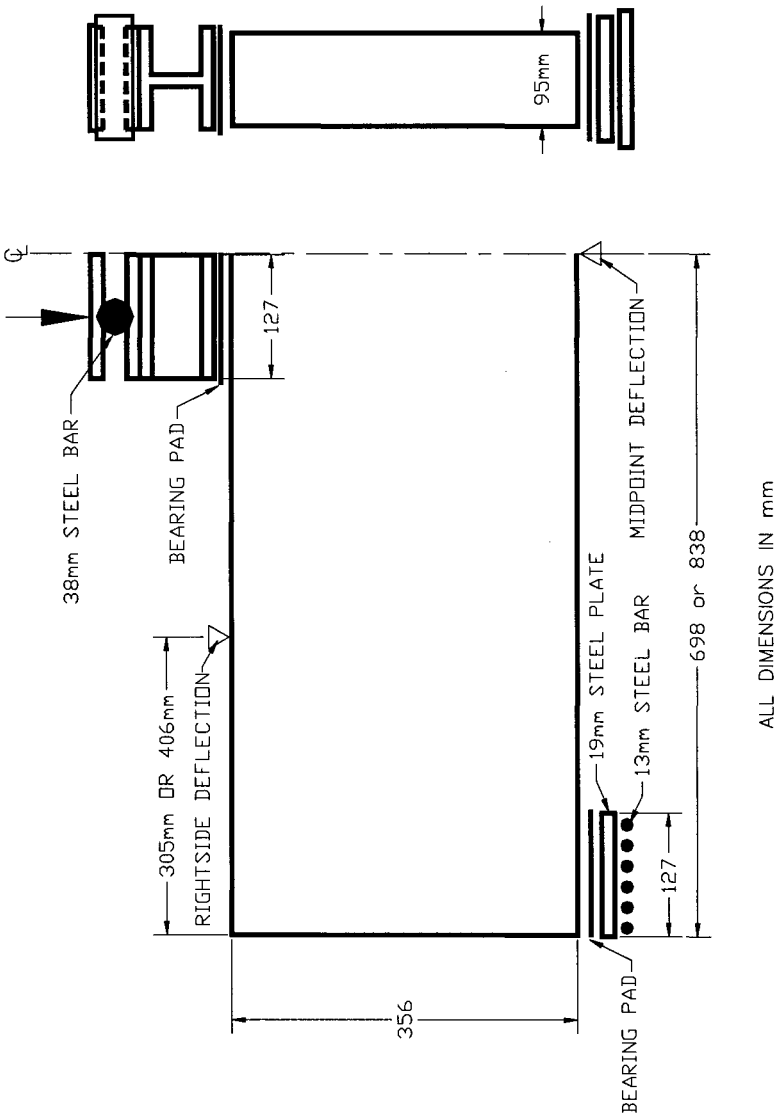

Figure 3-11. Schematic of test loading setup.

3.4.2 Test Setup

The specimens were positioned in the Tinius Olsen compression machine for midpoint loading as shown in Figure 3-11. The beams rested on two 19mm (3/4") steel plates which in turn rested on six 13mm (1/2") diameter steel bars.

A bearing pad was placed between the steel plates and the test samples to reduce the effects of surface irregularities. After the beam was centered and leveled, two W steel sections were placed atop the midspan. Cardboard was again placed between the surface of the beam and the loading plate. Throughout the setup procedure, care was taken to assure that the samples were vertically aligned with all load points and reactions in order to minimize the possibility of a stability failure.

For the samples with strain gauges, all wiring was connected on the morning of the testing. Prior to testing, the data acquisition system was electronically zeroed. Digital deflection gauges were placed and zeroed prior to testing.

3.5 Objective

The objective of the test program was to measure the stress and strain distribution parallel to the compression strut, as well as perpendicular to the compression strut. Test beams were designed with sufficient reinforcement to ensure a diagonal cracking failure. Beams were also designed with and without stirrups to determine their effect on the stress-strain distribution. The experimental findings will then be compared to a finite element analysis. The research work will then be compared to the current Canadian design code.

4 Test Results

4.1 Presentation of Results

In this chapter the experimental results are presented for the twelve test beams described in Chapter 3. Analysis of these results with comparison to the finite element predictions are discussed in Chapter 6.

The failure loads measured during the experimental testing are given in Section 4.2. The load versus displacement observations are given in Section 4.3.

Results for each of the individual beams tested along with strain data and crack patterns are presented in Section 4.4. The strain data is presented graphically to aid in the interpretation of the results.

4.2 Failure Loads

Failure loads were recorded by the Tinius Olsen compression machine. The applied load which resulted in failure for each of the twelve test beams are given in Table 4-1.

Table 4-1. Measured failure loads of the test beams.

Beam	f'_c (MPa)	f'_c (psi)	Failure load (kN)	Shear Span a (mm)	Depth h (mm)	Ratio a/h
B150S6	28.9	4191	371.9	559	356	1.57
B250S6	34.5	5003	496.4	559	356	1.57
B350S6	28.9	4191	422.6	559	356	1.57
B150S19	28.9	4191	356.7	559	356	1.57
B250S19	28.9	4191	378.1	559	356	1.57
B350S19	25.5	3698	311.4	559	356	1.57
B160S6	28.9	4191	392.8	711	356	2.00
B260S6	28.9	4191	371.9	711	356	2.00
B360S6	34.5	5003	355.8	711	356	2.00
B160S25	16.5	2393	169.9	711	356	2.00
B260S25	34.5	5003	355.8	711	356	2.00
B360S25	16.5	2393	151.2	711	356	2.00

4.3 Deflections

Deflections of eight deep beam specimen were measured at three locations as shown in Figure 3-11 on page 81.

- 305mm (12") from the right side for beams 1372mm (54") long or 406mm (16") from the right side for beams 1676mm (66") long

  This is designated as "Deflection Right" in Figures 4-1 to 4-8.

- 305mm (12") from the left side for beams 1372mm (54") long or 406mm (16") from the left side for beams 1676mm (66") long

  This is designated as "Deflection Left" in Figures 4-1 to 4-8.

- at the midspan

  This is designated as "Deflection Middle" in Figures 4-1 to 4-8.

The load versus deflection diagram for these eight test beams are shown in Figure 4-1 to Figure 4-8.

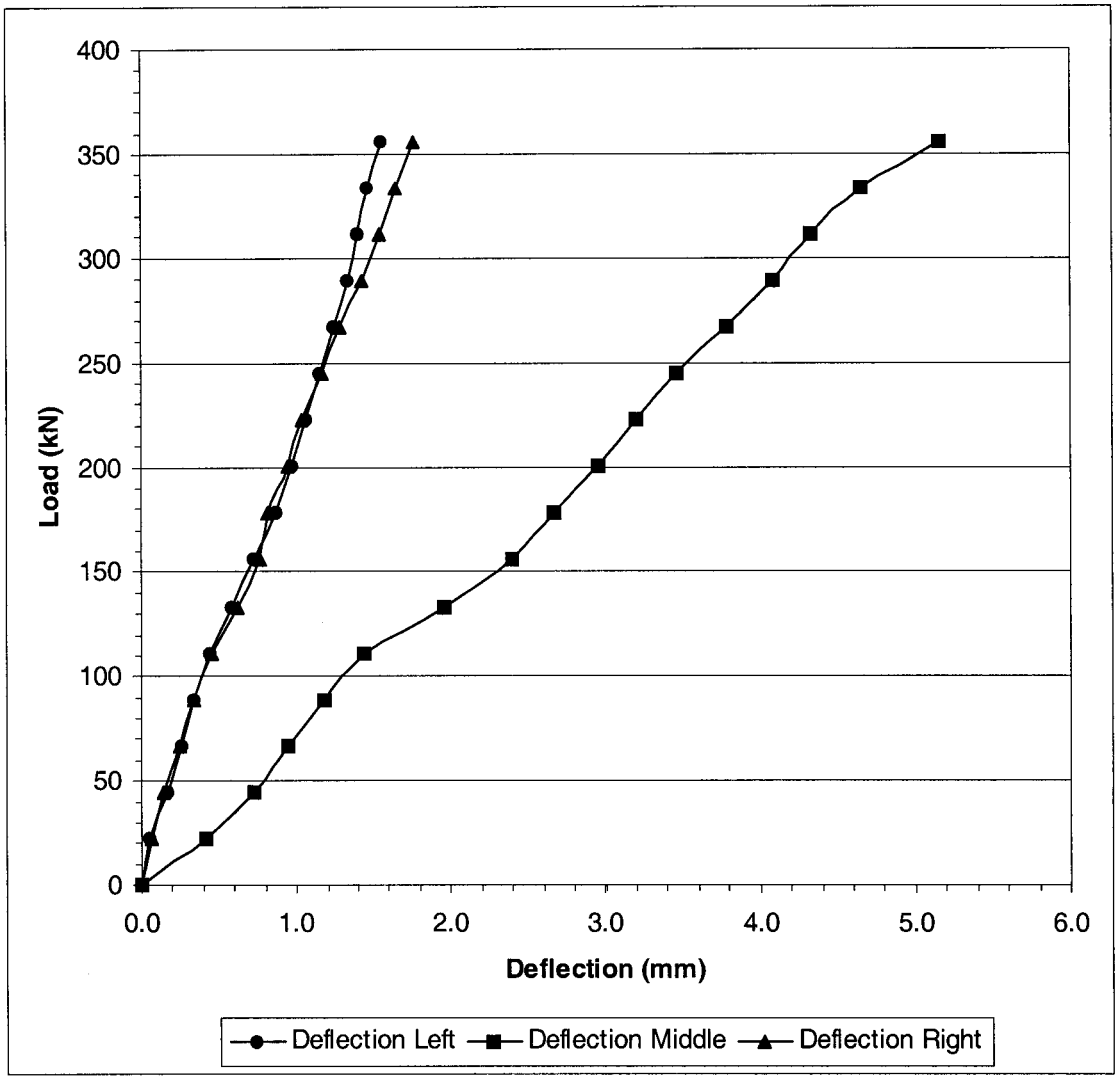

Figure 4-1. Deflection of beam B150S19.

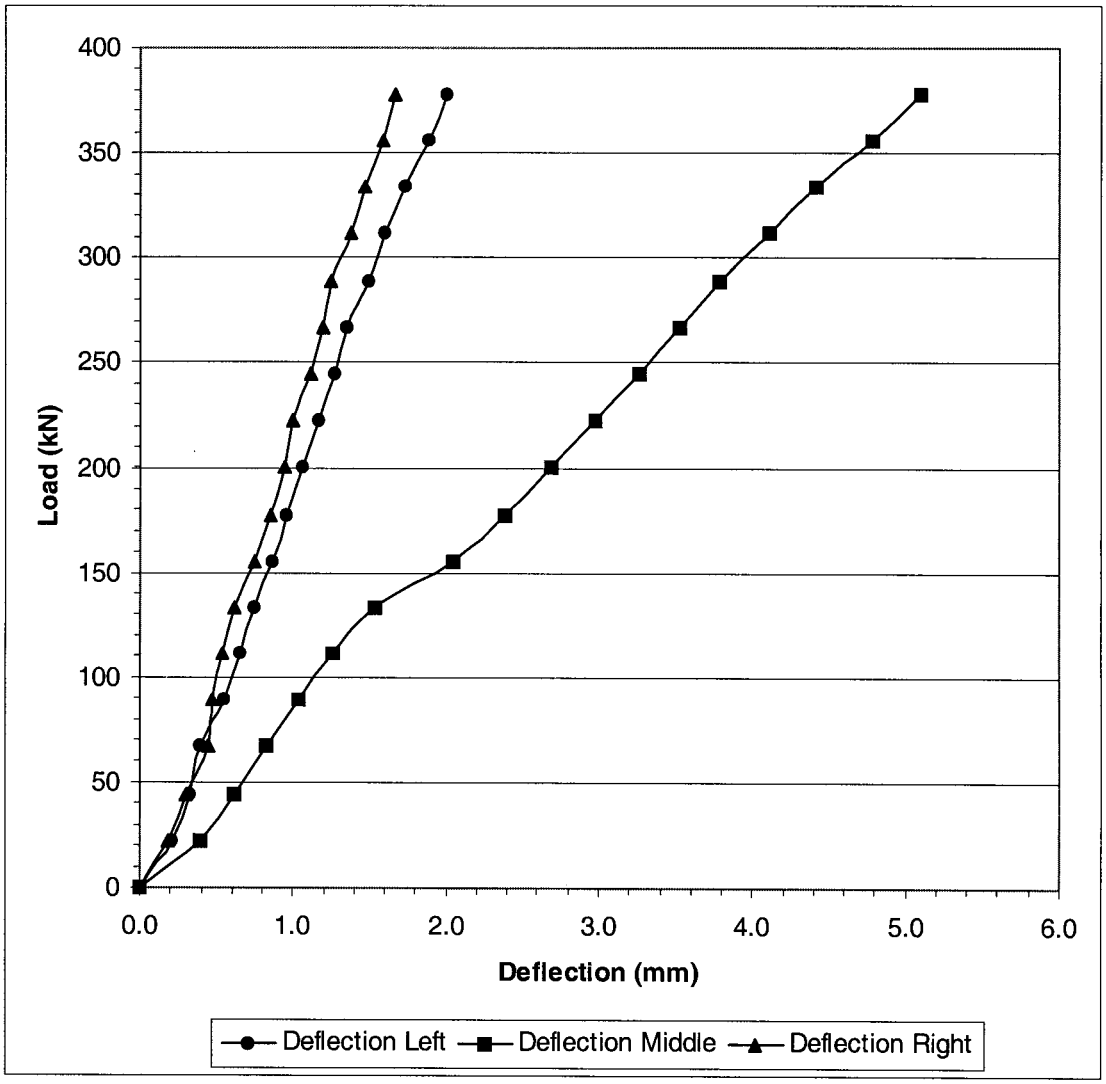

Figure 4-2. Deflection of beam B250S19.

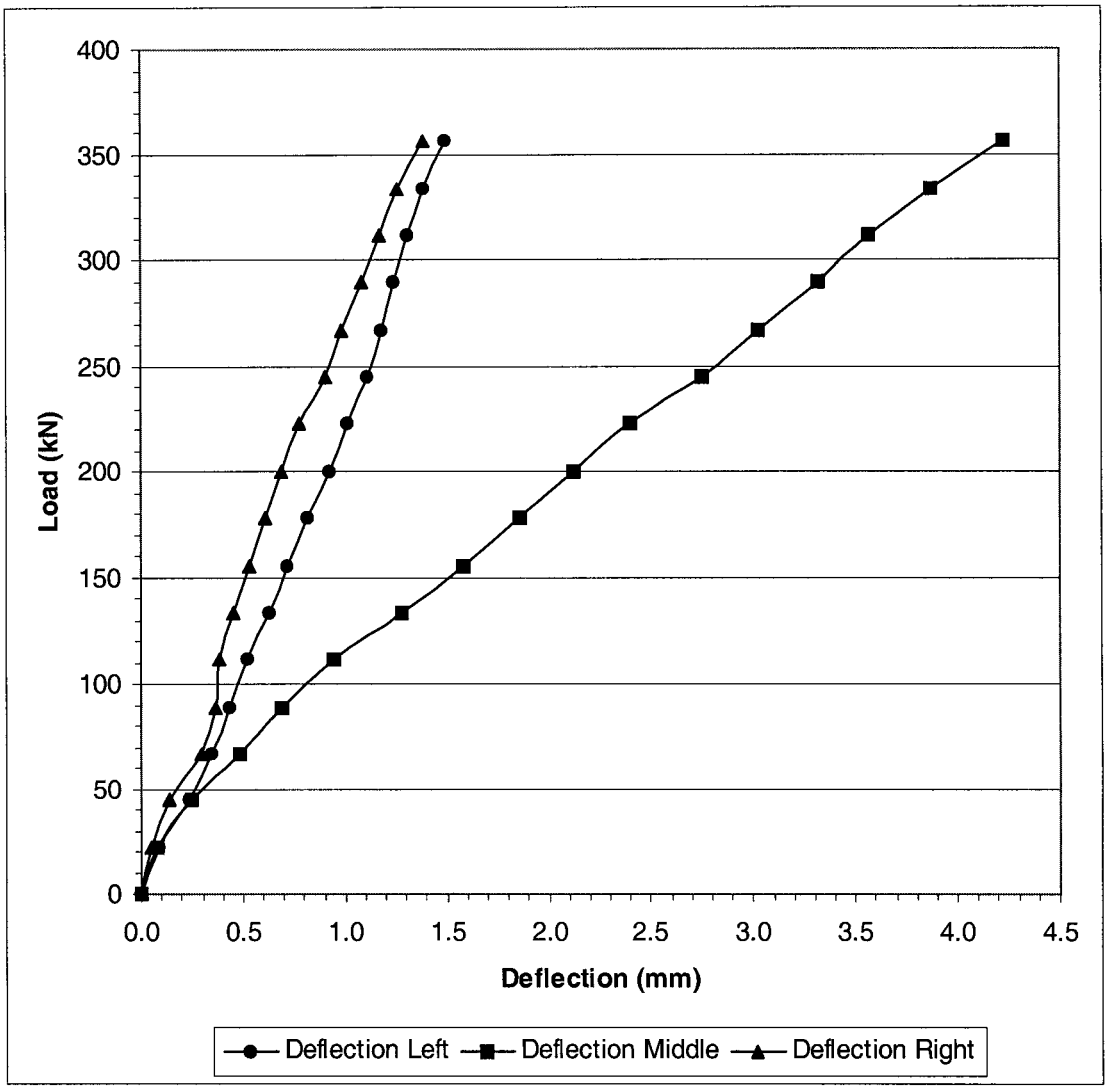

Figure 4-3. Deflection of beam B150S6.

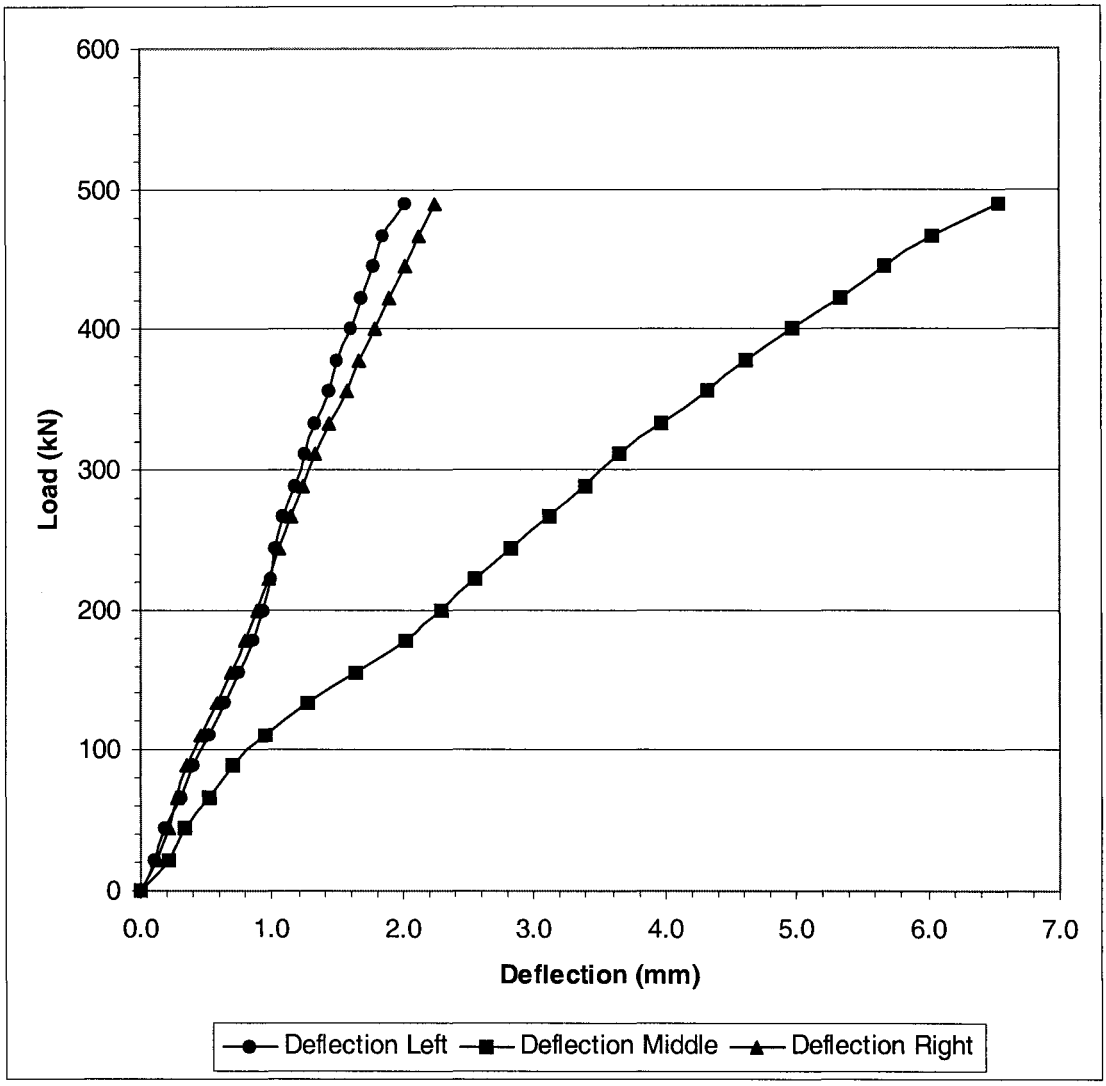

Figure 4-4. Deflection of beam B250S6.

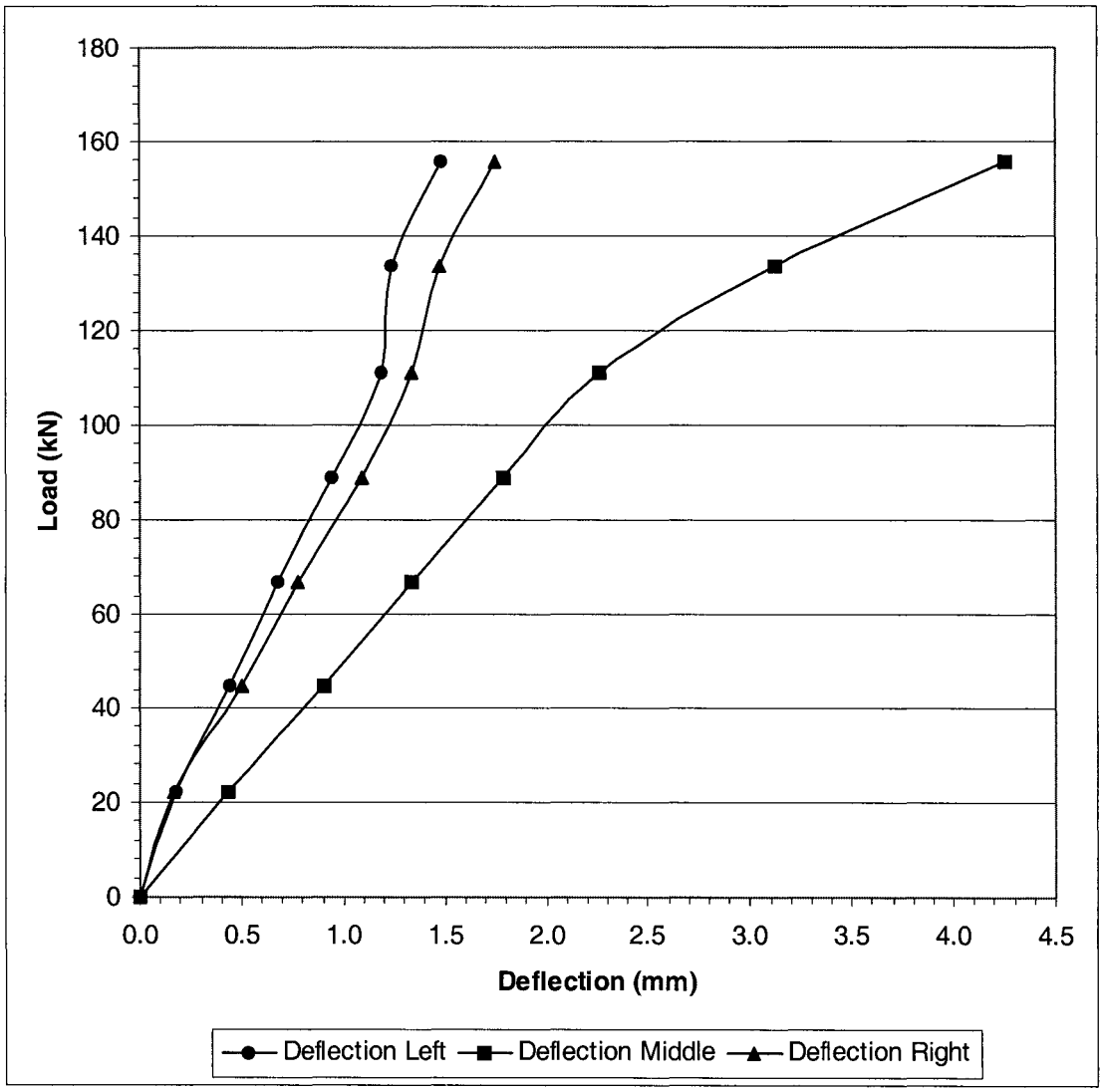

Figure 4-5. Deflection of beam B160S25.

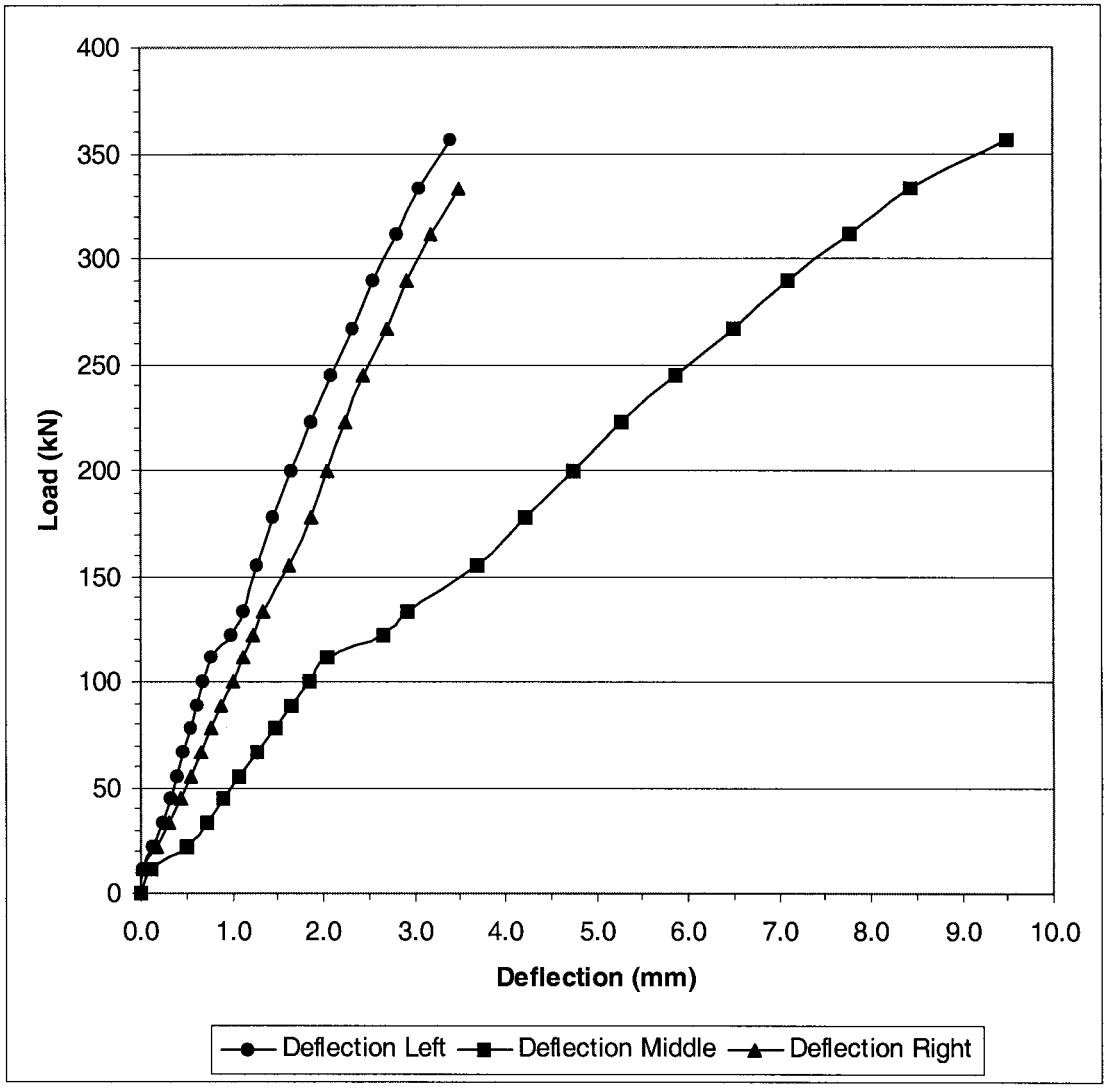

Figure 4-6. Deflection of beam B260S25.

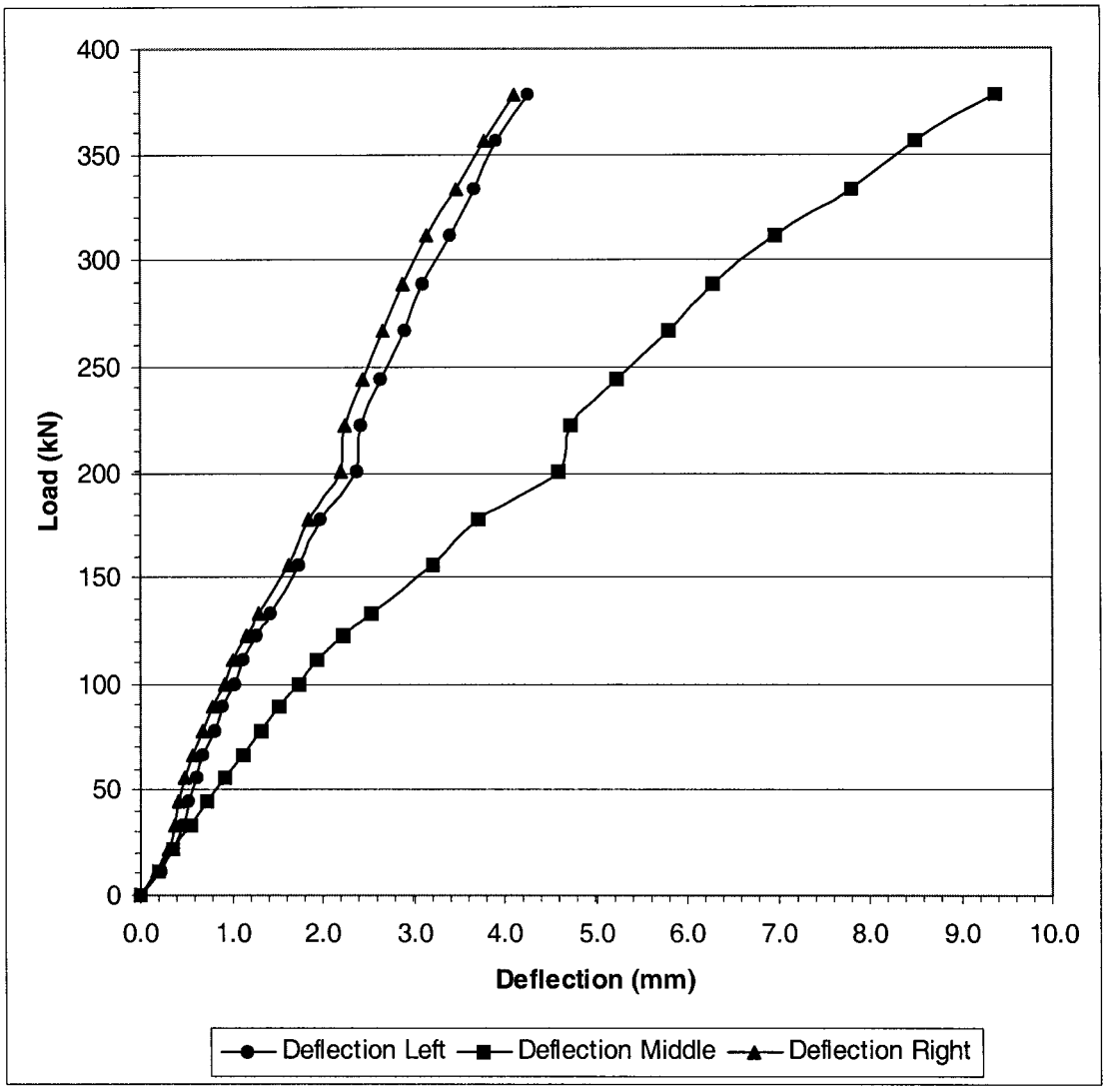

Figure 4-7. Deflection of beam B160S6.

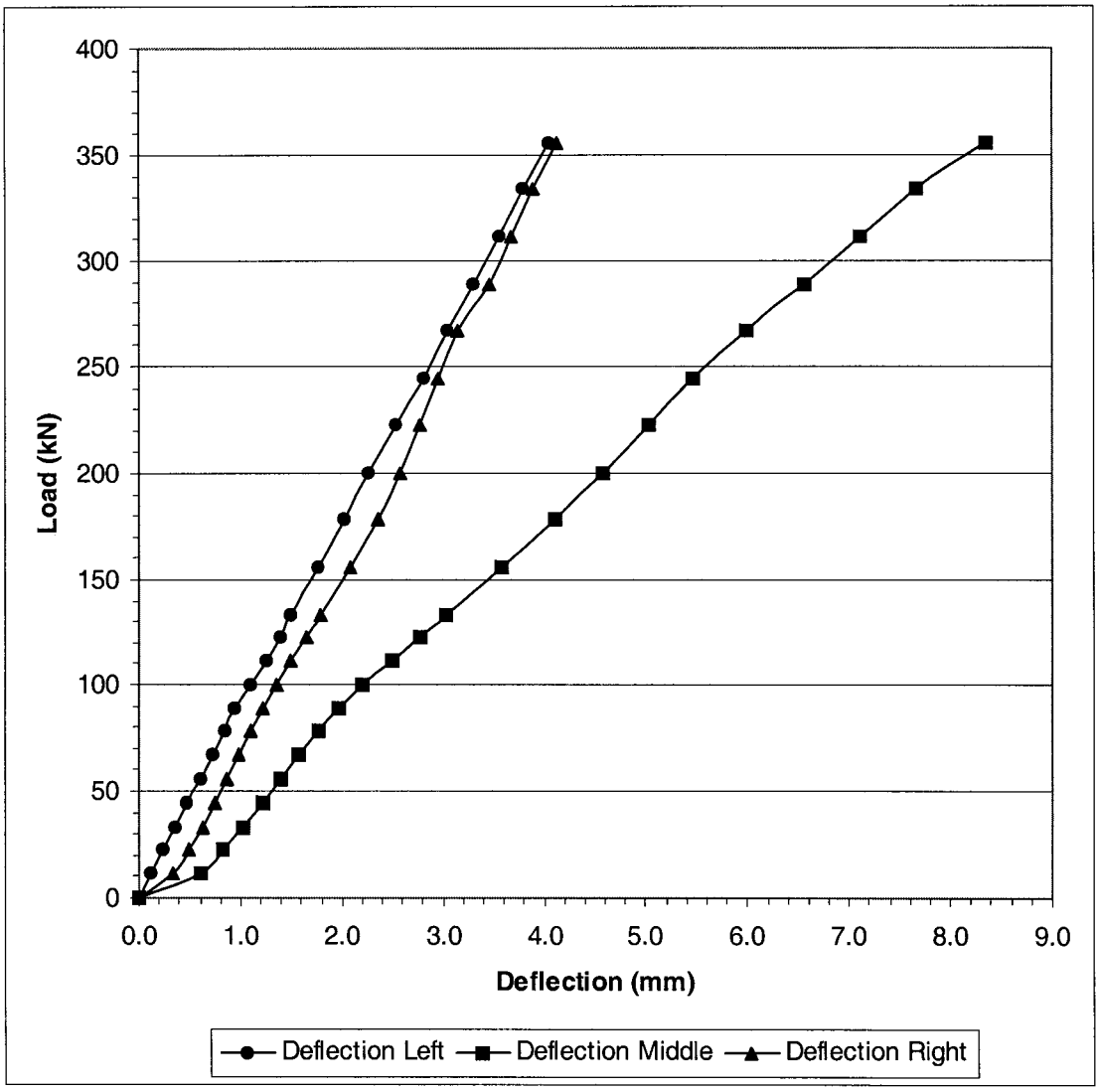

Figure 4-8. Deflection of beam B260S6.

4.4 Individual Beam Results

4.4.1 Beam B150S6

Beam B150S6 measured 1372mm in length, 356mm in height, and 95mm in width. The main horizontal reinforcement consisted of 4 - 20M bars. Eight closed loop stirrups, 6mm in diameter, were equally spaced at 152mm intervals.

The beam was loaded in 22 kN increments. First cracking occurred at a load of 133.4 kN along a diagonal from the support to the loading point as well as flexural cracking between the two supports. Failure of the test specimen occurred at 371.8 kN by diagonal cracking along the compression strut.

At each load increment, deflection readings were taken and the crack pattern drawn. Deflections were measured at midspan as well as 305mm from both the left and right sides. The crack pattern is shown in Figure 4-9. Loading is shown in kips (1 kip = 4.448 kN).

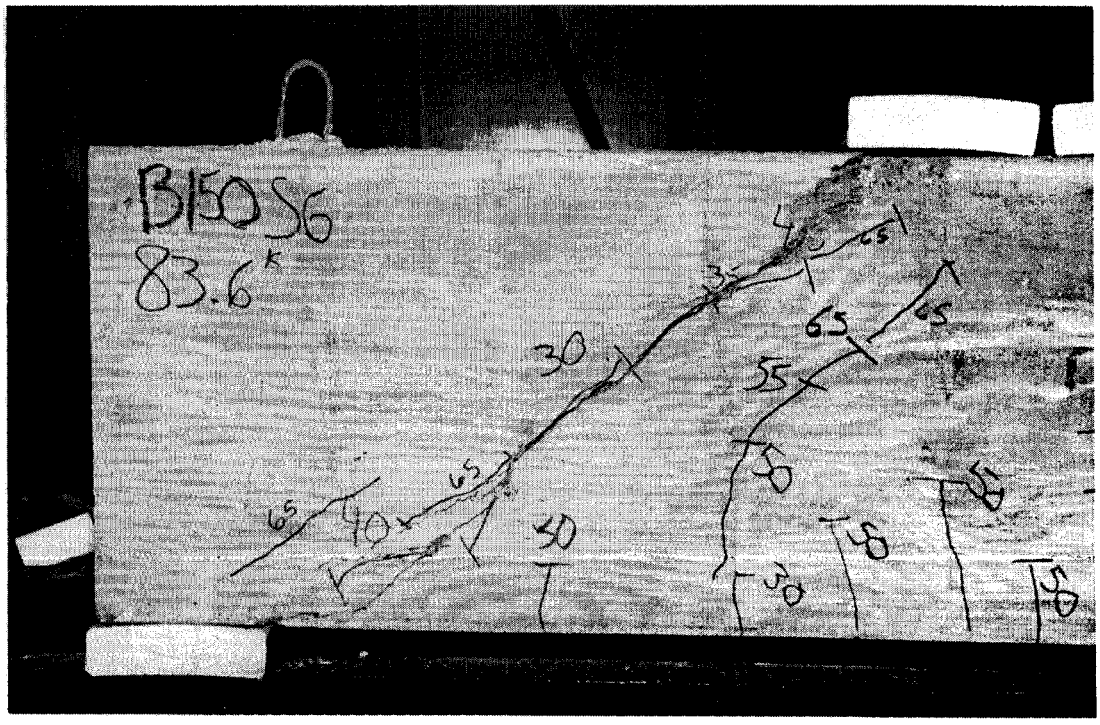

Figure 4-9. Crack pattern detail of left side of test beam B150S6.

4.4.2 Beam B250S6

Beam B250S6 measured 1372mm in length, 356mm in height, and 95mm in width. The main horizontal reinforcement consisted of 4 - 20M bars. Eight closed loop stirrups, 6mm in diameter, were equally spaced at 152mm intervals.

The beam was loaded in 22 kN increments. First cracking occurred at a load of 111.2 kN along a diagonal from the support to the loading point. Flexural cracking first occurred at 133.4 kN in the center of the beam. Failure of the test specimen occurred at 496.3 kN by diagonal cracking along the compression strut.

At each load increment deflection readings were taken and the crack pattern drawn. Deflections were measured at midspan as well as 305mm from both the left and right sides. The crack pattern is shown in Figure 4-10. Loading is shown in kips (1 kip = 4.448 kN).

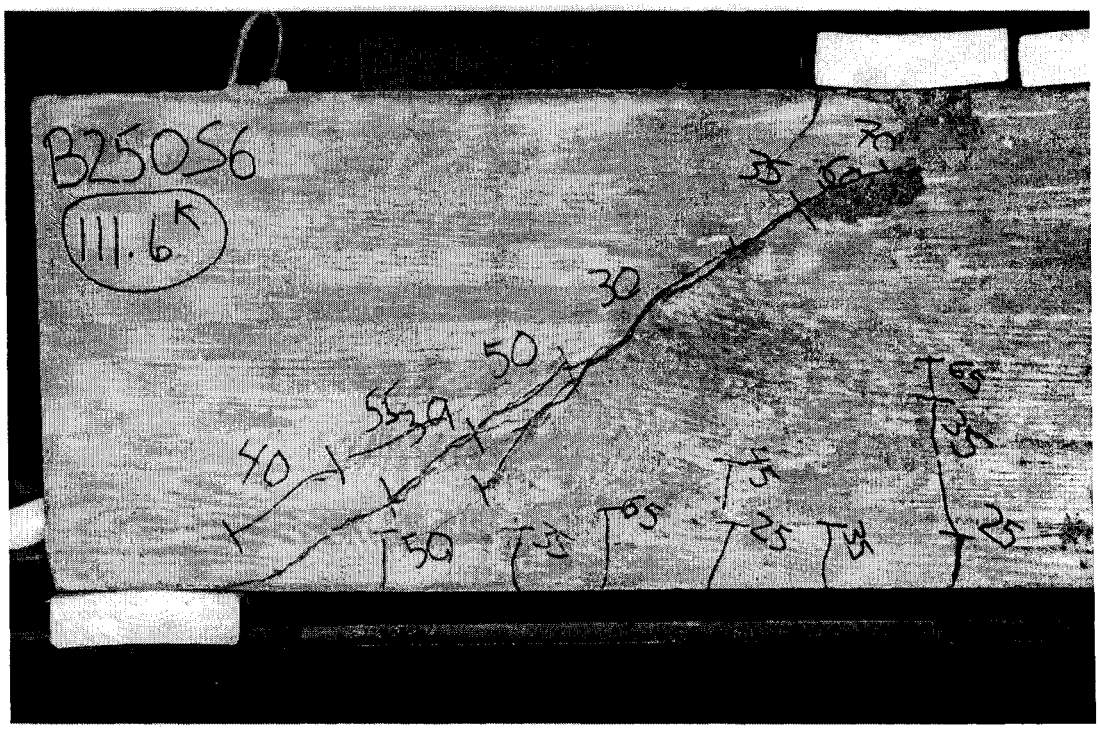

Figure 4-10. Left side crack pattern for beam B250S6.

4.4.3 Beam B350S6

Beam B350S6 measured 1372mm in length, 356mm in height, and 95mm in width. The main horizontal reinforcement consisted of 4 - 20M bars. Eight closed loop stirrups, 6mm in diameter, were equally spaced at 152mm intervals.

The beam was loaded in 11.1 kN increments until reaching 75 kN, then it was loaded at 22.2 kN increments until failure. First cracking occurred at a load of 155.7 kN along a diagonal from the support to the loading point. Flexural cracking first occurred at 155.7 kN at the center of the beam. Failure of the test specimen occurred at 422.6 kN by diagonal cracking along the compression strut.

At each load increment 25 strain gauge readings were taken. The crack pattern can be seen in Figure 4-11. Measured strain gauge readings are shown in Figure 4-12 to Figure 4-16.

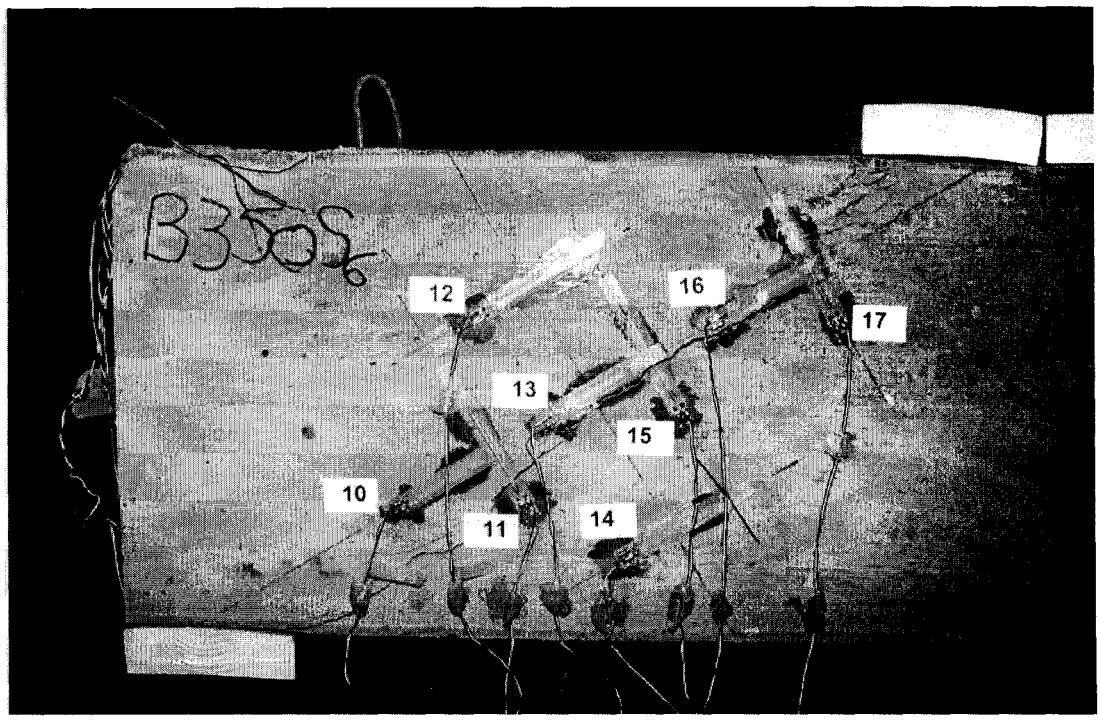

Figure 4-11. Left side crack pattern for beam B350S6.

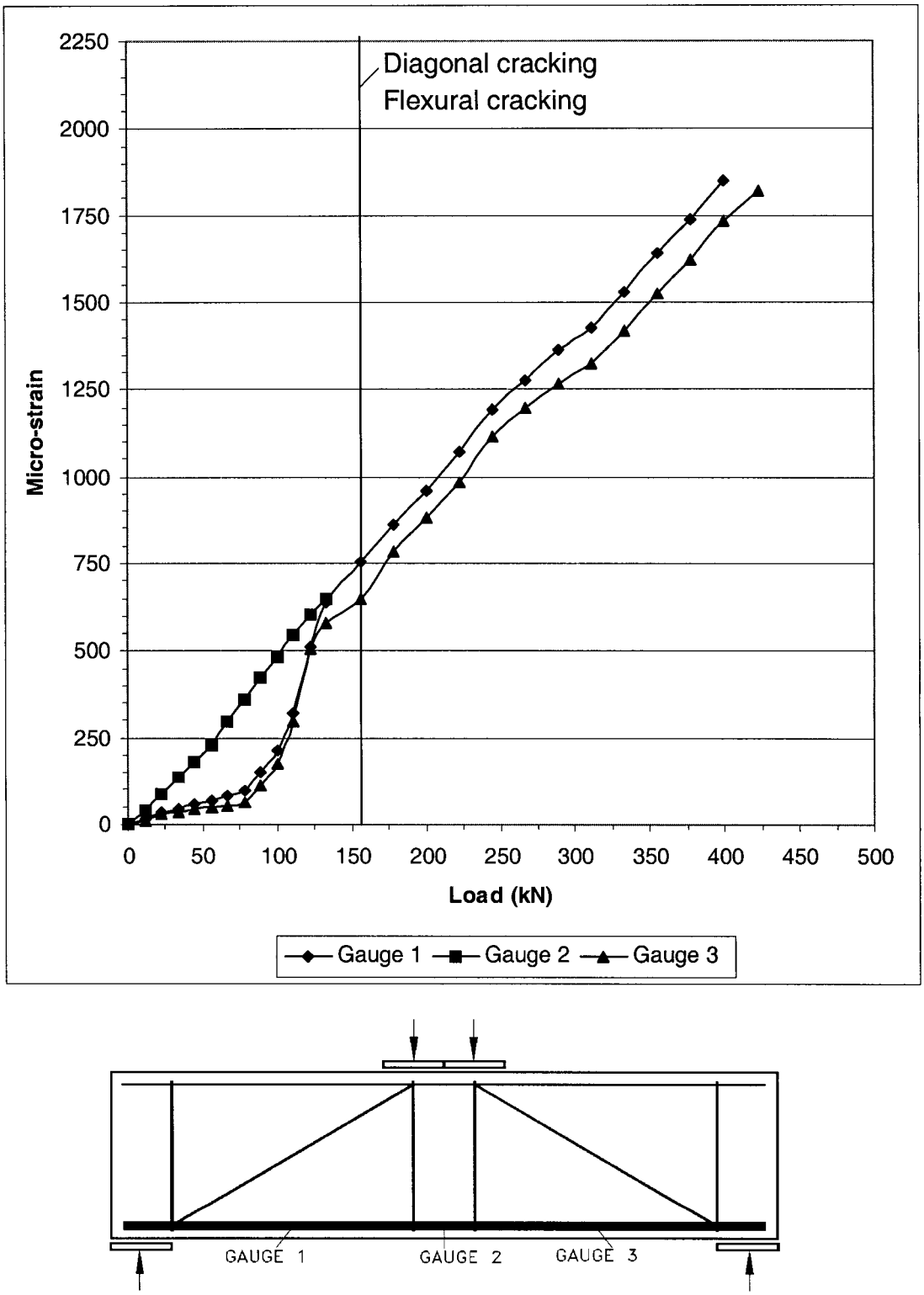

Figure 4-12. Main tension steel strain versus load for beam B350S6.

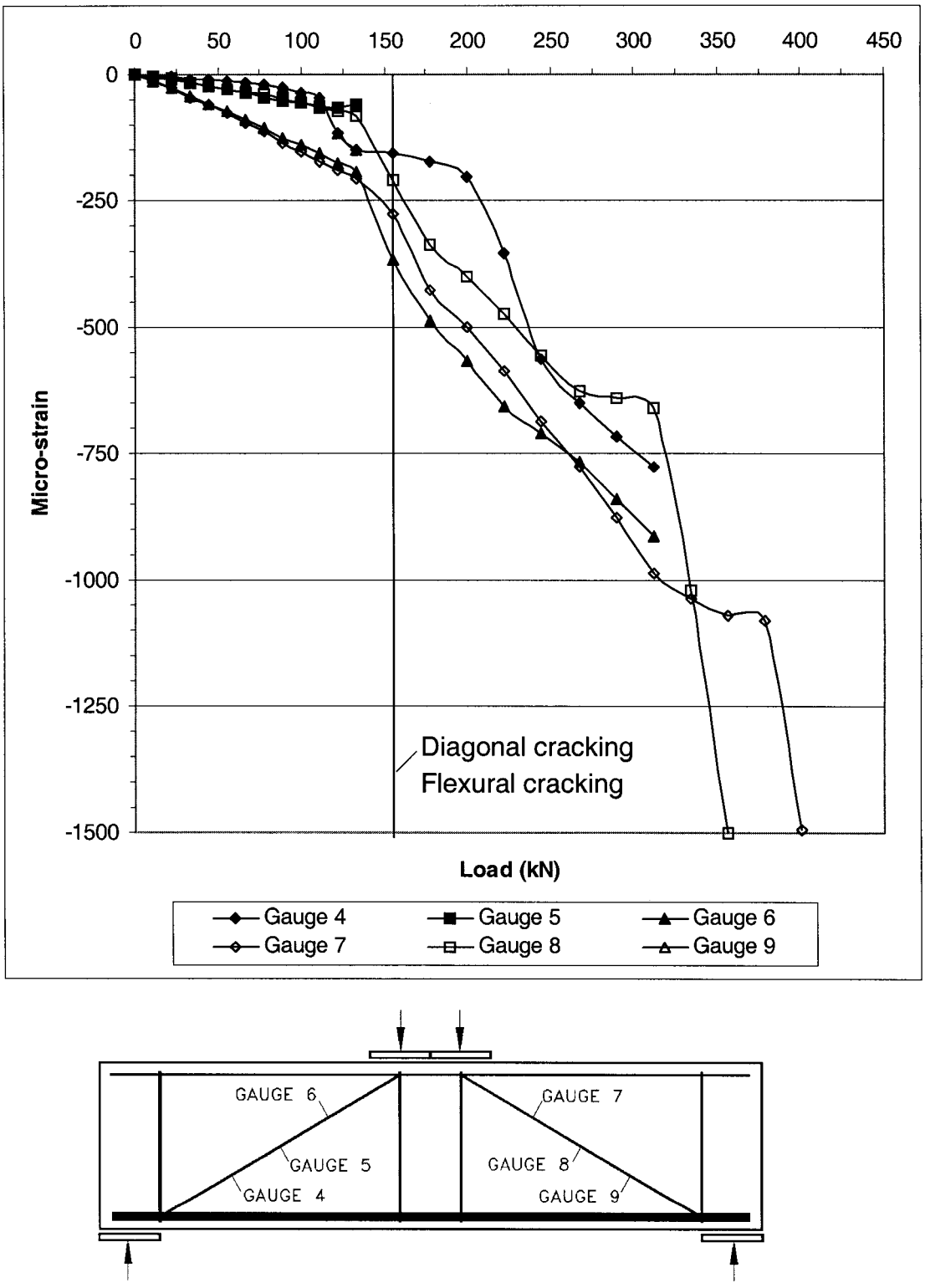

Figure 4-13. Diagonal steel strain versus load for beam B350S6.

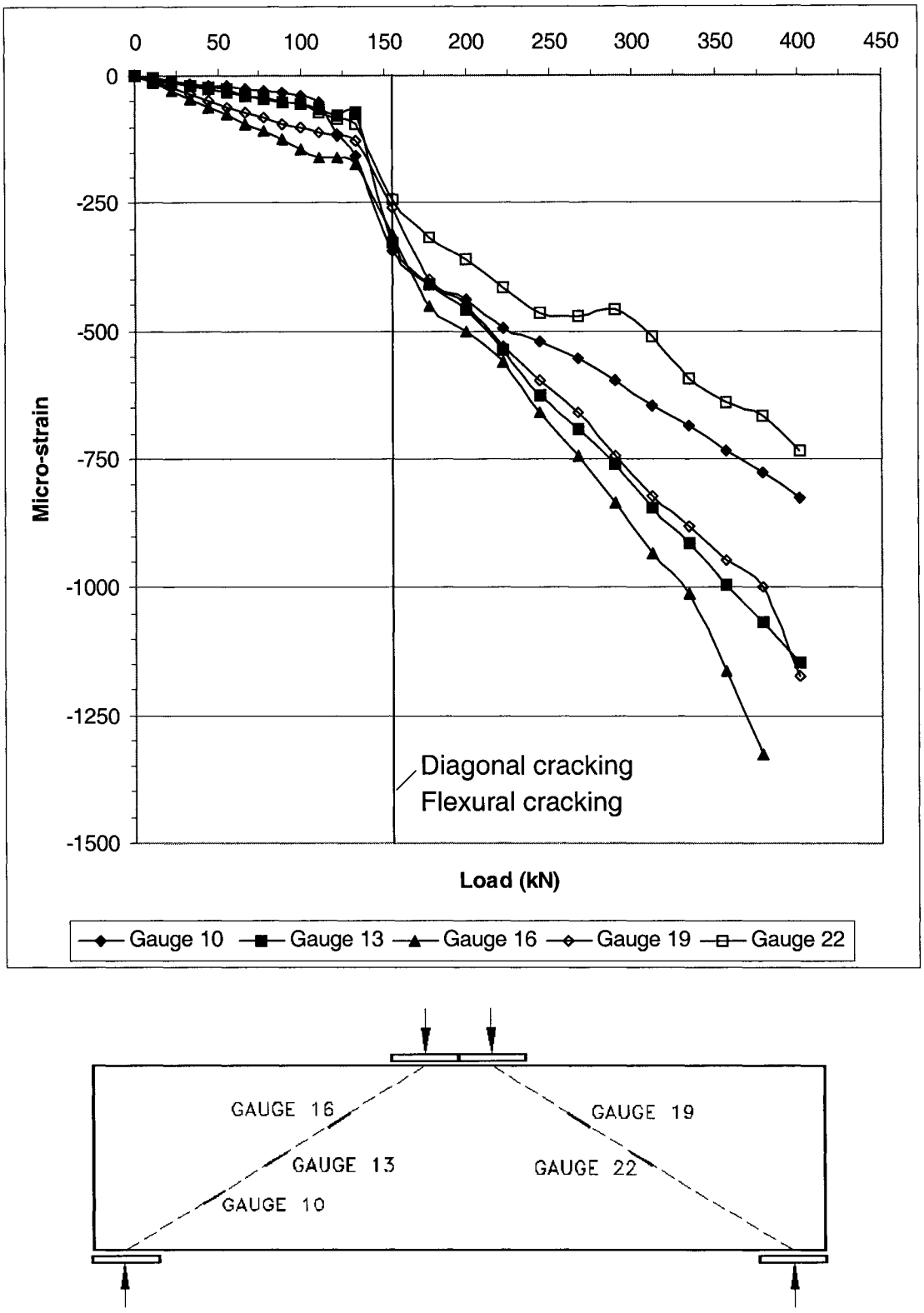

Figure 4-14. Concrete compression strain along diagonal versus load for beam B350S6.

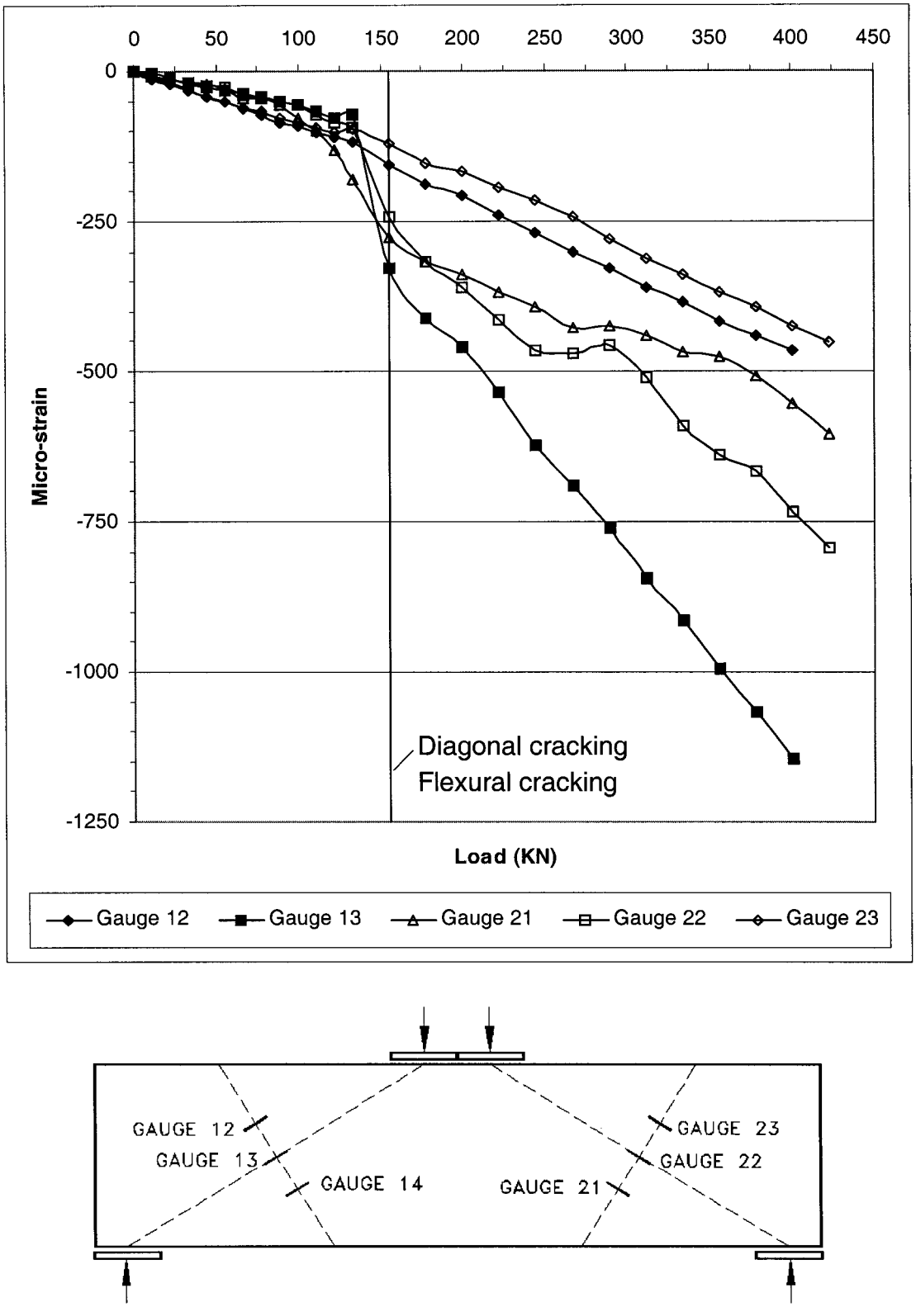

Figure 4-15. Concrete compression strain across the diagonal versus load for beam B350S6.

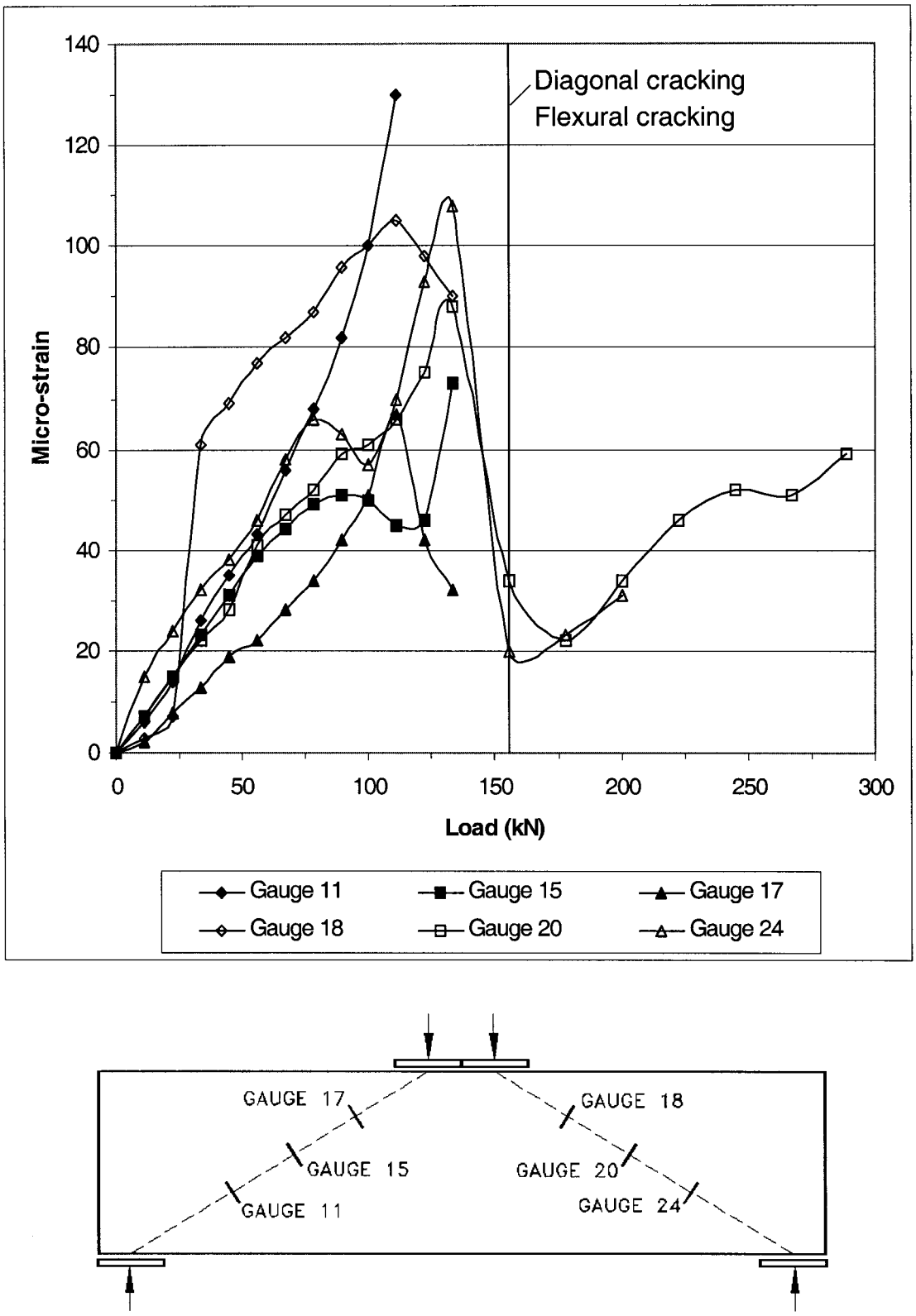

Figure 4-16. Concrete tension strain for beam B350S6.

Of the strain gauges placed on the steel reinforcement and the steel rods placed along the compression strut, strain gauges 2, 5 and 9 stop functioning just prior to the flexural and diagonal cracking. Gauge 14, which was placed on the concrete to measure compressive strains failed to work from the start. The strains measured along the compression strut by the gauges, by both the gauges on the concrete and on the diagonal steel rods, showed that the strains were much less than the Canadian Code proposed value of 0.002[5], the value recommended by the Canadian code[5] to be used when calculating the strength of the compression strut. The concrete strain gauges measuring tension perpendicular to the compression strut showed an increase in tensile strains with an increase in loading with a sudden drop just prior to diagonal cracking. After diagonal cracking, strain gauges 11, 15, 17, and 18 stop functioning. The remaining two strain gauges recorded that the tensile strains began to increase again as loading was applied.

4.4.4 Beam B150S19

Beam B150S19 measured 1372mm in length, 356mm in height, and 95mm in width. The main horizontal reinforcement consisted of 4 - 20M bars. A closed loop stirrup, 6mm in diameter, was placed near the loading points and supports, for a total of four stirrups.

The beam was loaded in 22.2 kN increments. First cracking occurred at a load of 133.4 kN along a diagonal from the support to the loading point. Flexural cracking first occurred at 155.7 kN at the center of the beam. Failure of the test specimen occurred at 356.7 kN by diagonal cracking along the compression strut.

At each load increment deflection readings were taken and the crack pattern drawn. Deflections were measured at midspan as well as 305 mm from both the left and right sides. The crack pattern is shown in Figure 4-17. Loading is shown in kips (1 kip = 4.448 kN).

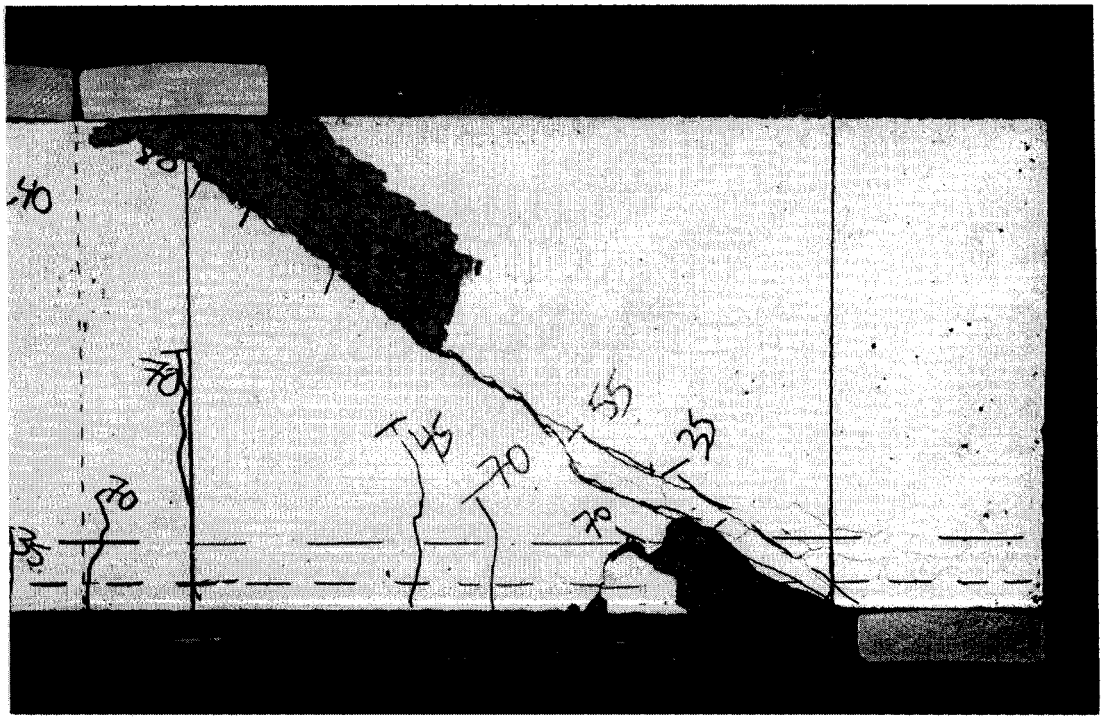

Figure 4-17. Right side crack pattern for beam B150S19.

4.4.5 Beam B250S19

Beam B250S19 measured 1372mm in length, 356mm in height, and 95mm in width. The main horizontal reinforcement consisted of 4 - 20M bars. A closed loop stirrup, 6mm in diameter, was placed near the loading points and supports, for a total of four stirrups.

The beam was loaded in 22.2 kN increments. First cracking occurred at a load of 133.4 kN along a diagonal from the support to the loading point. Flexural cracking first occurred at 155.7 kN between the two supports. Failure of the test specimen occurred at 378.0 kN by diagonal cracking along the compression strut.

At each load increment, deflection readings were taken and the crack pattern drawn. Deflections were measured at midspan as well as 305mm from both the left and right sides. The crack pattern is shown in Figure 4-18. Loading is shown in kips (1 kip = 4.448 kN).

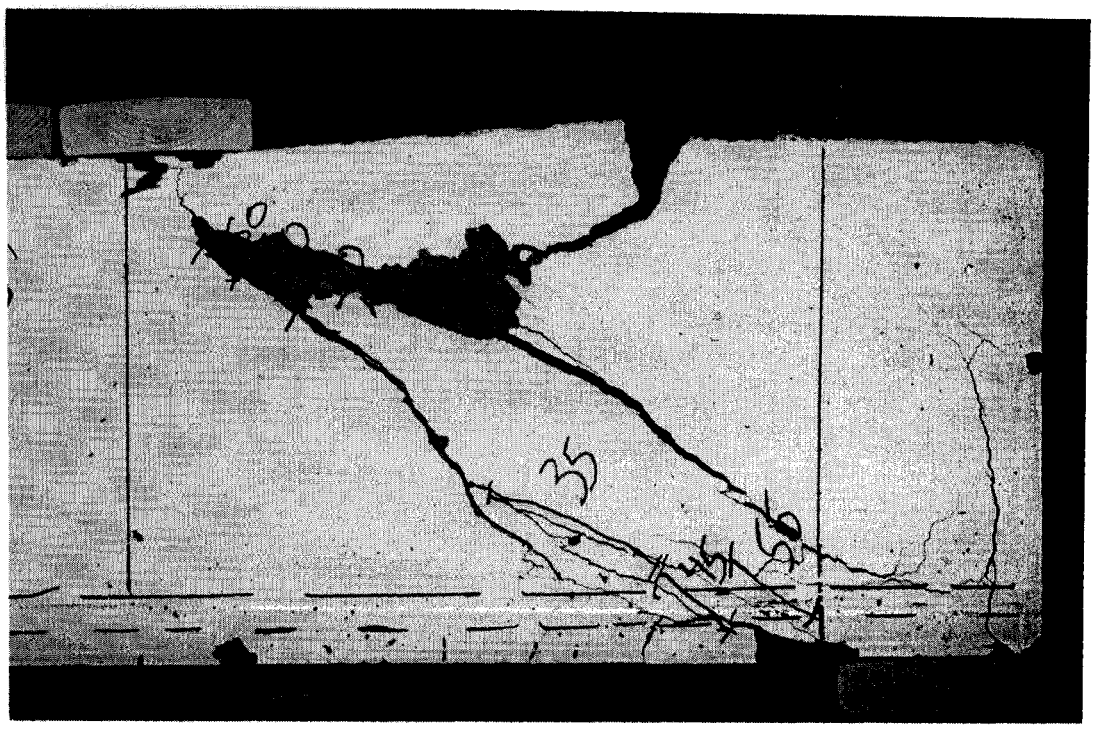

Figure 4-18. Right side crack pattern for beam B250S19.

4.4.6 Beam B350S19

Beam B350S19 measured 1372mm in length, 356mm in height, and 95mm in width. The main horizontal reinforcement consisted of 4 - 20M bars. A closed loop stirrup, 6mm in diameter, was placed near the loading points and supports, for a total of four stirrups.

The beam was loaded in 11.1 kN increments until reaching 133.4 kN, then loaded at 22.2 kN increments until failure. First cracking occurred at a load of 122.3 kN along a diagonal from the support to the loading point. Flexural cracking first occurred at 133.4 kN at the center of the beam. Failure of the test specimen occurred at 311.3 kN by diagonal cracking along the compression strut.

At each load increment 25 strain gauge readings were taken. The crack pattern is shown in Figure 4-19. Measured strain gauge readings are shown in Figure 4-20 to Figure 4-24.

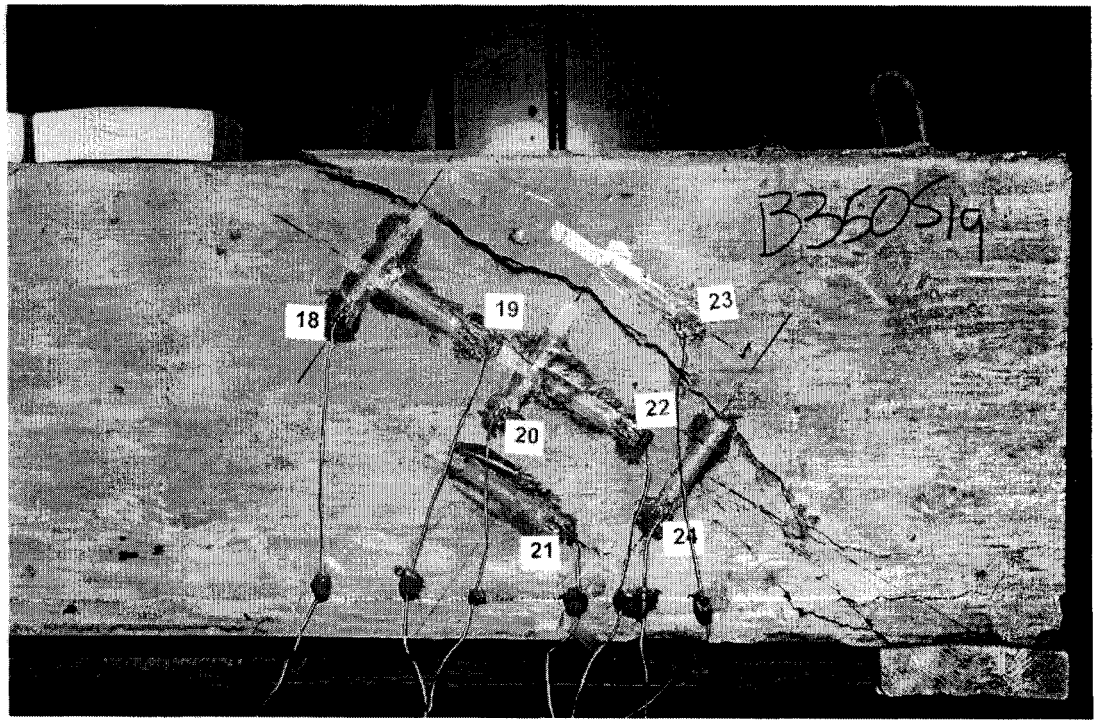

Figure 4-19. Right side crack pattern for beam B350S19.

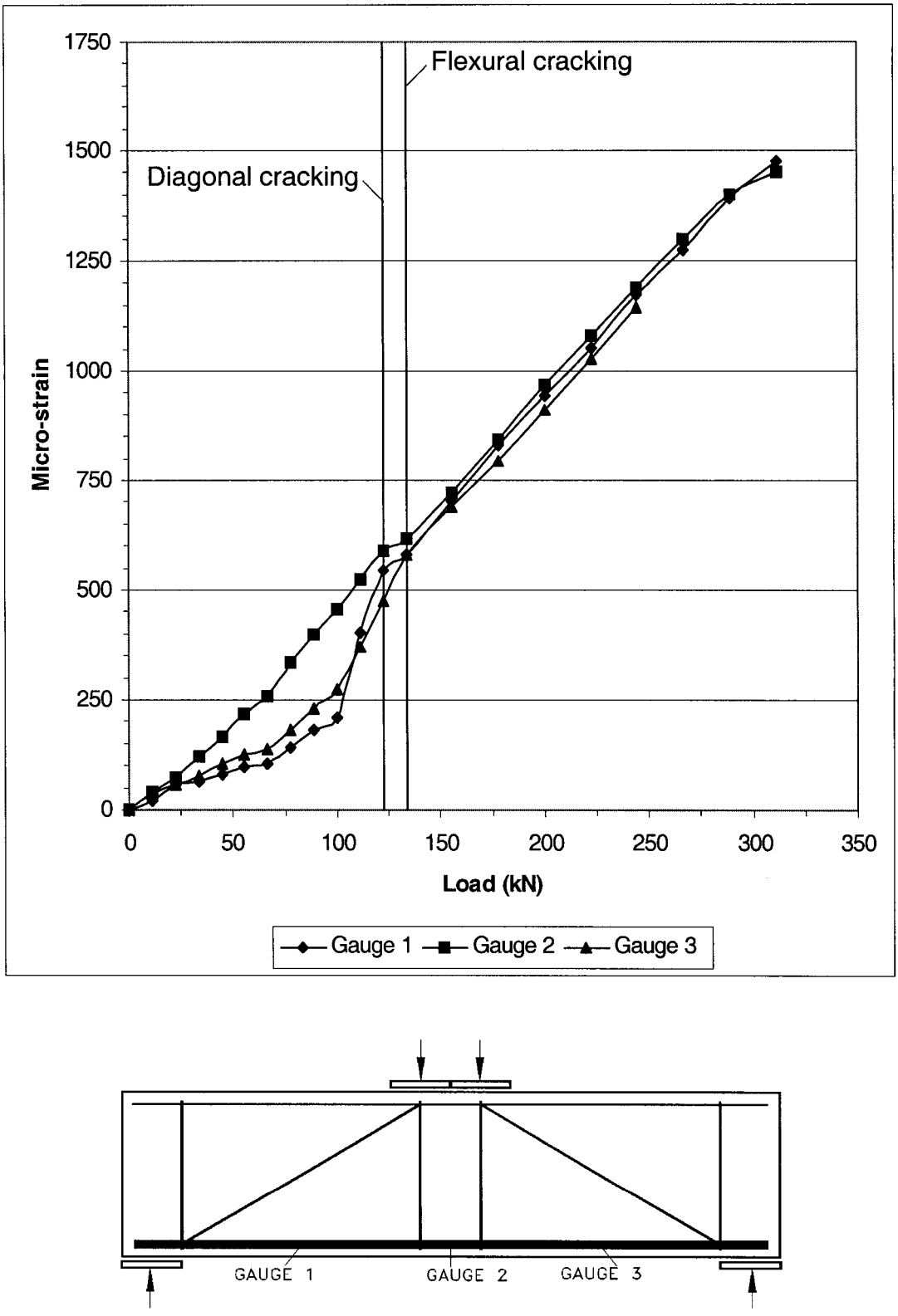

Figure 4-20. Main tension steel strain versus load for beam B350S19.

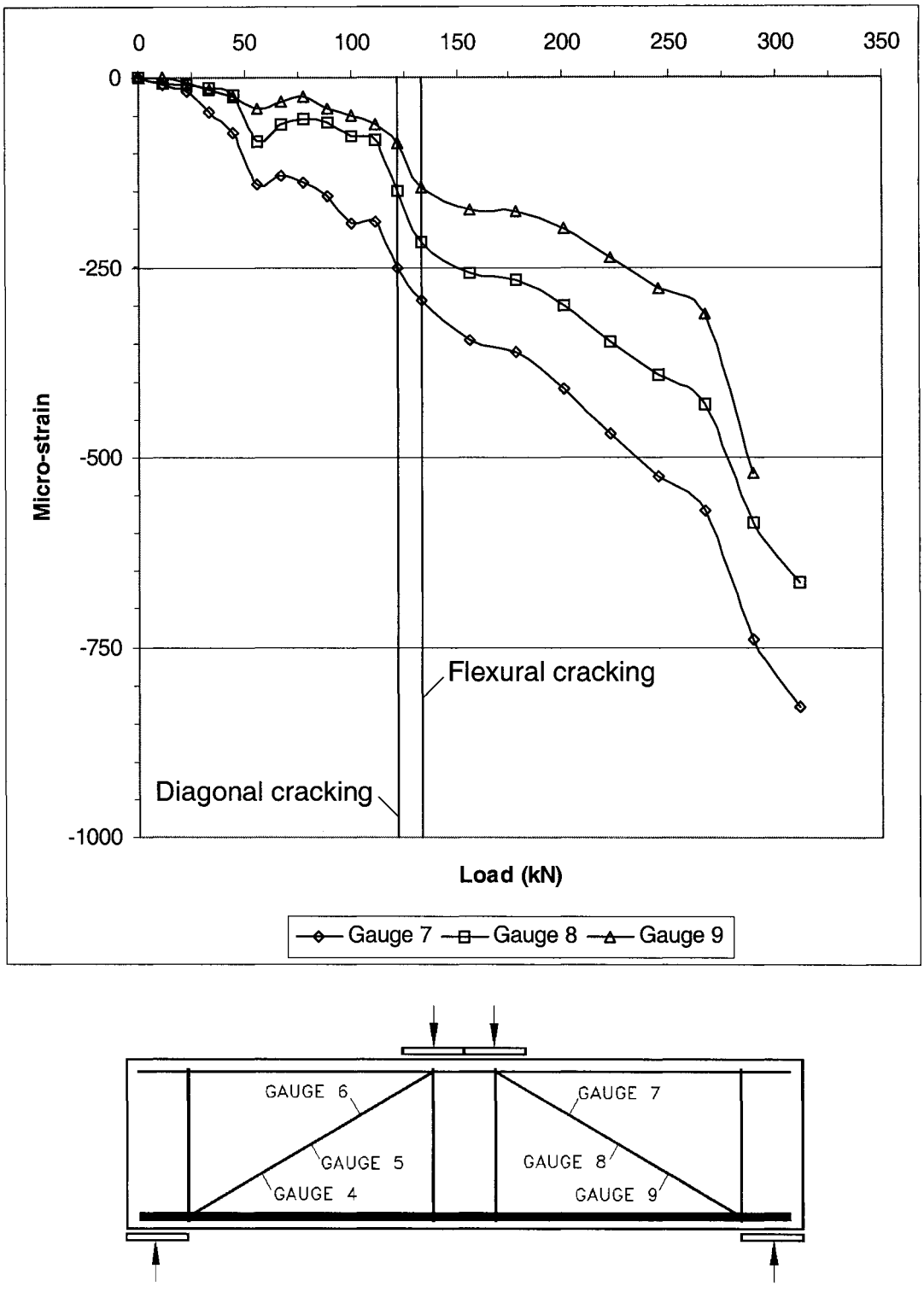

Figure 4-21. Diagonal steel strain versus load for beam B350S19.

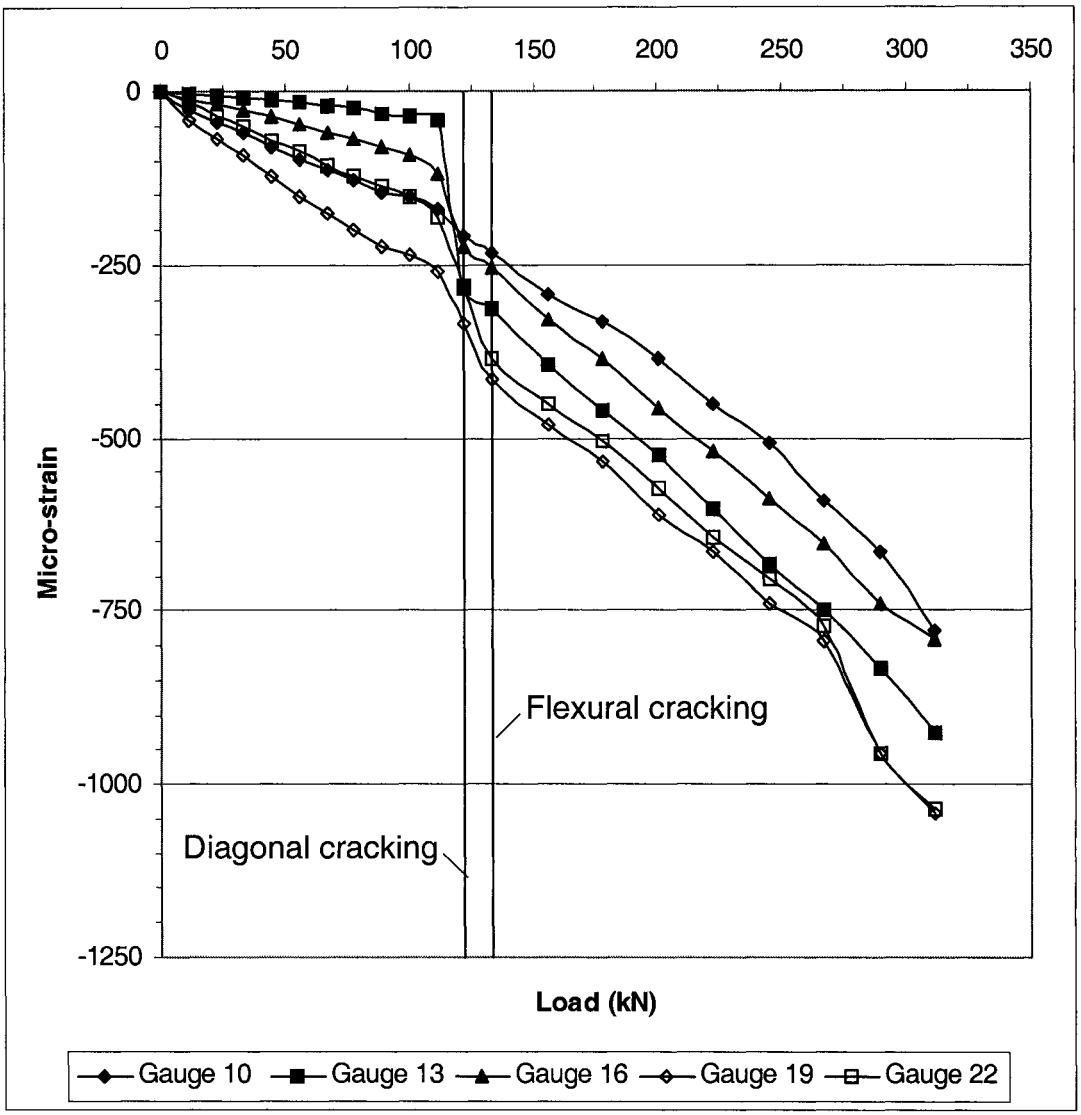

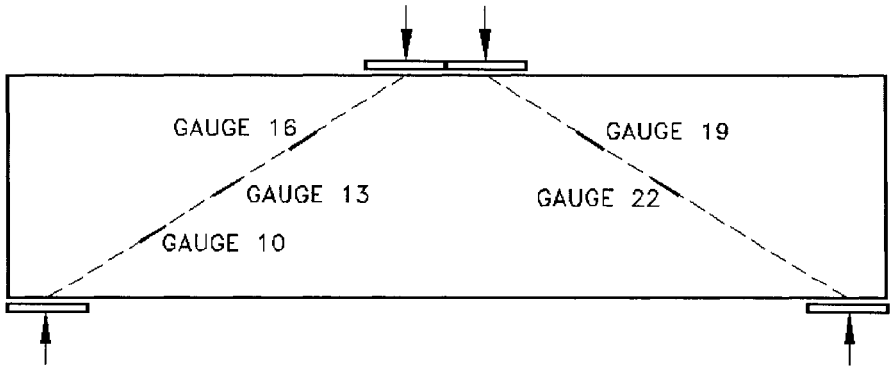

Figure 4-22. Concrete compression strain along diagonal versus load for beam B350S19.

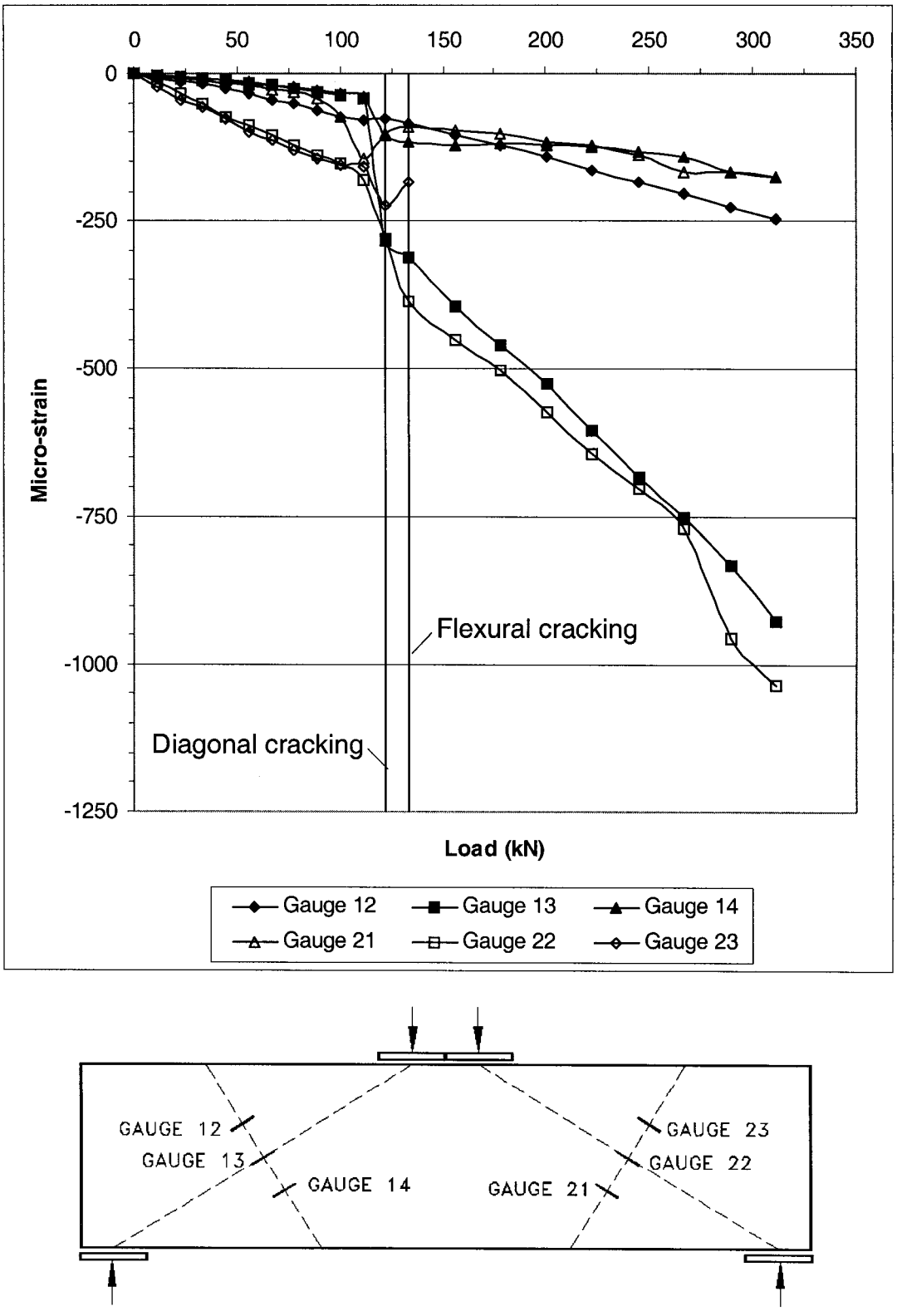

Figure 4-23. Concrete compression strain across the diagonal versus load for beam B350S19.

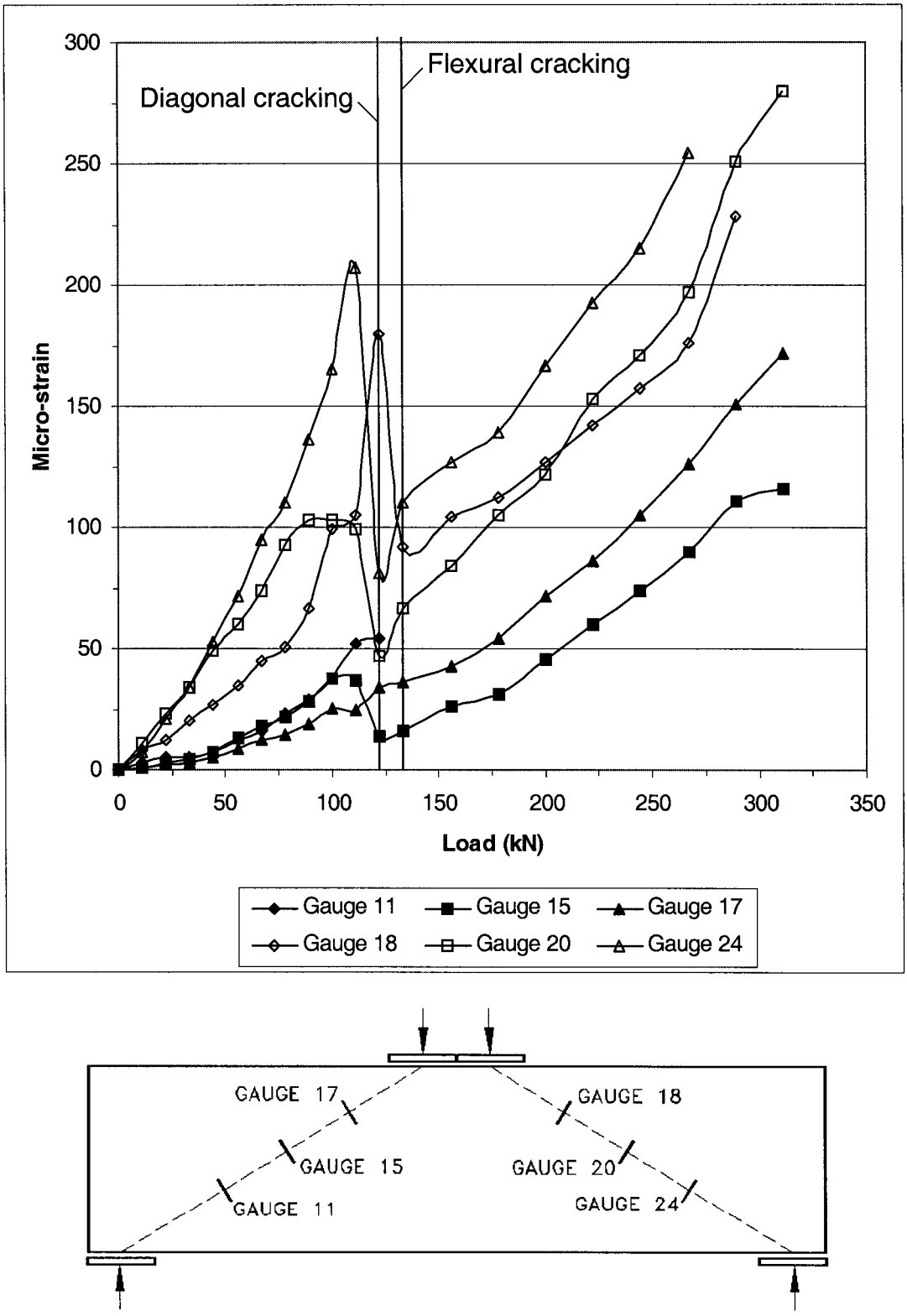

Figure 4-24. Concrete tension strain for beam B350S19.

The strain gauges on the main reinforcement showed that the strain along the length of the reinforcement was uniform after flexural cracking. This is consistent with the tied-arch model in that after the concrete deep beam experiences flexural cracking, the affect of the concrete in tension is negligible and the force in the tie is constant throughout it's length. Of the strain gauges measuring compressive strains, gauges 4,5, and 6 did not function from the start of the test. Gauge 23, measuring concrete compressive strains ceased functioning after diagonal cracking. Both the gauges on the steel rod placed along the compression strut and the gauges attached to the concrete surface measuring compressive strains once again showed that the strains along the compression strut are much lower than the Canadian Code proposed value of 0.002[5], with the highest measured strain just over 0.001.

The concrete strain gauges measuring tension perpendicular to the compression strut showed an increase in tensile strains with an increase in loading with a sudden drop just prior to diagonal cracking. After diagonal cracking, strain gauge 11 stop functioning. The remaining strain gauges recorded that the tensile strains began to increase again as loading was applied.

4.4.7 Beam B160S6

Beam B160S6 measured 1676mm in length, 356mm in height, and 95mm in width. The main horizontal reinforcement consisted of 4 - 20M bars. Ten closed loop stirrups, 6mm in diameter, were equally spaced at 152mm intervals.

The beam was loaded in 22.2 kN increments. First cracking occurred at a load of 66.7 kN along a diagonal from the support to the loading point. Flexural cracking first occurred at 133.4 kN at the center of the beam. Failure of the test specimen occurred at 392.7 kN by diagonal cracking along the compression strut.

At each load increment, deflection readings were taken and the crack pattern drawn. Deflections were measured at midspan as well as 406mm from both the left and right sides. The crack pattern is shown in Figure 4-25. Loading is shown in kips (1 kip = 4.448 kN).

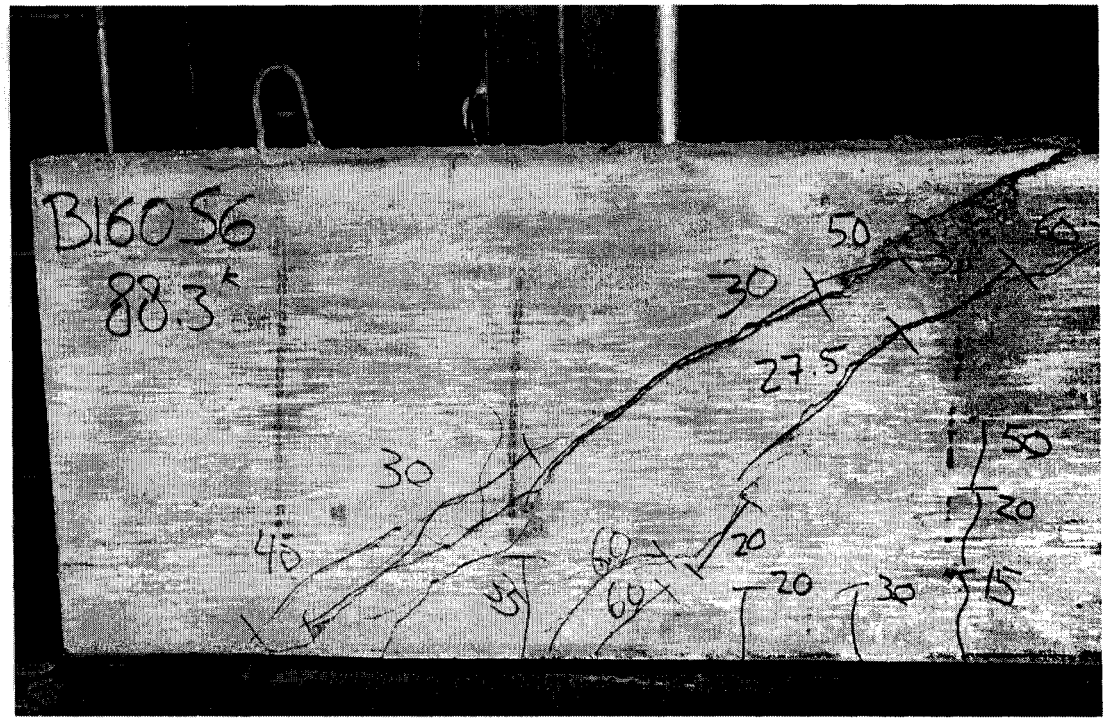

Figure 4-25. Left side crack pattern for beam B160S6.

4.4.8 Beam B260S6

Beam B260S6 measured 1676mm in length, 356mm in height, and 95mm. The main horizontal reinforcement consisted of 4 - 20M bars. Ten closed loop stirrups, 6mm in diameter, were equally spaced at 152mm intervals.

The beam was loaded in 22.2 kN increments. First cracking occurred at a load of 55.6 kN along a diagonal from the support to the loading point. Flexural cracking first occurred at 122.3 kN at the center of the beam. Failure of the test specimen occurred at 371.8 kN by diagonal cracking along the compression strut.

At each load increment, deflection readings were taken and the crack pattern drawn. Deflections were measured at midspan as well as 406mm from both the left and right sides. The crack pattern is shown in Figure 4-26. Loading is shown in kips (1 kip = 4.448 kN).

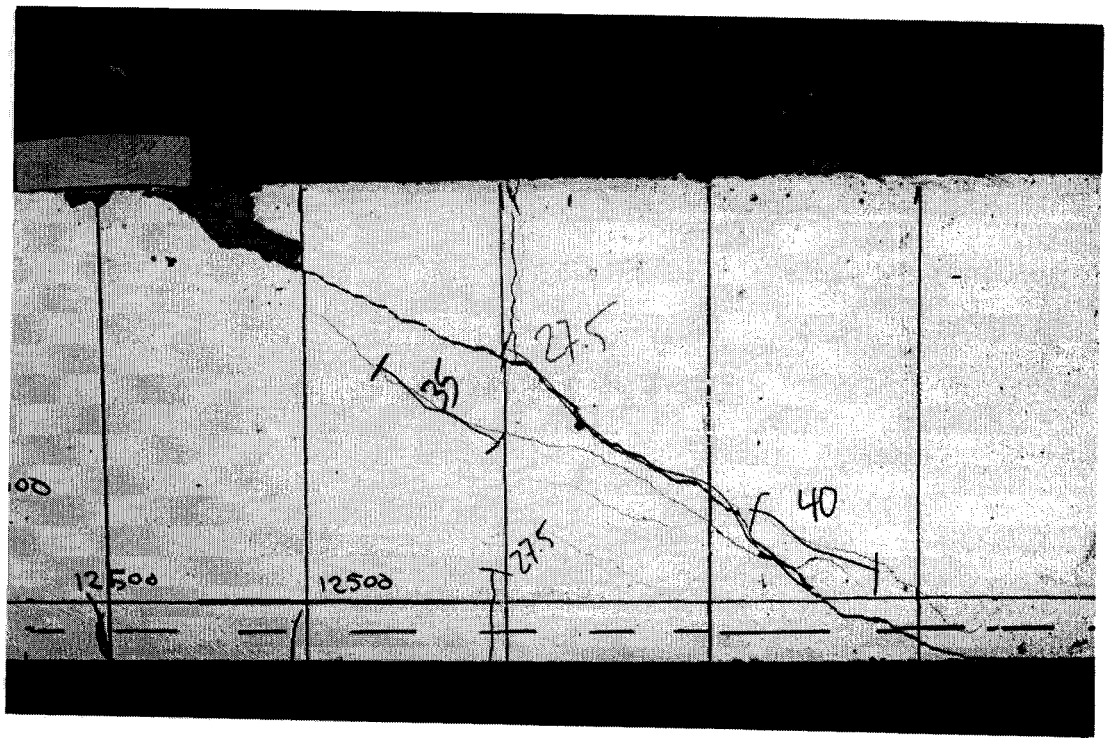

Figure 4-26. Right side crack pattern for beam B260S6.

4.4.9 Beam B360S6

Beam B360S6 measured 1676mm in length, 356mm in height, and 95mm. The main horizontal reinforcement consisted of 4 - 20M bars. Ten closed loop stirrups, 6mm in diameter, were equally spaced at 152.4mm intervals.

The beam was loaded in 11.1 kN increments until reaching 133.4 kN, then loaded at 22.2 kN increments until failure. First cracking occurred at a load of 66.7 kN along a diagonal from the support to the loading point. Flexural cracking first occurred at 133.4 kN at the center of the beam. Failure of the test specimen occurred at 355.8 kN by diagonal cracking along the compression strut.

At each load increment 25 strain gauge readings were taken. The crack pattern is shown in Figure 4-27. Measured strain gauge readings are shown in Figure 4-28 to Figure 4-32.

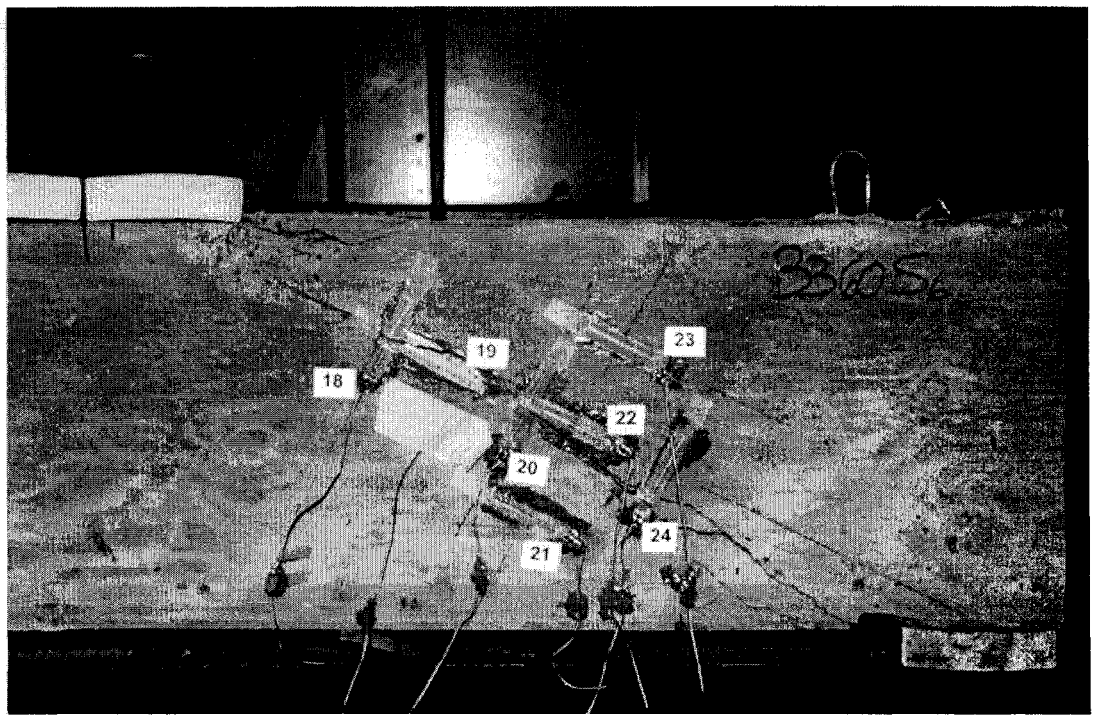

Figure 4-27. Right side crack pattern for beam B360S6.

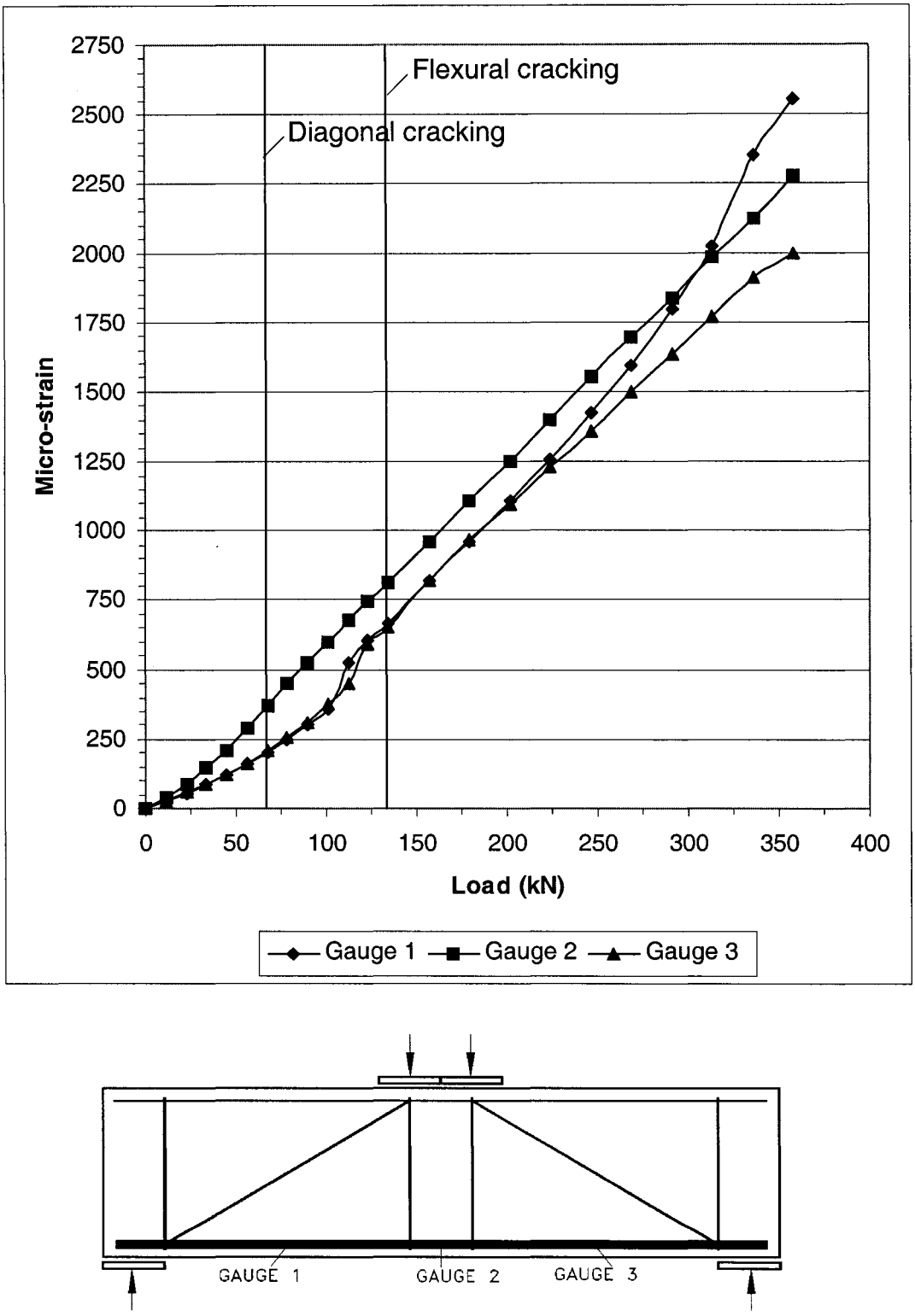

Figure 4-28. Main tension steel strain versus load for beam B360S6.

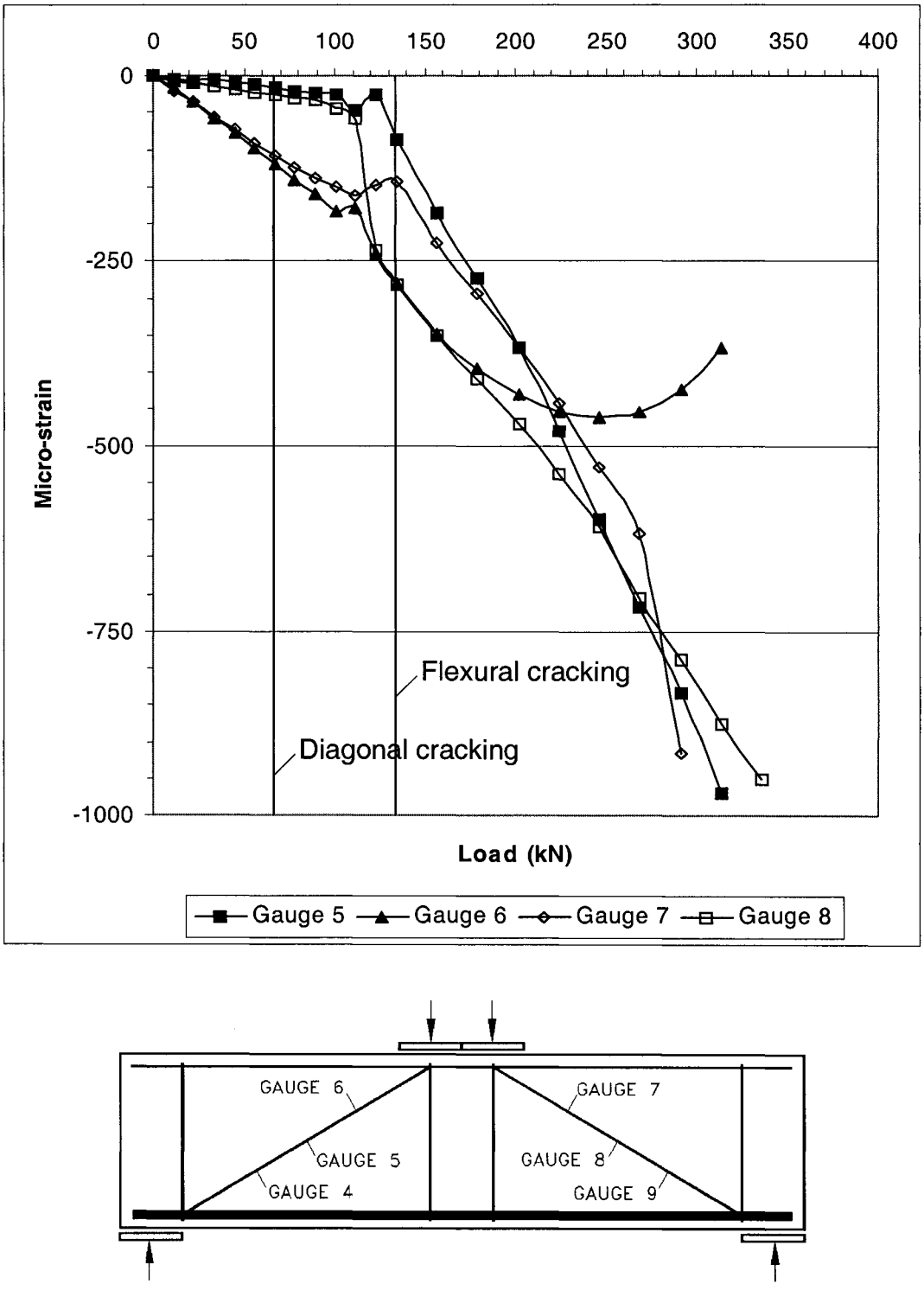

Figure 4-29. Diagonal steel strain versus load for beam B360S6.

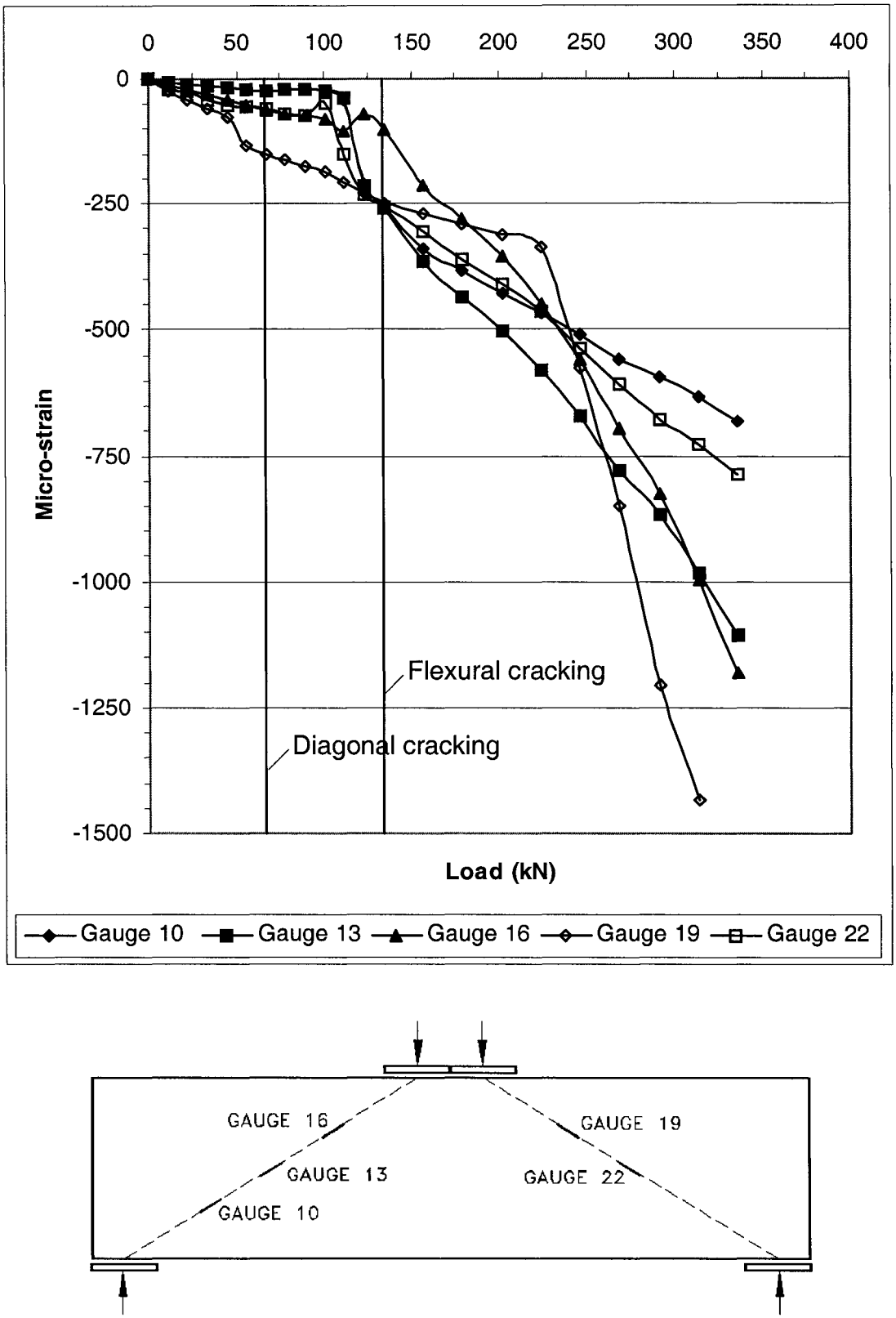

Figure 4-30. Concrete compression strain along diagonal versus load for beam B360S6.

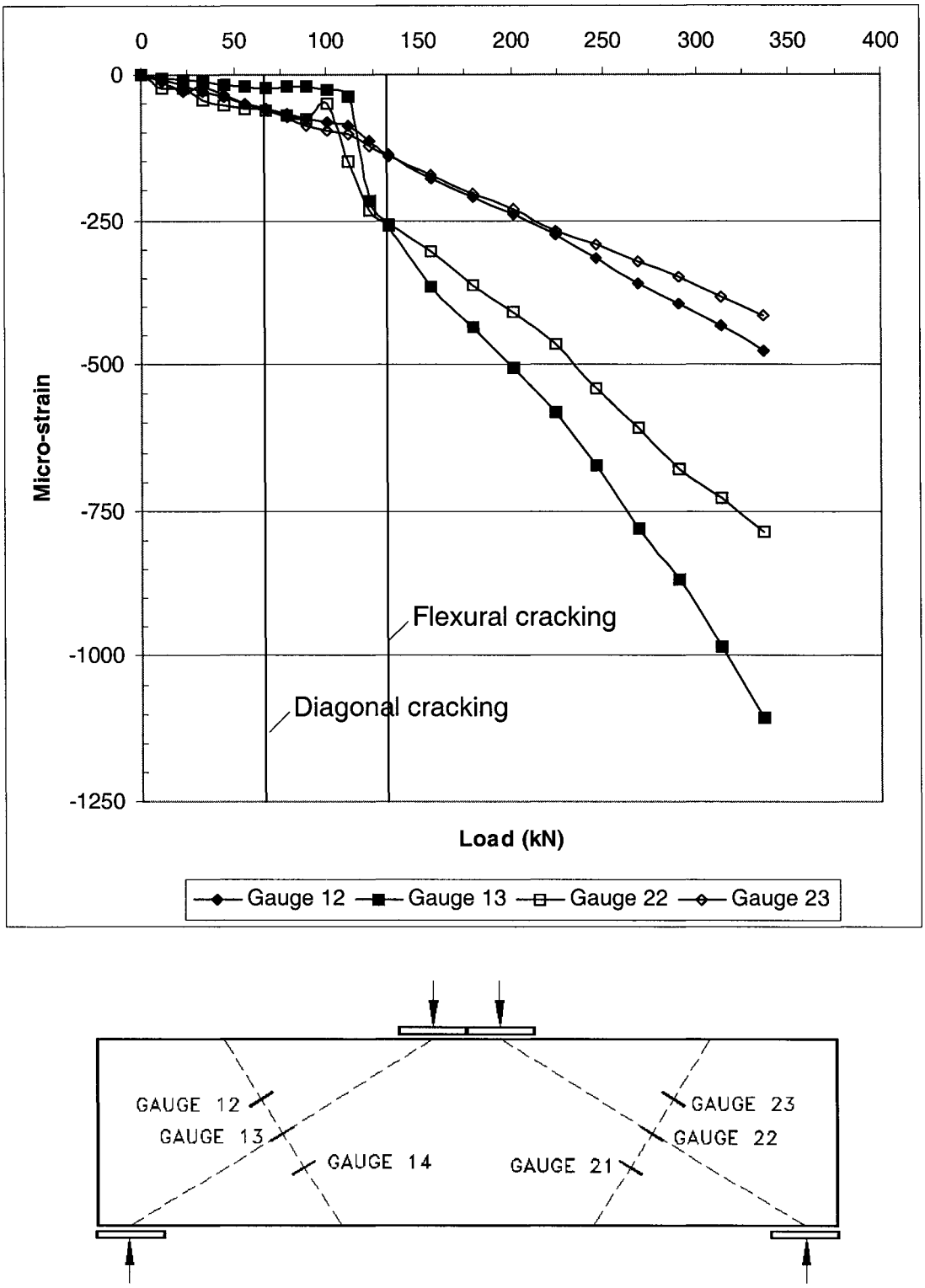

Figure 4-31. Concrete compression strain across the diagonal versus load for beam B360S6

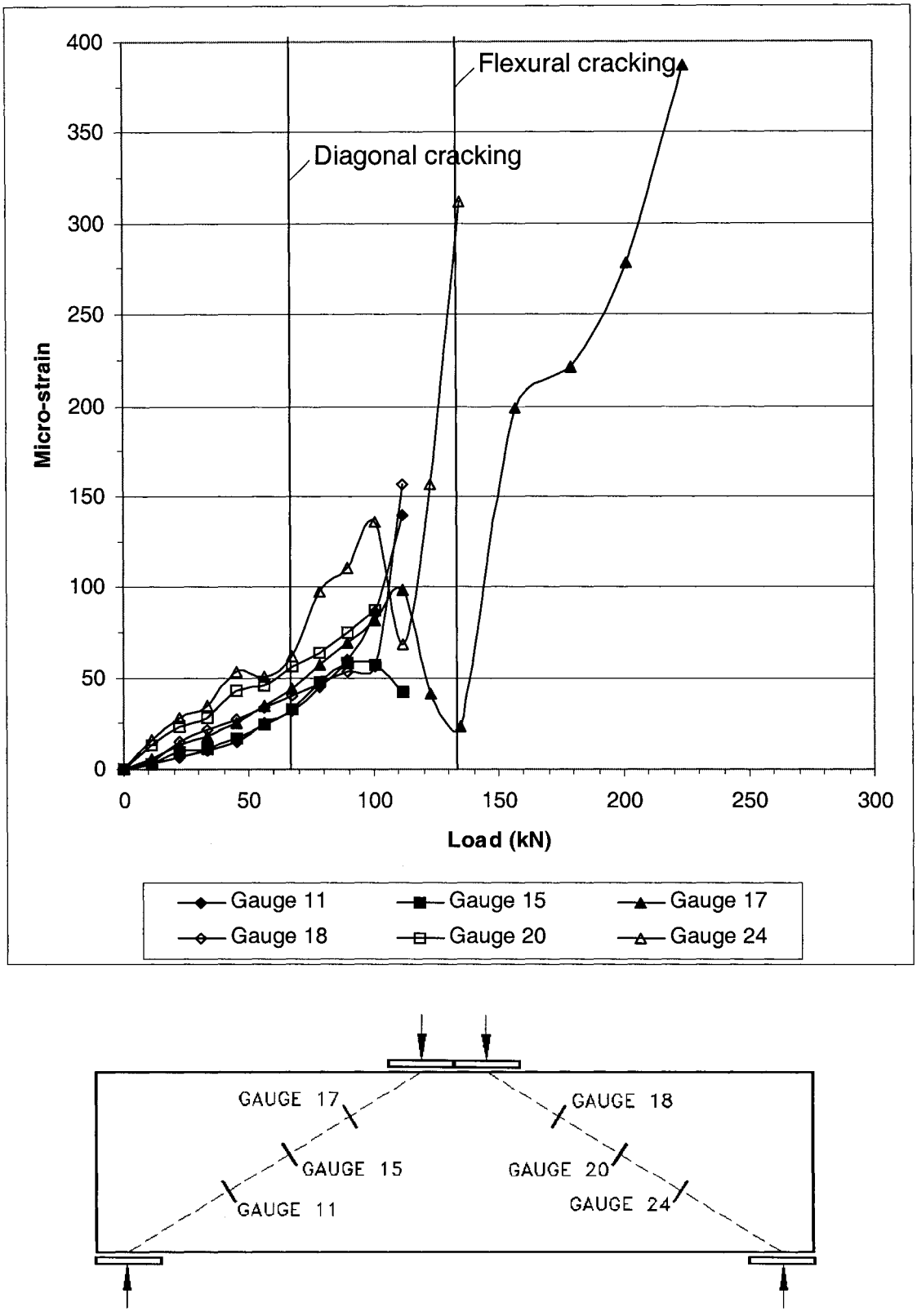

Figure 4-32. Concrete tension strain for beam B360S6.

The strain gauges on the main reinforcement showed that the strain along the length of the reinforcement was uniform after flexural cracking. This is consistent with the tied-arch model in that after the concrete deep beam experiences flexural cracking, the affect of the concrete in tension is negligible and the force in the tie is constant throughout it's length. Of the strain gauges measuring compressive strains, gauges 4, 9, 14 and 21 did not function from the start of the test. Both the gauges on the steel rod placed along the compression strut and the gauges attached to the concrete surface measuring compressive strains once again showed that the strains along the compression strut are much lower than the Canadian Code proposed value of 0.002[5], with the averaged measured strain just over 0.001.

The concrete strain gauges measuring tension perpendicular to the compression strut showed an increase in tensile strains with an increase in loading. After diagonal cracking and prior to flexural cracking, all strain gauges with the exception of gauge 17 stopped functioning. The remaining strain gauge recorded that the tensile strains began to increase again as loading was applied.

4.4.10 Beam B160S25

Beam B160S25 measured 1676mm in length, 356mm in height, and 95mm. The main horizontal reinforcement consisted of 4 - 20M bars. A closed loop stirrup, 6mm in diameter, was placed near the loading points and supports, for a total of four stirrups.

The beam was loaded in 22.2 kN increments. First cracking occurred at a load of 89.0 kN along a diagonal from the support to the loading point. Flexural cracking first occurred at 111.2 kN at the center of the beam. Failure of the test specimen occurred at 170.0 kN by diagonal cracking along the compression strut.

At each load increment deflection readings were taken and the crack pattern drawn. Deflections were measured at midspan as well as 406mm from both the left and right sides. The crack pattern is shown in Figure 4-33. Loading is shown in kips (1 kip = 4.448 kN).

Figure 4-33. Right side crack pattern for beam B160S25

4.4.11 Beam B260S25

Beam B260S25 measured 1676mm in length, 356mm in height, and 95mm. The main horizontal reinforcement consisted of 4 - 20M bars. A closed loop stirrup, 6mm in diameter, was placed near the loading points and supports, for a total of four stirrups.

The beam was loaded in 11.1 kN increments until 133.4 kN then in 22.2 kN increments until failure. First cracking occurred at a load of 77.8 kN along a diagonal from the support to the loading point. Flexural cracking first occurred at 111.2 kN at the center of the beam. Failure of the test specimen occurred at 355.8 kN by diagonal cracking along the compression strut.

At each load increment, deflection readings were taken and the crack pattern drawn. Deflections were measured at midspan as well as 406mm from both the left and right sides. The crack pattern is shown in Figure 4-34.

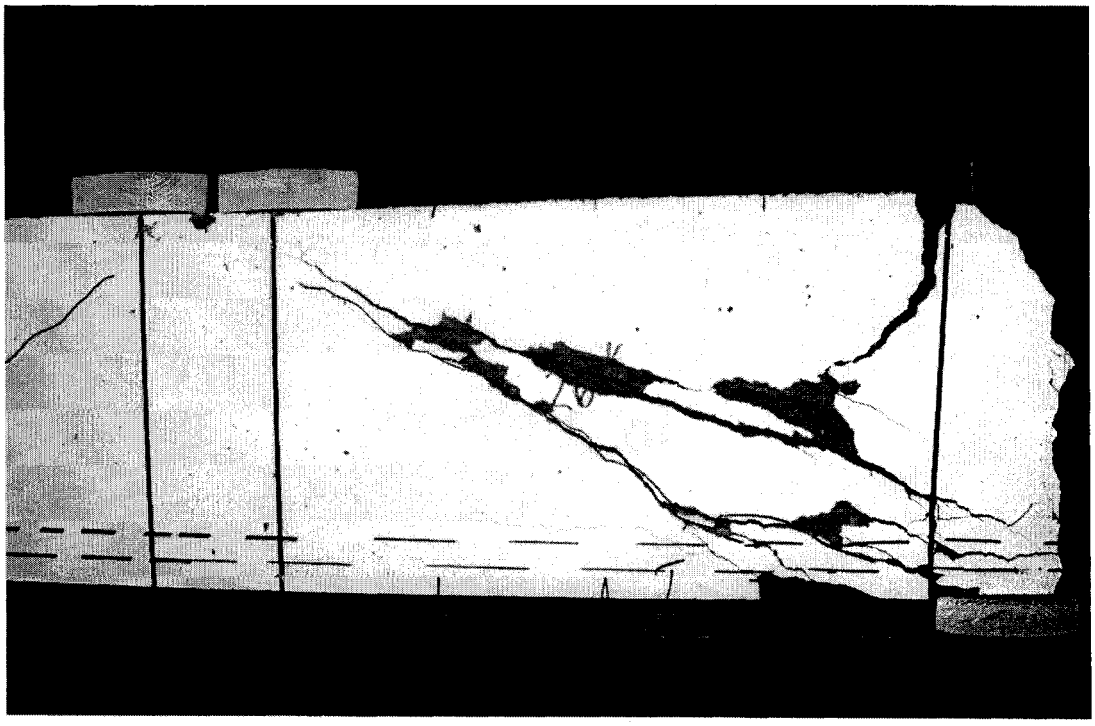

Figure 4-34. Right side crack pattern for beam B260S25.

4.4.12 Beam B360S25

Beam B360S25 measured 1676mm in length, 356mm in height, and 95mm. The main horizontal reinforcement consisted of 4 - 20M bars. A closed loop stirrup, 6mm in diameter, was placed near the loading points and supports, for a total of four stirrups.

The beam was loaded in 11.1 kN increments until reaching 133.4 kN, then loaded at 22.2 kN increments until failure. First cracking occurred at a load of 77.8 kN along a diagonal from the support to the loading point. Flexural cracking first occurred at 122.3 kN in the center of the beam. Failure of the test specimen occurred at 151.2 kN by diagonal cracking along the compression strut.

At each load increment 25 strain gauge readings were taken. The crack pattern is shown in Figure 4-35. Measured strain gauge readings are shown in Figure 4-36 to Figure 4-40.

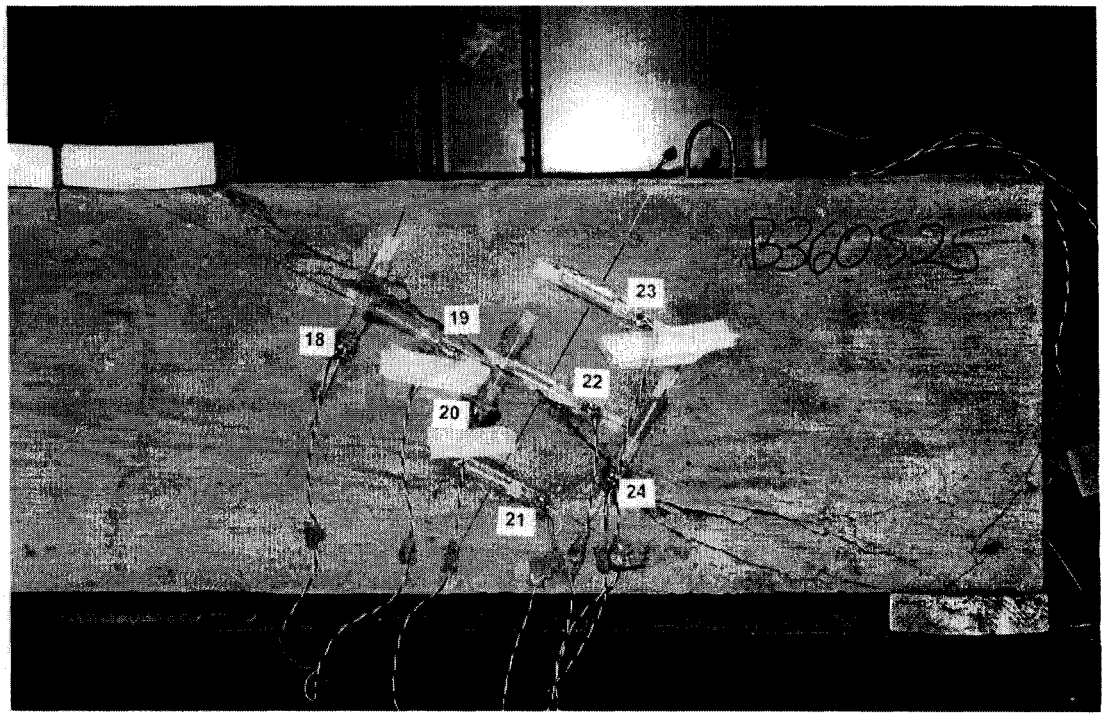

Figure 4-35. Right side crack pattern for beam B360S25.

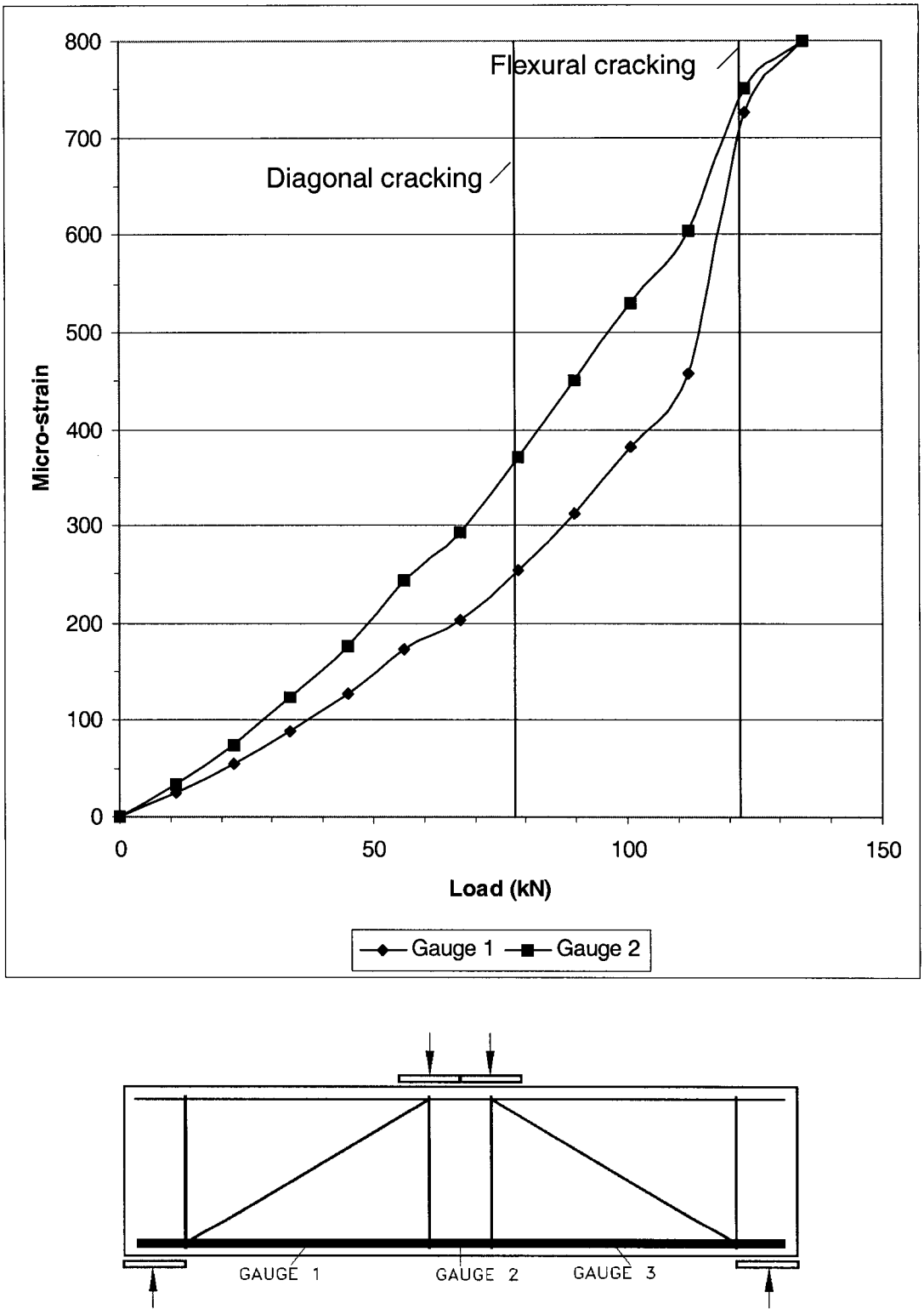

Figure 4-36. Main tensile steel strain versus load for beam B360S25.

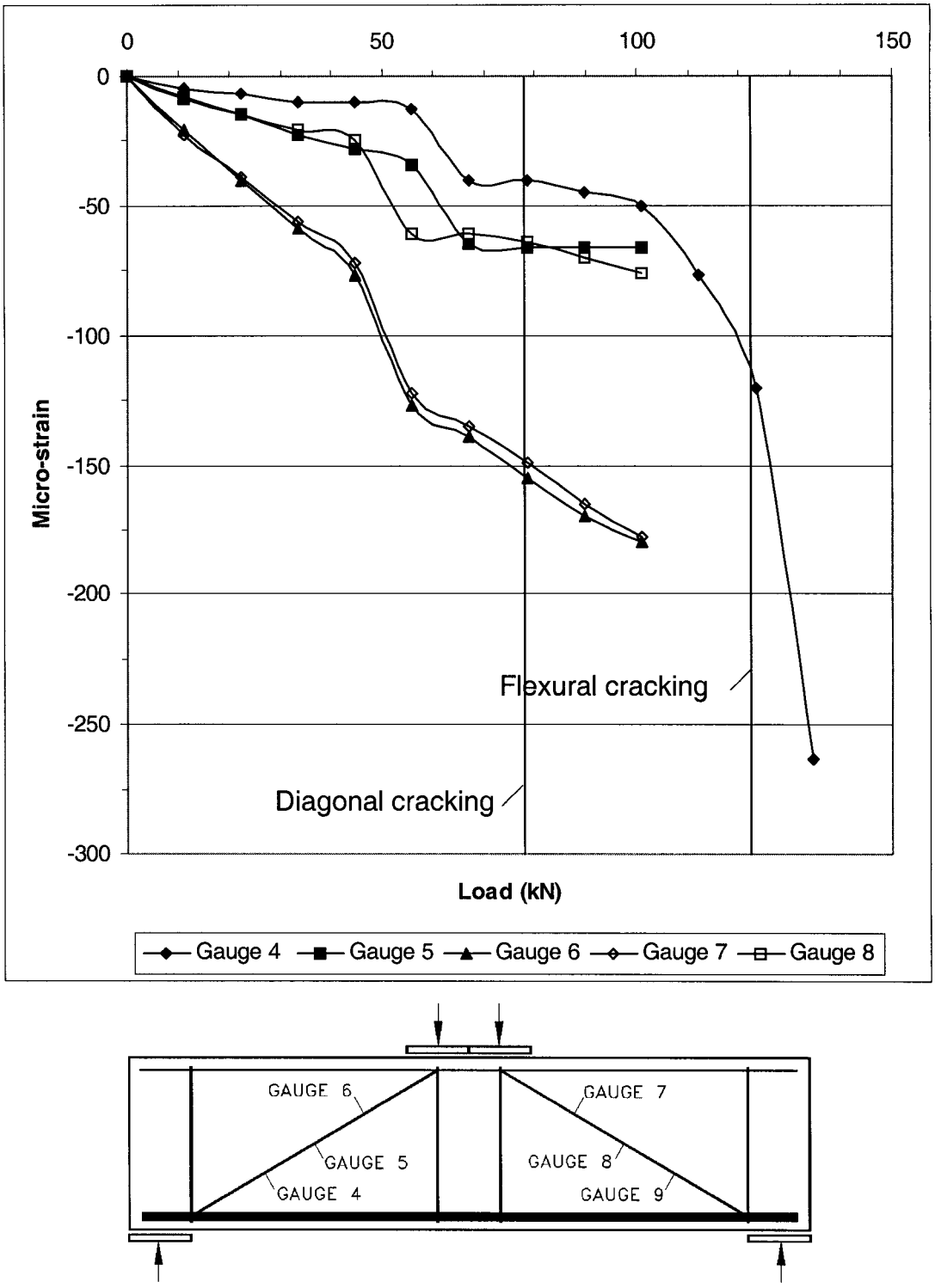

Figure 4-37. Diagonal steel strain versus load for beam B360S25.

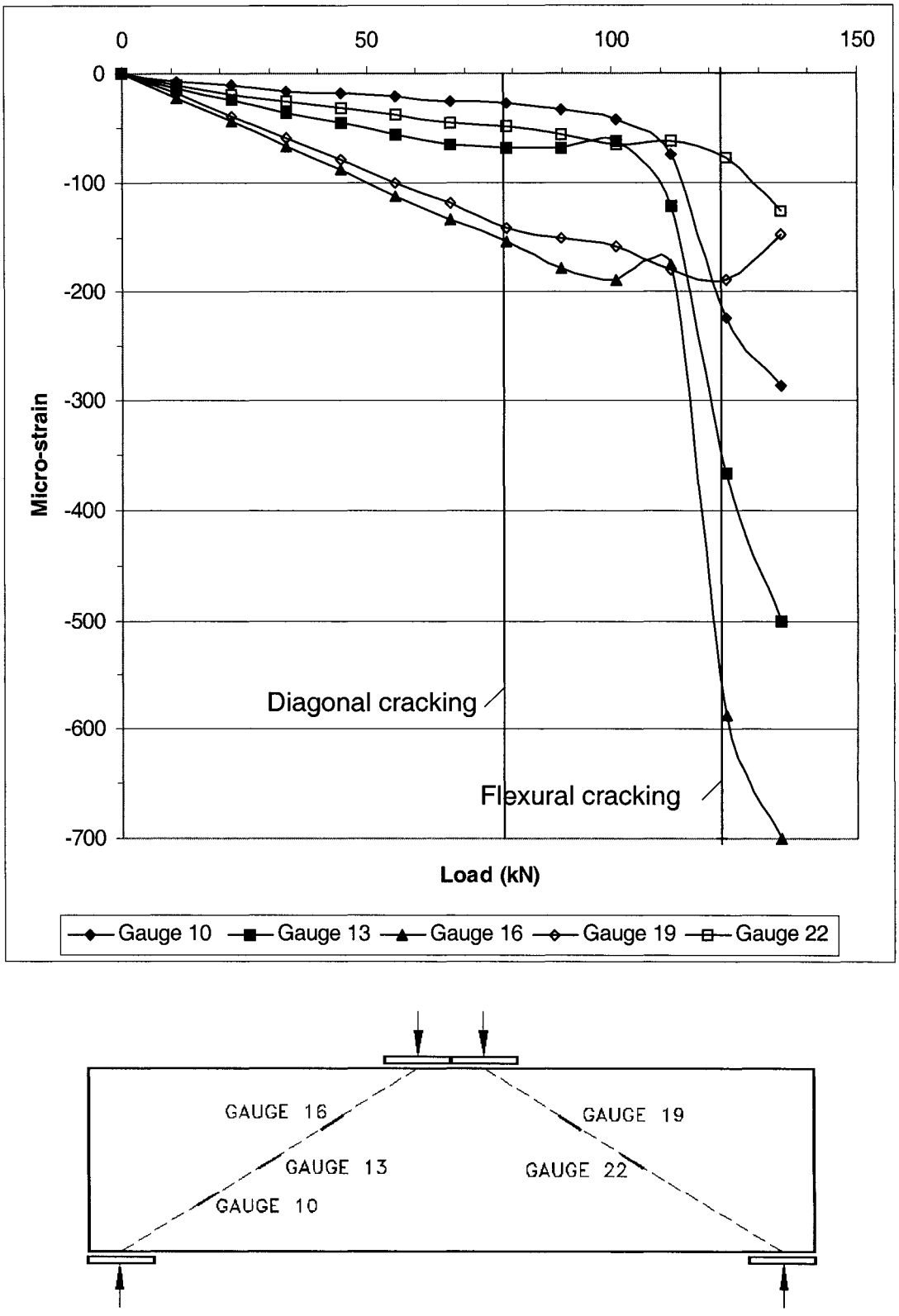

Figure 4-38. Concrete compression strain along diagonal versus load for beam B360S25.

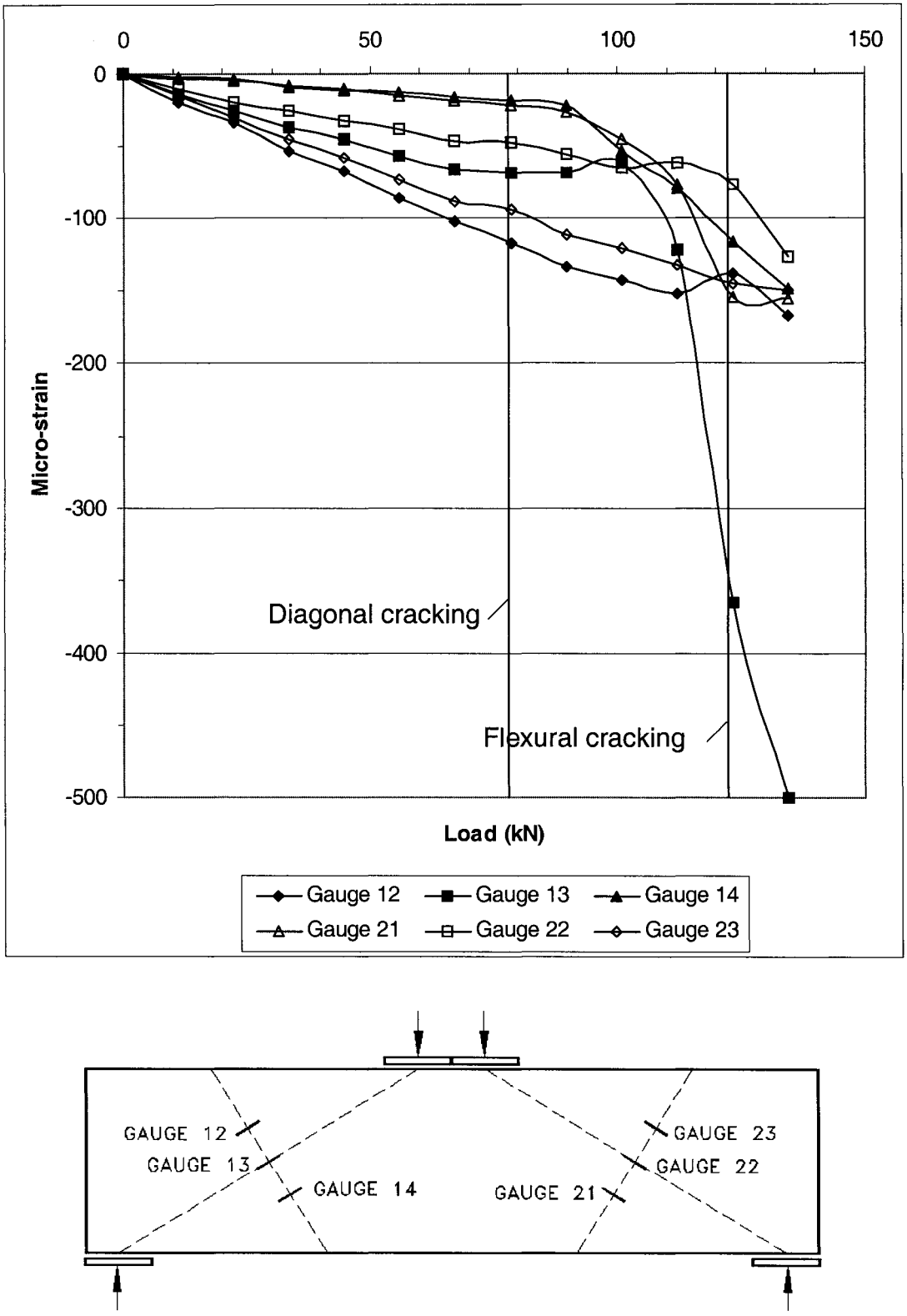

Figure 4-39. Concrete compression strain across the diagonal versus load for beam B360S25.

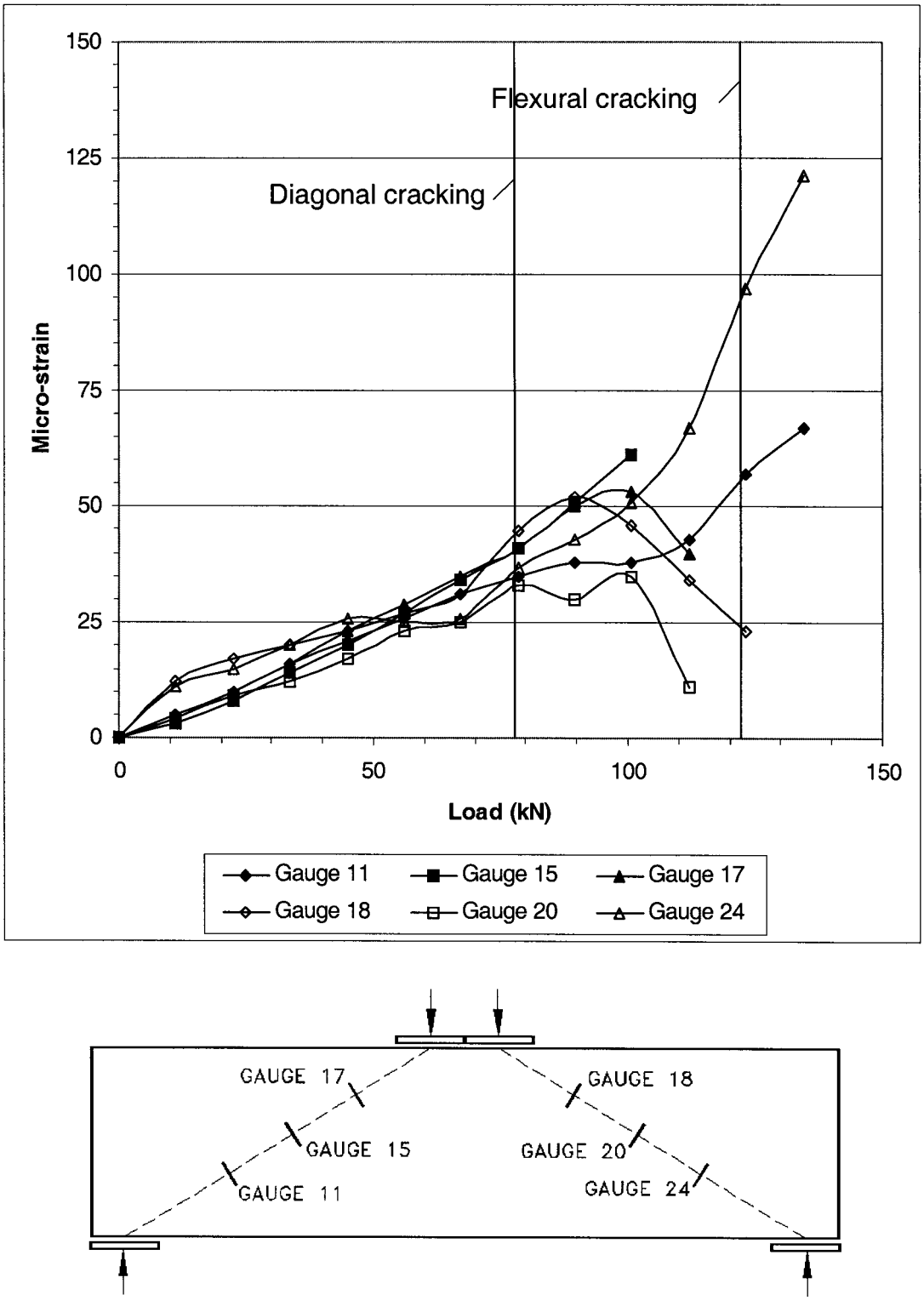

Figure 4-40. Concrete tension strain versus load for beam B360S25.

The strain gauge 3, which was to measure tensile strains on the main reinforcement did not function from the start of the test. Of the strain gauges measuring compressive strains on the steel rod placed diagonally along the compression strut, gauges 5, 6, 7, and 8 failed shortly after diagonal cracking. Strain gauge 9 did not function from the start of the test. All of the strain gauges measuring compressive strains on the concrete showed that the strains along the compression strut are much lower than the Canadian Code proposed value of 0.002[5], with the all of the measured strains below 0.0007.

The concrete strain gauges measuring tension perpendicular to the compression strut showed an increase in tensile strains with an increase in loading with a sudden drop after diagonal cracking. After diagonal cracking, strain gauge 15, 17, 18 and 20 stop functioning. The remaining two strain gauges recorded that the tensile strains began to increase again as loading was applied.

4.5 Modes of failure

All of the test beams failed by diagonal cracking. The strains measured in the tensile reinforcement showed that the beams did not fail by yielding of the reinforcement. Diagonal cracks were clearly visible from the point of loading to the supports.

5 Non-Linear Finite Element Analysis

5.1 Introduction

Finite Element Modeling was used to analyze the test results as reported in Chapter 4. The models were also used to help develop the strut and tie model introduced in Chapter 7. The commercial program ADINA[1] (Automatic Dynamic Incremental Nonlinear Analysis) was used.

5.1.1 Material Properties

5.1.1.1 Concrete

The concrete model in ADINA can be employed with 2-D or 3-D solid elements. The basic characteristics of the concrete model are:

- compression crushing failure at high compressive stresses,
- tension failures at relatively small tensile stresses,
- strain softening from compression crushing failure to an ultimate strain at which the material fails.

The tensile and compression failures are governed by stress strain envelopes. Consideration for the case of biaxial stress states is done by employing the stress-strain envelope proposed by Kupfer[29] as shown in Figure 5-1.

1. ADINA is a registered trademark of K.J. Bathe / ADINA R&D Inc.

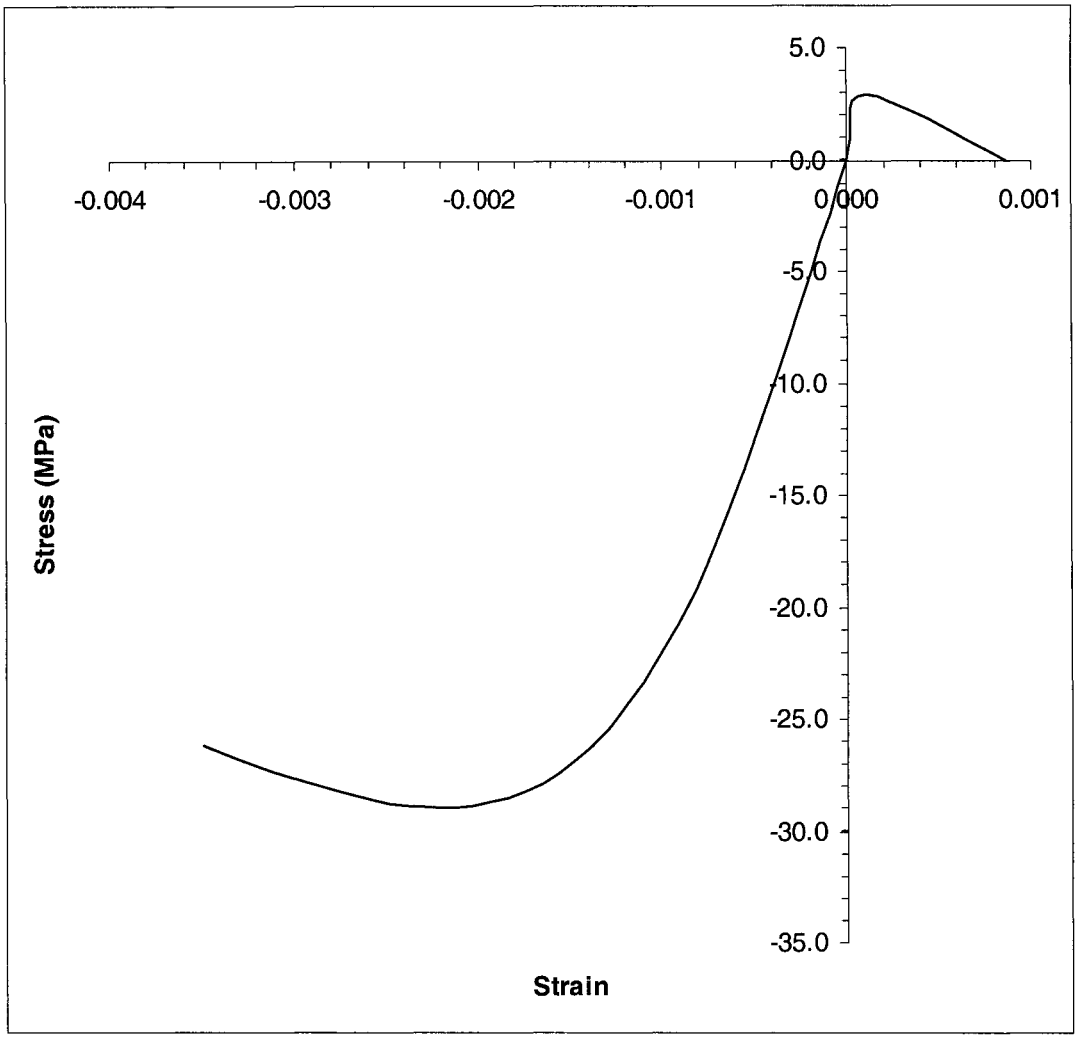

Figure 5-1. Concrete stress-strain curve used in the finite element analysis

5.1.1.2 Steel

The steel reinforcement was modeled using a plastic-bilinear material model. ADINA bases this material model on:

- The von Mises yield condition,
- An associated flow rule using the von Mises yield function,
- An isotropic or kinematic, bilinear hardening rule.

This material model can be used with truss elements. The stress-strain relationship is shown in Figure 5-2.

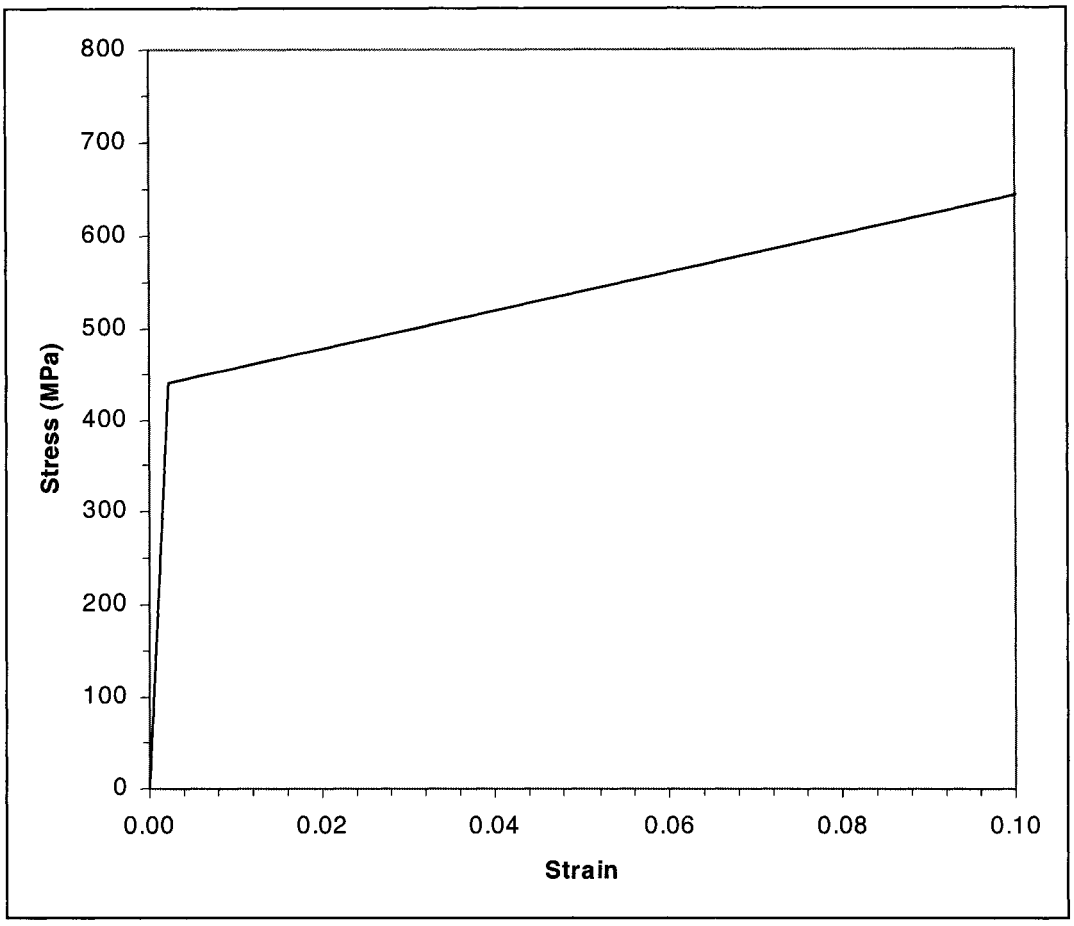

Figure 5-2. Stress-strain relationship for steel used in the finite element analysis

5.1.1.3 Concrete Post Tensile Failure

Tensile failure occurs when the tensile stress in the principal direction exceeds the tensile failure stress. When this occurs, it is assumed that a plane of failure develops perpendicular to the principal stress direction. The tensile failure plane is checked at each subsequent load step to determine whether the failure is still active. Failure is considered to be inactive when the normal strain across the plane becomes negative and less than the strain at the "last" failure. A tensile failure, may repeatedly become active and inactive. If a tensile failure plane has developed, the stress conditions along and normal to the material tensile failure plane are used to evaluate the stress-strain matrix.

5.1.1.4 Post Compression Failure

Compression crushing under multiaxial stress conditions is identified using the multiaxial failure envelope. Once the material has crushed, isotropic conditions are assumed using the uniaxial stress-strain law. The principal stresses are checked to see if a positive value has been reached, and if so, the stress in the corresponding direction is set to zero.

5.1.2 Modeling of Reinforcement

There are three alternative representations of reinforcement in a reinforced concrete member. These representations are known as distributed, embedded and discrete.

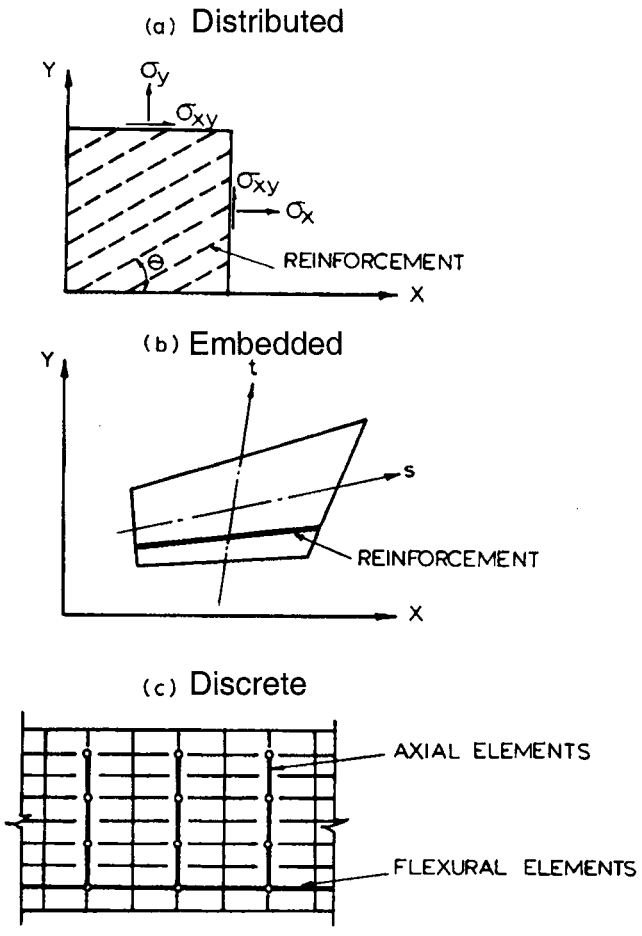

Figure 5-3. Alternate representation for steel reinforcement

Distributed representation assumes that the steel is distributed over the concrete element with a particular orientation. A composite concrete-reinforcement

constitutive relation is used. Perfect bond must be assumed between the concrete and steel.

An embedded representation may be used with higher order isoparametric concrete elements. The reinforcement is considered to be an axial member built into the isoparametric element such that the displacements are consistent with that of the element. Perfect bond is assumed between the concrete and steel.

With the discrete representation, axial force elements are assumed to be pin connected with two degrees freedom at the nodal points. The one dimensional reinforcement elements are superimposed on the two dimensional finite element mesh used to model the concrete. An advantage of this system is that it can account for possible displacement between the reinforcement with respect to the surrounding concrete. In this study, a discrete reinforcement representation is used.

5.1.3 Elements

5.1.3.1 Plane Stress Element

ADINA can model the following kinematic assumptions; plane stress, plane strain, generalized plane strain, axisymmetric and 3-D plane stress. The deep beams were modeled using eight node two dimensional plane stress elements. The eight node element is shown in Figure 5-4.

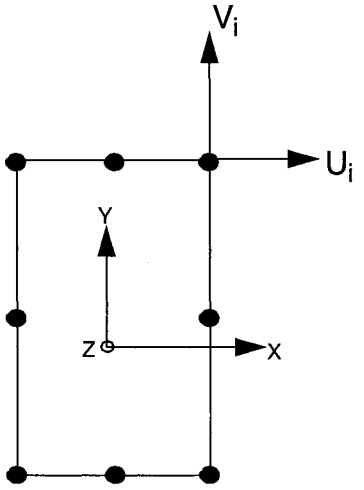

$$\sigma_{zz} = 0$$
$$\tau_{xz} = 0$$
$$\tau_{yz} = 0$$

Figure 5-4. Eight node plane stress element

5.1.3.2 Truss Element

ADINA can employ 2-node, 3-node or 4-node truss elements. The steel reinforcement was modeled using 3-node truss elements shown in Figure 5-5. Only longitudinal forces are transmitted by the truss element.

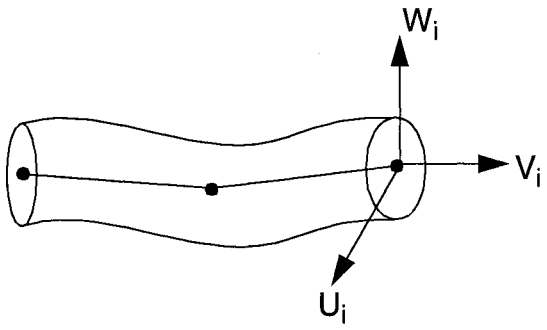

Figure 5-5. Three node truss element used to model the steel reinforcement

5.2 Finite Element Models

Although all beams were modeled, only two series are presented here. Beams B150S6, B150S19 and B250S19 were modeled using 981 nodes, 300 plane stress elements and 60 three node truss elements. The concrete elements used were 8-node plane stress elements, the steel was modeled with 3-node truss plastic-bilinear truss elements. The finite element models used are shown in Figure 5-6.

Beams B260S6, B360S6 and B260S25 were modeled using 1109 nodes, 340 plane stress elements and 68 three node truss elements. The concrete elements used were 8-node plane stress elements, the steel was modeled with 3-node truss plastic-bilinear truss elements. The finite element model used is shown in Figure 5-6.

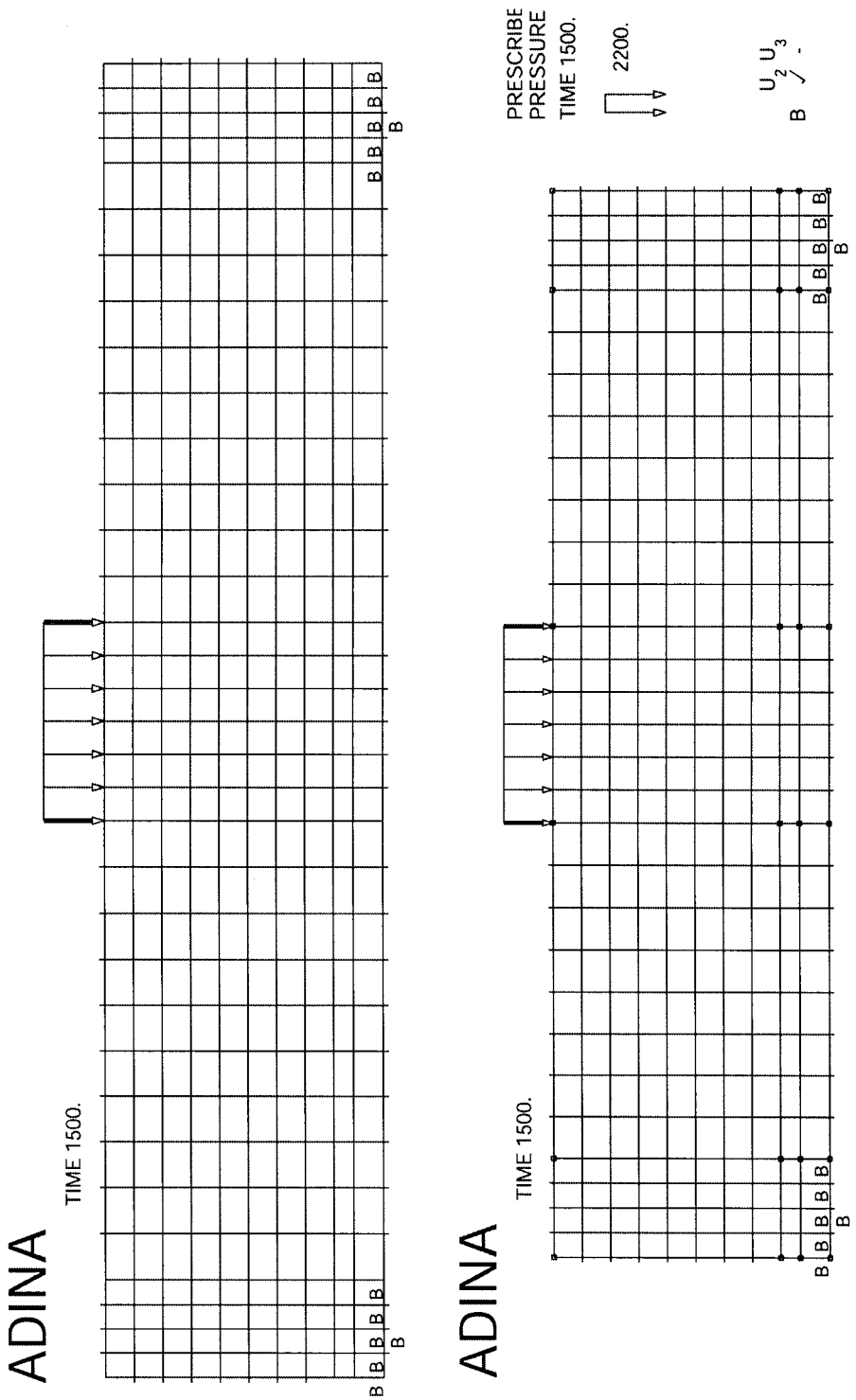

Figure 5-6. Finite element models used to simulate experimental tests

5.3 Finite Element Results

5.3.1 Beams B150S6, B150S19, and B250S19

The finite element model for beams B150S6, B150S19, and B250S19 predicted a failure load of 375.3 kN. This compares very well with the observed failures at 371.8 kN, 356.7 kN and 378.0 kN for beams B150S6, B150S19, and B250S19 respectively. The load versus deflection at the midpoint as well as 304 mm from the left side is shown in Figure 5-7. Plots of the tensile steel strain determined by the finite element analysis at midpoint and on the left side of the main reinforcement is shown in Figure 5-8. A comparison of finite element results with the experimentally measured values is done in Chapter 6.

Contour plots of compressive stresses at increasing loads are shown in Figure 5-9 and Figure 5-10. From these figures, the development of the compression strut is clearly shown. This supports the concept of strut and tie modeling of deep beams.

The finite element analysis predicted a diagonal cracking failure. The cracking pattern is shown in Figure 5-15 on page 147. Comparing this pattern to the photographs taken of the failed test beams shows that the patterns are quite similar. This leads us to believe that the finite element analysis is accurately modeling the test beams.

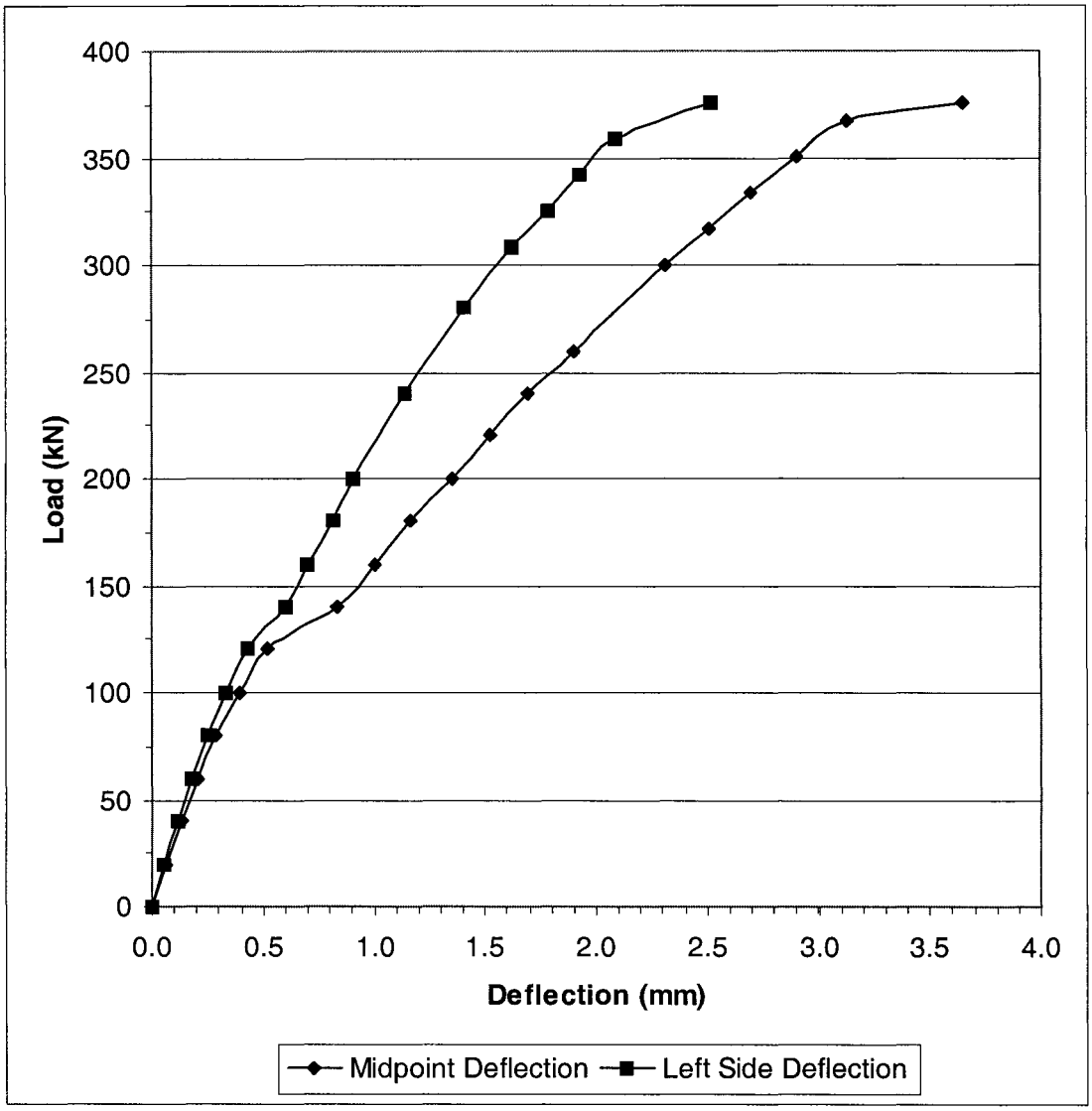

Figure 5-7. Deflection of series B50 as determined by the finite element analysis

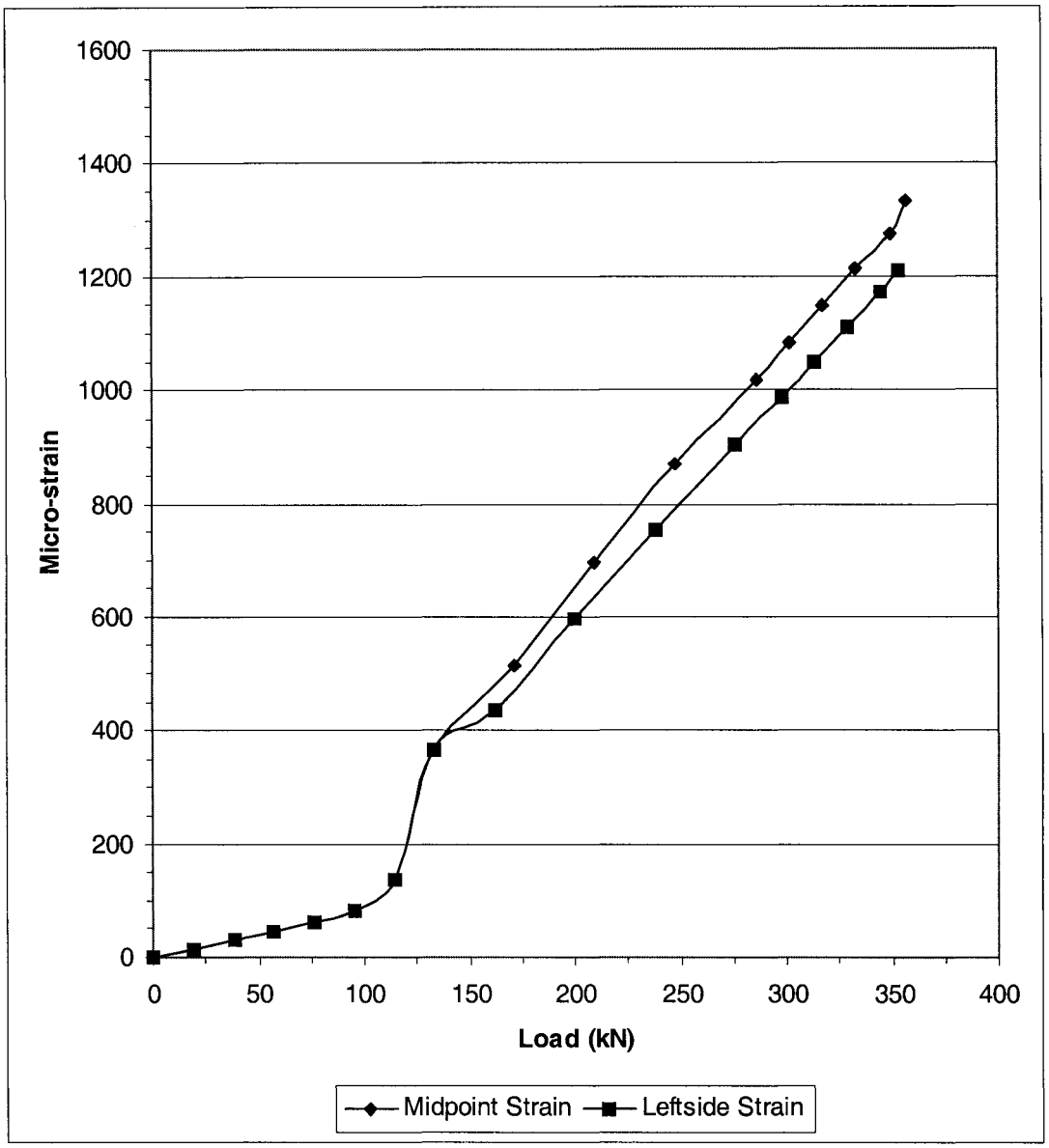

Figure 5-8. Steel strain at midpoint and leftside determined by finite element analysis

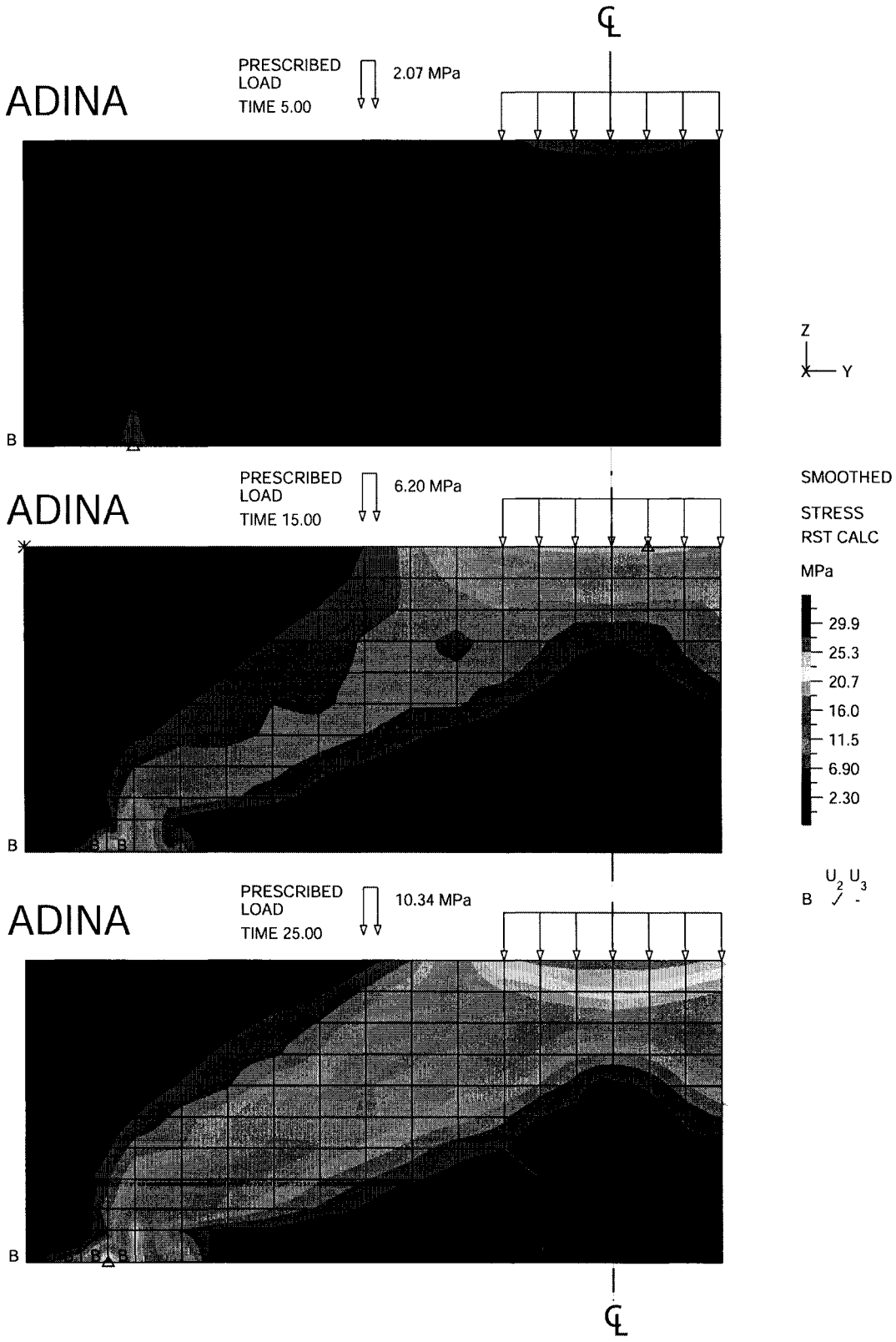

Figure 5-9. Compressive stresses at a loading of 50 kN, 150 kN and 250 kN

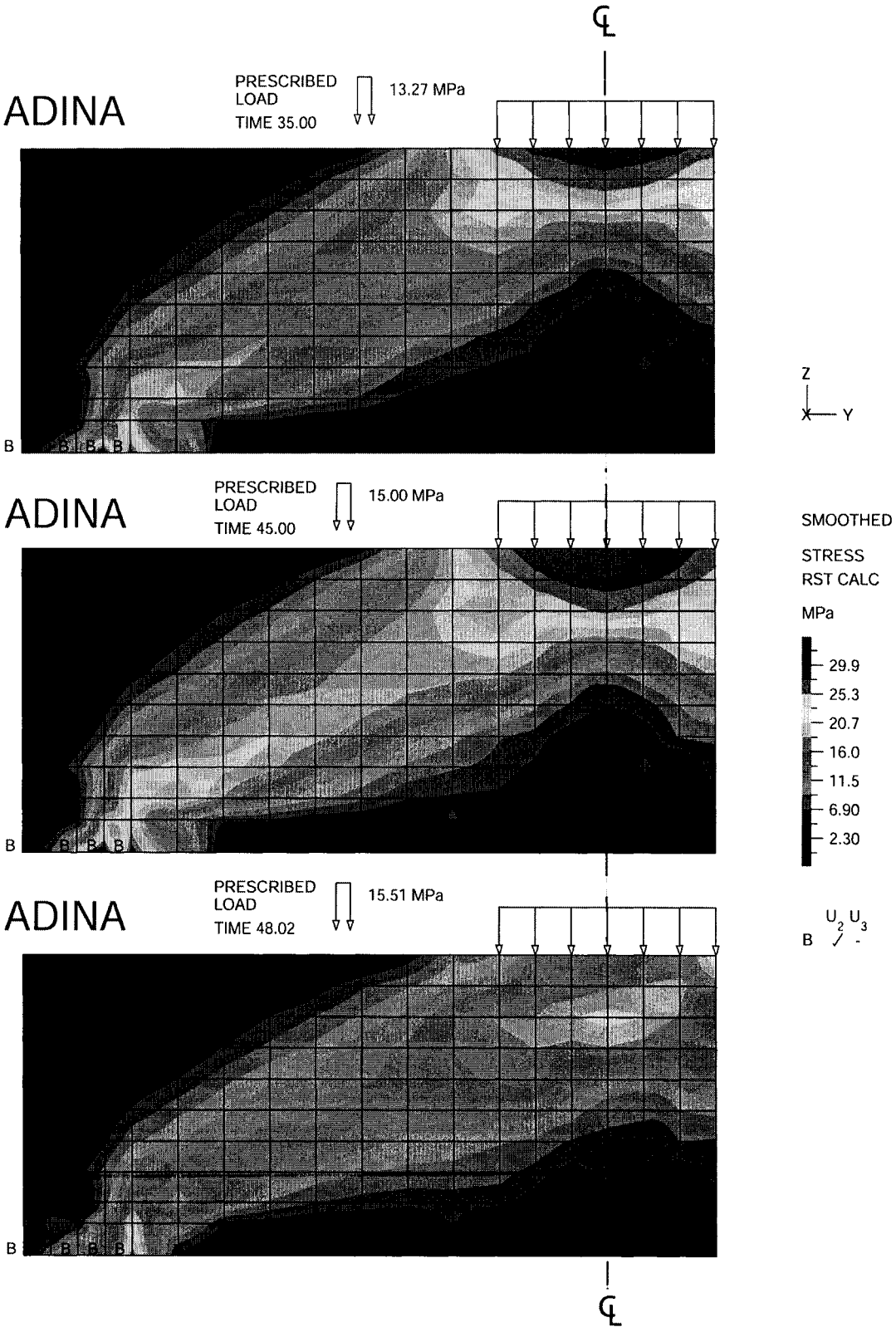

Figure 5-10. Compressive stresses at a loading of 321 kN, 362 kN and 375 kN

5.3.2 Beams B260S6, B360S6 and B260S25

The finite element model for beams B260S6, B360S6 and B260S25 predicted a failure load of 343.0 kN. This compares very well with the observed failures of 371.8 kN, 355.8 kN and 355.8 kN for beams B260S6, B360S6 and B260S25 respectively. The load versus deflection at the midpoint as well as 406 mm from the left side are shown in Figure 5-11. Plots of the tensile steel strain determined by the finite element analysis at the midpoint and on the left side of the main reinforcement are shown in Figure 5-12. A comparison of finite element results with the experimentally measured values is done in Chapter 6.

Contour plots of compressive stresses at increasing loads are shown in Figure 5-13 and Figure 5-14. From these figures, the development of the compression strut is clearly shown. This supports the concept of strut and tie modeling of deep beams.

The finite element analysis predicted a diagonal cracking failure. The cracking pattern is shown in Figure 5-15 on page 147. Comparing this pattern to the photographs taken of the failed test beams shows that the patterns are quite similar. This leads us to believe that the finite element analysis is accurately modeling the test beams.

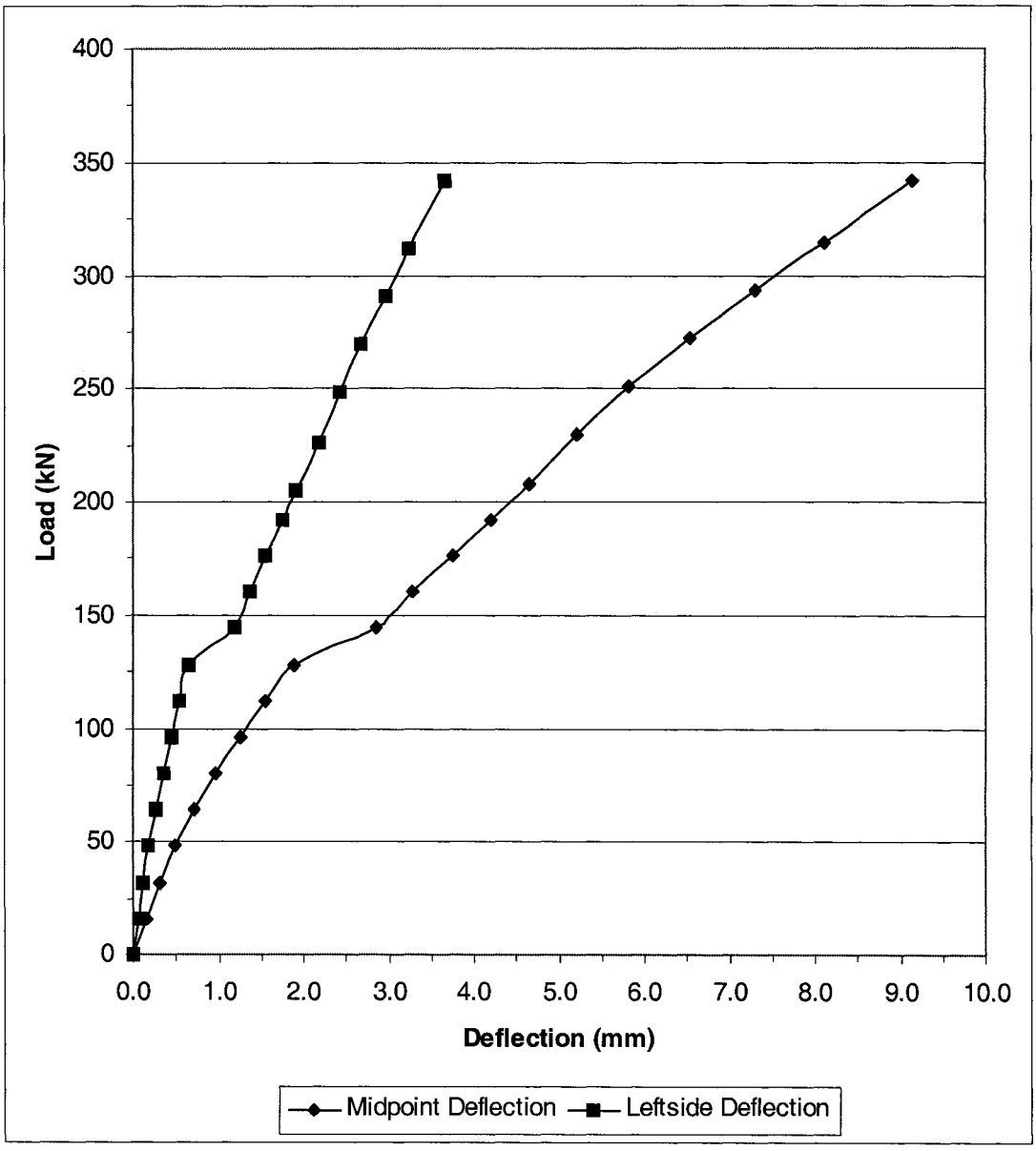

Figure 5-11. Deflection of deep beam series B60 as determined by finite element analysis

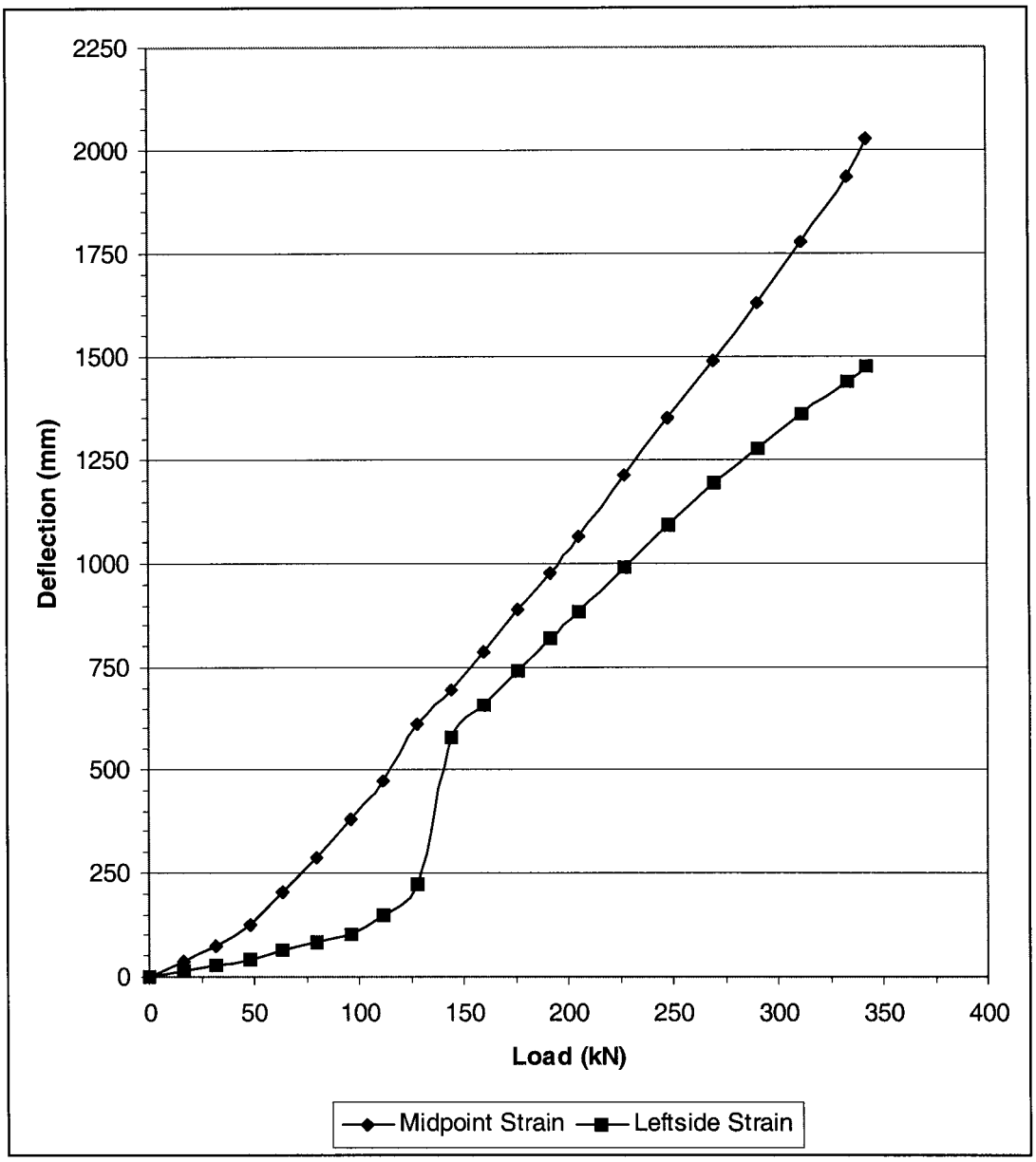

Figure 5-12. Steel strain at midpoint and leftside determined by finite element analysis

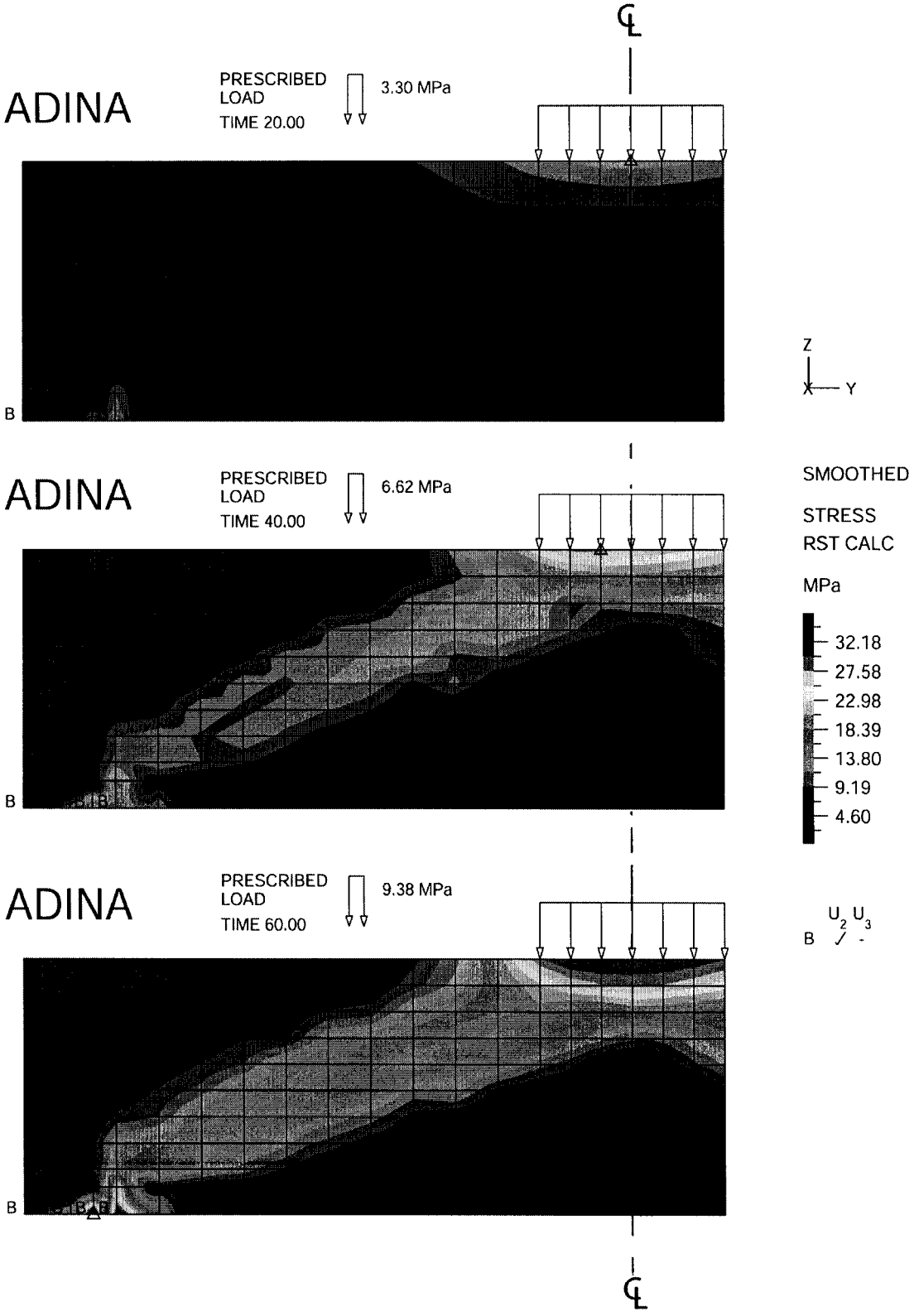

Figure 5-13. Compressive stresses at a loading of 80 kN, 160 kN and 227 kN

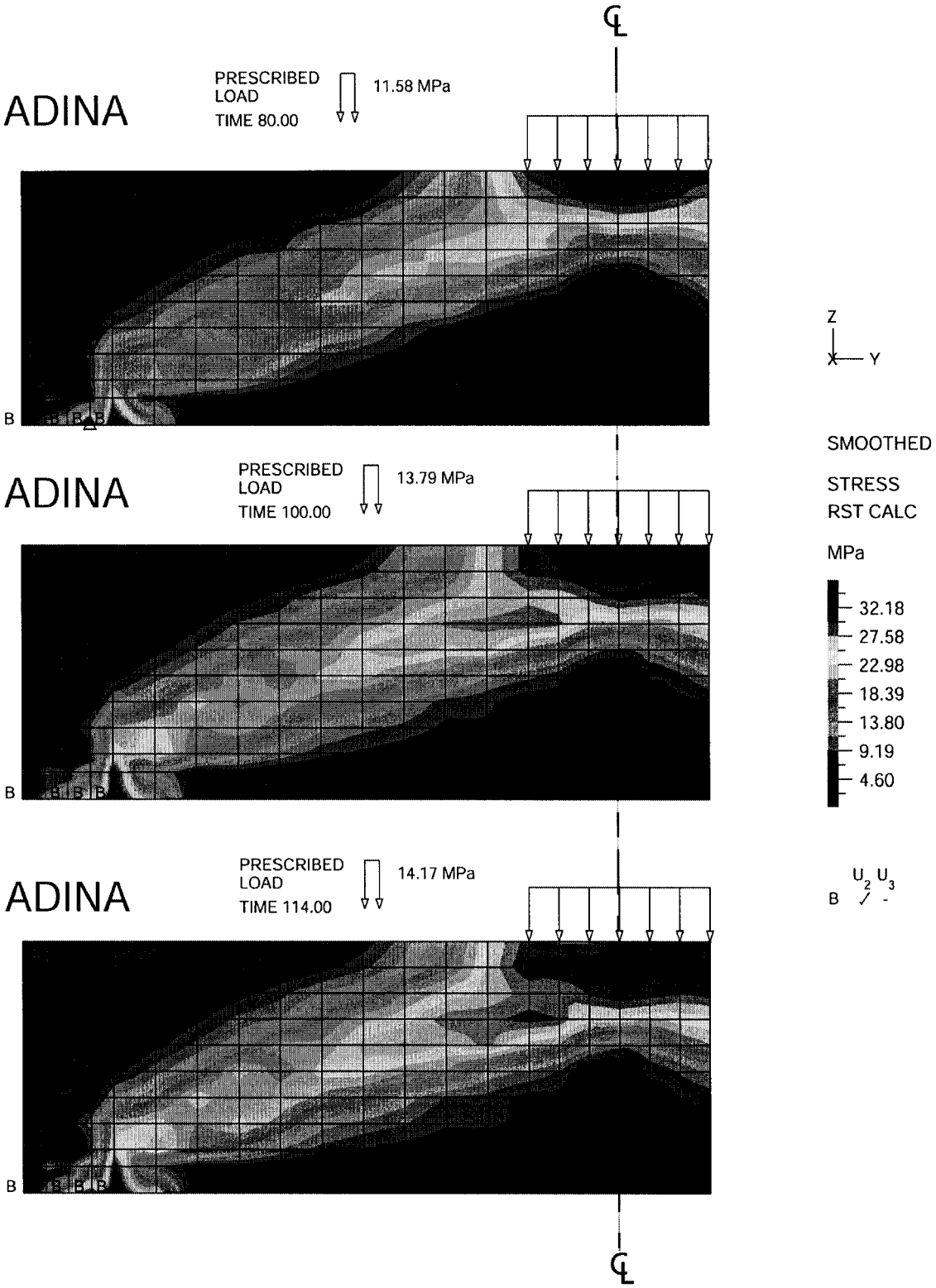

Figure 5-14. Compressive stresses at a loading of 280 kN, 334 kN and 343 kN

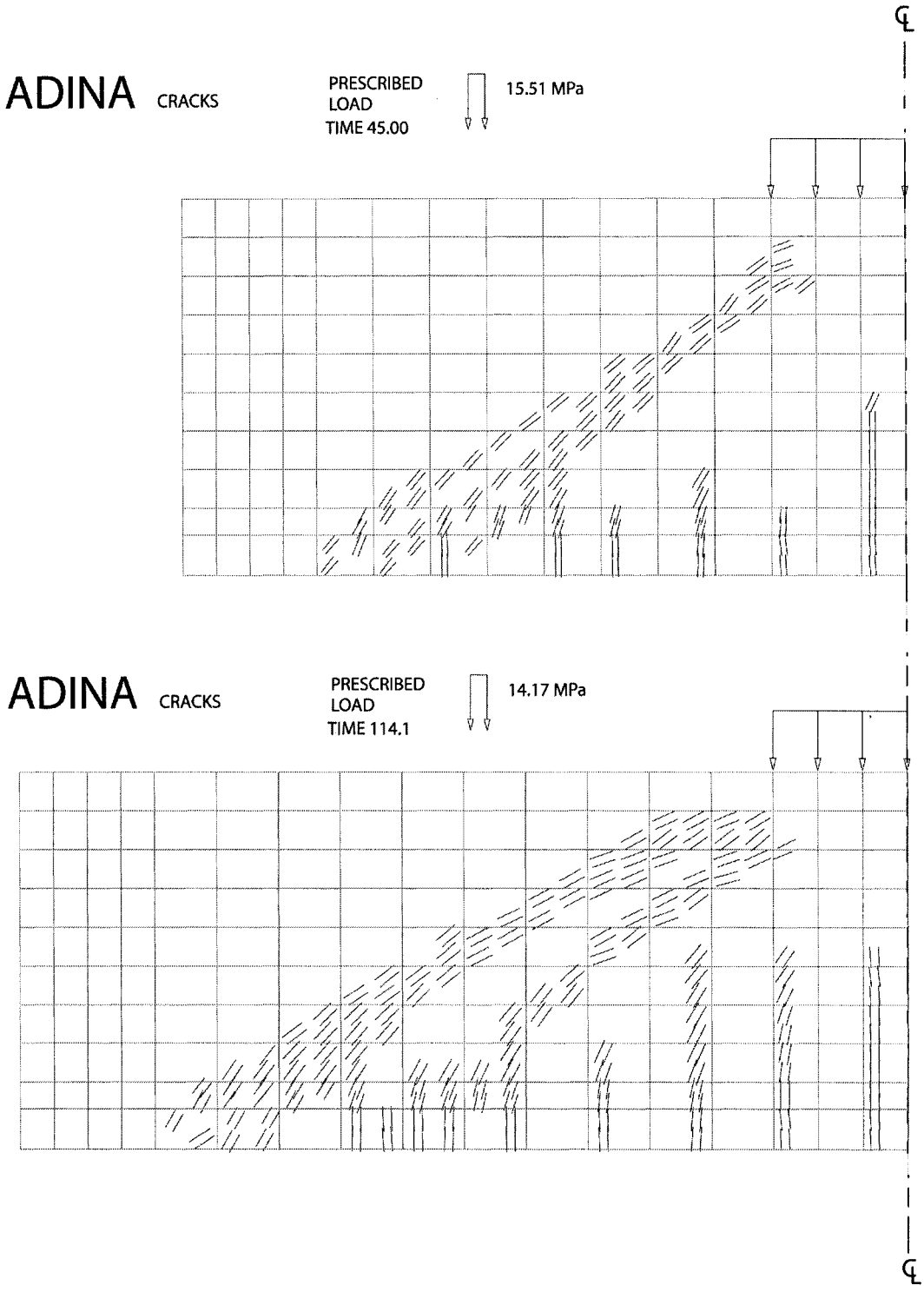

Figure 5-15. Cracking patterns as predicted by the finite element analysis

6 Analysis of F.E.M. Results

6.1 Introduction

Test results were presented in Chapter 4 with finite element modeling of the test samples in Chapter 5. This chapter will first examine the validity of the finite element models, then the behaviour of the compression strut will be studied using the results from the models. A strut and tie model will be defined based on the observations from the experimental work as well as from the finite element analysis. The strut and tie model, presented in Chapter 7, will be applied to the samples tested in this study as well as to other past research that was discussed in Chapter 2.

6.2 Finite Element Model

Before conclusions can be drawn from the finite element models, it is necessary to determine their validity. Table 6-1 lists the calculated capacity of the test samples as determined by the ADINA finite element models. The ratio of the experimental failure load to the finite element analysis is also provided for clarity. As can be seen from this table, the models accurately predicted the ultimate capacity of the test samples.

Ultimate capacity prediction by itself is not sufficient in determining the overall accuracy of the models, other factors must also be checked. It was shown in Chapter 5 that the cracking patterns and mode of failure predicted by the finite element analysis was similar to that observed in the laboratory. Deflection graphs were drawn comparing the experimental model with the ADINA predictions. As can be seen in Figure 6-1, Figure 6-2, Figure 6-3, and Figure 6-4, the predicted

deflection of the deep beam samples compared well to the actual recorded deflections. This is a very good indication that the models are behaving in a similar fashion to that of the experimental samples.

Figure 6-5, Figure 6-6, Figure 6-7, and Figure 6-8 show the comparison of the calculated tensile strain in the steel reinforcement with the strains recorded from the strain gauges applied to the test samples. As can be seen from these graphs, the predicted strains are in good agreement with the recorded ones indicating that the steel reinforcement was modeled correctly and that the behavior of the finite element model is similar to that of the test samples.

Table 6-1. Measured failure loads of the test samples.

Sample	Concrete Compressive Strength (MPa)	Measure Ultimate Load (kN)	Computed Failure Load (kN)	$\frac{\text{Measured Ultimate Load}}{\text{Computed Failure Load}}$
B150S6	29.0	371.9	358.5	1.04
B250S6	34.5	496.4	439.9	1.13
B350S6	29.0	422.6	358.5	1.17
B150S19	29.0	356.7	358.5	0.99
B250S19	29.0	378.1	358.5	1.05
B350S19	25.5	311.4	300.2	1.04
B160S6	29.0	392.8	367.0	1.07
B260S6	29.0	371.9	367.0	1.01
B360S6	34.5	355.8	342.9	1.04
B160S25	16.5	169.9	164.1	1.03
B260S25	34.5	355.8	342.9	1.04
B360S25	16.5	151.2	164.1	0.92

Important observations can now be made from the finite element models since they have been shown to accurately depict the experimental test results.

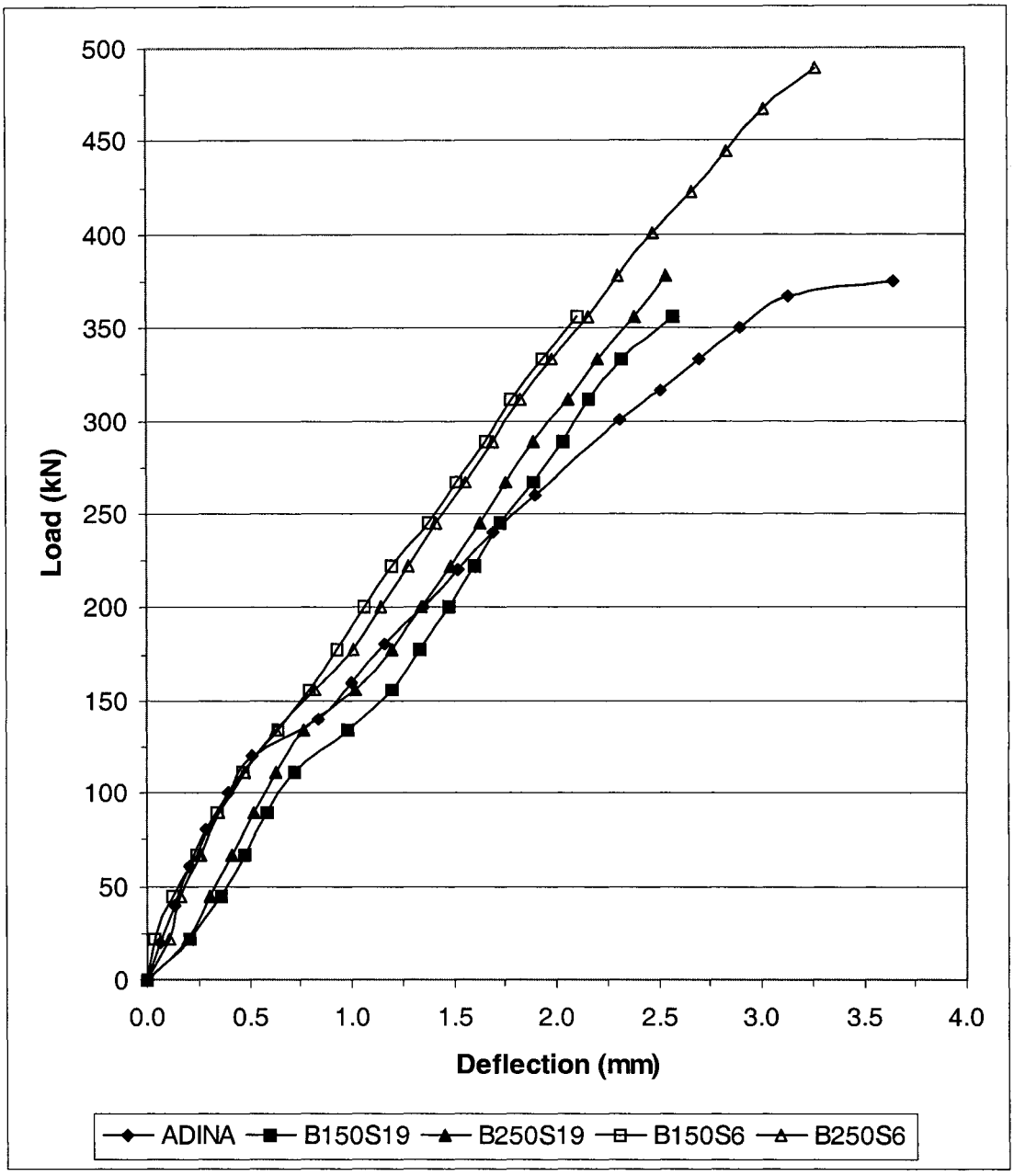

Figure 6-1. Midpoint deflection from experimental test results and finite element analysis

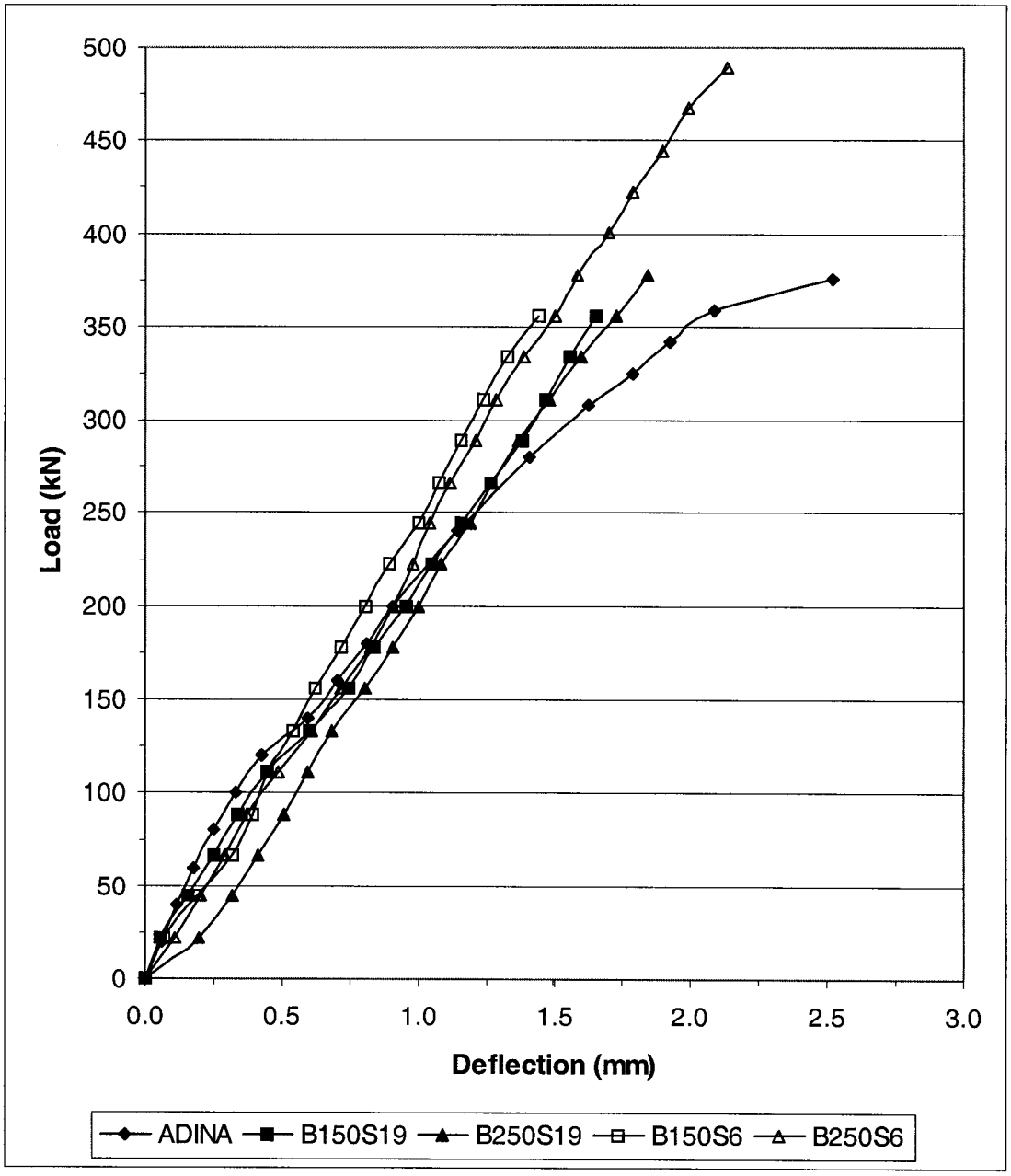

Figure 6-2. Left side deflection from experimental test results and finite element analysis

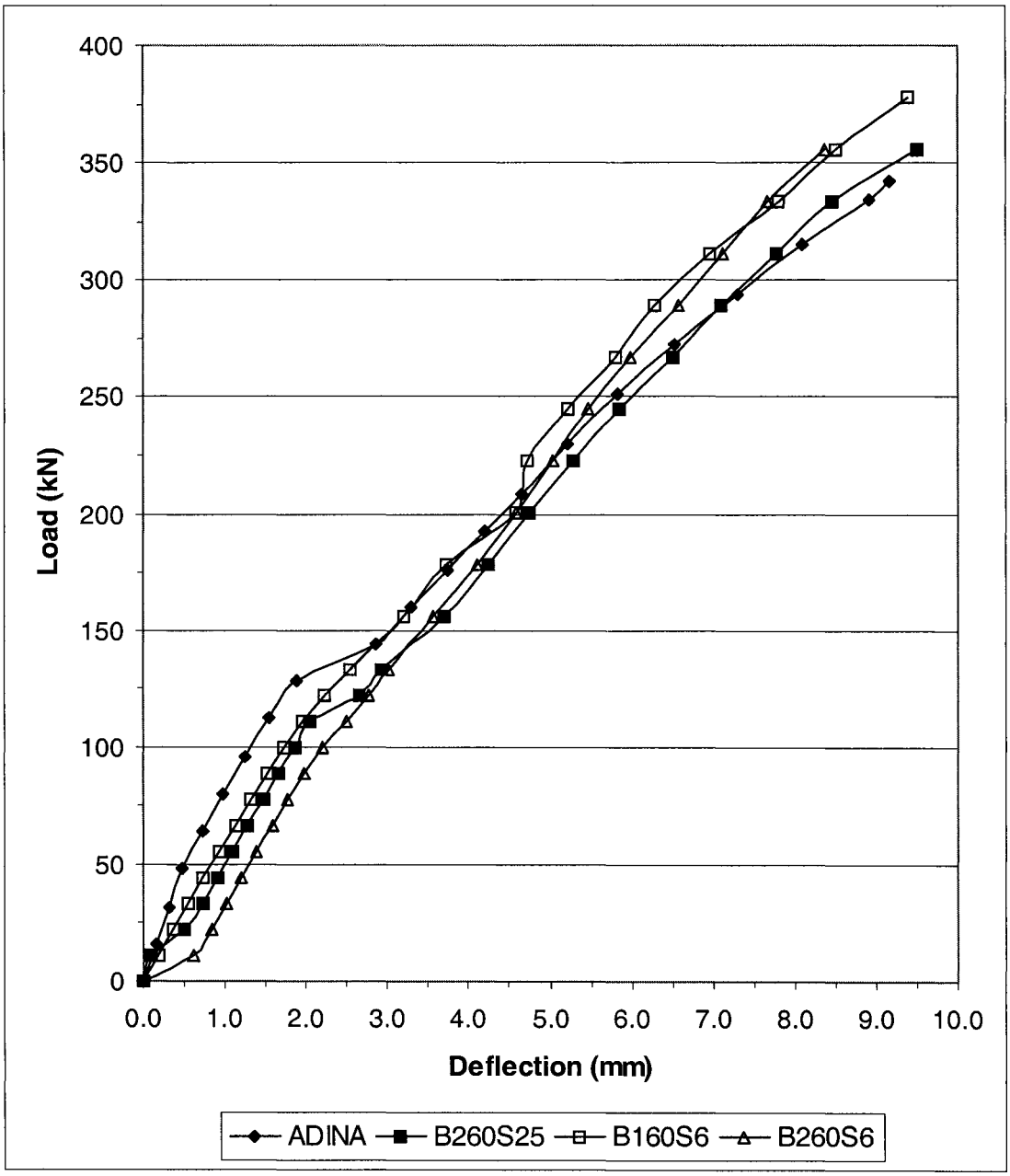

Figure 6-3. Midpoint deflection from experimental test results and finite element analysis

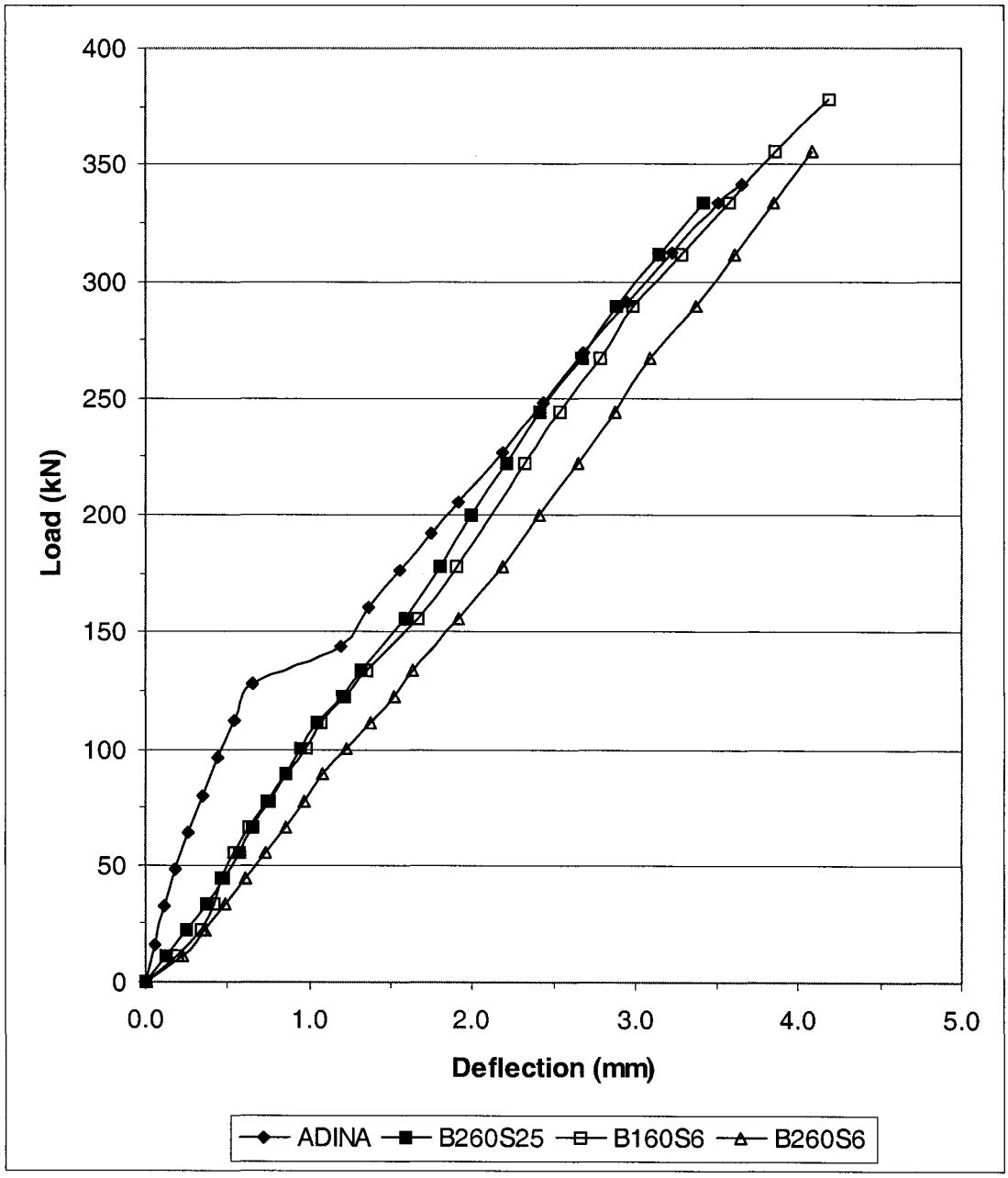

Figure 6-4. Left side deflection from experimental test results and finite element analysis

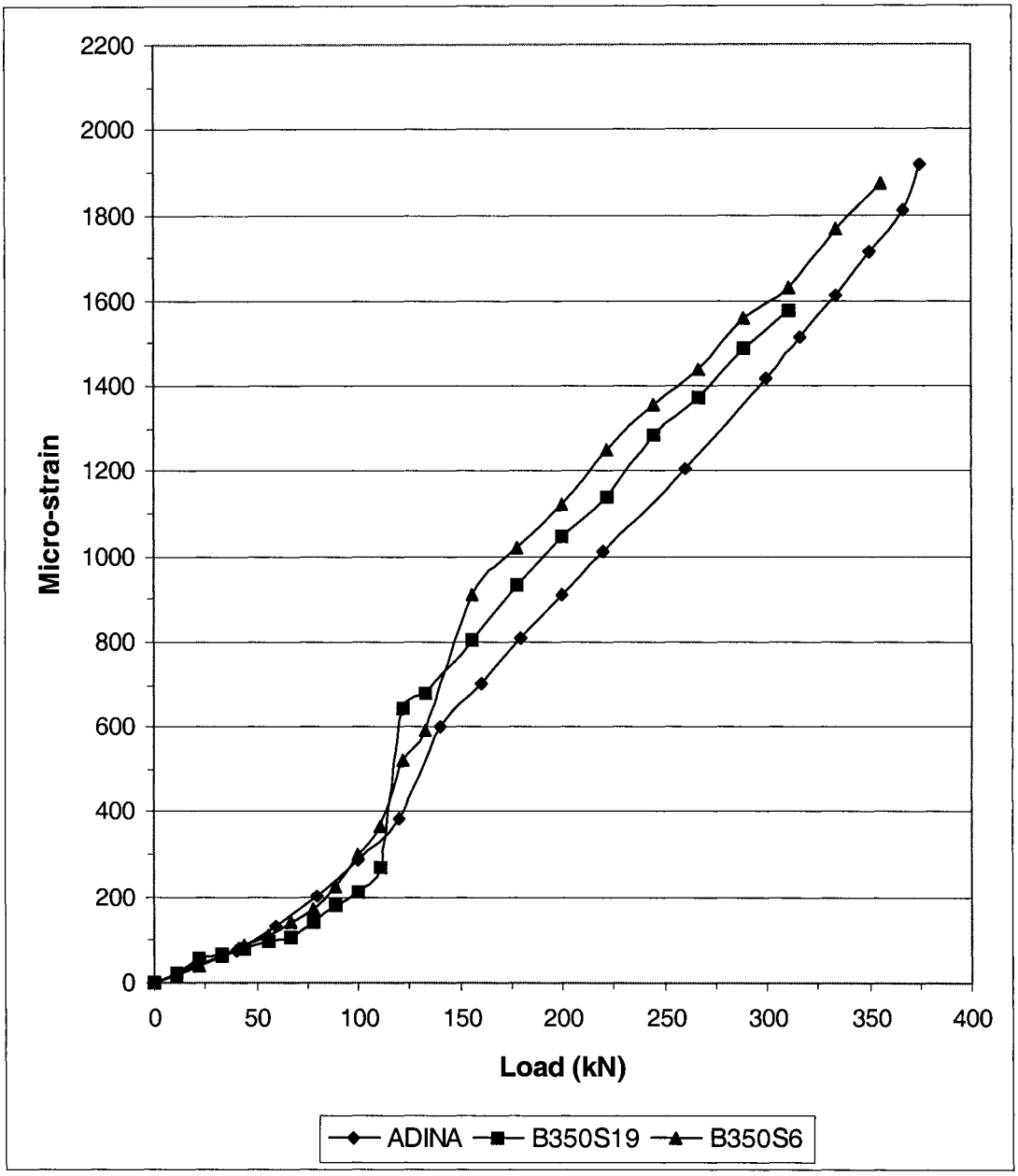

Figure 6-5. Comparison of main tension steel strain at midpoint for series B350

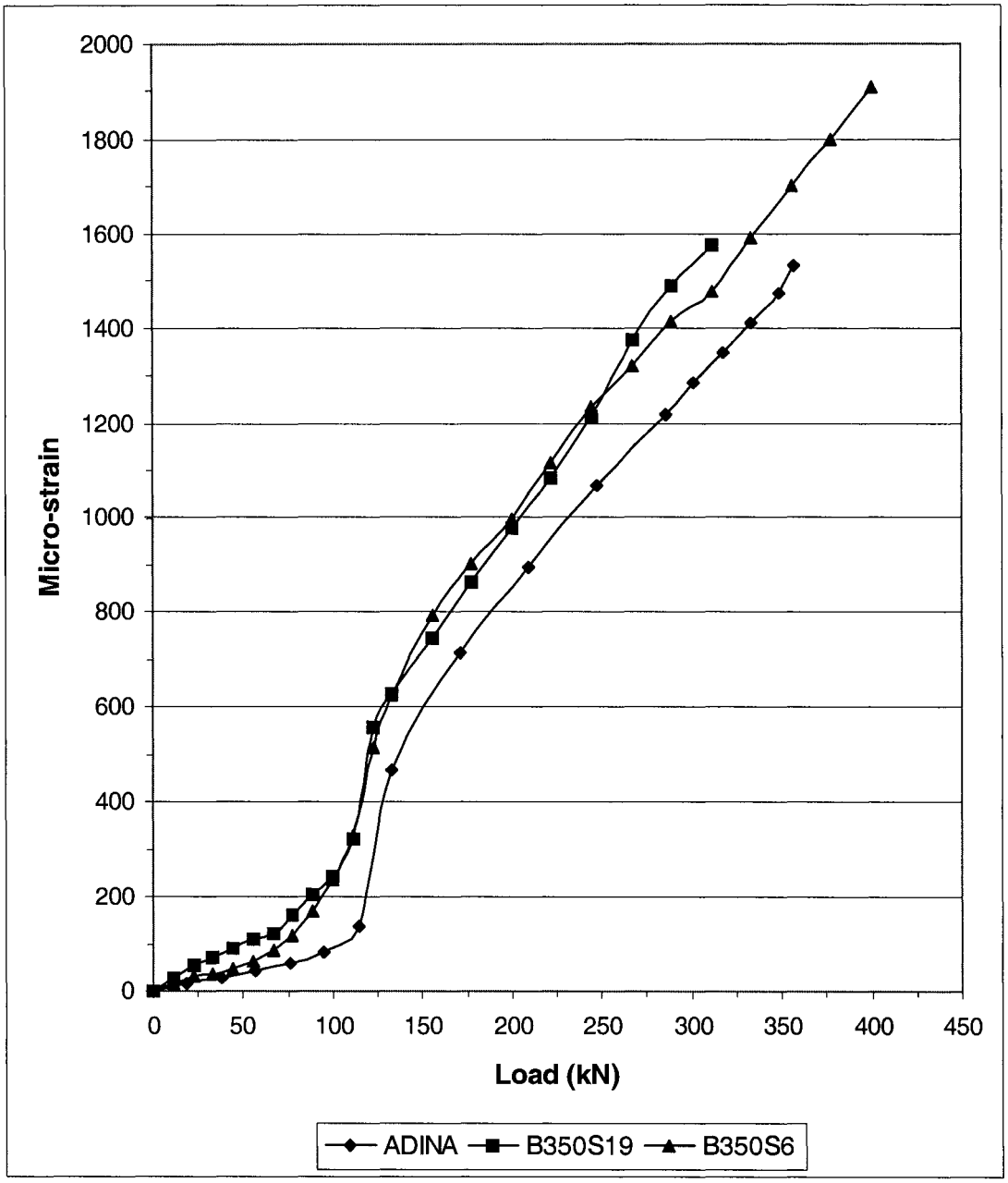

Figure 6-6. Comparison of main tension steel strain at left side for series B350

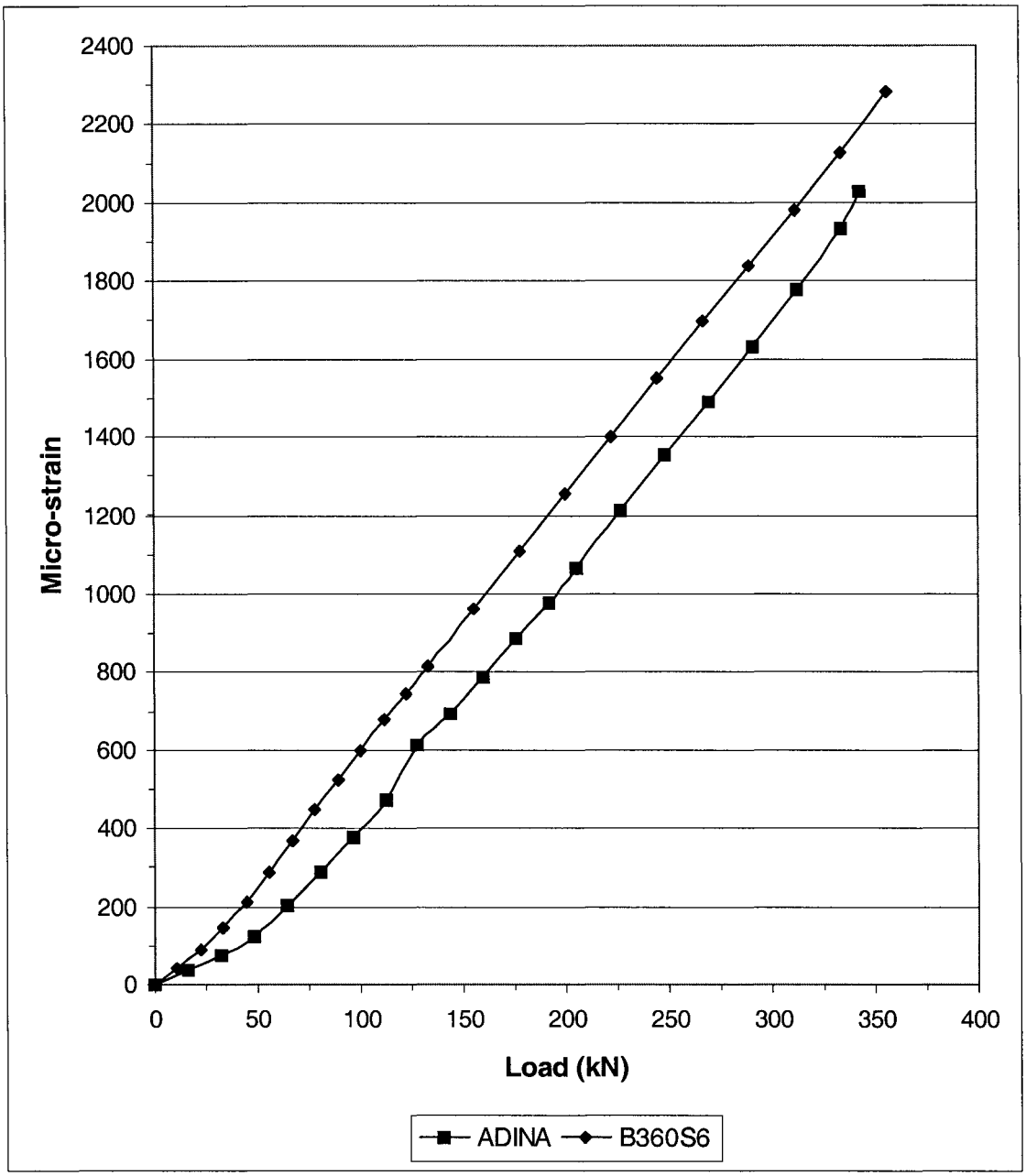

Figure 6-7. Comparison of main tension steel strain at midpoint for series B360

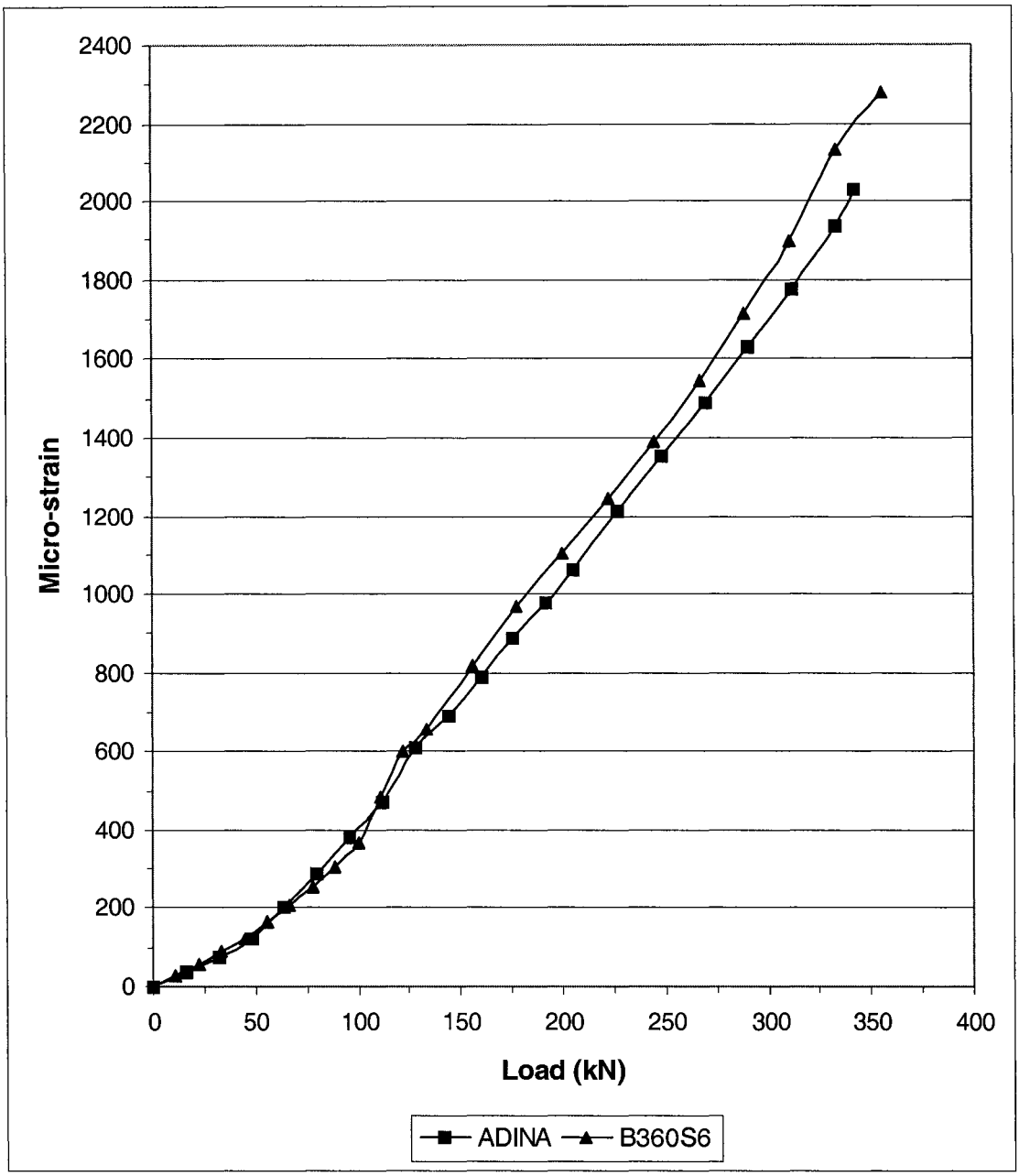

Figure 6-8. Comparison of main tension steel strain at left side for series B360

6.2.1 Stress and strain distribution

The first important observation can be made by examining the load transmission. As can be seen in Figure 6-9, the finite element analysis shows the development of the compression strut from the point of loading to the supports.

It stands to reason that if the load transmission acts from the loading points to the supports, then the effective stress[1] will likewise have a similar behaviour. Figure 6-10 to Figure 6-11 verifies this observation.

A significant observation can be seen in Figure 6-12 to Figure 6-15. From these figures, it can be seen that the compression strut is under biaxial stress and strain. This is in good agreement with the cracking pattern discussed in the introduction and with that developed on the test samples. Under biaxial compression and tension, the concrete compressive strength must be reduced. When defining the compression strut, steps must be taken to consider the biaxial stress state that exists along the compression strut.

The preliminary results of the finite element modeling indicates that there is no need to design deep beams and corbels for "shear". It has been shown that the behaviour of these structures is in developing a compression strut and tension ties. By designing the strut and tie, the design of the structure is complete. Not only will the design reflect the behaviour of these elements, but more economical and efficient designs can be made.

A close examination of the stress-strain distribution along the compression strut as well as perpendicular to the compression strut is needed. In the following section, such an examination is carried out.

---

1. Although maximum shear stress theory provides a reasonable hypothesis for yielding, maximum distortion energy theory correlates with test data better. ADINA uses the following equation to determine effective stress. $\sigma_Y = \sqrt{\frac{1}{2}[(\sigma_x - \sigma_y)^2 + (\sigma_y - \sigma_z)^2 + (\sigma_x - \sigma_z)^2 + 6(\tau_{xy}^2 + \tau_{yz}^2 + \tau_{xz}^2)]}$.

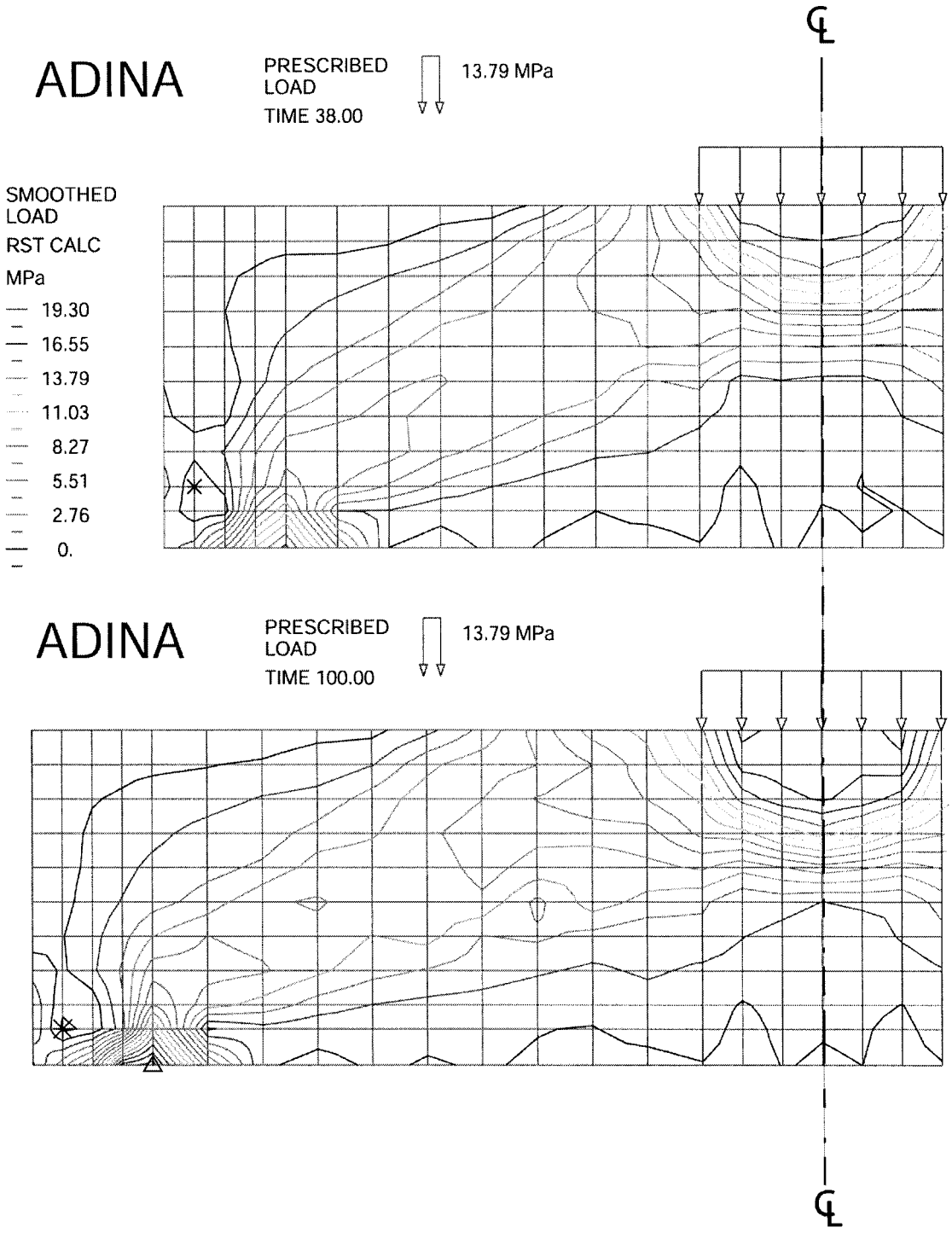

Figure 6-9. Load transmission for test beams at a loading of 333.6 kN

Figure 6-10. Effective stress of left side for beams B150S6, B150S19, and B250S19

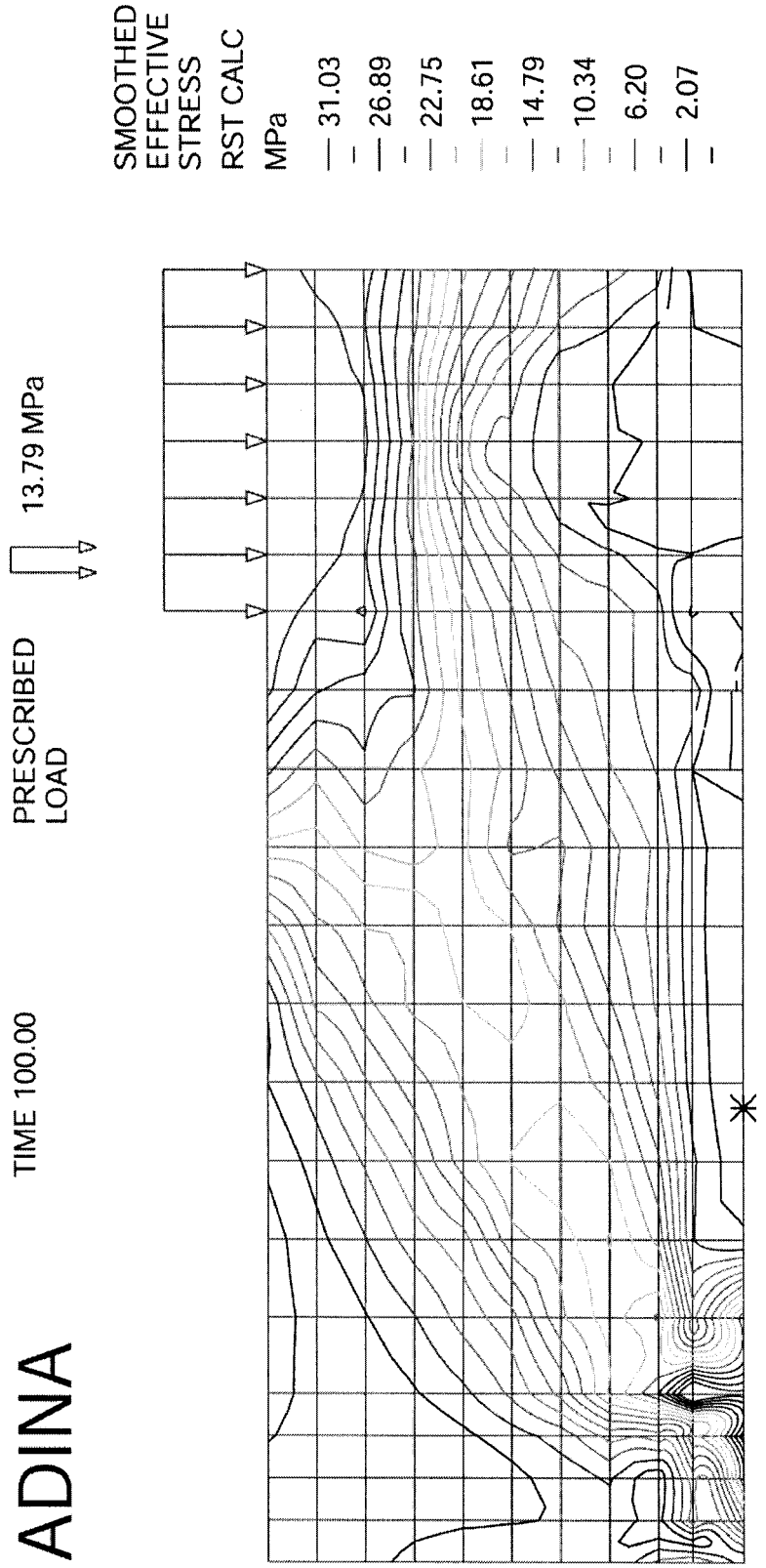

Figure 6-11. Effective stress of left side for beams B260S6, B360S6, and B260S25

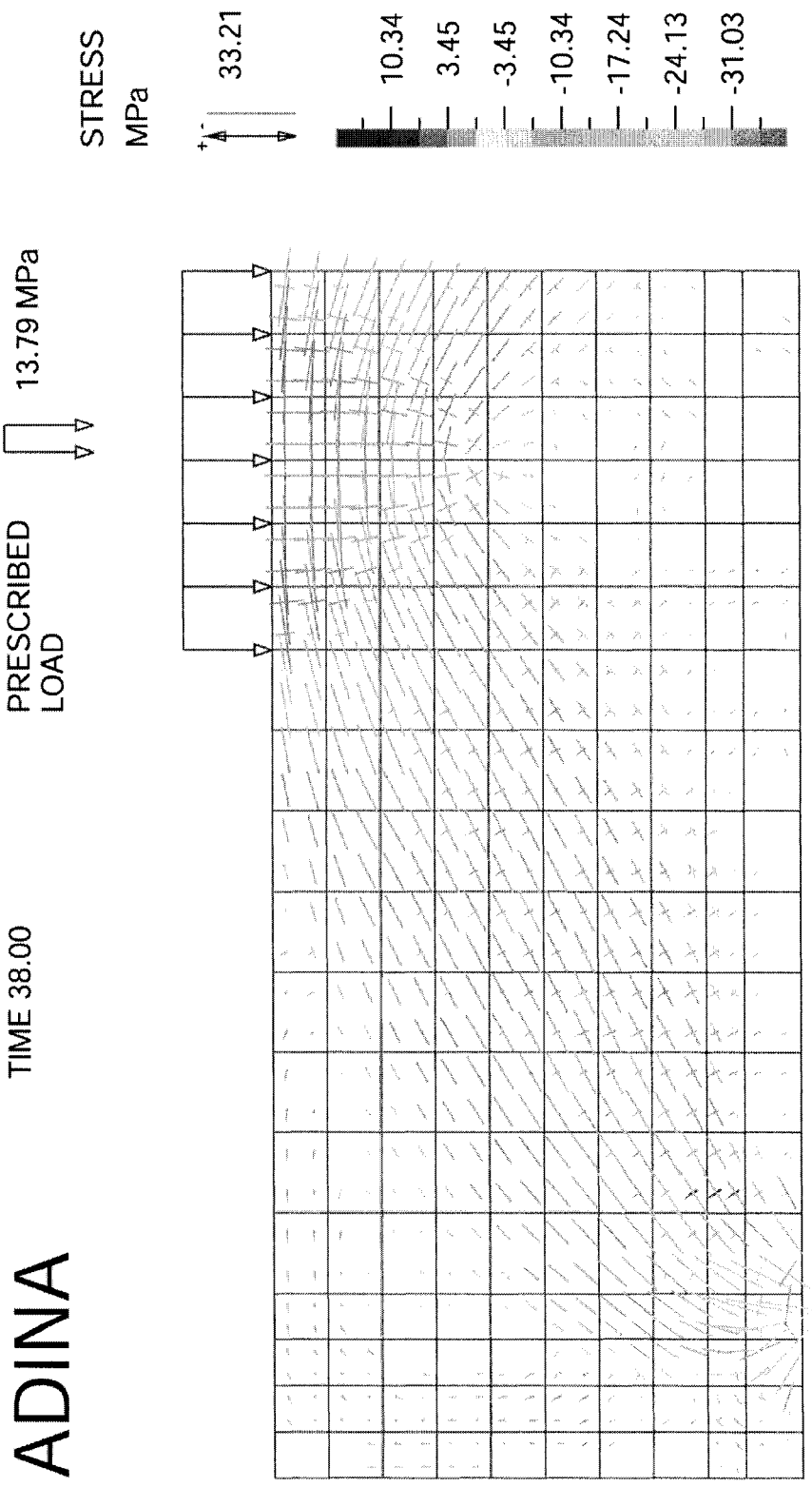

Figure 6-12. Left side stress distribution for beams B150S6, B150S19, and B250S19

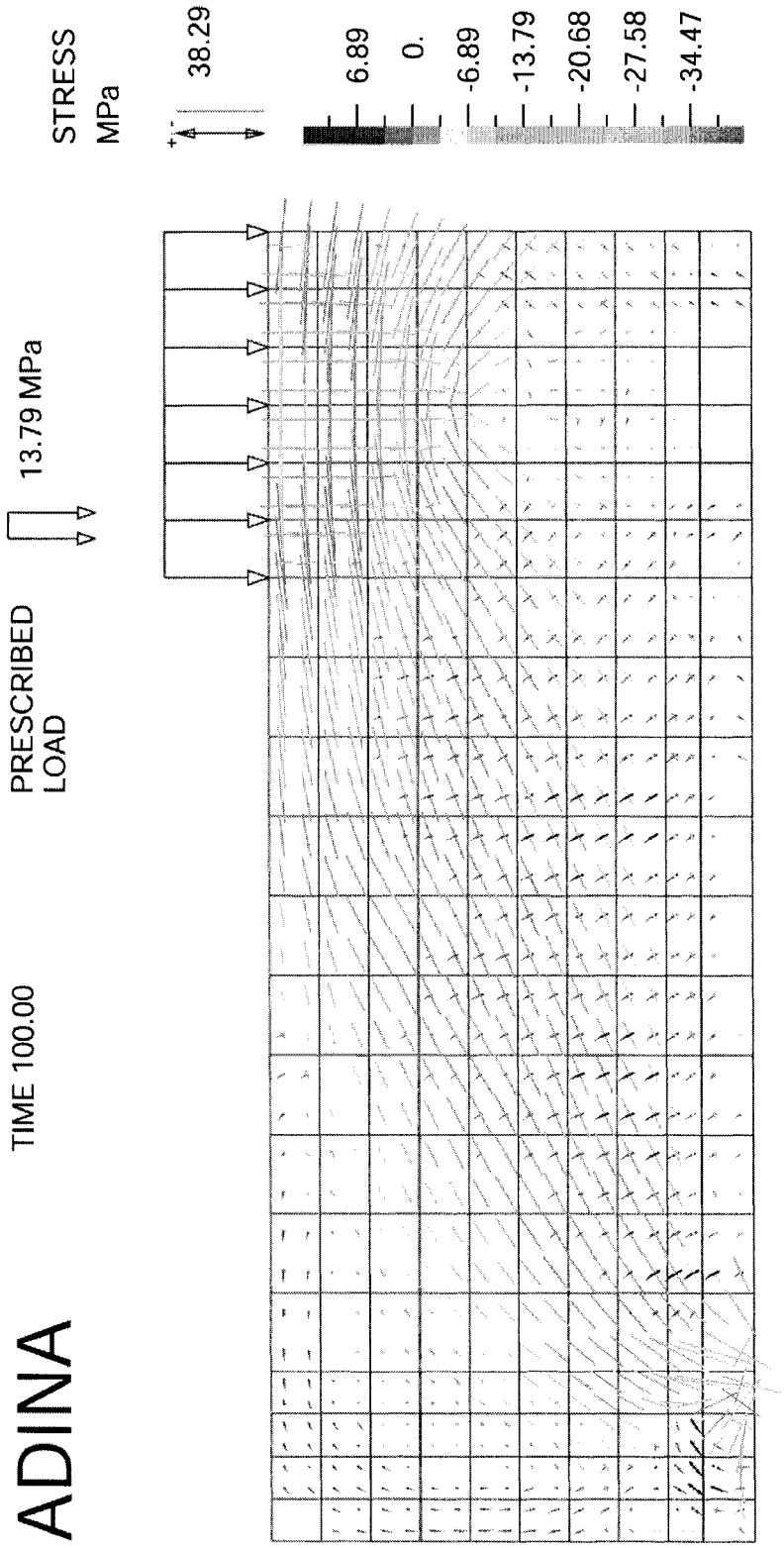

Figure 6-13. Left side stress distribution for beams B260S6, B360S6, and B260S25

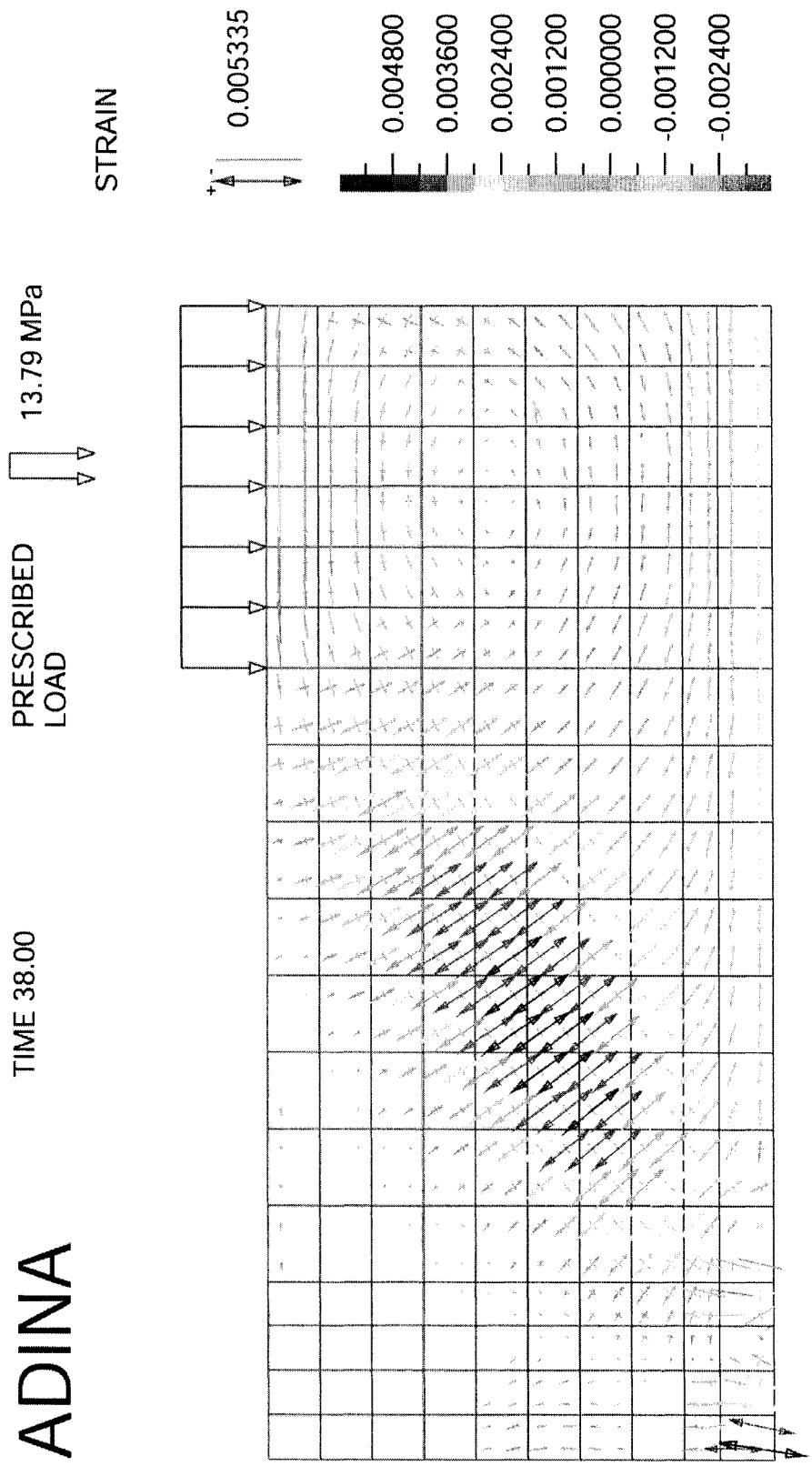

Figure 6-14. Left side strain distribution for beams B150S6, B150S19, and B250S19

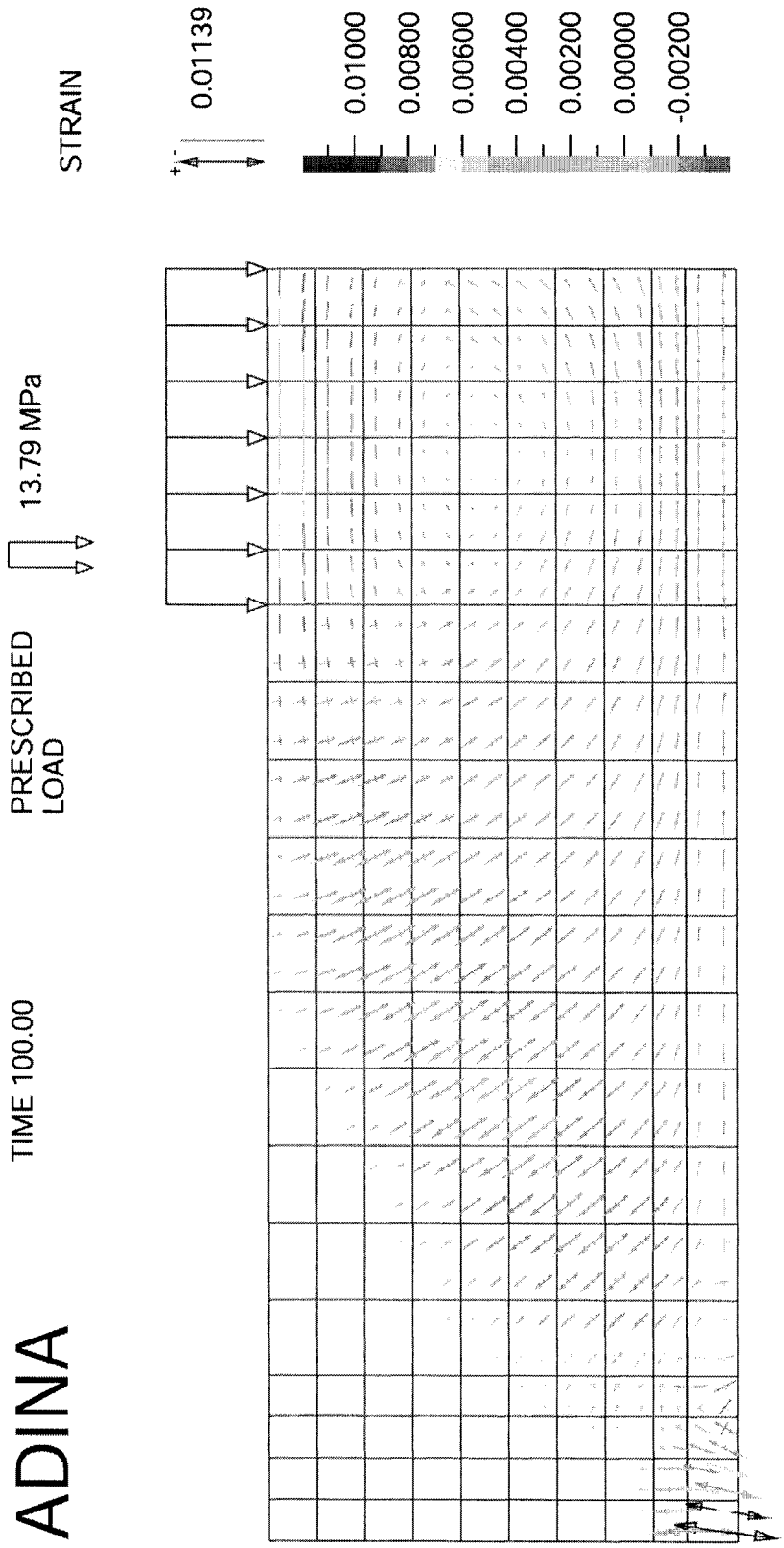

Figure 6-15. Left side strain distribution for beams B260S6, B360S6, and B260S25

6.2.2 Strain along the compression strut

As previously mentioned, in order to design a strut and tie model that accurately depicts the behaviour of the compression strut, an examination of the stresses along the strut and perpendicular to the strut will be necessary. In anticipation that such detail would be required, strain gauges were placed on the concrete test samples along the diagonal from the point of loading to the support (line A-A). As well, strain gauges were placed on a line perpendicular (line B-B) to the main diagonal intersecting the midpoint of line A-A.

Lines A-A and B-B for the left side of the test samples are shown in Figure 6-16 while Figure 6-17 shows the right side of the test sample.

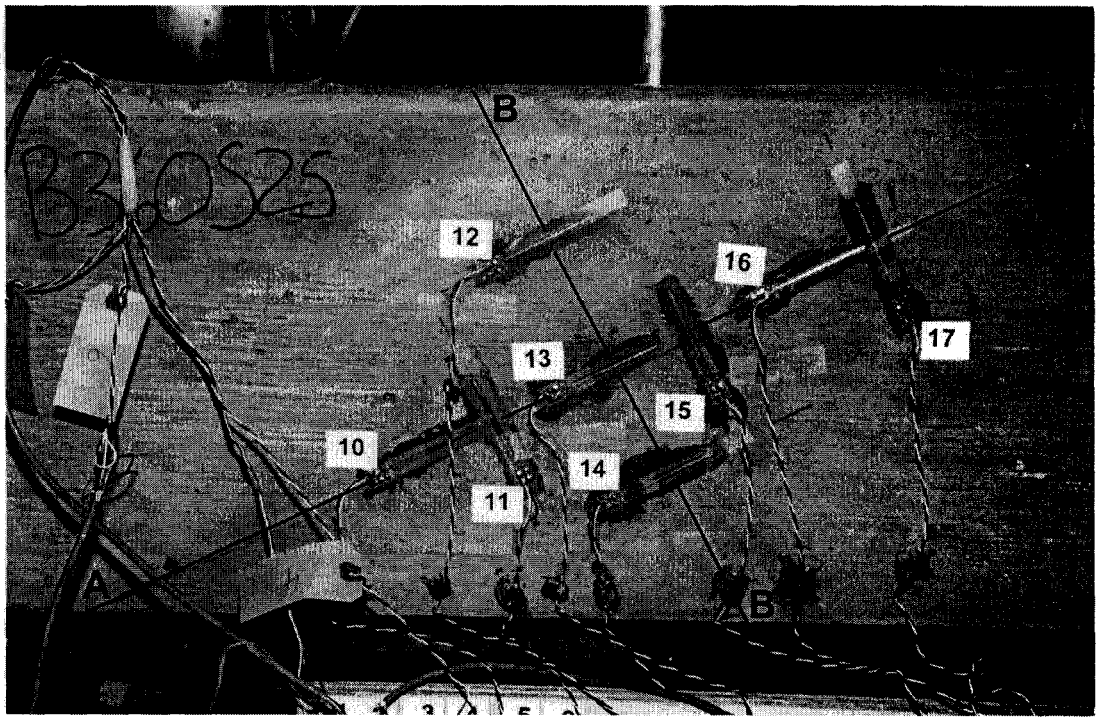

Figure 6-16. Location of left side strain gauges on lines A-A and B-B

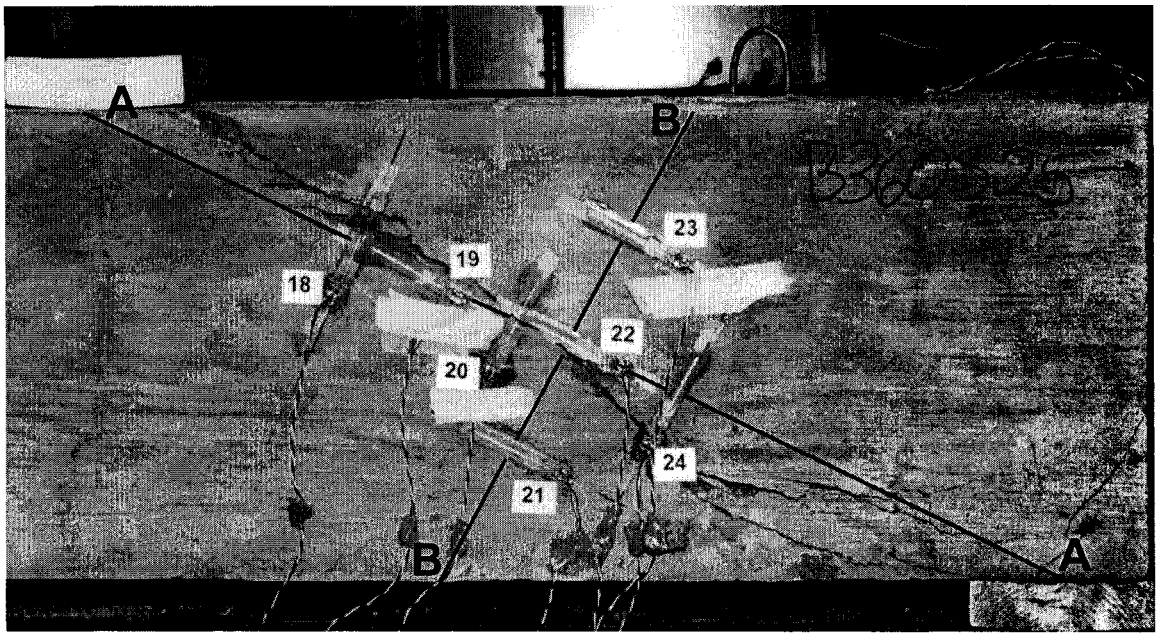

Figure 6-17. Location of right side strain gauges on lines A-A and B-B

Figure 6-18 to Figure 6-25 show the strain perpendicular to line B-B as measured during testing along with the strain calculated by the finite element analysis. In these diagrams, the left side strain gauges are numbered 12,13, and 14, while the right side gauges are numbered 21, 22, 23. In all, two load steps are shown for each of the four samples that had strain gauges. In each of these diagrams, the measured strains recorded during the testing phase match closely to the strain calculated by ADINA. This further demonstrates that the finite element modeling accurately describes the test samples. The compressive concrete strains shown in these figures show that the strain is much less than 0.002, the value which is recommended by the Canadian Code[5].

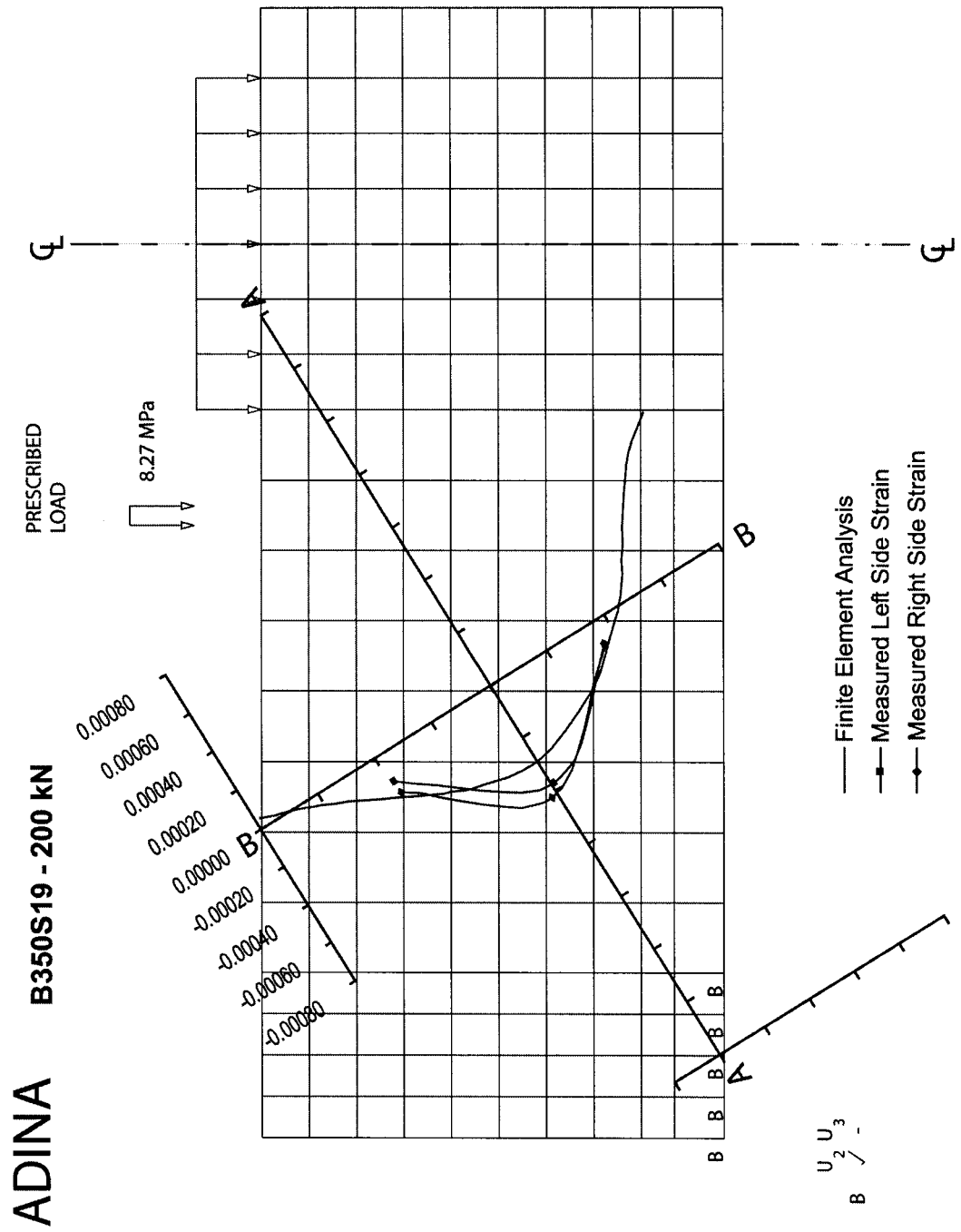

Figure 6-18. Strain perpendicular to B-B for sample B350S19 at 200 kN

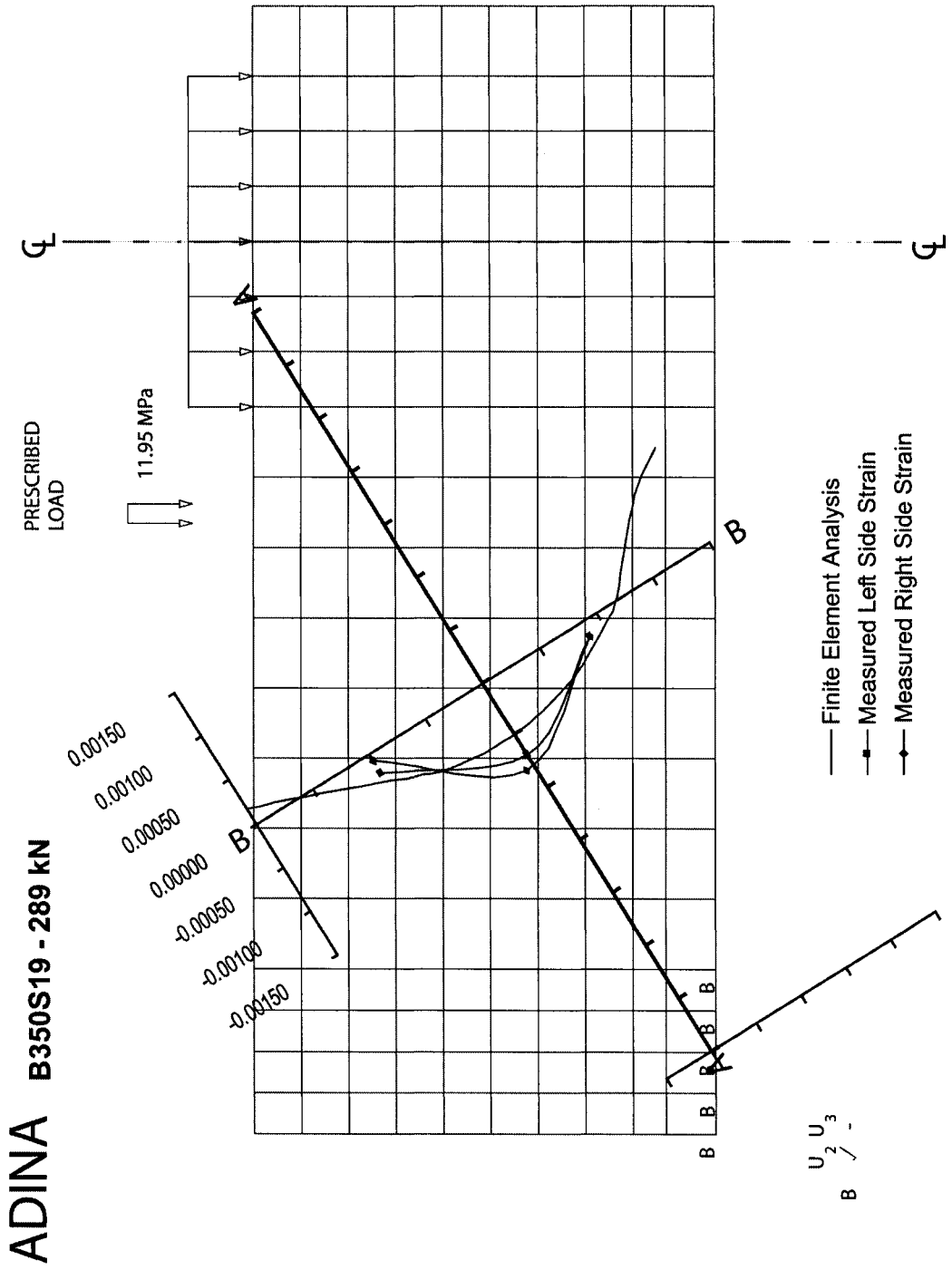

Figure 6-19. Strain perpendicular to B-B for sample B350S19 at 289 kN

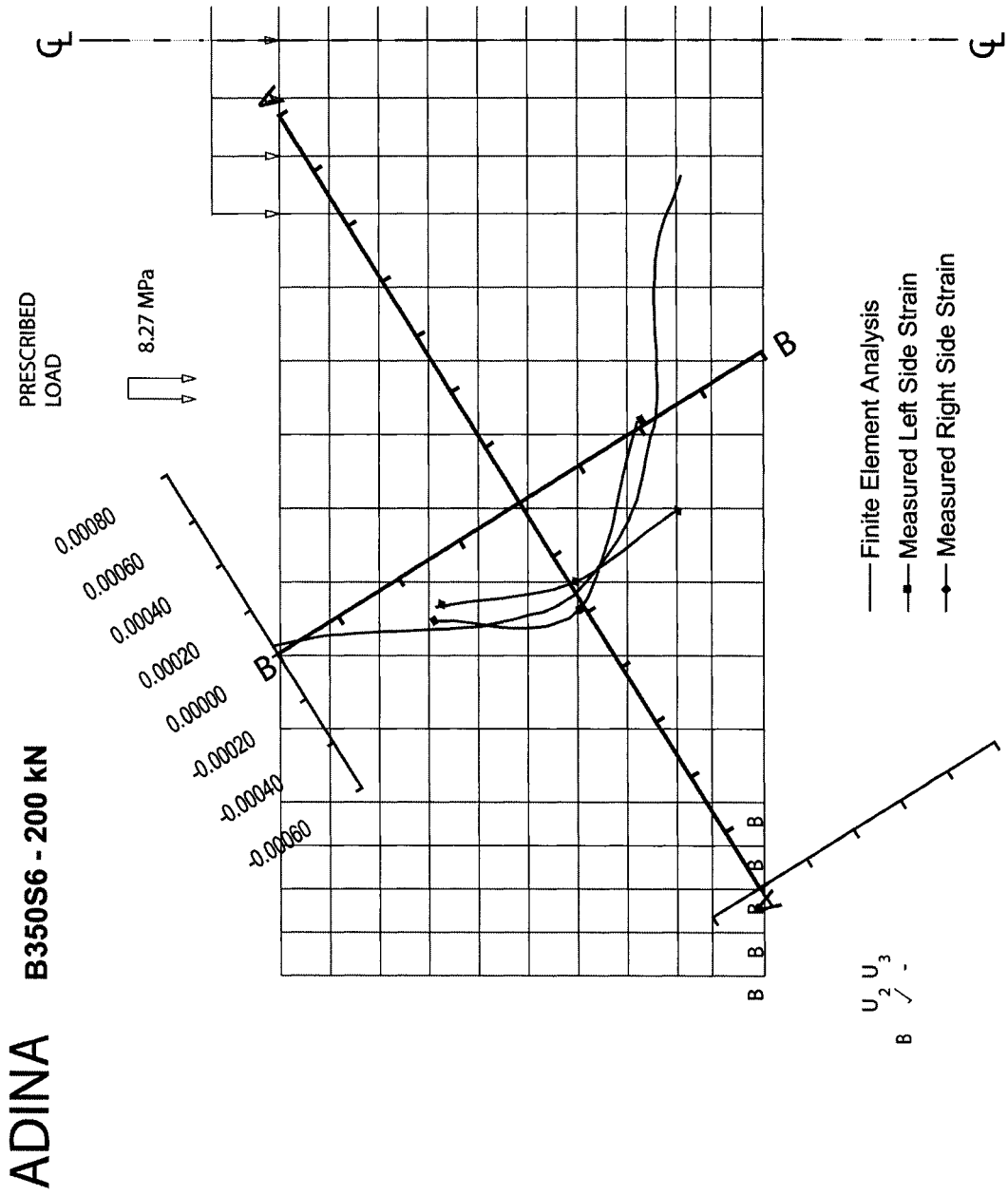

Figure 6-20. Strain perpendicular to B-B for sample B350S6 at 200 kN

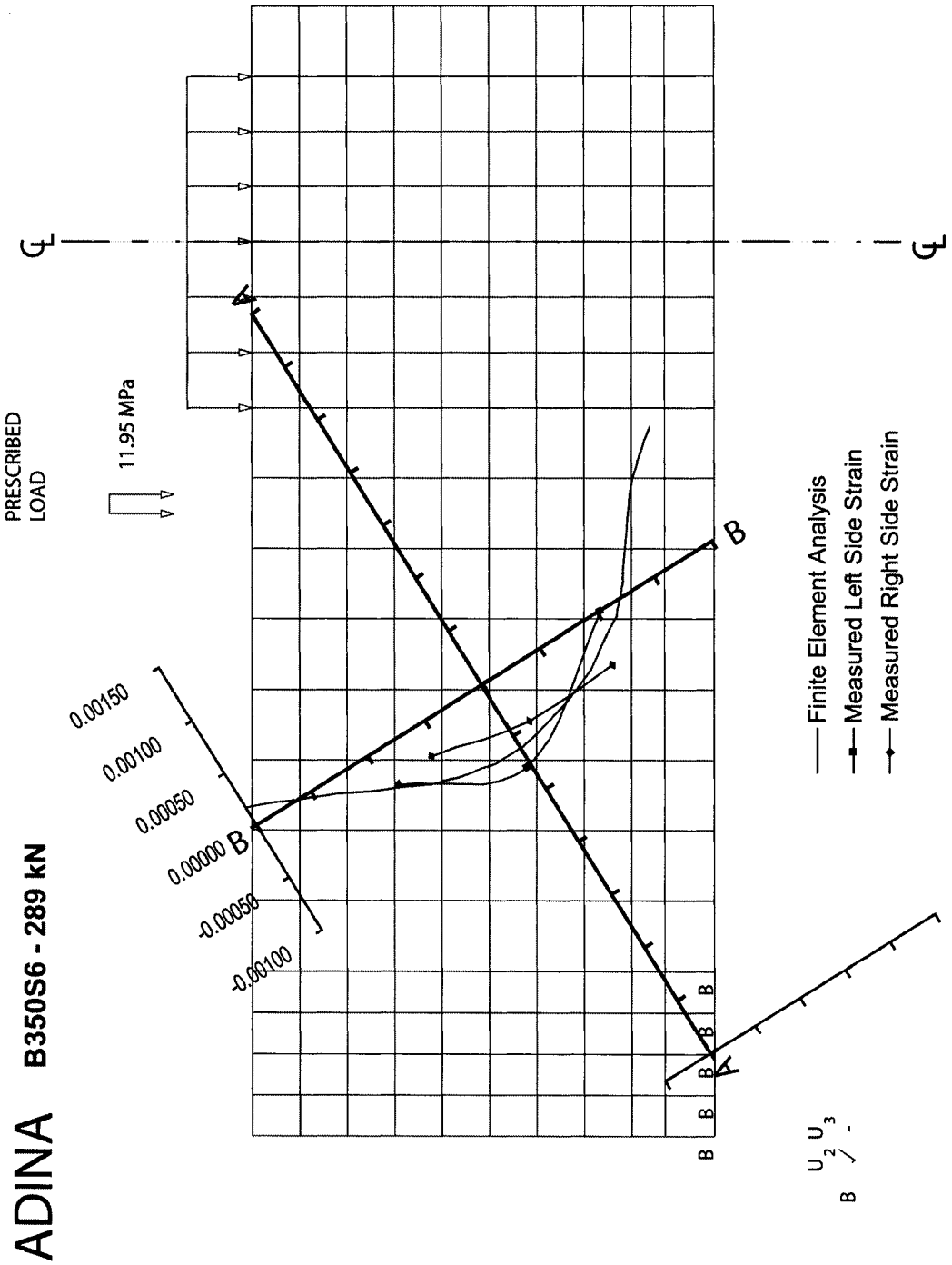

Figure 6-21. Strain perpendicular to B-B for sample B350S6 at 289 kN

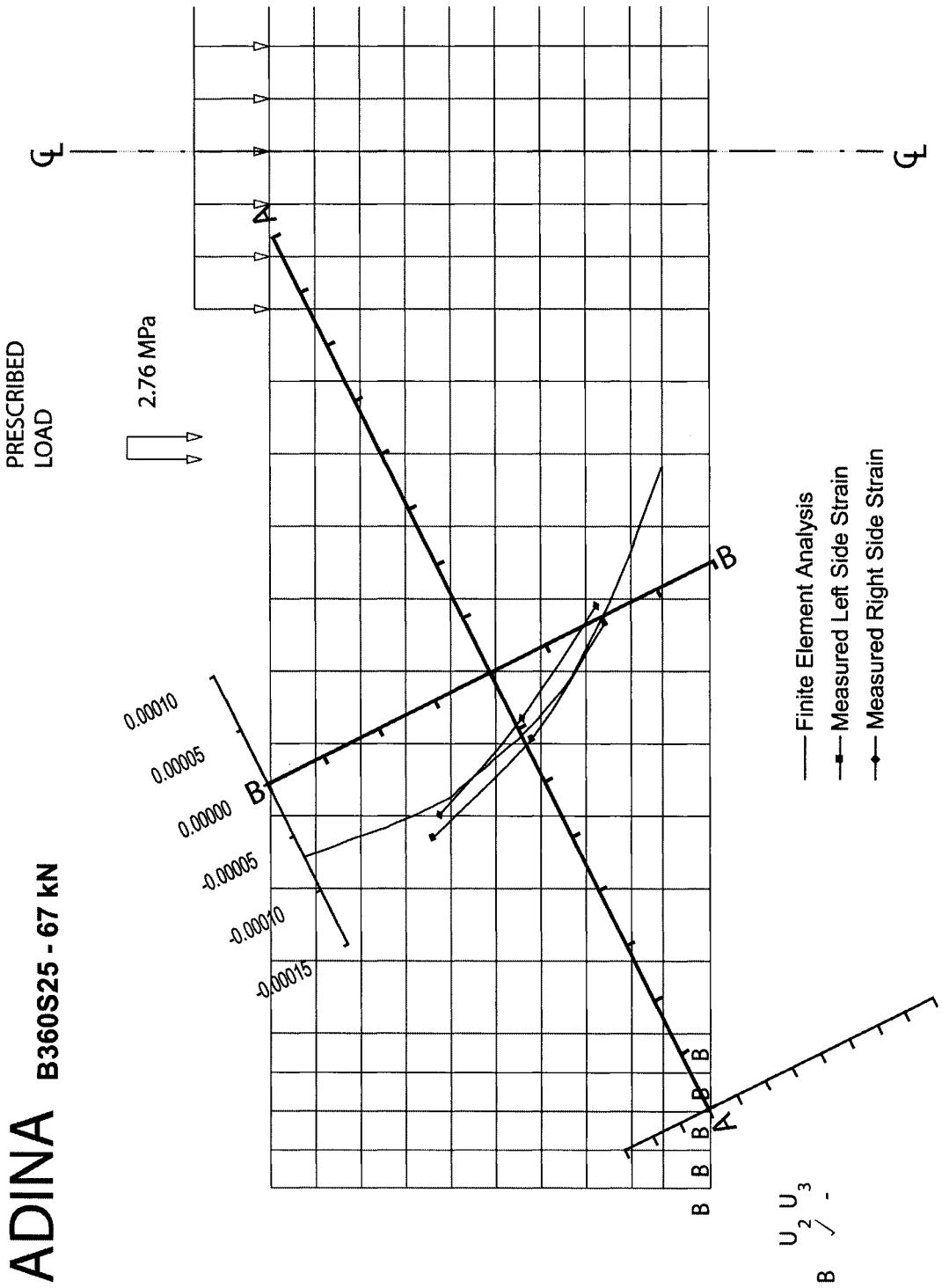

Figure 6-22. Strain perpendicular to B-B for sample B360S25 at 67 kN

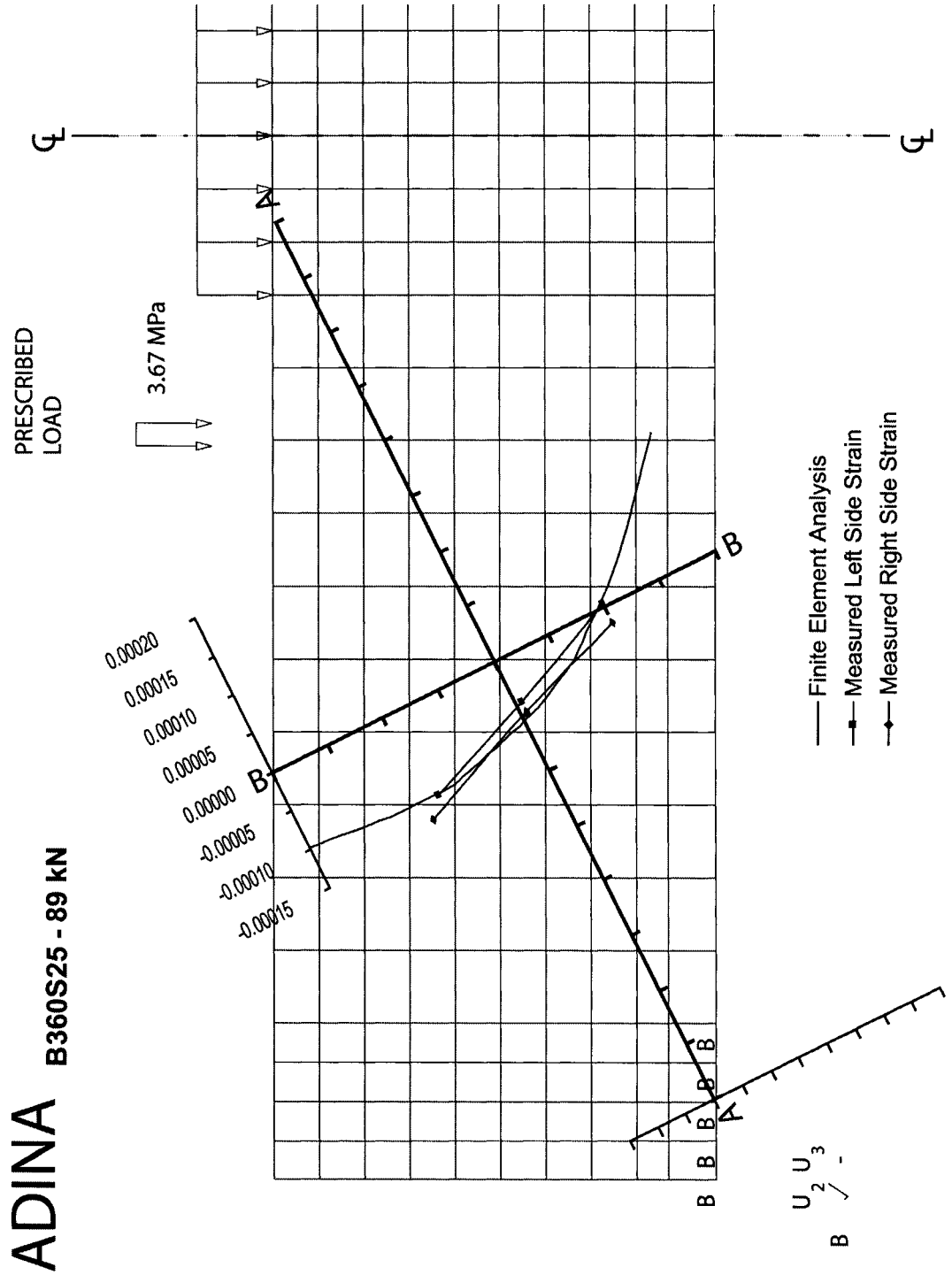

Figure 6-23. Strain perpendicular to B-B for sample B360S25 at 89 kN

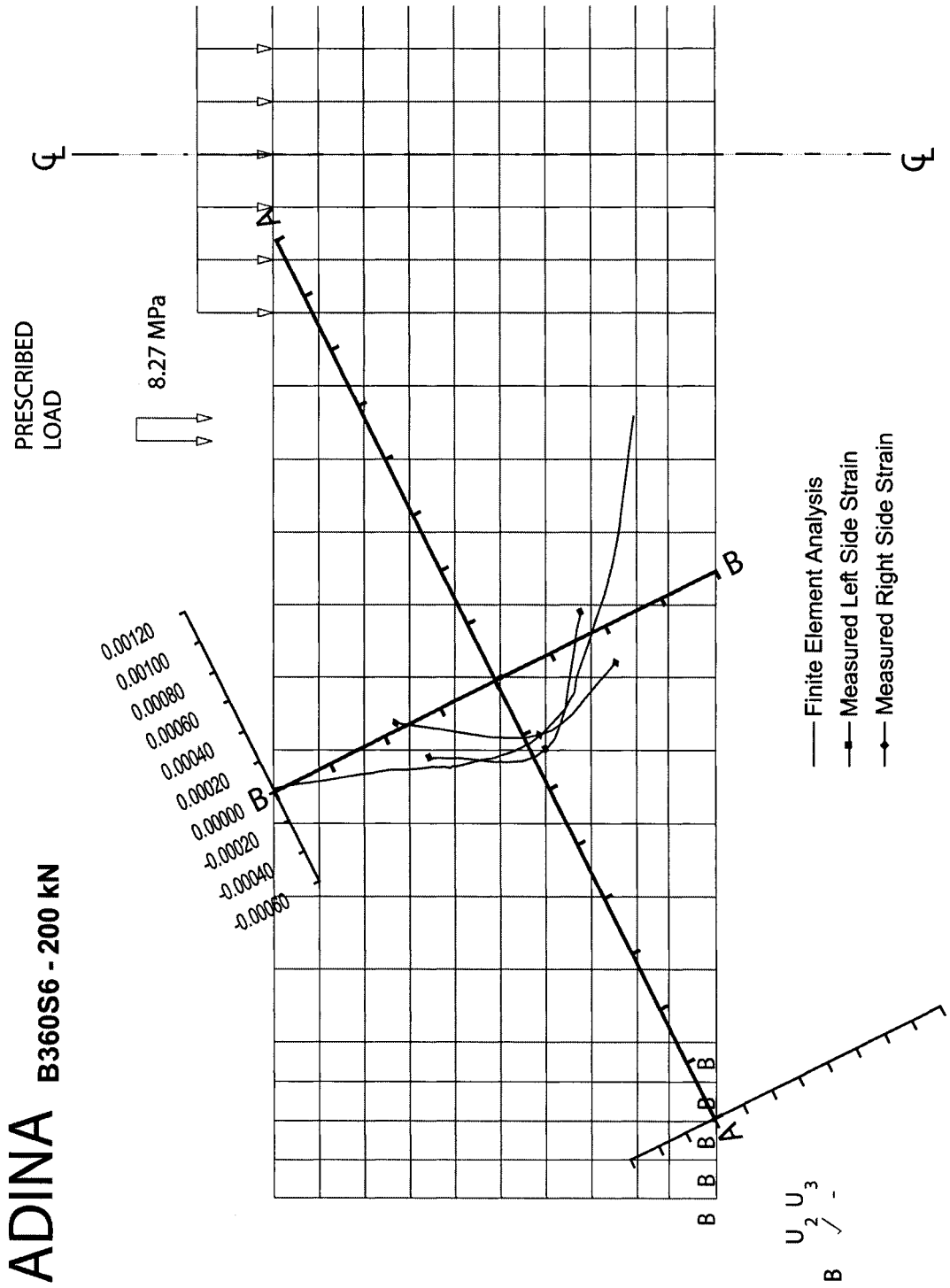

Figure 6-24. Strain perpendicular to B-B for sample B360S6 at 200 kN

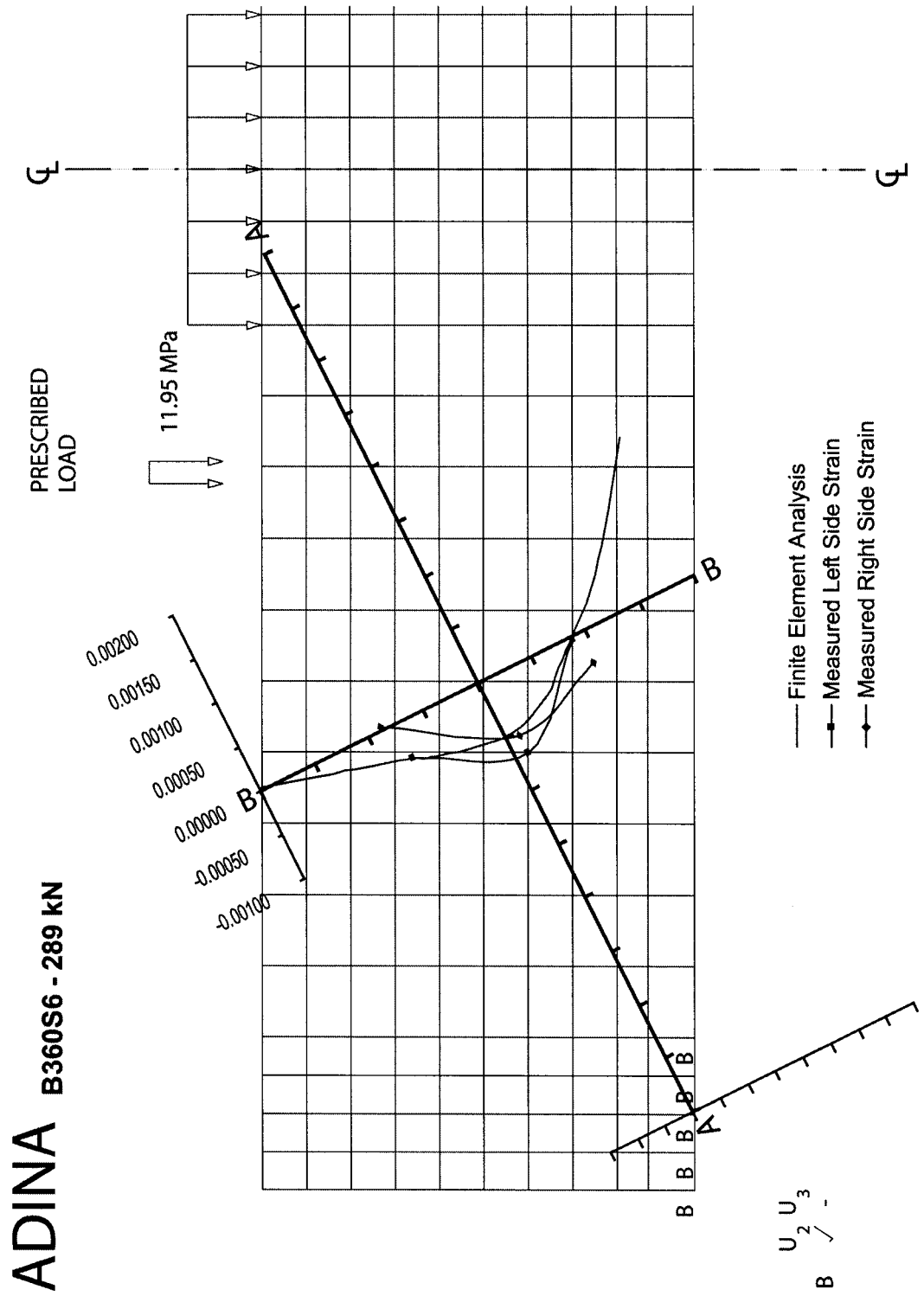

Figure 6-25. Strain perpendicular to B-B for sample B360S6 at 289 kN

Figure 6-26 to Figure 6-33 show the strain perpendicular to line A-A as measured during testing along with the strain calculated by the finite element analysis. In these diagrams, the left side strain gauges are numbered 11,15, and 17, while the right side gauges are numbered 18, 20, 24. In all, two load steps are shown for each of the four samples that had strain gauges. In each of these diagrams, the measured strains recorded during the testing phase match closely to the strain calculated by ADINA. This further demonstrates that the finite element modeling accurately describes the test samples. An important observation is that the tension strain along line A-A is almost constant. The strain becomes compressive in the area of the main reinforcement and under the loading point.

The figures show that the tensile strains which act perpendicularly to the compression strut were present whether or not there were stirrups crossing the strut. This is contrary to the design recommendation of the Canadian Code[5], which calls for a reduction of concrete strength only when the compression strut is crossed by a tension tie. The biaxial stress state exists along the compression strut regardless of the reinforcement provided. Therefore, the strength of concrete should be reduced accordingly.

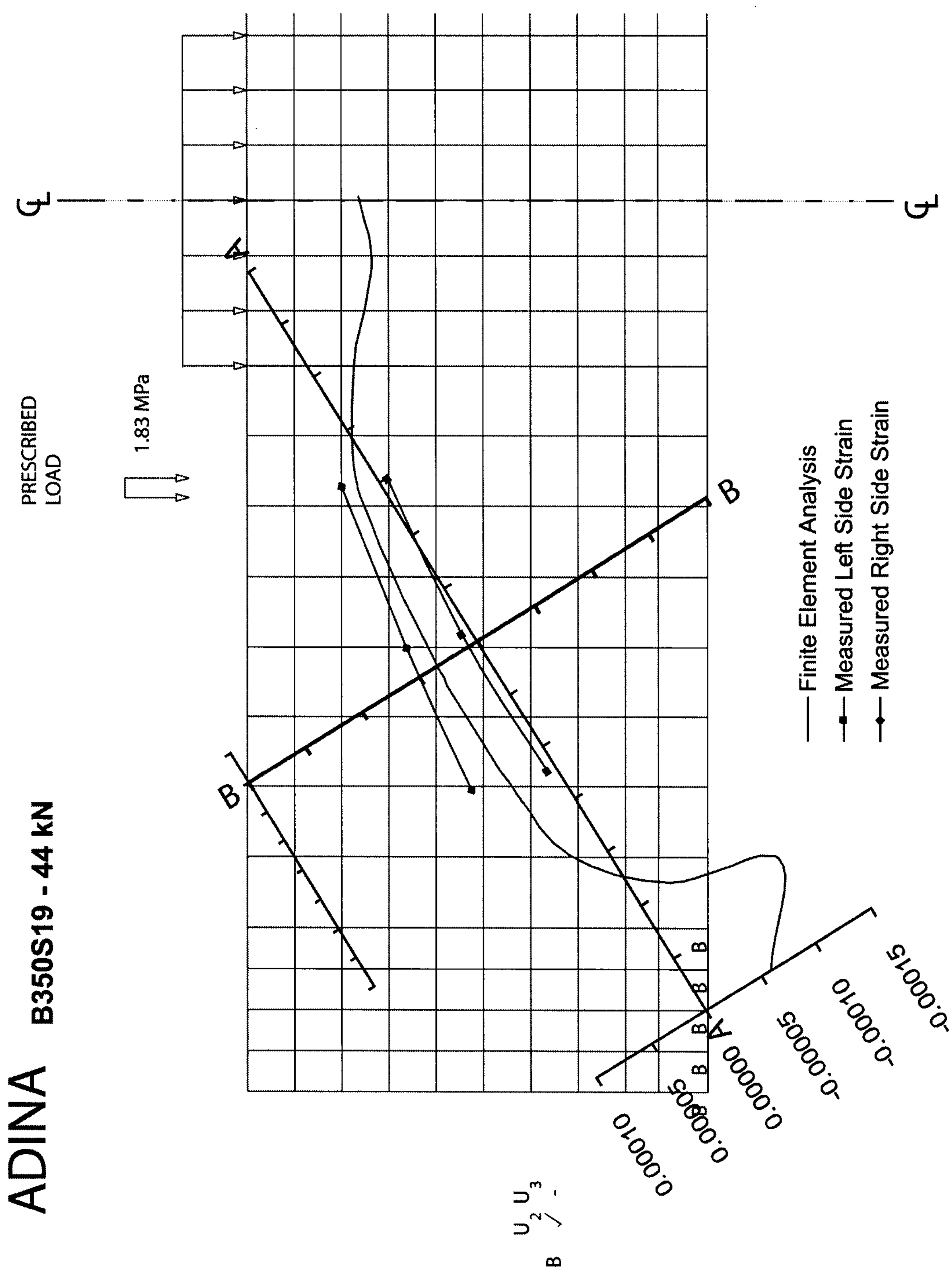

Figure 6-26. Strain perpendicular to A-A for sample B350S19 at 44 kN

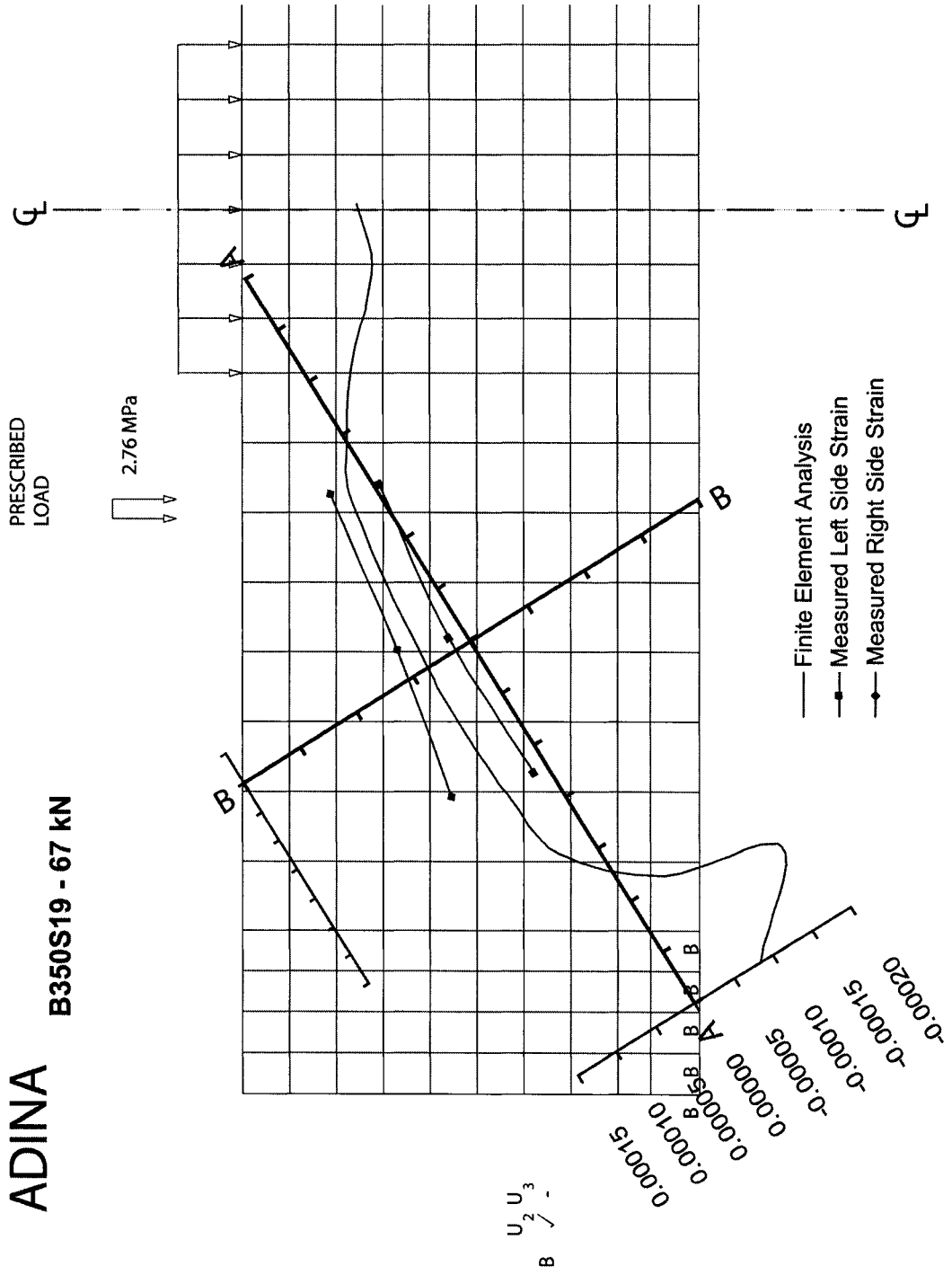

Figure 6-27. Strain perpendicular to A-A for sample B350S19 at 67 kN

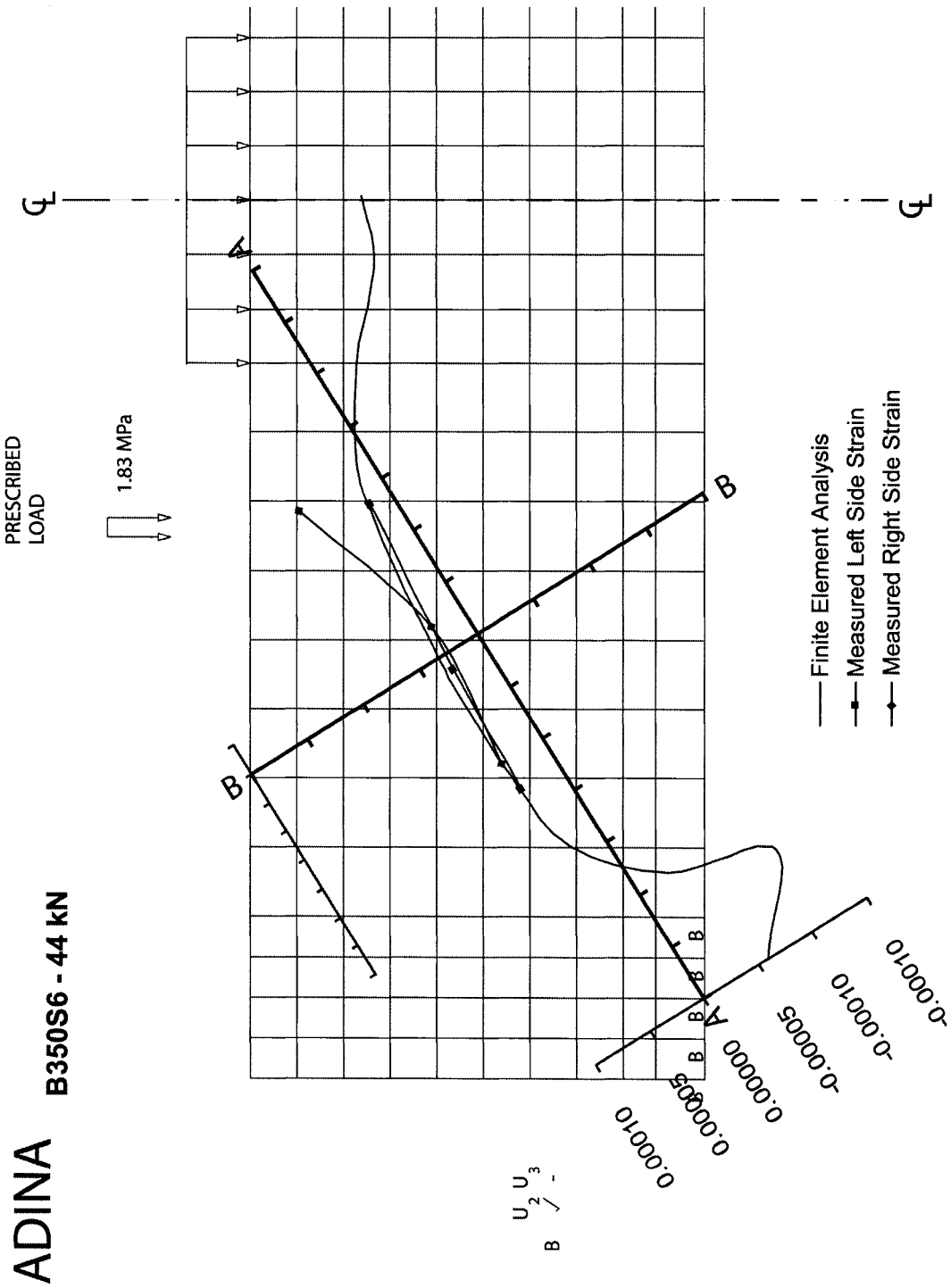

Figure 6-28. Strain perpendicular to A-A for sample B350S6 at 44 kN

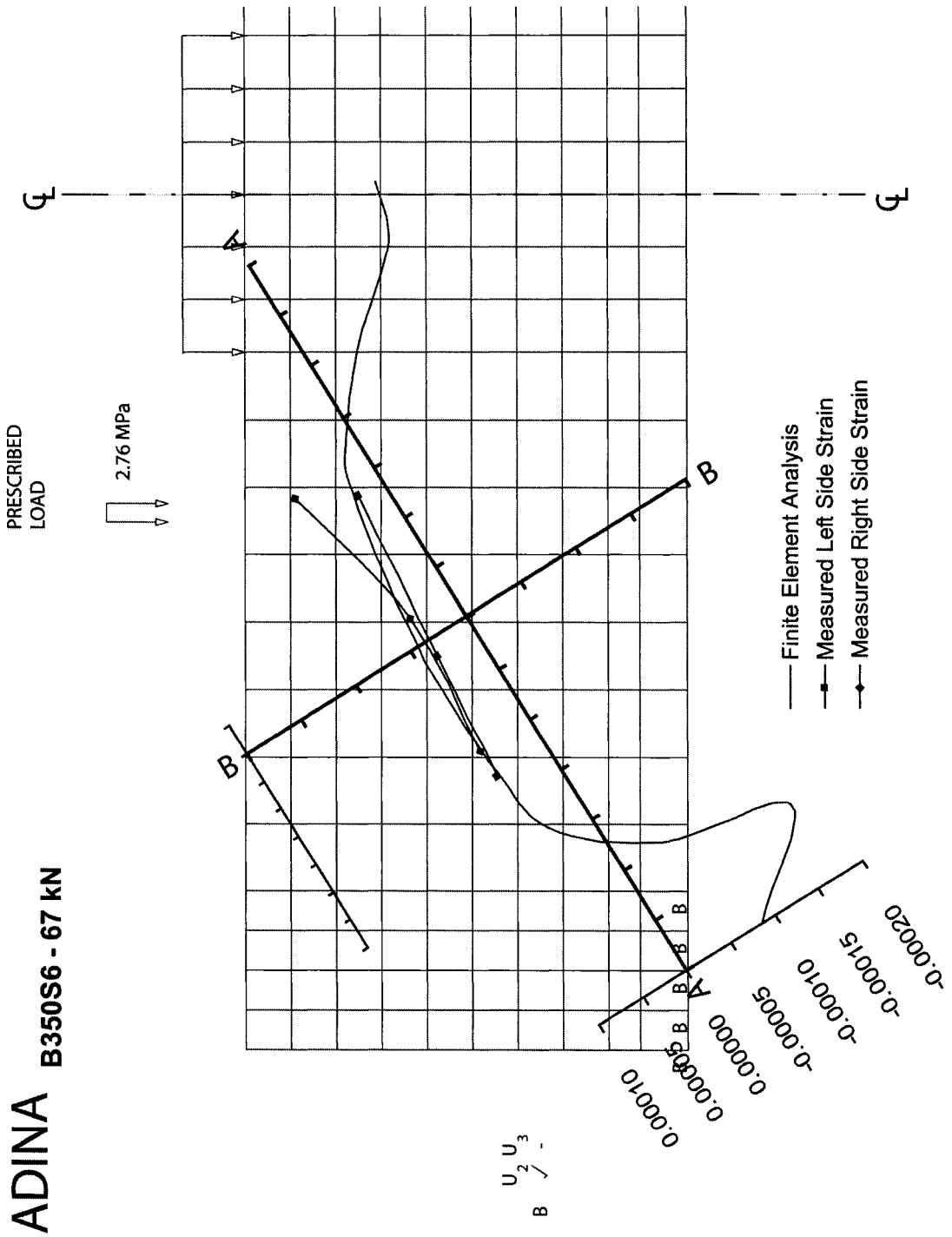

Figure 6-29. Strain perpendicular to A-A for sample B350S6 at 67 kN

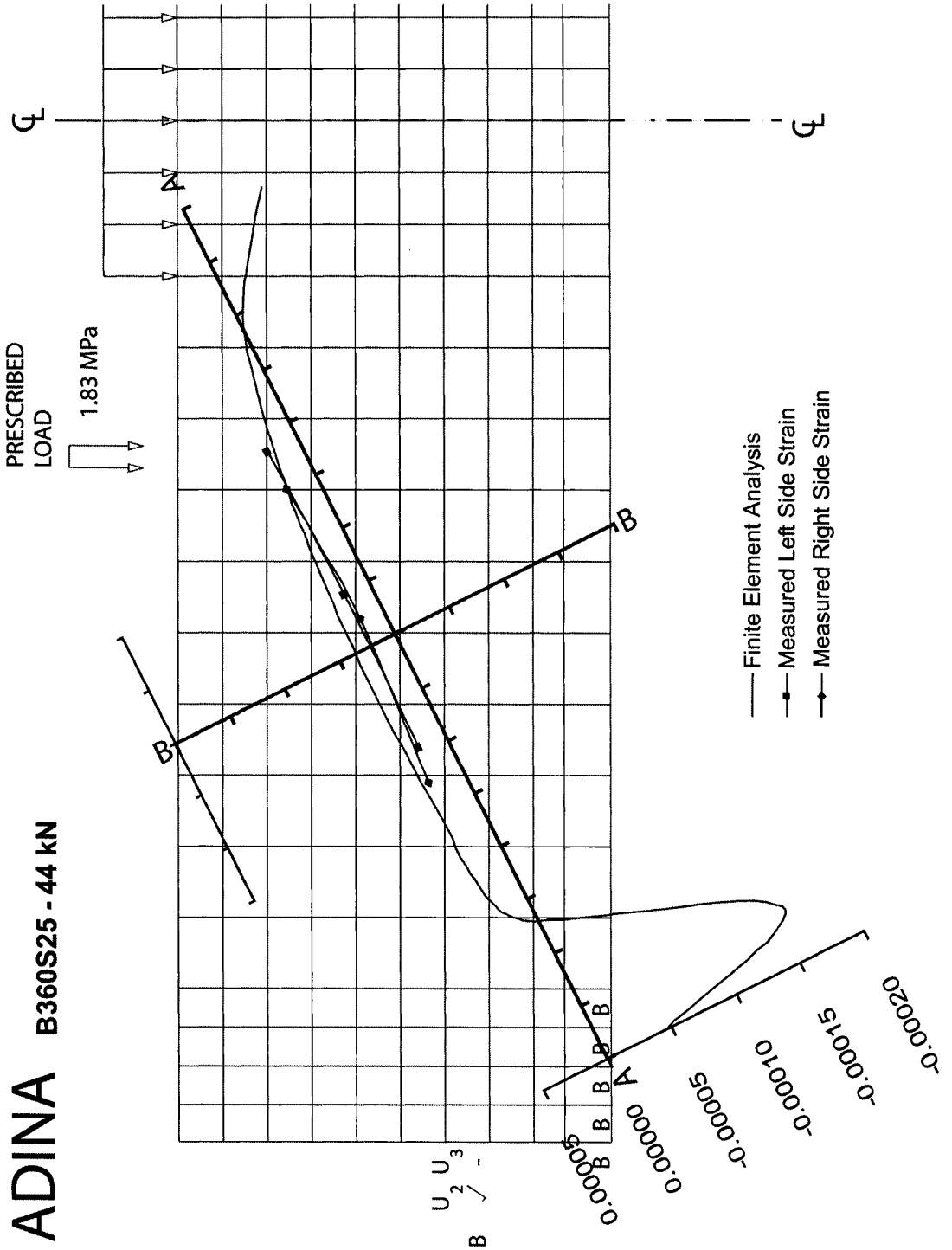

Figure 6-30. Strain perpendicular to A-A for sample B360S25 at 44 kN

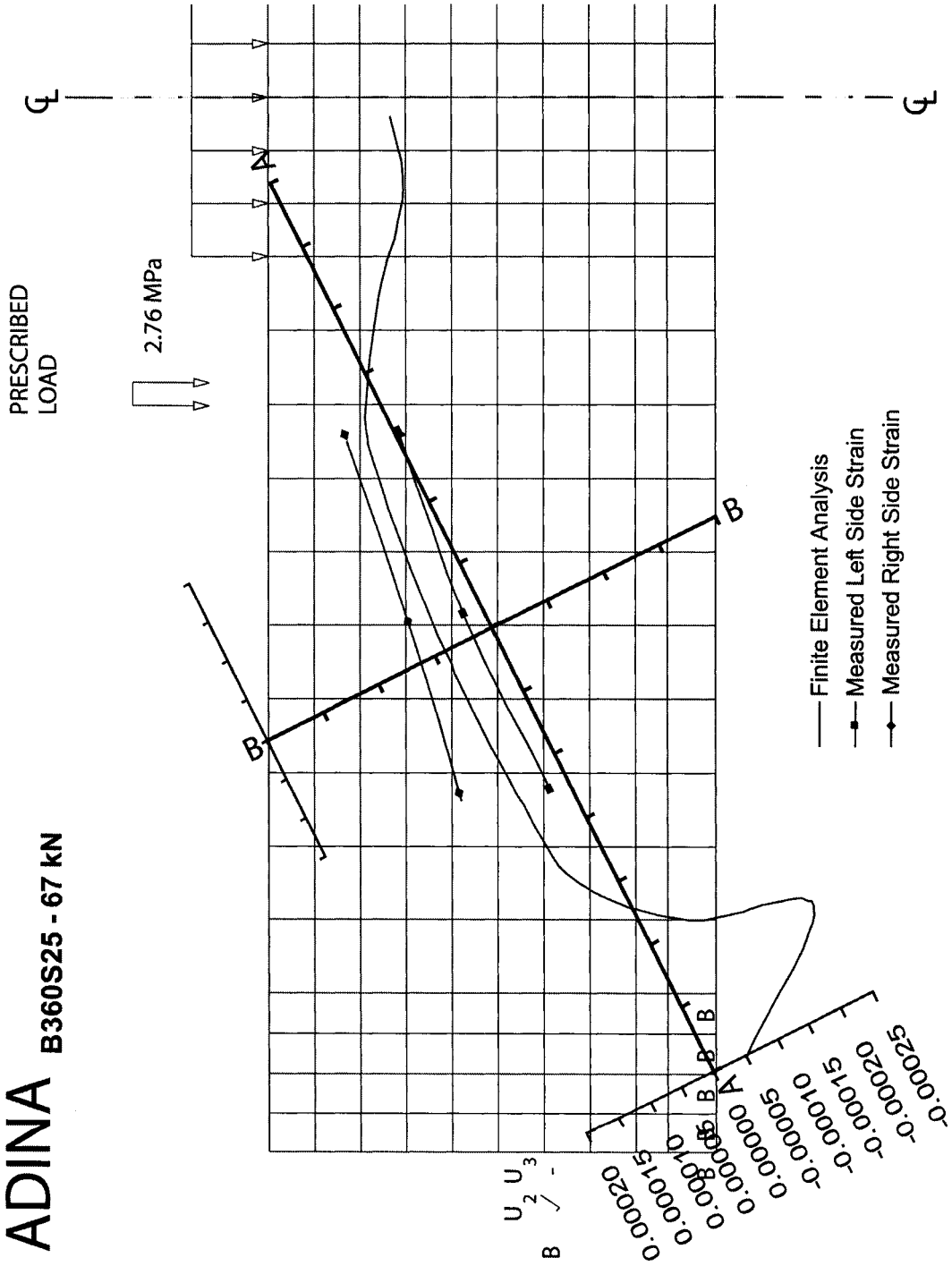

Figure 6-31. Strain perpendicular to A-A for sample B360S25 at 67 kN

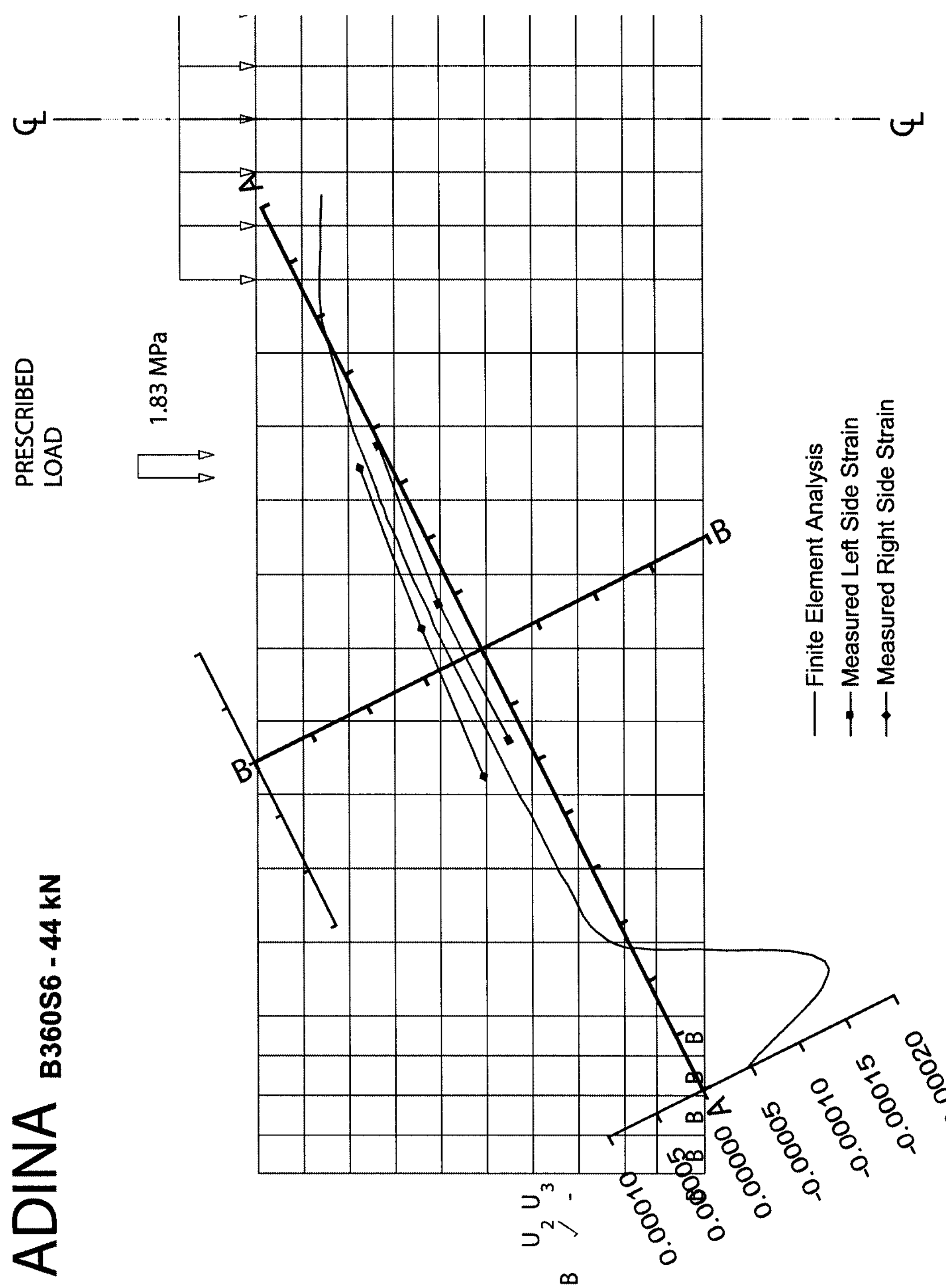

Figure 6-32. Strain perpendicular to A-A for sample B360S6 at 44 kN

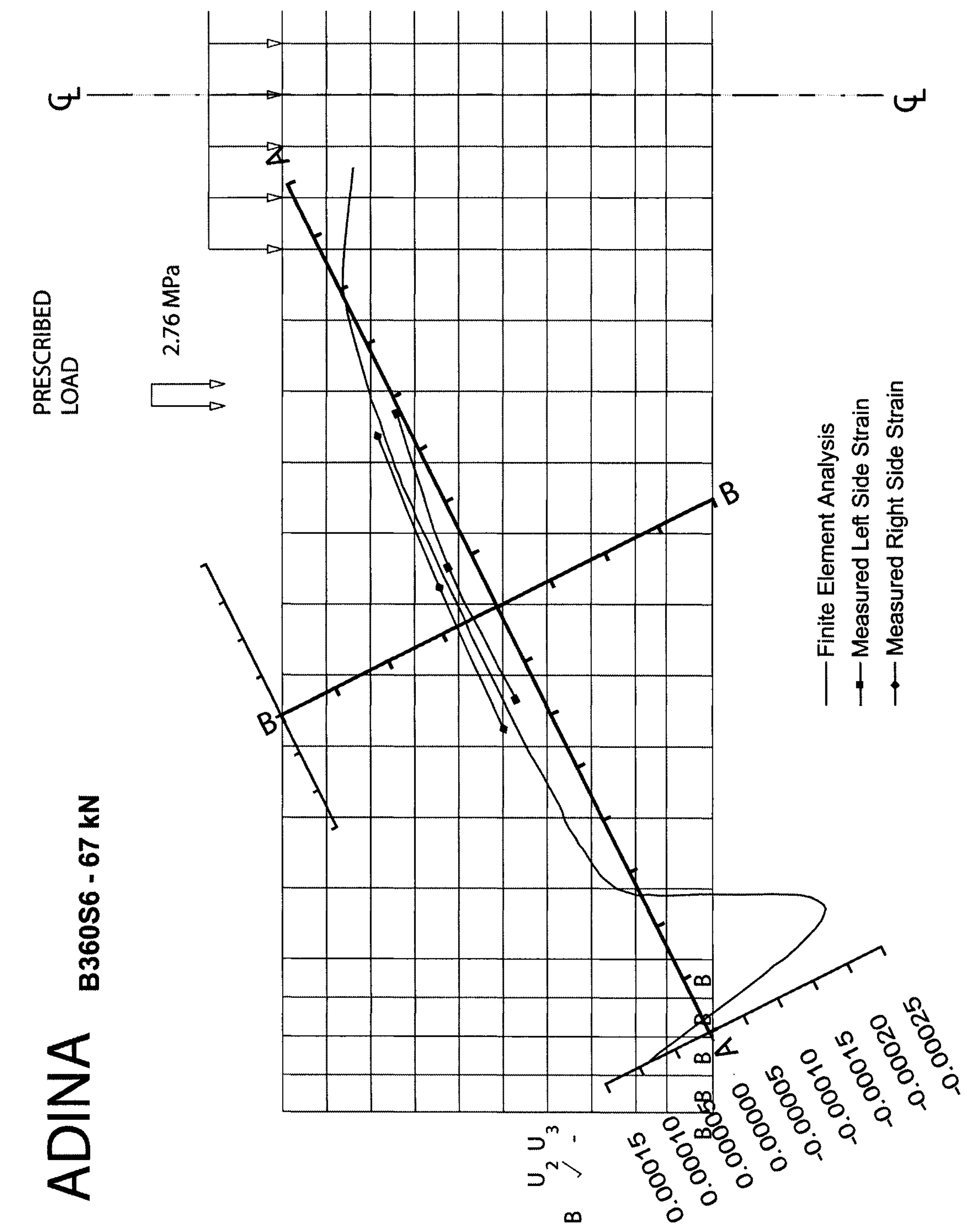

Figure 6-33. Strain perpendicular to A-A for sample B360S6 at 67 kN

6.2.3 Stress along the compression strut

After determining that the calculated strains closely matched the measured values, our attention turned to an examination of the stresses. Figure 6-35 to Figure 6-36 show the stress perpendicular to line B-B as calculated by the finite element analysis. In all, three load steps are shown for each of the two different shear span length samples. The first significant observation was that the stresses are distributed over the entire area perpendicular to the strut. This shows that the compression strut is not a narrow column of compressive stresses. At higher loads, the stress is parabolic in shape, with the maximum value peaking along the main diagonal. The area under the finite element curves was calculated in order to compare with an internal force strut and tie diagram shown in Figure 6-34. Table 6-2 lists the compression force values along with the ratio of the finite element results to the free body diagram values.

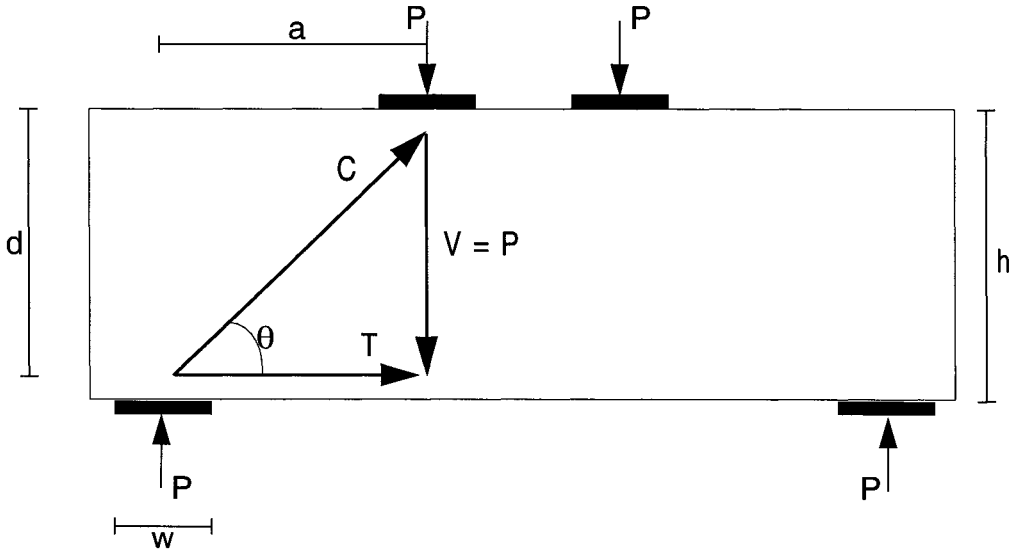

Figure 6-34. Internal force diagram strut and tie schematic

Table 6-2. Force along the compression strut

Sample	Load (kN)	Force under the finite element curve (kN)	Force from strut and tie (kN)	$\frac{\text{Finite element}}{\text{Strut and tie}}$
B350S19	180.1	43.0	44.7	0.96
	270.2	67.6	67.1	1.00
	362.8	96.1	90.1	1.07
B360S25	132.1	31.9	39.4	0.81
	176.1	50.9	52.5	0.97
	213.5	63.6	63.7	1.00

Figure 6-37 to Figure 6-38 show the stress perpendicular to line A-A as calculated by the finite element analysis. In all, three load steps are shown for each of the two different shear span length samples. An important observation is that the tension stress along line A-A is constant along the length of the strut, with the area near the loading point and near the support being in compression.

This phenomena has been documented before. The American Society for Testing and Materials tensile test (ASTM C496) places a standard concrete cylinder, 6" x 12" (152mm x 305mm) on its side and then loads it in compression along the diameter as shown in Figure 6-39 on page 191. As can be seen from Figure 6-39d, the vertical axis is stressed in biaxial compression and tension. The stresses acting across the vertical diameter range from high compressive stresses (in the perpendicular direction) at the top and bottom to a nearly constant uniform tensile stress across the rest of the cylinder. The strength of the cylinder, tested in this fashion, defines the splitting strength of concrete as:

$$f_{ct} = \frac{2P}{\pi l d} \qquad \textbf{Equation 6-1.}$$

where

P = maximum applied load,

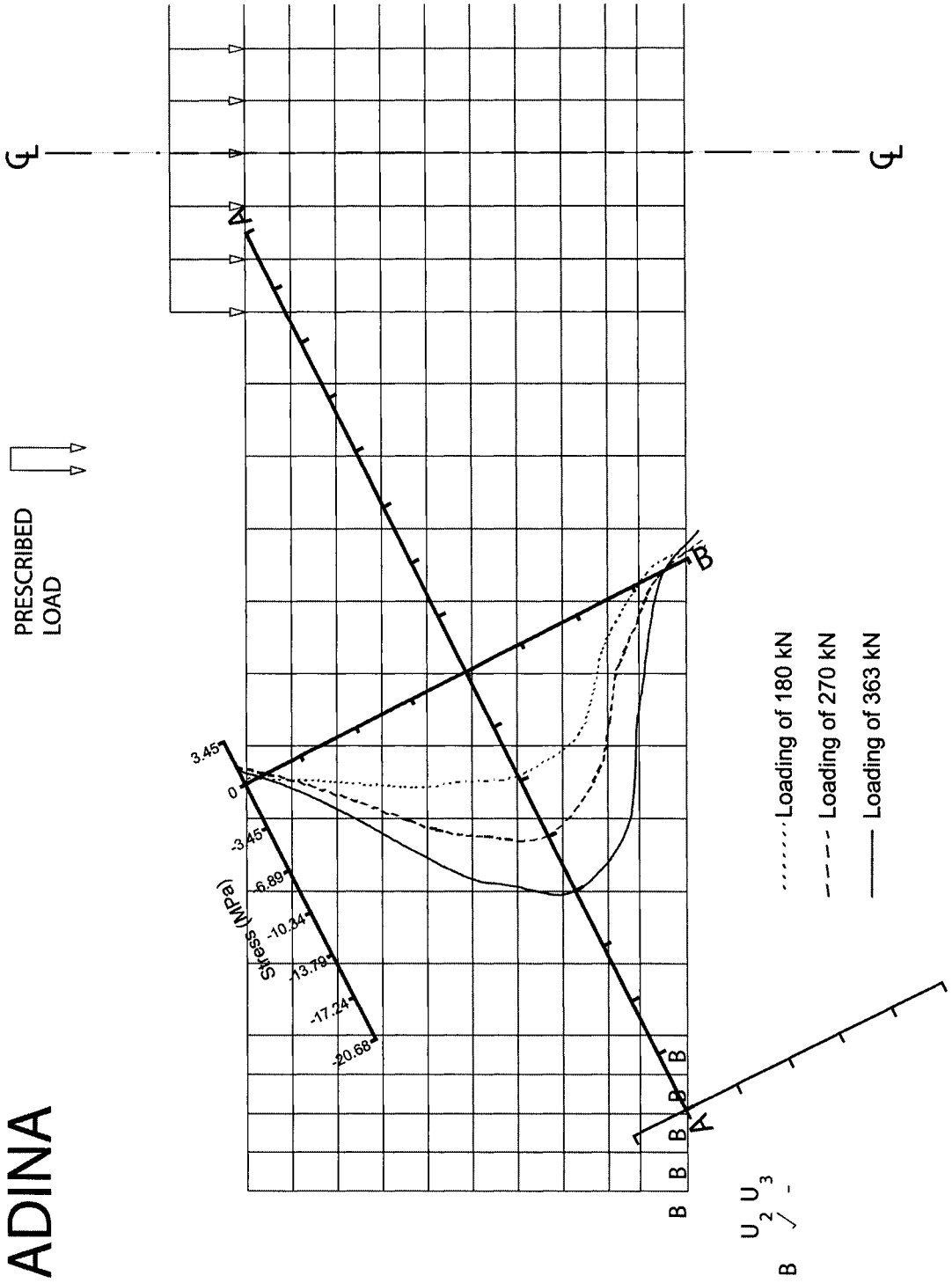

Figure 6-35. Finite element stress perpendicular to B-B for sample B350S19

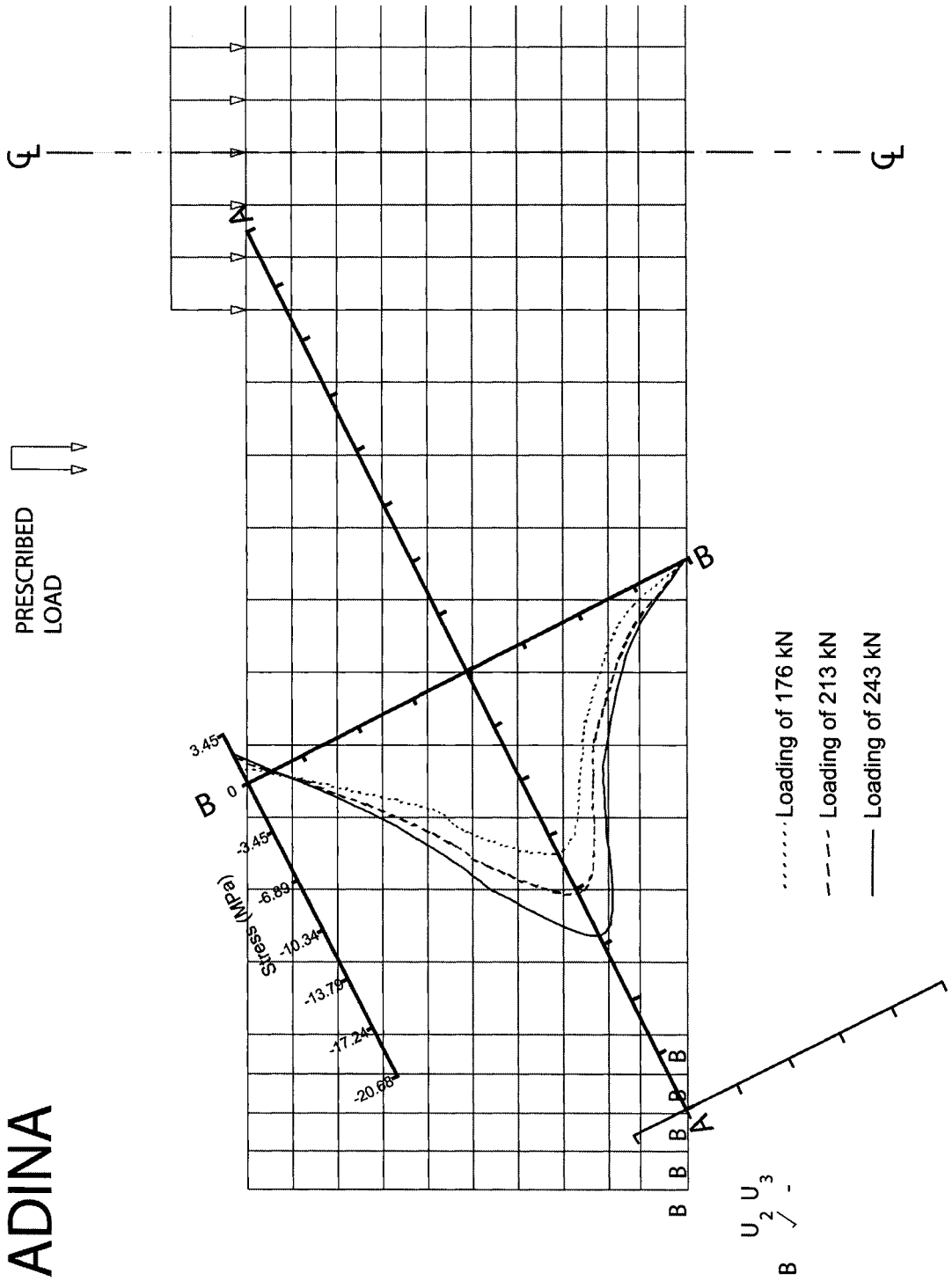

Figure 6-36. Finite element stress perpendicular to B-B for sample B360S25

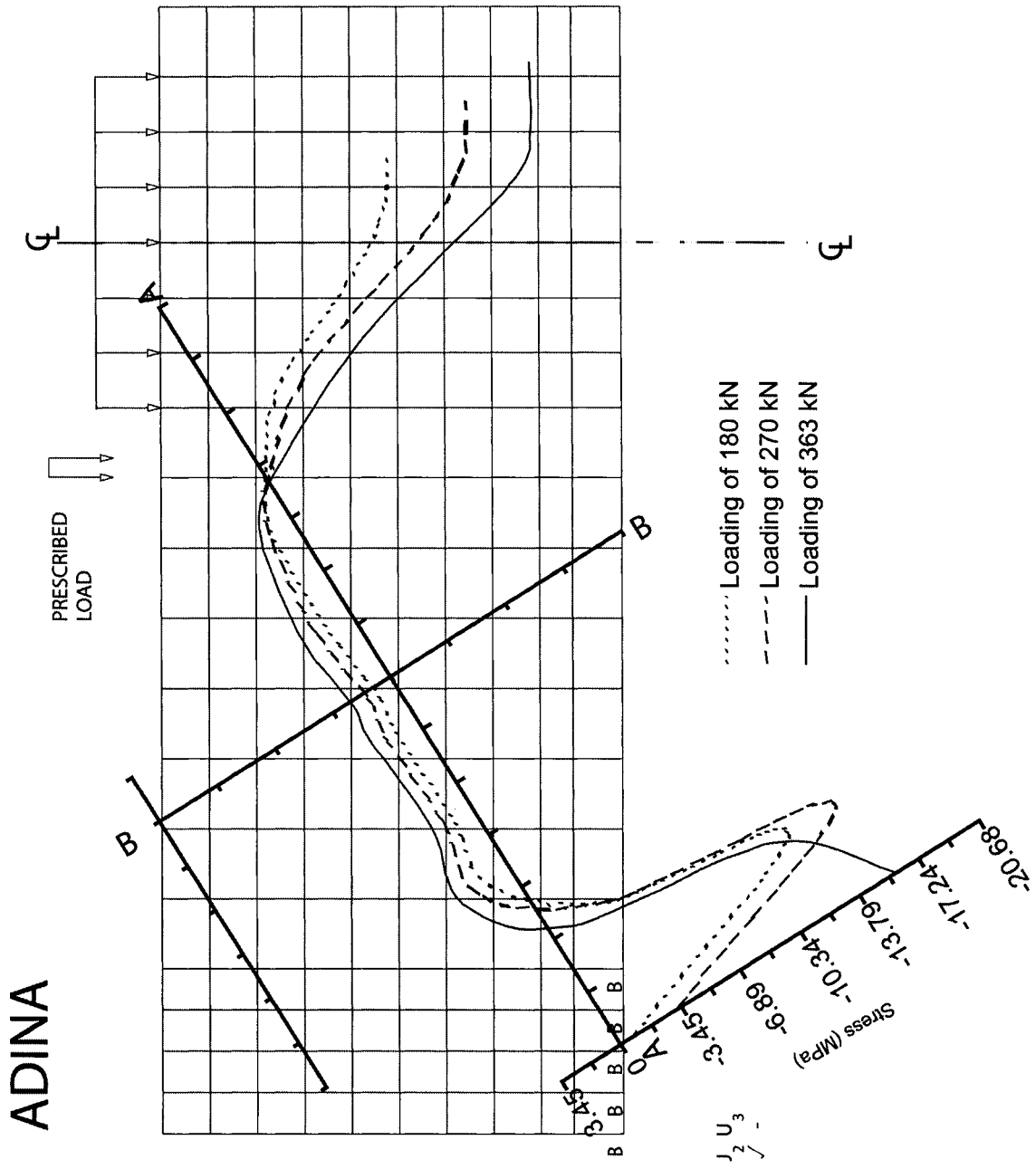

Figure 6-37. Finite element stress perpendicular to A-A for sample B350S19

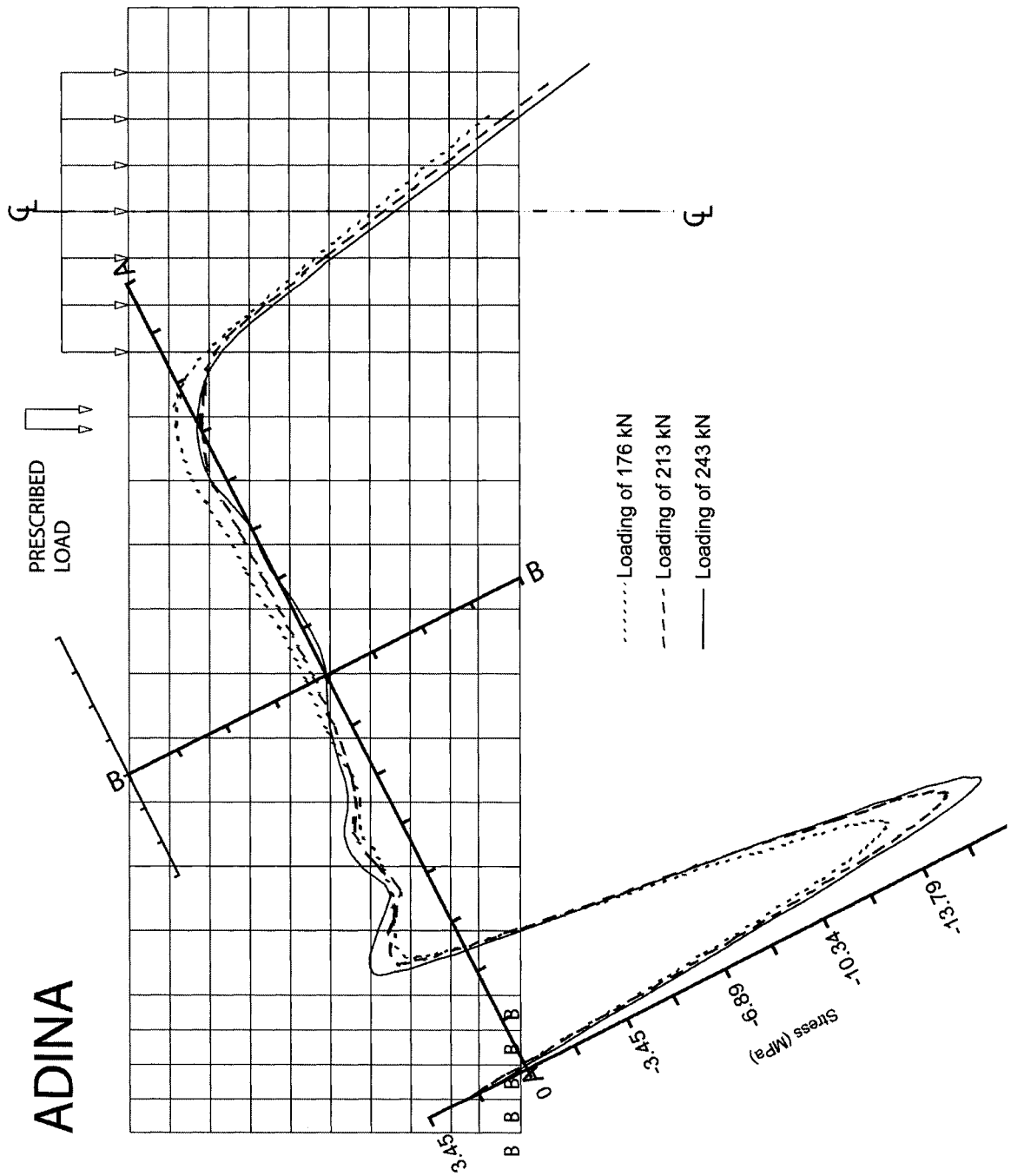

Figure 6-38. Finite element stress perpendicular to A-A for sample B360S25

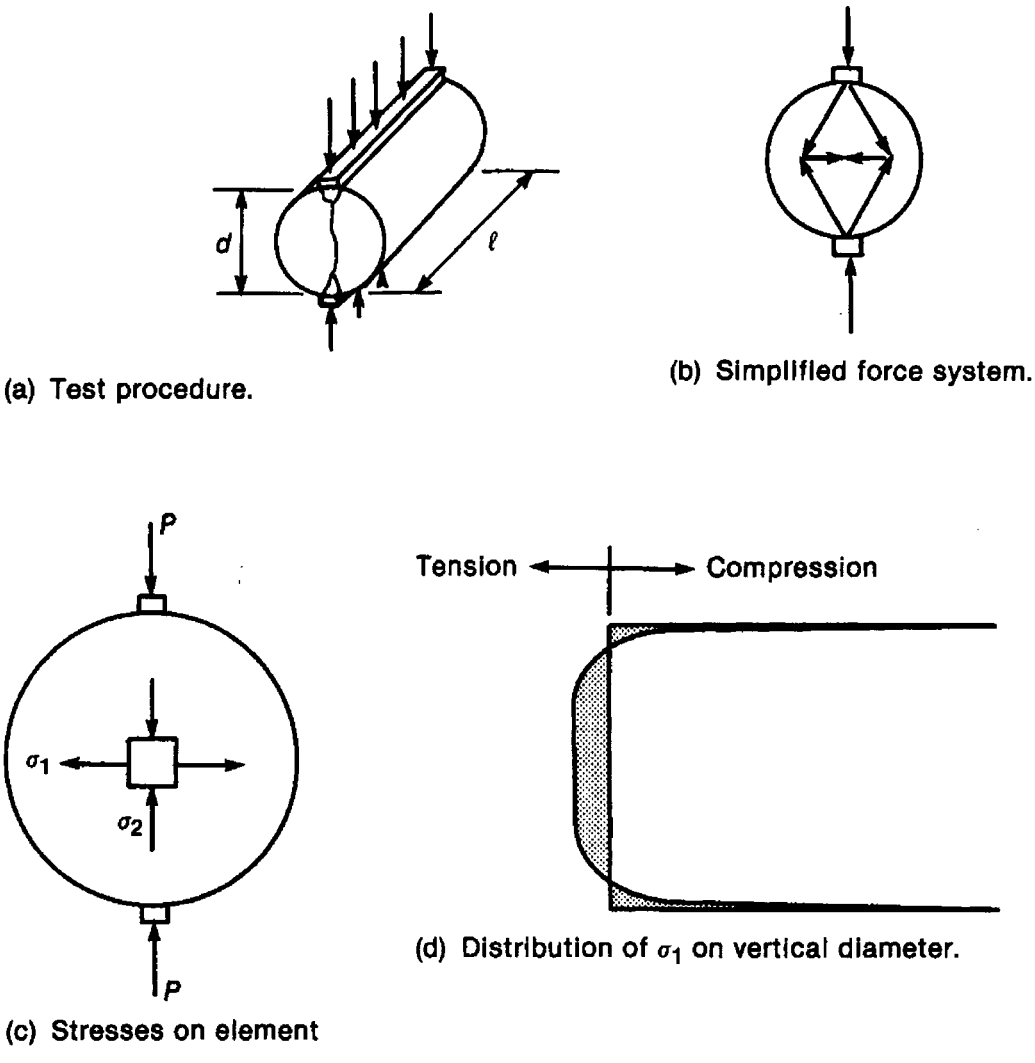

Figure 6-39. ASTM (C496) split cylinder test

l = the length of the concrete cylinder, and

d = the diameter of the cylinder.

Comparing Figure 6-39d to the finite element work shown in reveals that diagonal splitting of deep beams is similar to the splitting test adopted by ASTM.

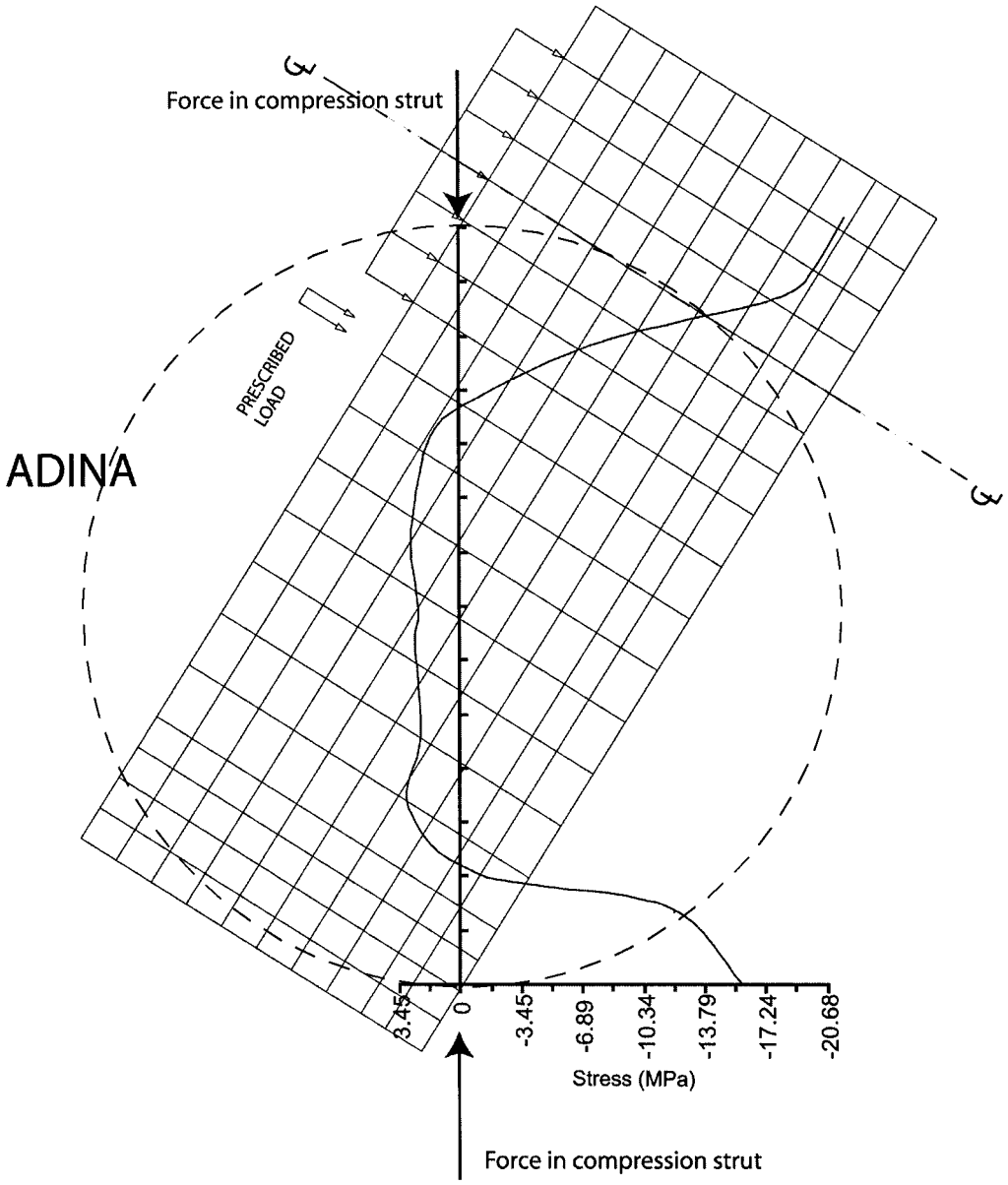

Figure 6-40. Tension stresses perpendicular to compression strut

6.2.4 Summary

Numerous comparisons were carried out between the finite element modeling and the experimental work. The following is a list of observations that can be made from the experimental and finite element work:

1. The finite element modeling done using ADINA was shown to accurately represent the test samples.
2. The stresses and strains along the compression strut are biaxial in nature whether or not the strut is crossed by a tension tie.
3. The compression stresses in the strut, are distributed over the entire area perpendicular to the strut. The strut is not a narrow column of stresses as assumed by many strut-and-tie models.
4. Tensile stresses exist perpendicular to the compression strut. These stresses are constant over the length of the strut, with two areas of compressive stress, one near the loading point, the other near the support.
5. Concrete can continue to carry tensile stresses after cracking. The tensile stress at the crack is zero, however between two cracks the concrete continues to carry tensile stresses.
6. The strains in the concrete strut are much less than the value [5][8] of 0.002 used by the Canadian code.

A strut and tie model used to describe the behaviour of deep beams and corbels must consider a reduction of compressive strength of concrete subjected to biaxial tension and compression stresses. Based on these observations, a strut and tie model is defined in Chapter 7. This model accurately predicts the failure loads of deep beams and corbels, while considering the behaviour of these structures.

7 Truss Model

7.1 Truss Model

The finite element and experimental work presented suggests that deep beams behave as tied arches comprised of concrete compression struts, acting between the points of loading and the supports, and steel tension ties. For the case of a deep beam subjected to two point loads, the load path can be idealized as shown in Figure 6-34. Failure of the deep beam will occur by failure of the compression strut, failure of the tension tie, or a simultaneous failure of both the compression strut and tension tie. It was also shown that the compression stress perpendicular to line B-B in Figure 7-1 is symmetrically distributed about line A-A. The stress perpendicular to line A-A is also uniformly distributed, with two isolated areas of compression, one where the main tension reinforcement is located and the other in the compression zone due to bending. Any truss model derived to calculate the capacity of such structures should account for the biaxial stress state that exists along these diagonals.

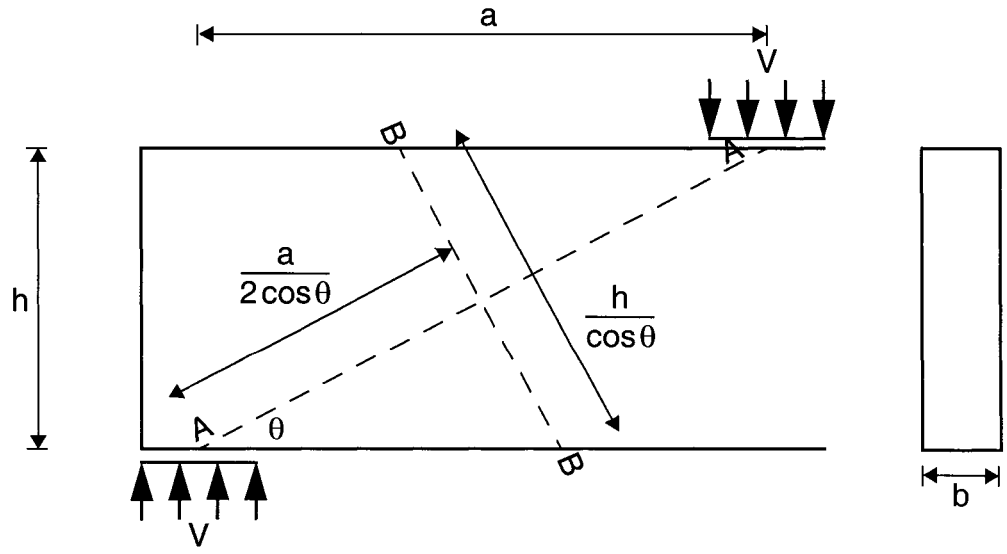

Figure 7-1. Schematic detailing main diagonal and perpendicular diagonal

7.1.1 Compression strut

For simplicity, it will be assumed that the compression stress is uniformly distributed, much like it is done for conventional bending stresses. In this way, the stress distribution can be seen as shown in Figure 7-2.

From the free body diagram shown in Figure 6-34, the compression strut can be defined as

$$C = \frac{V}{\sin\theta} = \frac{P}{\sin\theta}$$ **Equation 7-1.**

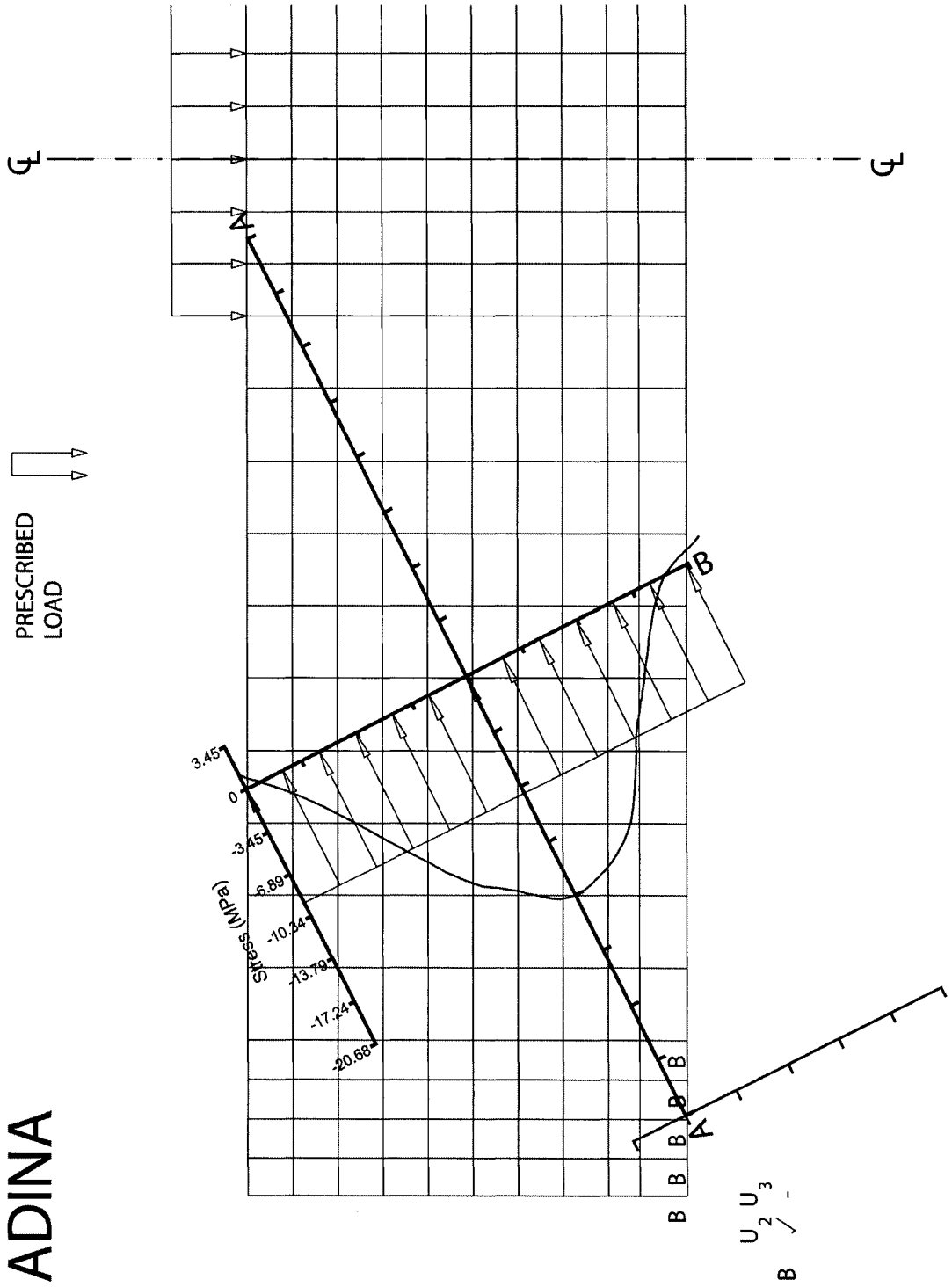

Figure 7-2. Simplified compressive stress distribution

From this, the uniformly distributed compression stress perpendicular to line B-B can be defined.

$$f_{ct} = \frac{C}{b\frac{h}{\cos\theta}} = \frac{V\cos\theta}{bh\sin\theta}$$ **Equation 7-2.**

$$\text{since } \tan\theta = \frac{\sin\theta}{\cos\theta} = \frac{h}{a}$$ **Equation 7-3.**

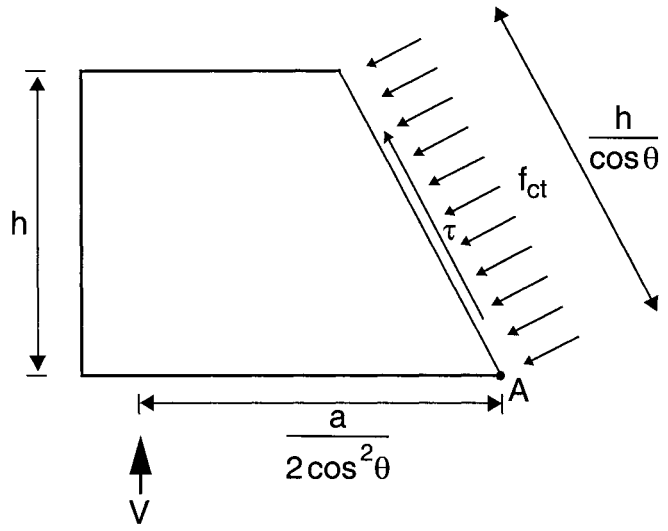

Figure 7-3. Assumed compression stress distribution

substituting equation Equation 7-3 into Equation 7-2 yields

$$f_{ct} = \frac{V\cos\theta}{bh\sin\theta} = \frac{Va}{bh^2}$$ **Equation 7-4.**

In defining the tension stress perpendicular to the main diagonal, an internal force diagram as shown in Figure 7-4 is proposed. The compression force is replaced with two struts radiating at an angle of 2:1 from the point of application. The ratio of 2:1 was adopted from research conducted by Schlaich[53][54]. For equilibrium, tension forces are introduced in the perpendicular direction.

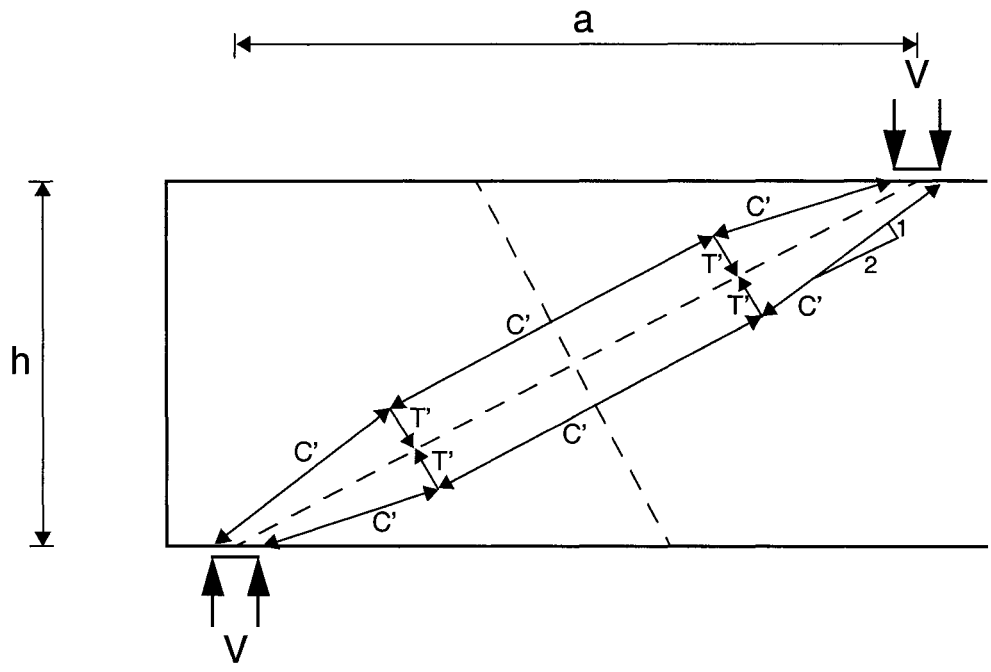

Figure 7-4. Internal force distribution of the compression strut

From the above diagram, the compression strut can be defined as

$$C' = \frac{C}{2} = \frac{V}{2\sin\theta}$$ **Equation 7-5.**

The corresponding tension force can be defined as

$$T' = \frac{C'}{2} = \frac{V}{4\sin\theta}$$ **Equation 7-6.**

In terms of stress

$$f_{tc} = \frac{2T'}{\frac{a}{\cos\theta}b} = \frac{V\cos\theta}{2ab\sin\theta}$$ **Equation 7-7.**

Substituting from Equation 7-3

$$f_{tc} = \frac{V\cos\theta}{2ab\sin\theta} = \frac{Va}{2abh} = \frac{V}{2bh}$$ **Equation 7-8.**

As previously mentioned, the biaxial concrete stress state must be considered when defining the strength of the compression strut. The linear strength envelope (shown in Figure 7-5) describing the biaxial strength of concrete as proposed by Zielinski[73] will be adopted.

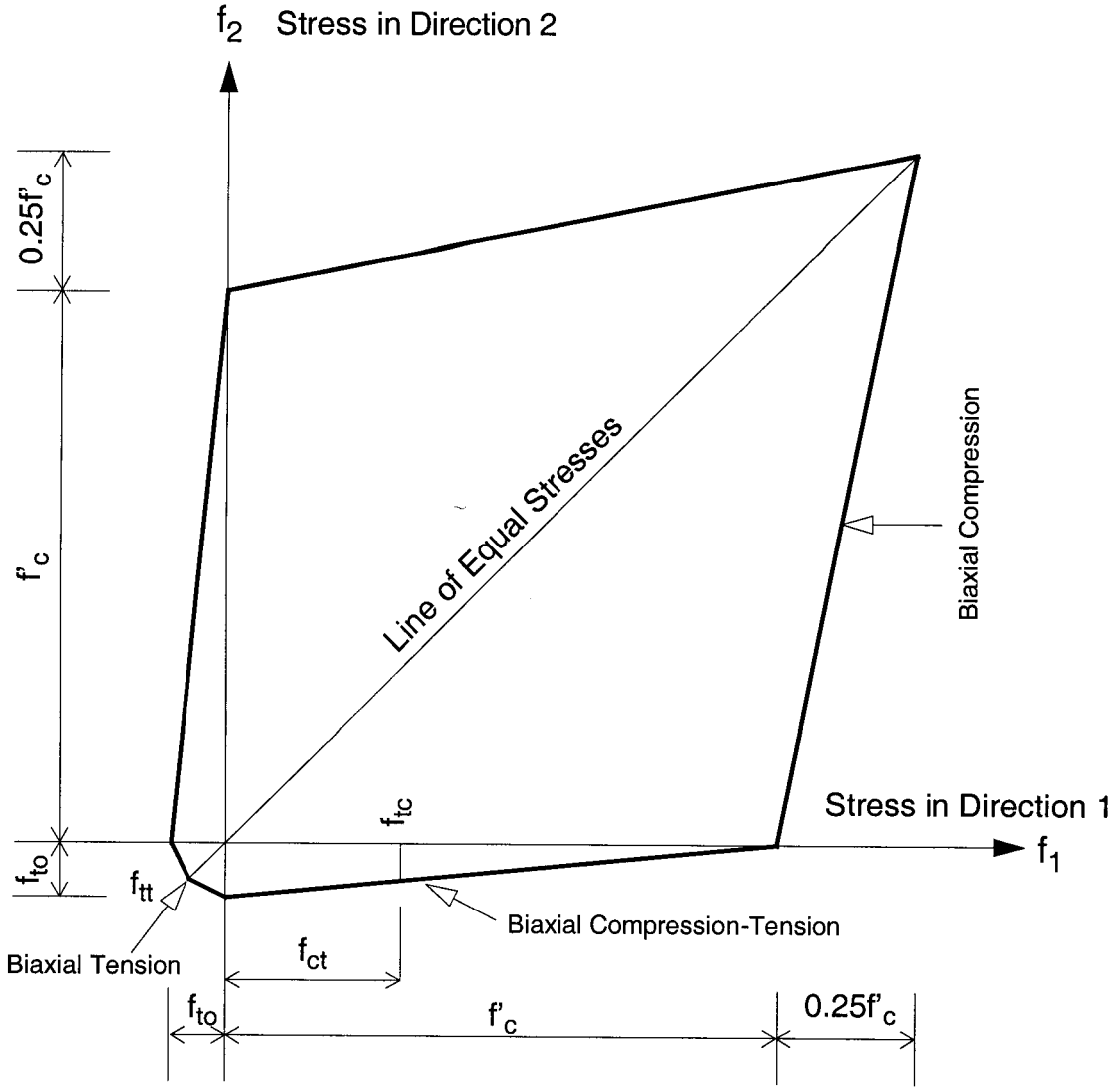

$$f_{to} \cong 0.1f'_c \qquad f_{tc} \cong f_{to}\left[1-\frac{f_{ct}}{f'_c}\right] \qquad f_{ct} \cong f'_c\left[1-\frac{f_{tc}}{f_{to}}\right]$$

Figure 7-5. Biaxial strength envelope for concrete as proposed by Zielinski[73]

$$f_{ct} = f'_c\left(1 - \frac{f_{tc}}{f_t}\right)$$ **Equation 7-9.**

$$\frac{f_{tc}f'_c}{f_t} + f_{ct} = f'_c$$ **Equation 7-10.**

$$f_{tc}\left(\frac{f'_c}{f_t} + \frac{f_{ct}}{f_{tc}}\right) = f'_c$$ **Equation 7-11.**

$$f_{tc} = \frac{f'_c}{\frac{f'_c}{f_t} + \frac{f_{ct}}{f_{tc}}}$$ **Equation 7-12.**

From Equation 7-4 and Equation 7-8

$$\frac{f_{ct}}{f_{tc}} = \frac{\frac{Va}{bh^2}}{\frac{V}{2bh}} = \frac{2a}{h}$$ **Equation 7-13.**

Substituting into Equation 7-12

$$f_{tc} = \frac{f'_c}{\frac{f'_c}{f_t} + \frac{2a}{h}}$$ **Equation 7-14.**

Equation 7-13 implies that tension stresses decrease with an increase in clear span to depth ratio. From the geometry of the deep beam and the material properties, the tension stress can be calculated from Equation 7-14. By substituting into Equation 7-9, the maximum compression stress capacity can be found. The maximum load can then be calculated from Equation 7-4.

$$V = \frac{f_{ct}bh^2}{a}$$ **Equation 7-15.**

The presence of web reinforcement will increase the capacity of the compression strut. Considering the portion of web reinforcement parallel to the diagonal.

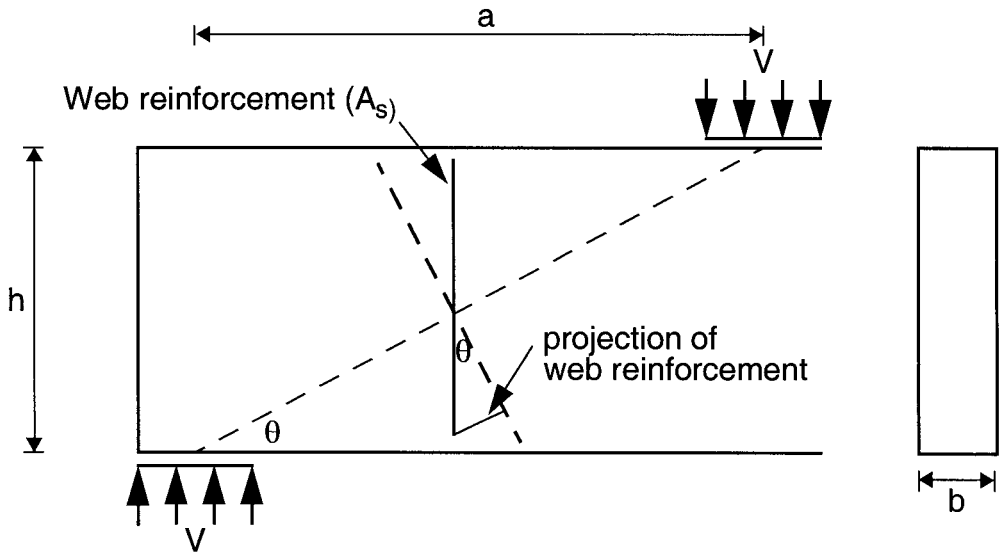

Figure 7-6. Projection of reinforcement along compression strut

$$V = f_{ct}\left(\frac{bh^2}{a} + \frac{E_s}{E_c}\sum A_s \sin\theta\right)$$ **Equation 7-16.**

Failure of the deep beam can be defined by the above equation, provided that the tension tie is well anchored and has sufficient capacity.

7.1.2 Tension tie

The tension tie, assuming that it is well anchored and that adequate development length is present, can be defined as having a maximum capacity of:

$$T = \sum A_s f_y$$ **Equation 7-17.**

where:

A_s = the area of main horizontal tensile reinforcement

f_y = the yield strength of the steel reinforcement

From the free body diagram shown in Figure 6-34, the total load, V, that can be carried by the deep beam based on the capacity of the tension tie is:

$$V = T\tan\theta = \sum A_s f_y \tan\theta = \sum A_s f_y \frac{h}{a}$$ **Equation 7-18.**

Failure occurs when the capacity of the compression strut or the tension tie is reached. At the balanced condition, failure of the compression strut occurs simultaneously with the failure of the tension tie. A comparison of Equation 7-18 to the force in the reinforcement as determined by ADINA is shown in Figure 7-7. For both test series at various loadings, Equation 7-18 was in good agreement with the force determined by ADINA.

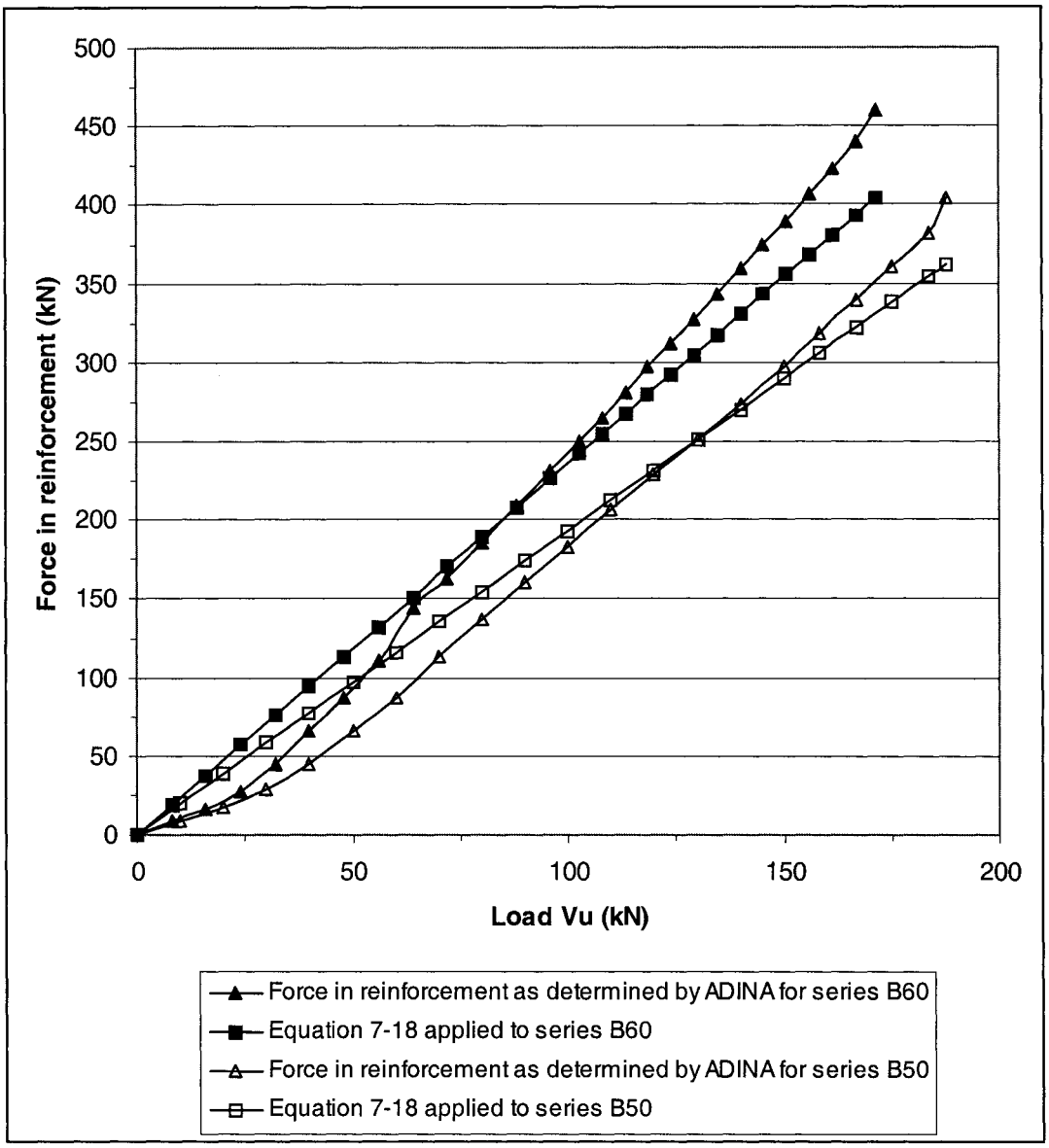

Figure 7-7. Comparison of Equatio n7-18 to force in reinforcement as determined by ADINA

The above equations were applied to the current research to determine their adequacy. A comparison was also made with the current Canadian Code[5].

Table 7-1. Truss model equations applied to experimental results

Sample	a/h ratio	V_u (kN)	V_{calc} (kN) (Equation 7-16)	$\frac{V_u}{V_{calc}}$	$\frac{V_u}{V_{CSA}}$
B150S6	1.57	185.9	178.9	1.04	1.35
B250S6	1.57	258.0	210.0	1.23	1.78
B350S6	1.57	211.3	178.9	1.18	1.60
B150S19	1.57	178.4	178.9	1.00	1.27
B250S19	1.57	189.0	178.9	1.06	1.38
B350S19	1.57	155.7	159.3	0.98	1.21
B160S6	2.00	196.4	169.6	1.16	2.35
B260S6	2.00	185.9	169.6	1.10	2.18
B360S6	2.00	177.9	199.0	0.89	1.72
B160S25	2.00	85.0	102.4	0.83	1.34
B260S25	2.00	177.9	199.0	0.89	1.72
B360S25	2.00	75.6	102.4	0.74	1.16
			Average	0.99	1.59
			Coefficient of variation	0.15	0.24

From Table 7-1, it can be seen that the equations developed here are in good agreement with the experimental work done. The Canadian Code[5] underestimated the capacity of the test beams by an average of 59%. The model presented predicted the capacity much more accurately and with a smaller coefficient of variation than the Canadian Code[5]. It is important to note that the defined truss model utilizes a much wider compression strut than defined by the Canadian Code, and that the concept of strain-softening is not completely lost. By utilizing a concrete biaxial stress curve, we are reducing the concrete capacity due to the presence of perpendicular tensile stresses.

The equations derived in this chapter were applied to test beams available in literature. Test results reported by Smith and Vantsiotis[58], Kong, Robins and Cole[20] were used to test the accuracy of the presented model. These test beams were selected because they satisfied the following conditions.

1. the test beams failed in web shear mode, not in a flexural or bearing mode,

2. the span to depth ratio was less than 2 (thus making them deep beams),

3. the test beams were simply supported.

7.2 Comparison to Other Research

The equations derived in this chapter were applied to fifty-two samples tested by Smith and Vantsiotis[58]. Their research, conducted in 1981, studied deep beams with shear span to depth ratios ranging from 0.77 to 2.01. As shown in Table 7-2, the derived equations are in good agreement with their experimental test results.

Table 7-2. Comparison to work done by Smith and Vantsiotis[58]

Sample	a/d	V_u (lbs)	V_{calc} (lbs) (Equation 7-16)	$\frac{V_u}{V_{calc}}$	$\frac{V_u}{V_{CSA}}$
0A0-44	0.77	31370	29385	1.07	0.59
0A0-48	0.77	30600	30028	1.02	0.56
1A1-10	0.77	36250	27097	1.34	0.76
1A3-11	0.77	33350	26420	1.26	0.72
1A4-12	0.77	31750	23833	1.33	0.76
1A4-51	0.77	38430	30366	1.27	0.75
1A6-37	0.77	41385	31371	1.32	0.80
2A1-38	0.77	39230	31423	1.25	0.73
2A3-39	0.77	38350	28919	1.33	0.77
2A4-40	0.77	38650	30065	1.29	0.76
2A6-61	0.77	36400	28595	1.27	0.75
3A1-42	0.77	36200	26699	1.36	0.77
3A3-43	0.77	38830	28169	1.38	0.81
3A4-45	0.77	40140	30768	1.30	0.78
3A6-46	0.77	37800	29756	1.27	0.75
0B0-49	1.01	33500	30025	1.12	0.74
1B1-01	1.01	33150	30905	1.07	0.72
1B3-29	1.01	32275	28492	1.13	0.76
1B4-30	1.01	31550	29850	1.06	0.72
1B6-31	1.01	34475	28337	1.22	0.86
2B1-05	1.01	29000	26871	1.08	0.70

Table 7-2. Comparison to work done by Smith and Vantsiotis[58]

Sample	a/d	V_u (lbs)	V_{calc} (lbs) (Equation 7-16)	$\frac{V_u}{V_{calc}}$	$\frac{V_u}{V_{CSA}}$
2B3-06	1.01	29500	26946	1.09	0.72
2B4-07	1.01	28350	25135	1.13	0.75
2B4-52	1.01	33700	31210	1.08	0.74
2B6-32	1.01	32650	28679	1.14	0.79
3B1-08	1.01	29400	22787	1.29	0.84
3B1-36	1.01	35735	28600	1.25	0.86
3B3-33	1.01	35600	26946	1.32	0.92
3B4-34	1.01	34850	27615	1.26	0.88
3B6-35	1.01	37350	29950	1.25	0.90
4B1-09	1.01	34500	23989	1.44	0.98
0C0-50	1.34	26000	27323	0.95	0.78
1C1-14	1.34	26750	25775	1.04	0.87
1C3-02	1.34	27750	29677	0.94	0.81
1C4-15	1.34	29450	31133	0.95	0.84
1C6-16	1.34	27500	30313	0.91	0.80
2C1-17	1.34	27900	26600	1.05	0.90
2C3-03	1.34	23300	26123	0.89	0.73
2C3-27	1.34	25925	26215	0.99	0.84
2C4-18	1.34	28000	28114	1.00	0.87
2C6-19	1.34	27900	28910	0.97	0.86
3C1-20	1.34	31650	28159	1.12	1.00
3C3-21	1.34	28100	22519	1.25	1.08
3C4-22	1.34	28700	25184	1.14	1.01
3C6-23	1.34	30850	26523	1.16	1.07
4C1-24	1.34	32950	26233	1.26	1.13
4C3-04	1.34	28900	25199	1.15	1.00
4C3-28	1.34	34250	26123	1.31	1.22
4C4-25	1.34	34300	25510	1.34	1.27
4C6-26	1.34	35850	29565	1.21	1.17
0D0-47	2.01	16500	23573	0.70	0.88
4D1-13	2.01	19650	24177	0.81	1.35
			Average	1.16	0.85
			Coefficient of variation	0.14	0.19

1 lb = 4.448222 N, 1 psi = 0.00689476 MPa

The current Canadian Code over estimated the capacity of these deep beams by and average of 15%, while the model presented here had an under estimated the same beams by 16%. The model presented here yielded results on the conservative side with a smaller coefficient of variation.

Further comparisons were also carried out with work done by Kong, Robbins and Cole[20] in 1970. This time, thirty-five samples with shear span to depth ratios ranging from 0.35 to 1.18 were studied. Once again, the equations presented in this chapter proved to accurately predict the experimental test results.

Table 7-3. Comparison to work done by Kong, Robbins and Cole [20]

Sample	a/d	V_u (lbs)	V_{calc} (lbs) (Equation 7-16)	$\frac{V_u}{V_{calc}}$
1-30	0.35	53700	53888	1.00
1-25	0.43	50400	50979	0.99
1-20	0.54	42600	35287	1.21
1-15	0.74	36900	26490	1.39
1-10	1.18	20100	18170	1.11
2-30	0.35	56000	47408	1.18
2-25	0.43	50400	37969	1.33
2-20	0.54	48400	31991	1.51
2-15	0.74	31400	26944	1.17
2-10	1.18	22400	15436	1.45
3-30	0.35	62100	58795	1.06
3-25	0.43	50700	45555	1.11
3-20	0.54	46700	33408	1.40
3-15	0.74	35800	28040	1.28
3-10	1.18	19400	18545	1.05
4-30	0.35	54400	55084	0.99
4-25	0.43	45200	43392	1.04
4-20	0.54	40600	32922	1.23
4-15	0.74	24600	26312	0.93
4-10	1.18	21500	17153	1.25

Table 7-3. Comparison to work done by Kong, Robbins and Cole [20]

Sample	a/d	V_u (lbs)	V_{calc} (lbs) (Equation 7-16)	$\frac{V_u}{V_{calc}}$
5-30	0.35	53800	46496	1.16
5-25	0.43	46800	39883	1.17
5-20	0.54	38800	33020	1.18
5-15	0.74	28600	26461	1.08
5-10	1.18	17500	17511	1.00
6-30	0.35	69200	64630	1.07
6-25	0.43	59800	51463	1.16
6-20	0.54	55000	42345	1.30
6-15	0.74	38800	31299	1.24
6-10	1.18	22100	19611	1.13
7-30A	0.35	56800	61425	0.92
7-30B	0.35	67400	64091	1.05
7-30C	0.35	58300	61954	0.94
7-30D	0.35	59300	53034	1.12
7-30E	0.35	66800	53277	1.25
			Average	1.16
			Coefficient of variation	0.13

1 lb = 4.448222 N, 1 psi = 0.00689476 MPa

Comparisons were also carried out with work done by Mattock et al.[37][38][39][40][41]. This time, twenty-seven samples with shear span to depth ratios ranging from 0.23 to 1.01 were studied. Only the corbels that failed in "beam shear" were considered. Once again, the equations presented in this chapter proved to accurately predict the experimental test results.

Table 7-4. Comparison to work done by Mattock et al.[37][38][39][40][41]

Sample	a/d	V_u (lbs)	V_{calc} (lbs) (Equation 7-16)	$\frac{V_u}{V_{calc}}$
a2	0.67	35600	39354	0.90
a3	1.01	28000	39093	0.72

Table 7-4. Comparison to work done by Mattock et al.[37][38][39][40][41]

Sample	a/d	V_u (lbs)	V_{calc} (lbs) (Equation 7-16)	$\frac{V_u}{V_{calc}}$
b2	0.67	38900	36944	1.05
b3	1.01	38900	38179	1.02
b3a	1.01	42100	42291	0.99
c1	0.45	44000	44514	0.99
c2	0.68	40000	39718	1.00
c2a	0.68	40500	39611	1.02
c3	1.02	37600	44457	0.85
d1	0.45	28000	43404	0.65
d2	0.68	34000	40680	0.83
d3	1.01	32800	37570	0.87
e1	0.22	55000	38765	1.42
e2	0.45	46000	41165	1.12
e3	0.68	48500	37598	1.29
e4	1.01	35500	34312	1.03
f2	0.45	36500	34366	1.06
f3	0.68	24000	33232	0.72
f4	1.01	24000	34142	0.70
f4a	1.01	23500	31435	0.75
g4	0.99	24000	31828	0.75
h1	0.23	67000	37641	1.78
h2	0.45	50000	36355	1.37
h3	0.68	47400	34346	1.38
h3a	0.68	39600	35281	1.12
h3b	0.68	46100	34034	1.35
j4	1.01	21500	30842	0.70
			Average	1.01
			Coefficient of variation	0.26

1 lb = 4.448222 N, 1 psi = 0.00689476 MPa

The results shown in the previous tables have been graphed, and are shown in Figure 7-8. As can be seen, the equations presented here can predict the failure load of corbels and deep beams. Differences between the calculated and

measured values tend to be on the conservative side, with the calculated values generally predicting a slightly lower value than actually recorded.

The equations presented in this study have been applied to ninety-nine deep beam test samples and twenty-seven corbels. Overall, good agreement was seen between the predicted failure loads and the actual failure load. The model presented here differs from other truss models in that it takes into account the biaxial stress state that exists. Of course, this is only true if failure does not first occur by some other means such as, the crushing of the bearing area.

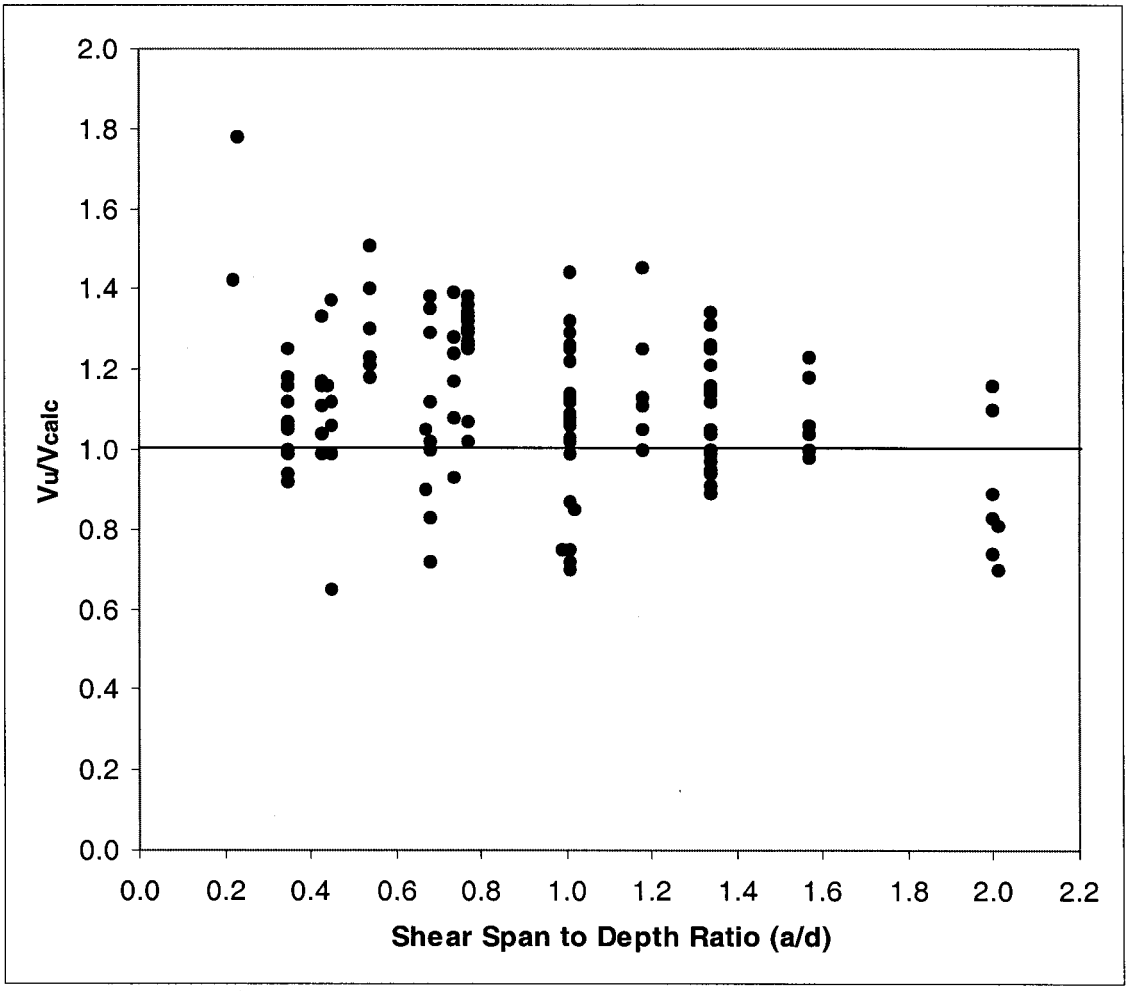

Figure 7-8. Calculated versus measured failures for various shear span to depth ratios

8 Conclusion

8.1 Conclusion

Reinforced concrete, being a heterogeneous material, depends on the strength of both concrete and steel. Failure results when either of these materials fail independently or simultaneously.

Given there is sufficient reinforcement, after flexural cracking, a concrete deep beam will work as a tied arch. The compression strut formed between the loading point and the support is under biaxial compression tension stresses. Beams with a shear span to depth ratio of less than 2.32[73] will work as tied arches provided that the main reinforcement is well anchored beyond the support.

The current Canadian Code[5] uses the work done by Collins and Mitchell[8][9] to establish guidelines in the design of "regions of discontinuity". However the Compression Field Theory was developed using beam theory, and requiring that plane sections remain plane, which is clearly not the case when designing deep beams or corbels. As well, the code does not provide a rationale for how the design recommendations for the width of the compression strut are derived. A significant weakness of the code is the need to assume the values of the strain in the compressive strut as well as in the tension ties.

The research presented here discusses the analysis, behaviour and ultimate strength in diagonal cracking of reinforced concrete deep beams. In all, twelve deep beams, categorized in four groups were tested. Test variables included the shear span, the amount of web reinforcement and the concrete compressive strength. A single beam from each of the four test groups was fitted with twenty-five strain gauges to measure the tensile strain in the main tensile reinforcement, as well as the concrete strain along the main diagonal from between the support

and the loading points. The experimental work showed the development of diagonal cracking. These cracks appeared above the supports and propagated towards the loading point. The strain gauges on the concrete surface confirmed that the stresses along the compression strut were under biaxial compression tension stresses.

The finite element analysis presented was compared to the experimental failure loads, deflections, the concrete and steel strains cracking patterns and modes of failure. On confirmation that the finite element analysis accurately represented the test beams, further results were considered. The following observations were made:

1. Compressive strains along the compression strut are below the Canadian Code[5] (and the Compression Field Theory) recommended value of 0.002. Values as low as 0.001 were measured by the strain gauges as well as predicted by the finite element analysis.
2. The width of the compression strut was found to be much wider than that recommended by the Canadian Code[5]. The finite element analysis demonstrated that the width of the compression strut was as wide as the perpendicular projection of the beam depth to the compression strut.
3. Tensile strains are found perpendicular to the compression strut, whether or not there are any tension ties crossing the strut at that point. The tensile stresses are uniformly distributed along the length of the compression strut. The current Canadian Code[5] only reduces the concrete capacity if a tension tie is present.
4. The Compression Field Theory requires that the strain perpendicular to the compression strut be greater than 0.00117 before the concrete compressive strength is reduced. This high value of strain is probably due to the heavy reinforcement used in the experimental work by Collins and Mitchell. For deep beams without heavy or with no web reinforcement, this value is unreasonably high. The compressive strength of concrete is significantly reduced in the presence of biaxial tensile strains.

With this information, a strut and tie model is defined. This model calculates the average tensile stress perpendicular to the compression strut. Then using a biaxial concrete stress capacity curve, the reduced compression capacity of concrete is used to calculate the maximum compression load each strut can carry. The strain softening concept is still somewhat maintained, in that the strength of concrete is reduced due to the presence of biaxial stresses. This differs from all other strut and tie models. The model was applied to the twelve test beams used in this study confirms an accuracy of 99%. A comparison with the current Canadian Code[5] revealed that the work done here yielded more accurate results than the code. The current code underestimated the capacity of the test beams by an average of 59%. The model was also applied to 114 other test samples available in literature (from Smith and Vantsiotis[58], Kong, Robbins and Cole[20], and Mattock et al.[37][38][39][40][41]) and yielded an accuracy of 112%. The models presented, on average, were on the conservative side, under estimating the failure values by 12%.

Designing for diagonal splitting failures using the models presented here will decrease the amount of concrete and steel used while considering the behaviour of these structures. In order to accurately predict the capacities, the real stress state of the concrete must be considered, i.e. that the compression strut is under biaxial compression and tension.

The advantages of the system proposed here are:

- the concept is simple and avoids complicated empirical equations.
- the model more accurately reflects the behaviour of structures failing in diagonal splitting.
- the designer does not have to assume strain values in the compression strut or the tension ties.
- the formulas have been shown to yield accurate results to 115 beam and corbel test samples available in literature as well as the 12 beams tested in the course of this study

8.2 Recommendations for future study

Recommendations for future work includes expanding the current study:

- to include continuous span beams,
- to consider variations in the loading, perhaps by adding more point loads or by considering distributed loads,
- by changing the horizontal and vertical web reinforcement patterns, and
- by using inclined reinforcement, which is perpendicular to the compression strut.

Bibliography

[1] ACI Committee 318; "Building Code Requirements for Reinforced Concrete, ACI-71" ,American Concrete Institute, 1971.

[2] ACI Committee 318; "Building Code Requirements for Reinforced Concrete, ACI-95,American Concrete Institute, 1995.

[3] Bathe, K.J., Walczak J., Welch A., and Mistry N., "Nonlinear Analysis of Concrete Structures", Computers and Structures, 1989, Vol. 32, pp 563-590

[4] Besser, I.I. and Cusens, A.R.; "Reinforced Concrete Deep Beam Panels with High Depth over Span Ratios"- Proceedings of the Institution of Civil Engineers, June 1984, pp. 265-278.

[5] Canadian Standards Association; "Design of Concrete Structures A23.3-94", Rexdale 1994, 199 pp.

[6] CEB-FIP Model Code for Concrete Structures, Comite Euro-International du Beton/Federation Internationale de la Precontrainte, Paris, 1978.

[7] Cement and Concrete Association (UK), "Handbook on the Unified Code for Structural Concrete - CP110: 1972".

[8] Collins, M.P. and Mitchell, D.; "A Rational Approach to Shear Design -The 1984 Canadian Code Provisions", ACI Journal, Nov-Dec 1986, pp. 925-933.

[9] Collins, M.P. and Mitchell, D.; "Prestressed Concrete Basics", Canadian Prestressed Concrete Institute, 1987, 614 pgs.

[10] Franz G., and Niedenhoff, H., "Reinforcement for Brackets and Short Beams", Beton und Stahlbetonbau (Berlin), V.48, No.5, 1963, pp. 112-120.

[11] Hagberg, T., "Design of Concrete Brackets: On the Application of the Truss Analogy", ACI Journal, V.80, No.I, Jan-Feb 1983, pp. 3-12.

[12] Hagberg, T., "On the Design of Brackets", Beton und Stahlbetonbau, V.61, No.3, 1966, pp. 68-72.

[13] Hermansen, B. R., "Conventionally Reinforced Concrete Brackets", BSc Thesis, Heriot-Watt University, Edinburgh, Apr. 1971, 163 pp.

[14] Hermansen, B. R., and Cowan, J., "Modified Shear - Friction Theory for Bracket Design", ACI Journal, V.71, No.2, Feb. 1974, pp. 55-60.

[15] Hermansen, B. R., and Cowan, J., "Second Thoughts on Shear Friction", Concrete(UK), Aug. 1975, pp. 31-32.

[16] Hwang S., Lu W., and Lee H., "Shear Strength Prediction for Deep Beams", ACI Structural Journal, May 2000 Vol. 97, No. 3, pp 367-376.

[17] Hwang S., Lu W., and Lee H., "Shear Strength Prediction for Reinforced Concrete Corbels", ACI Structural Journal, July 2000 Vol. 97, No. 4, pp 543-552.

[18] Kong, F.K.; "Reinforced Concrete Deep Beams"- Blackie (London & Glasgow); Van Nostrand-Reinhold (New York), 1990.

[19] Kong, F.K. and Robins, P.J.; "Web Reinforcement Effects on Lightweight Concrete Deep Beams"- ACI Journal, July 1971, pp. 514-520.

[20] Kong, F.K., Robins, P.J. and Cole, D.F.; "Web Reinforcement Effects on Deep Beams"- ACI Journal Dec 1970, pp. 1010-1017.

[21] Kong, F.K., Robins, P.J., Kirby, D.P., and Short, D.R.; "Deep Beams with Inclined Web Reinforcement "- ACI Journal, March 1972, pp. 172-176.

[22] Kong, F.K., Robins, P.J., Singh, A. and Sharp, G.R.; "Shear Analysis and Design of Reinforced Concrete Deep Beams"- The Structural Engineer, Vol. 50, No.10, October 1972, pp 405-409.

[23] Kong, F.K., and Sharp, G.R.; "Shear Strength of Lightweight Concrete Deep Beams with Web Openings"- The Structural Engineer, Vol. 51,No.8, August 1972, pp 267-275.

[24] Kong, F.K., and Sharp, G.R.; "Structural Idealization for Deep Beams with Web Openings"- Magazine of Concrete Research, Vol. 29, No.99, June 1977, pp 81 -91.

[25] Kong, F.K. and Singh. A.; "Diagonal Cracking and Ultimate Loads of Lightweight Concrete Deep Beams"- ACI Journal, August 1972, pp. 513-521.

[26] Kotsovos, M.D.; "Compressive Force Path Concept: Basis for Reinforced Concrete Ultimate Limit State Design"- ACI Structural Journal, Jan-Feb 1 988, pp 68-75.

[27] Kotsovos, M. D.; "Design of Reinforced Concrete Deep Beams" - The Structural Engineer, Vol. 66, No.2, Jan. 1988 pp 28-32.

[28] Kriz, L. B., and Raths, C. H., "Connections in Precast Concrete Structures- Strength of Corbels", PCI Journal, V.10, No.I, N.4, Feb.1965, pp. 16-61.

[29] Kupfer, H., Hilsdorf, H.K., and Ruesch, H., "Behavior of Concrete Under Biaxial Stresses", Journal ACI, Proc. V. 66, No. 8, Aug. 1969, pp. 656-666.

[30] Leonhardt, F., "Reducing the Shear Reinforcement in Reinforced Concrete Beams and Slabs", Concrete Research, V.17, No.53, Dec. 1965, p. 187

[31] Leonhardt, F. and Walther, R.; "Wandartige Trager"- Bulletin No. 178, Wilhelm Ernst und Sohn, Berlin, 1966, 159 pp.

[32] Leonhardt, F., and Monning, E., "Lectures on the Design of Concrete Structures", Springer Verlag, Berlin-Hiedelberg, 1974.

[33] Marti, P., "Plastic Analysis of Reinforced Concrete Shear Walls", Bericht No.87, Institut fur Baustatik und Konstruktion, Zurich, 1978

[34] Marti, P., "Basic Tools of Reinforced Concrete Design", ACI Journal, Jan-Feb. 1985, pp. 46-56.

[35] Marti, P., "Truss Models in Detailing"- Concrete International, Dec 1985, pp 66-73.

[36] Mast. R. F., "Auxiliary Reinforcement in Concrete Connections", Proceedings of the American Society of Civil Engineers, V.94, No.ST6, Jun. 1968, pp. 1485- 1504.

[37] Mattock, A. H., "Design Proposals for Reinforced Concrete Corbels", PCI Journal, Prestressed Concrete Institute, V.21, No.3, May-June 1976, pp. 18 - 42.

[38] Mattock, A. H., "Shear Transfer Friction in Concrete having Reinforcement at an Angle to the Shear Plane", ACI SP42-2, 1974, pp. 17-42.

[39] Mattock, A. H., "Shear Transfer Friction in Reinforced Concrete", First Progress Report to National Science Foundation, Jun. 1973.

[40] Mattock, A. H., and Lee, D. W., "Discussion of the Paper authored by B.R. Hermansen and J. Cowan: Modified Shear- Friction Theory for Bracket Design", ACI Journal, Aug. 1974, pp. 420-423.

[41] Mattock, A. H., Chen K. C., and Soonswang K., "The Behaviour of Reinforced Concrete Corbels", PCI Journal, Prestressed Concrete Institute. V.21, No.2, Mar - Apr. 1976, pp. 53 - 75.

[42] Mau, S.T. and Hsu, T.C.; "Formula for the Shear Strength of Deep Beams" - ACI Structural Journal, Vol. 86, No.5, Sept. 1989, pp 516-523.

[43] Mau, S.T. and Hsu, T.C., "Shear Strength Prediction for Deep Beams with Web Reinforcement"- ACI Structural Journal, Nov-Dec 1987, pp 513-523.

[44] Mitchell, D. and Collins, M.P.; "Diagonal Compression Field Thoery - A Rational Model for Structural Concrete in Pure Torsion", ACI Journal , V.71, Aug. 1974, pp. 649-666.

[45] Morsch, E., "Reinforced Concrete Theory and Application", Stuttgart, Verlag Konrad Wittwer, 1912.

[46] Mueller, P., "Plastic Analysis of Reinforced Concrete Beams", Bericht No.83, Institut fur Baustatik und Konstruktion, ETH Zurich, Jul. 1978.

[47] Nielsen, M. P., Braestrup, M. W., Jensen, B. C., and Finn Bach, "Concrete Plasticity, Beam Shear- Shear in Joints - Punching Shear", Special Publication of the Danish Society for Structural Science and Engineering, Technical University of Denmark, Lyngby/Copenhagen, 1978

[48] de Pavia, H.A.R. and Siess, C. P.; "Strength and Behaviour of Deep Beams in Shear"- ASCE Proceedings, Oct 1965, pp 19-41.

[49] Ramakrishnan, V. and Ananthanarayana, Y.; "Ultimate Strength of Deep Beams in Shear"- ACI Journal, Proceedings, Vol. 65, No. 2, Feb 1968, pp 87-97.

[50] Rogowsky, D.M. and MacGregor, J.G.; "Design of Reinforced Concrete Deep Beams"- Concrete International, August 1986, pp 49-58.

[51] Rogowsky, D.M. and MacGregor, J.G.; "Shear Strength of Deep Reinforced Concrete Continuous Beams"- Structural Engineering Report No. 110, Dept. of Civil Engineering, University of Alberta, Edmonton, Canada, Nov 1983.

[52] Rogowsky, D.M., MacGregor, J.G. and Ong, XX.; "Tests of Reinforced Concrete Deep Beams"- ACI Journal, July-Aug 1986, pp 614-623.

[53] Schlaich, J., and Schafer, K., "Design and Detailing of Structural Concrete using Strut and Tie Models", The Structural Engineer, Proceedings, V.69, No.6, 19 Mar. 1991, pp. 113 - 125.

[54] Schlaich, J., and Schafer, K., "Towards a Consistent Design of Structural Concrete", PCI Journal, E32, No.3, May-Jun. 1987, pp. 74 - 150.

[55] Siao, W.B.; "Deep Beams Revisited"- ACI Structural Journal, Vol. 92,No.1, Jan-Feb 1995, pp 95-102.

[56] Siao, W.B., "Shear Strength of Short Reinforced Concrete Walls, Corbels and Deep Beams"- ACI Structural Journal, Vol. 91, No.2, March 1994, pp 123-132.

[57] Siao, W.B., "Strut and Tie Model for Shear Behaviour in Deep Beams and Pile Caps Failing in Diagonal Splitting"- ACI Structural Journal, Vol. 90, No.4, July 1993, pp 356-363.

[58] Smith, K.N. and Vantsiotis, A.S.; "Shear Strength of Deep Beams"- ACI Journal, May-June 1982, pp 201-213.

[59] Solanki, H., and Sabnis, G. N., "Reinforced Concrete Corbels- Simplified", ACI Structural Journal, Sept. - Oct. 1987, pp. 428 -432.

[60] Somerville, G., "The Behaviour and Design of Reinforced Concrete Corbels", Shear in Reinforced Concrete, SP -42, American Concrete Institute, Detroit, 1974, pp. 477-502."

[61] Tan K.H., Lu H.Y., "Shear Behavior of Large Reinforced Concrete Deep Beams and Code Comparisons", ACI Structural Journal, Sept. - Oct. 1999, pp. 836-845.

[62] Thurlimann, B., "Advanced Lecture for Civil Engineers", Institut fur Bautechnik und Konstruktion, ETH Zurich, 1983.

[63] Thurlimann, B., "Plastic Analysis of Reinforced Concrete Beams", Bericht No.86, Institut fur Baustatik urld Kondstruktion, Zurich, Nov. 1978.

[64] Thurlimann, B.; "Shear Strength of Reinforced and Prestressed Concrete Beams"- CEB Bulletin 126, Paris, June 1978.

[65] Vecchio, F., and Collins, M. P., "The Response of Reinforced Concrete to In-Plane Shear and Normal Stresses", Publication No.82-03, Department of Civil Engineering, University of Toronto, Mar. 1982, 332 pp.

[66] Vecchio, F.J. and Collins, M.P.; "The Modified Compression Field Theory for Reinforced Concrete Elements Subjected to Shear"- ACI Journal, March-April 1986, pp 219-231.

[67] Vecchio, F. and Collins, P.; "Stress-Strain Characteristics of Reinforced Concrete in Pure Shear"- Final Report, IABSE Colloquium on Advanced Mechanics of Reinforced Concrete (Delft 1981), International Association for Bridge and Structural Engineering, Zurich, pp 211-225.

[68] Wagner, H., "Ebene Blechwandtrager mit sehr dunnem Stegblech", Zeitschrift fur Flugtechnik und Motorluftschiffahr, V.20, Nos 8 to 12, Berlin, 1929.

[69] Zielinski, Z.A., "Precast prestressed concrete girders", published by Arkady, Warsaw (Polish), 1st edition 1957, pp 1-309.

[70] Zielinski, Z.A., "Entwurfs - und Verwendungsprobleme wirtschaftlicher Spannbetontragern", Federation Internationale de la Precontraine, Proceedings, Paper No. 17, 1958, pp. 1-6.

[71] Zielinski, Z.A., "Behaviour and ultimate strength of rectangular reinforced concrete beams in bending and high shear", Bulletin No. 81, North Carolina State University, Raleigh, 1967

[72] Zielinski, Z.A., "Research on ultimate strength in shear of bonded and unbonded reinforced concrete beams", International Symposium Shear, Torsion and Bond in Reinforced and Prestressed Concrete, P.S.G. College of Technology, Coimbatore, India, 1969.

[73] Zielinski, Z.A., "A new approach to ultimate strength of reinforced concrete beams in inclined cracking and reduction of web reinforcement in bridge girders", 2nd International Symposium Concrete Bridge Design, ACI Publication, 1971, pp. 411-456.